

APPLYING DESIGN OF EXPERIMENTS PRINCIPLES TO
THE INVESTIGATION OF CHEMICAL REACTIONS
VIA MATHEMATICAL MODELING

by

Elizabeth N. Bess

A dissertation submitted to the faculty of
The University of Utah
in partial fulfillment of the requirements for the degree of

Doctor of Philosophy

Department of Chemistry

The University of Utah

May 2015

Copyright © Elizabeth N. Bess 2015

All Rights Reserved

The University of Utah Graduate School

STATEMENT OF DISSERTATION APPROVAL

The following faculty members served as the supervisory committee chair and members for the dissertation of Elizabeth N. Bess.

Dates at right indicate the members' approval of the dissertation.

Matthew S. Sigman, Chair 5 November 2014
Date Approved

Elena A. Cherkaev, Member 5 November 2014
Date Approved

Jennifer M. Heemstra, Member 5 November 2014
Date Approved

Ryan E. Looper, Member 5 November 2014
Date Approved

Ryan P. Steele, Member 5 November 2014
Date Approved

The dissertation has also been approved by Cynthia J. Burrows Chair of the Department of Chemistry and by David B. Kieda, Dean of The Graduate School.

ABSTRACT

Selectivity in chemical reactions is a matter of distinguishing between pathways of little energetic difference. From reactions affording no selectivity in product formation to those achieving selectivity levels of >99:1, the energy differences responsible for these disparate isomer ratios range from 0 to ~ 3 kcal mol⁻¹, respectively. It is astounding that such a seemingly trivial amount of energy, on the order of the energetic barrier to carbon-carbon bond rotation in ethane (~ 2.9 kcal mol⁻¹), can precipitate products in exquisitely high isomeric purity. Identifying the origin of the small energy differences that afford selectivity has, historically, been a daunting endeavor and predominantly characterized by empiricism.

In recent years, the Sigman group has been developing a more efficient alternative to the typical guess-and-check approach to optimizing catalyst-substrate interactions for high site- and enantioselective outcomes. This methodology relies on the quantification and systematic modulation of various reaction features that putatively induce selectivity, ultimately enabling the identification of mathematical equations to describe these effects. Detailed herein is the process for developing reliably predictive mathematical constructs of reaction selectivity. In the context of three distinct reactions—iridium-catalyzed asymmetric hydrogenation (Chapter 2), rhodium-catalyzed site-selective C-H amination (Chapter 3), and rhodium-catalyzed asymmetric transfer hydrogenation (Chapter 4)—means for effective model development are put forth. Namely, this work describes the

examination of the unconventional application of design of experiments principles, the identification of parameters capable of describing selectivity, and the process by which linear regression models are developed and validated.

Through this approach, mathematical equations are developed that relate the differential free energy of selectivity to numerical depictions of steric, electronic, and hydrophobic effects. By identifying underlying predictive trends, developed models serve as a unique avenue by which mechanistic insight may be gained about selectivity engendering interactions. Consequently, these models enable the energetic optimization of substrate-catalyst interactions and the quantitative prediction of how such changes will influence reaction selectivity. Through the work of myself and my colleagues in the Sigman group, we are learning how reactions may be investigated and understood so as to make the ~ 3 kcal mol⁻¹ energy range that is responsible for selectivity a vast window of opportunity for shaping reaction partners to achieve desired reaction outcomes.

To Ken, my best friend and supporter

TABLE OF CONTENTS

ABSTRACT.....	iii
LIST OF TABLES.....	viii
LIST OF ABBREVIATIONS.....	ix
ACKNOWLEDGEMENTS.....	xiv
CHAPTER	
1. QUANTITATIVE PREDICTIONS IN PHYSICAL ORGANIC CHEMISTRY.....	1
Introduction.....	1
Hammett and the Development of LFER.....	2
Extending LFER to Asymmetric Catalysis via the Curtin-Hammett Principle ...	6
Hammett σ LFER and Mn(salen)-Catalyzed Asymmetric Epoxidation.....	9
Quantitating Steric Effects Using LFER.....	11
Applying Charton ν and Hammett σ to NHK Asymmetric Propargylation.....	15
Broadening the Scope of Free-Energy Relationships.....	17
Quantitative Structure-Activity Relationships.....	18
Development of Multidimensional Free-Energy Relationship Models.....	20
References.....	24
2. IDENTIFYING MECHANISTICALLY RELEVANT CHEMICAL DESCRIPTORS FOR LINEAR REGRESSION MODELLING.....	27
Introduction.....	27
Selecting Suitable Chemical Descriptors.....	28
Application of Design of Experiments Principles.....	38
Principal Component Analysis (PCA) to Streamline DoE Application.....	41
A Qualitative DoE Approach.....	45
A Quantitative Model from a Qualitatively Developed DoE Library.....	50
Conclusions.....	58
Experimental Information.....	59
References.....	111

3. A DESIGN OF EXPERIMENTS-GUIDED APPROACH TO THE INVESTIGATION OF RHODIUM-CATALYZED C–H AMINATION SITE SELECTIVITY	117
Introduction.....	117
Investigating the Reaction.....	121
Parameter Selection	123
Model Development.....	129
Assessing Model Robustness via External Validation.....	134
Analyzing and Interpreting the Model	135
Predicting an Improved Sulfamate Ester	136
Conclusions.....	140
Experimental Information.....	141
References.....	176
4. A DESIGNER SUBSTRATE SCOPE LIBRARY AMENABLE TO QUANTITATIVE DESCRIPTION AND PREDICTIVE MODELLING OF SELECTIVITY.....	180
Introduction.....	180
Identify Substrate Parameters and Define the Ketone Experimental Space	185
Organize and Evaluate Ketones that Systematically Sample the Experimental Space.....	193
Quantitatively Connect Reaction Outcomes and Molecular Descriptors of Ketones	194
Predict the Performance of New Ketone Substrates	204
Conclusions.....	204
Methods.....	207
Experimental Information.....	210
References.....	242
5. ONGOING AND PROPOSED APPLICATIONS OF MODEL DEVELOPMENT	249
Introduction.....	249
Extending Free-Energy Relationships to Enzyme Engineering.....	250
Conclusions.....	256
References.....	257

LIST OF TABLES

2.1	Exploration of substrate <i>meta</i> -directing group effects.....	46
2.2	Substrate scope for iridium(PhosPrOx)-catalyzed hydrogenation.....	48
2.3	Design of Experiments matrix for optimization of reaction conditions	105
2.4	Parameter set used for descriptive modelling	108
3.1	Training set (entries 1–23), external validations (entries 24–61), and predictions (entries 62–64).....	132
3.2	Training, external validation, and prediction data sets for model development.....	143
4.1	Aryl/alkyl ketone DoE library and external validations	229
4.2	Alkyl/alkyl ketone DoE library and external validations	234
5.1	Parameter measurements on which Principal Component Analysis (PCA) was performed.....	254

LIST OF ABBREVIATIONS

A	Winstein-Holness values
Å	Angstrom
a.u.	arbitrary units
A [‡]	diastereomeric transition state
AcCl	acyl chloride
Ala	Alanine
aq	Aqueous
Ar	Aryl
asym	Asymmetric
ATH	asymmetric transfer hydrogenation
B:T	benzylic-to-tertiary ratio
B ₁	Sterimol minimum radius
B ₅	Sterimol maximum radius
BA _{TF}	tetrakis[3,5-bis(trifluoromethyl)phenyl]borate
Boc	<i>tert</i> -butyloxycarbonyl
bs	broad singlet
°C	degree Celsius
C	Chemical
<i>c</i>	concentration
C=C	carbon-carbon double bond
Cbz	carboxybenzyl
C-H	carbon-hydrogen bond
COD	cyclooctadiene
Conv.	conversion
Cp*	pentamethylcyclopentadienyl
Cy	cyclohexyl
ΔΔG [‡]	differential transition state free energy
ΔG _{AB}	difference in free energy between A and B
d	Doublet
d[A _{Pdt}]	change in concentration of product A over time
DCE	1,2-dichloroethane
DCM	dichloromethane
dd	doublet of doublets

ddd	doublet of doublet of doublets
DFT	density functional theory
Dist ^B 1 _{Aryl}	measure of minimum arene radius distal to carbonyl
Dist ^B 5 _{Alkyl}	measure of maximum alkyl radius distal to carbonyl
Dist ^B 5 _{Aryl}	measure of maximum arene radius distal to carbonyl
Dist ^L Alkyl	measure of alkyl substituent length
Dist ^L Aryl	measure of arene length
dm	decimeter
DMA	dimethylacetamide
DMAP	4-(dimethylamino)pyridine
DMSO	dimethylsulfoxide
DoE	design of experiments
d _{tor}	torsion between aryl rings
δ	chemical shift
ee	enantiomeric excess
EI	electron ionization
equiv	equivalents
er	enantiomeric ratio
E _s	Taft's measure for steric bulk
ESI	electrospray ionization
Et	ethyl
EtOAc	ethyl acetate
EtOH	ethanol
<i>f</i>	mathematical function
F ₂₅₄	fluorescence at 254 nm
FCC	face-centered-cubic
FT-IR	Fourier Transform-Infrared
g	gram
GC	gas chromatography
GC-MS	gas chromatography-mass spectrometry
h	hour
HPLC	high performance liquid chromatography
HRMS	high-resolution mass spectrometry
IBCF	<i>isobutylchloroformate</i>
I _{C=O}	intensity of carbonyl IR stretch
<i>i</i> _{C-H}	intensity of alkene C-H bond asymmetric IR vibration
I _{CO}	intensity of sulfamate ester C-O stretch
Ile	isoleucine
I _{OSN}	intensity of sulfamate ester O-S-N asymmetric stretch
<i>i</i> Pr	<i>isopropyl</i>

<i>i</i> PrOAc	<i>isopropyl acetate</i>
IR	<i>infrared</i>
Ir	<i>Iridium</i>
I _{Scissor}	<i>intensity of carbonyl substituent scissoring</i>
I _{SO₂asym}	<i>intensity of sulfamate ester SO₂ asymmetric stretch</i>
I _{SO₂sym}	<i>intensity of sulfamate ester SO₂ symmetric stretch</i>
<i>i</i> _{sym}	<i>intensity of aryl ring symmetric IR vibration</i>
<i>J</i>	<i>coupling constant</i>
<i>K</i>	<i>equilibrium constant</i>
<i>k</i>	<i>reaction rates</i>
kcal	<i>kilocalorie</i>
<i>k</i> _{Nuc}	<i>reaction rate of nucleophilic attack</i>
L	<i>Sterimol length</i>
LCTOF	<i>liquid chromatography time-of-flight</i>
Leu	<i>leucine</i>
LFER	<i>linear free-energy relationship</i>
ln	<i>natural logarithm</i>
log	<i>logarithm</i>
logP	<i>hydrophobicity partition coefficient</i>
LOO	<i>leave-one-out</i>
LRGC-MS	<i>low-resolution gas chromatography-mass spectrometry</i>
m	<i>multiplet or meter</i>
M	<i>molar</i>
m/z	<i>mass to charge ratio</i>
Me	<i>methyl</i>
Meas.	<i>measured</i>
MeOH	<i>methanol</i>
mg	<i>milligram</i>
MHz	<i>megahertz</i>
min	<i>minute</i>
mL	<i>milliliter</i>
mm	<i>millimeter</i>
mmol	<i>millimole</i>
Mn	<i>manganese</i>
mol	<i>mole</i>
M.P.	<i>melting point</i>
NBO	<i>natural bond orbital</i>
<i>n</i> Bu	<i>normal butyl</i>
<i>n</i> BuLi	<i>normal butyl lithium</i>
NEt ₃	<i>triethylamine</i>

NHK	Nozaki-Hiyama-Kishi
nm	nanometers
NMM	<i>N</i> -methylmorpholine
NMR	nuclear magnetic resonance
Nuc	nucleophile
ν	Charton's measure for steric bulk
$\nu_{C=O}$	frequency of carbonyl IR stretch
ν_{CO}	frequency of sulfamate ester C–O stretch
ν_{OSN}	frequency of sulfamate ester O–S–N asymmetric stretch
$\nu_{Scissor}$	frequency of carbonyl substituent scissoring
ν_{SO_2asym}	frequency of sulfamate ester SO ₂ asymmetric stretch
ν_{SO_2sym}	frequency of sulfamate ester SO ₂ symmetric stretch
p	pentet
P/N	Phosphorous/Nitrogen
PC	principal component
PCA	principal component analysis
Pd/C	palladium on carbon
Ph	phenyl
Phe	phenylalanine
PhI(OAc) ₂	(diacetoxyiodo)benzene
PhMe	toluene
PhosPrOx	phosphoramidite ligand bearing proline and oxazoline moieties
PMA	phosphomolybdic acid
ppm	parts per million
Pr	propyl
Pred.	predicted
$Prox B1_{Alkyl}$	measure of minimum alkyl radius proximal to carbonyl
$Prox B1_{Aryl}$	measure of minimum arene radius proximal to carbonyl
$Prox B5_{Alkyl}$	measure of maximum alkyl radius proximal to carbonyl
$Prox B5_{Aryl}$	measure of maximum arene radius proximal to carbonyl
π	pi orbital
psi	pounds per square inch
q	quartet
q ⁺	positive point charge
q ⁻	negative point charge
QSAR	quantitative structure-activity relationship
qt	quartet of triplets
ρ	Hammett value sensitivity factor
R	ideal gas constant
R ²	adjusted coefficient of determination

R _f	retention factor
Rh	Rhodium
rt	room temperature
R _T	retention time
r _v	minimum van der Waals radius
σ	Hammett value
σ ⁺	Hammett sigma plus value
σ _I	inductive effect measure
σ _R	resonance effect measure
s	singlet
sep	septet
sex	sextet
SFC	super-critical fluid chromatography
sym	symmetric
θ	physiological response
t	Triplet
T	temperature
<i>t</i> Bu	<i>tert</i> -butyl
td	triplet of doublets
THF	tetrahydrofuran
TLC	thin-layer chromatography
TMS	tetramethylsilane
TOF	time-of-flight
<i>Tor</i>	degree of torsion
tq	triplet of quartets
TsCl	tosyl chloride
TZVP	triple-zeta valence basis set with polarization
μm	micrometer
UV	ultraviolet
Val	valine
vol	substituent volume
vs	versus
°	Degree

ACKNOWLEDGEMENTS

Many people have journeyed with me through the triumphs and difficulties of my time in graduate school, and each one has profoundly impacted me as a person and as a scientist. First, I am very appreciative of my adviser, Matt Sigman, for his continuous confidence in my potential, which has pulled me through difficult times and helped me to develop self-confidence as a scientist. Matt created a positive, safe learning environment where I was able to engage in scientific discussions, explore eccentric ideas, and challenge myself with difficult problems. Matt's trust in me and my abilities is the greatest gift a student can ask for.

The Sigman research group has drawn to it many people who are exceptionally bright, motivated, and enthusiastic, and who have become dear friends. Rachel Vaden has been my confidante and someone on whom I can always rely for support. Through many long discussions over the years, she has provided advice and perspective on navigating academia and life. As the student that I looked up to throughout my PhD, Rachel's energy, passion, and dedication to scientific discovery shaped my approach to research.

I also offer my sincere gratitude to Anat Milo for her scientific insight, enthusiasm, and innovation that opened my eyes to new ways of approaching research. Much of this work was made possible due to her creative contributions to the field of mathematical model development. To Kaid Harper, for training me in chemical synthesis and mathematical modelling, for many stimulating discussion during the development of

the concepts described herein, and for his boldness to initiate this unconventional approach to reaction investigation. To Ryan DeLuca, for showing me how to laugh about life and be serious about science. To Margaret Hilton, Susi Opra, Ajara Raman, Celine Santiago, and Sarah Vilardi, who have each added a bit of sparkle to my days and made coming to work fun. To Amanda Bischoff and Christina Hughes, who were fantastic undergrads that patiently helped me learn how to teach and mentor students. And to each member of the Sigman group who has added to the scientifically intense, yet friendly, atmosphere where thought-provoking questions are asked, where hard work happens, and where lots of laughs are had.

I am appreciative of the perceptive comments, questions, and discussions that I have had with my PhD committee members and for the advice and support that they have provided, both scientifically and professionally.

I am grateful to my parents, Richard and Nancy Black, who taught me from a young age the satisfaction and excitement that comes from learning and that, with enough hard work, anything can be accomplished. This philosophy ultimately led me to pursue graduate education and continues propelling my desire to learn about the world around me. I am also particularly grateful for the time my father spent teaching me how to write. As we sat side-by-side to edit every paper I wrote from seventh through twelfth grades, he taught me the capabilities of language and how the writing process illuminates new connections in information. An ability to articulate my thoughts and construct logical arguments through writing has made writing papers, grants, and even my dissertation some of the most satisfying experiences in graduate school.

Finally, I am most grateful to my best friend and partner in everything, Ken, for

his unwavering love, support, patience, and confidence and for showing me how to relax, have fun, and enjoy life a bit more. During my graduate school experience, everything that I thought I knew about life has been poked and prodded and sometimes turned on its head. Ken has always been there to help me pick up the pieces and reassure me that everything will be okay.

CHAPTER 1

QUANTITATIVE PREDICTIONS IN PHYSICAL ORGANIC CHEMISTRY

Introduction

Organic chemistry is founded in the identification of patterns in chemical behavior. The field has been propelled by a desire to precisely understand these observations, identify the foundational principles governing chemical behavior, and combine this knowledge in order to control the synthesis of organic molecules. Thus, discerning the mechanism of organic transformations informs and furthers reaction development.

As early as 1868, Crum-Brown and Fraser postulated that a chemical's (C) influence on a biological system's measured physiological response (θ) could be described as a mathematical function (f) (Eq. 1.1).¹ That is, changes to chemical structure manifest as changes in physiological responses. From the perspective of catalysis, it is conceivable that a similar relationship may be developed to describe the connection between molecular features, such as steric, electronic, and hydrophobic effects, and the outcomes of catalytic reactions, e.g., site-selectivity, enantioselectivity, turnover number, rate (Eq. 1.2). Ideally, describing chemical reactions in this quantitative manner would significantly augment mechanistic understanding and enable the precise formulation of substrates and catalysts to achieve desired reaction outcomes.

$$\theta = f(C) \quad \text{Eq. 1.1}$$

$$\text{reaction outcomes} = f(\text{molecular features}) \quad \text{Eq. 1.2}$$

Hammett and the Development of LFER

This idealized mathematical construct began to become a reality in the 1930s when Hammett pioneered the development of linear free-energy relationships (LFER) in the context of benzoic acid ionization.^{2,3} He postulated that the electronic effects exerted by substituents on arenes could be quantitatively described. Furthermore, a constant could be determined for each arene substituent that defines the substituent's electronic properties and that is not dependent on the specific reaction from which the constant was derived. Hammett had deduced that the log of equilibrium constants, $\log(K_{eq})$, for two distinct reactions of variously substituted arenes could be equated to each other with the addition of a correction factor (σ), which would describe the electronic impact of the substituent differences between the arene substrates. Mathematical representation of this idea, and the pattern after which LFERs are now constructed, is given in Eq. 1.3.

$$\log(K_x) = \log(K_{ref}) + \sigma \quad \text{Eq. 1.3}$$

To bring this theory to fruition, it was first necessary to derive values for the correction factor and substituent constant, σ , in Eq. 1.3. This was achieved by comparing equilibrium constants of ionization for substituted benzoic acids, K_x , to the ionization equilibrium constant of unsubstituted benzoic acid (K_{ref}), which was designated the reference reaction (Figure 1.1). Simply solving Eq. 1.3 for σ afforded a value representative

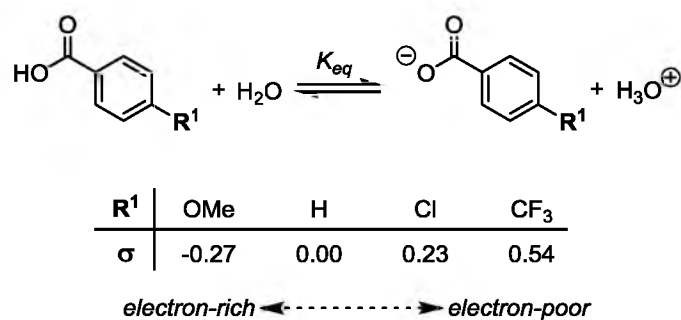


Figure 1.1. Derivation of Hammett σ values. Substituted benzoic acid ionization reaction, which was used to establish values representative of the electronic effects that substituents impart on arenes.

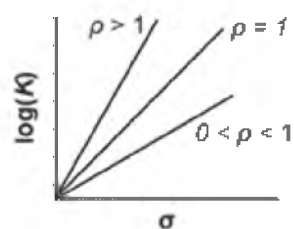
of the electronic effect exerted by the arene substituent on the ionization reaction.

From Eq. 1.3, a relationship is identified that allows for equating the σ value to the differential logs of the equilibrium constants (Eq. 1.4). Addition of the coefficient ρ to this relationship allows the equation to be applied to different reactions of arenes, accounting for the variation in the magnitude of substituents' electronic effects, where the relative influence of these effects is maintained.

$$\log(K_x/K_{ref}) = \rho\sigma \quad \text{Eq. 1.4}$$

The linear nature of the relationship in Eq. 1.4 enables its facile graphing and visual interpretation (Figure 1.2). From this mathematical model of a reaction, significant mechanistic information is gleaned. The equation's slope, ρ , defines 1) the sensitivity of the evaluated reaction to Hammett σ -like changes and 2) the nature of the charge build-up in the transition state. For instance, ρ values greater than 1 indicate that the reaction is more sensitive to the electronic influences of substituents than the reaction from which the σ constants were derived, i.e., benzoic acid ionization. With a $\rho > 1$, reaction rates increase with increasingly electron-withdrawing arene substituents. This signifies that negative charge builds up in the transition state and, when stabilized by electron-withdrawing groups, enables rate enhancement through a reduction in transition state energy.

Conversely, $\rho < 0$ indicates that positive charge develops in the transition state, which is stabilized by electron-donating groups. Regarding the interpretation of the reaction's sensitivity to electronic influences, the absolute value of ρ is considered. ρ with an absolute value between $0 < \rho < 1$ indicates that the reaction evaluated is less sensitive



	$\rho > 1$	$\rho = 1$	$0 < \rho < 1$	$\rho < 0$	$\rho = 0$
reaction's sensitivity to substituent-induced electronic effects relative to benzoic acid ionization	more	equal	less	see text	not sensitive
transition state charge build-up	neg.	neg.	neg.	pos.	no build-up

Figure 1.2. Interpreting the plot of the log of reaction rates versus σ values.

to electronic perturbation than benzoic acid ionization. As above, $|\rho > 1|$ denotes that the reaction is more sensitive to the effects of electronic change.

Extending LFER to Asymmetric Catalysis via the Curtin-Hammett Principle

While numerous applications of Hammett σ values have been demonstrated to yield valuable mechanistic insight for studying relative reaction rates via LFER, a subtle variation on this treatment is the analysis of product selectivity in catalytic reactions. This extension is made by first considering that catalytic processes are often considered to be a Curtin-Hammett, kinetically controlled process (Figure 1.3).⁴ A Curtin-Hammett scenario in asymmetric catalysis is defined by rapid equilibration between two diastereomeric complexes (**A** and **B**, Figure 1.3), one of which has a lower free-energy of activation barrier (**A**[‡]), leading to a predominance of the corresponding enantiomer (**A**_{Pat}). Thus, for systems where there is a greater energy difference between the two diastereomeric transition states ($\Delta\Delta G^\ddagger$)—a high energetic barrier reducing the probability of one of the enantiomer-forming reaction pathways—greater enantioselectivity is observed.

As LFER analysis is the correlation between σ values and the logarithm of relative rate data, selectivity ratios, i.e., relative rates of isomer formation, can also be correlated to σ values. The application of LFER analysis to selectivity ratios is understood through consideration of Curtin-Hammett conditions (Figure 1.3). Enantioselective catalytic reactions governed by the Curtin-Hammett kinetic scenario are characterized by rapid equilibration between two catalyst-substrate diastereomeric complexes (**A** and **B**, Figure 1.3) and relatively slower reaction rates (k_A and k_B) that lead to enantiomeric products. Thus, the enantiomeric excess of one enantiomer relative to the other is a function only of

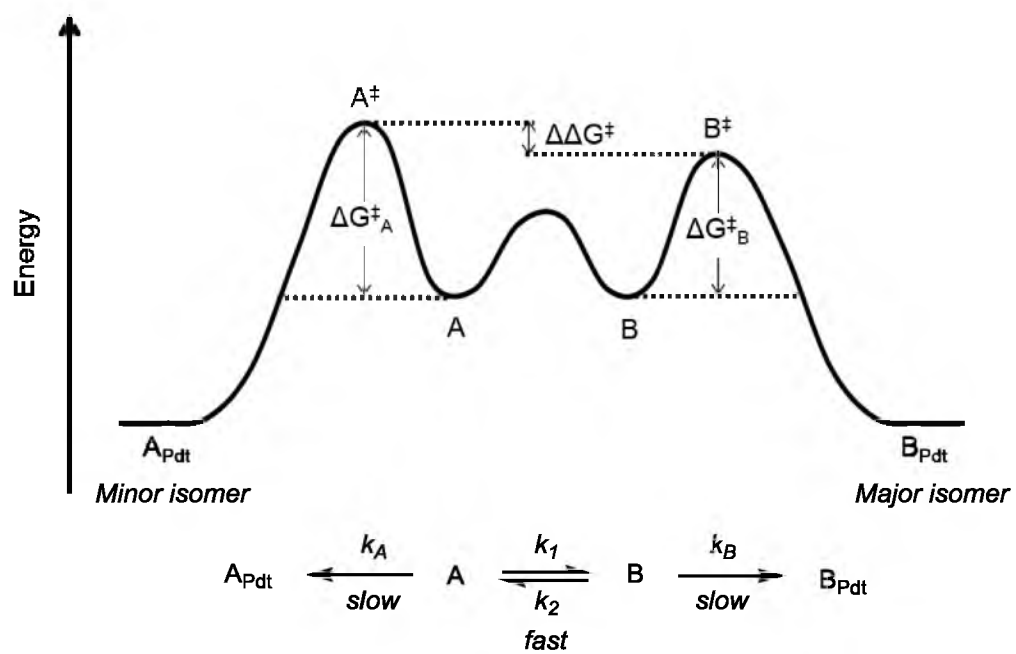


Figure 1.3. Representation of the energy profile and kinetic necessities for Curtin-Hammett reaction dynamics.

the differential Gibbs free energy of activation of the rate-limiting step. Eq. 1.5, relating differential Gibbs free energy to concentrations of enantiomers, is derived by first forming the rate laws for production of \mathbf{A}_{Pdt} and \mathbf{B}_{Pdt} , as given in Eq. 1.6 and Eq. 1.7, respectively.

The quotient of Eq. 1.6 and Eq. 1.7 and expansion of the changes in product concentration ($d[\mathbf{A}_{\text{Pdt}}]$, $d[\mathbf{B}_{\text{Pdt}}]$) yields Eq. 1.8. The left side of this equation reduces to that seen in Eq. 1.9, as there is no product observed at $t = 0$. As \mathbf{A} and \mathbf{B} are in rapid equilibrium, their relative concentration is a constant (K_{eq}) and equates to the Gibbs free energy of their interconversion. In the example given (Figure 1.3), there is no energetic difference between \mathbf{A} and \mathbf{B} (ΔG_{AB}), and so their relative concentration is reduced to one according to Eq. 1.10. Substituting Eq. 1.10 into Eq. 1.8 results in Eq. 1.9. Inserting the relationship in Eq. 1.11 into Eq. 1.9 yields Eq. 1.12, which can be converted to Eq. 1.5 by performing the natural logarithm (\ln) of Eq. 1.12 and rearranging the relationship. With the demonstrated link between the concentration of enantiomeric products and their relative rates of formation, the derived $\Delta\Delta G^\ddagger$ equation (Eq. 1.5) can be appropriately related to LFER parameters.

$$\Delta\Delta G^\ddagger = -RT\ln([A]/[B]) \quad \text{Eq. 1.5}$$

$$d[\mathbf{A}_{\text{Pdt}}]/dt = k_A[\mathbf{A}] \quad \text{Eq. 1.6}$$

$$d[\mathbf{B}_{\text{Pdt}}]/dt = k_B[\mathbf{B}] \quad \text{Eq. 1.7}$$

$$([\mathbf{A}_{\text{Pdt}}]_t - [\mathbf{A}_{\text{Pdt}}]_{t=0})/([\mathbf{B}_{\text{Pdt}}]_t - [\mathbf{B}_{\text{Pdt}}]_{t=0}) = (k_1/k_2)([A]/[B]) \quad \text{Eq. 1.8}$$

$$[\mathbf{A}_{\text{Pdt}}]/[\mathbf{B}_{\text{Pdt}}] = (k_A/k_B) \quad \text{Eq. 1.9}$$

$$\Delta G_{AB} = 0 \quad \therefore e^{-\Delta G_{AB}/RT} = K_{eq} = 1 \quad \text{Eq. 1.10}$$

$$e^{-\Delta G^\ddagger/RT} = k \quad \text{Eq. 1.11}$$

$$[\mathbf{A}_{\text{Pdt}}]/[\mathbf{B}_{\text{Pdt}}] = (e^{-\Delta G^\ddagger_A/RT})/(e^{-\Delta G^\ddagger_B/RT}) \quad \text{Eq. 1.12}$$

Hammett σ LFER and Mn(salen)-Catalyzed
Asymmetric Epoxidation

An effective illustration of the mechanistic insight that LFER can lend to enantioselective reactions comes from Jacobsen and coworkers' (salen)Mn(III)-catalyzed asymmetric epoxidation (Figure 1.4a).^{5,6} In this system, the salen's arene moiety provides an apt conduit through which electronic effects may be relayed from the ligand to the manganese, altering the complex's reactivity and selectivity profiles. The effects of the complex's X^1 substituents were evaluated by synthesizing a series of electron-rich ($X^1 = \text{OMe}$) to electron-poor ($X^1 = \text{NO}_2$) arenes. The logarithm of enantiomeric ratios (er) resulting from the corresponding reactions of these complexes were plotted in relation to the substituents' Hammett σ values. The line best fitting these data points is given in Figure 1.4b, where the absolute value of ρ (1.37, where ρ is -1.37) indicates that the transformation is more responsive to the electronic changes in the arene than is the ionization of benzoic acid, providing a reference point for sensitivity.

The negative sign of ρ must be considered in mechanistic context in order to infer its meaning. Enantioselectivity is determined when the Mn(V) oxidant accepts a single electron from the substrate's alkenyl functionality and is reduced to Mn(IV). At the metal center in the transition state, positive charge is decreasing; alternatively, negative charge is increasing. If the negative ρ were interpreted as prescribed in the context of benzoic acid ionization (Figure 1.2), then it would be expected that electron-withdrawing groups would stabilize the transition state and increase the reaction rate. However, for LFER's of enantioselectivity, analysis is not simply a comparison of reaction rates relative to a standard, but each $\Delta\Delta G^\ddagger$ represents a relative rate itself, making the interpretation of ρ less apparent.

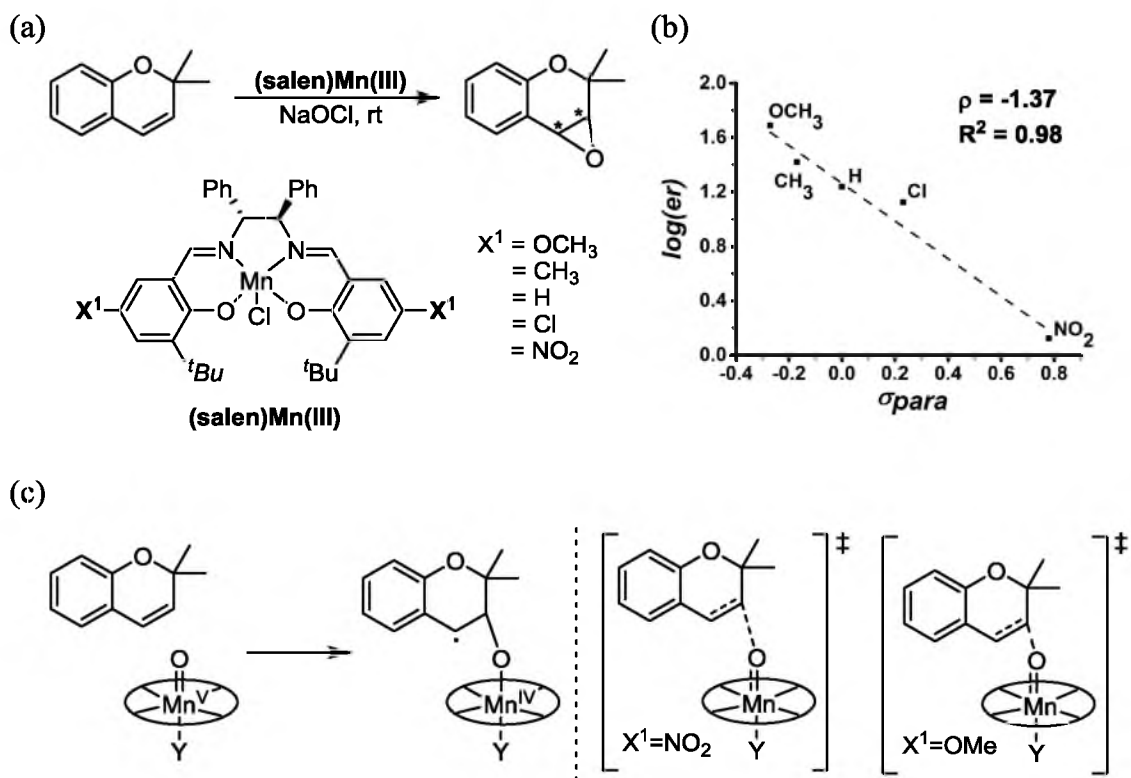


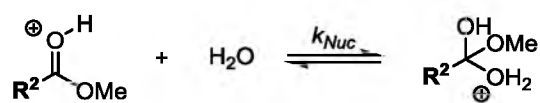
Figure 1.4. Linear free-energy relationship analysis of (salen)Mn(III)-catalyzed asymmetric epoxidation. (a) Reaction scheme. (b) Hammett σ LFER plot. (c) Reaction's enantio-determining step and postulated transition state structures. Support for these structures and the origin of enantioselection comes from LFER analysis and the Hammond postulate.

As electron-donating X^1 groups have the effect of enhancing enantioselectivity, despite the increase of manganese negative charge upon reduction in the enantio-determining step, it was considered that the opposition that electron-donation imposes on metal reduction engenders the requirement of a shorter distance between metal and alkene upon alkene oxidation. Presumably, in a more tightly packed transition state, the chiral catalyst complex can more precisely distinguish between enantiotopic alkene faces, enabling higher levels of asymmetric induction.

Conversely, electron-deficient manganese complexes become more reactive as the positive charge on manganese becomes further destabilized. In accordance with the Hammond postulate, increased reactivity would cause the transition state to be more reactant-like than product-like.⁷ With electron-transfer from the alkene to manganese occurring with a greater distance between these species, the chiral catalyst engages in a less ordered transition state, resulting in decreased precision of differentiation between enantiotopic faces.

Quantitating Steric Effects Using LFER

The ability of Hammett values to effectively describe the electronic effects of arene substitution prompts inquiry about other reaction features that may be similarly quantitatively described and analyzed via LFER. One of many such descriptor sets developed is the Taft/Charton parameter for steric bulk depiction.⁸⁻¹⁰ Taft initiated this description of steric bulk by measuring the rates of nucleophilic attack (k_{Nuc}) in the acid-catalyzed hydrolysis of variously R^2 -substituted methyl esters (Figure 1.5).^{11,12} Analogous to the derivation of Hammett values, this measure of steric bulk, termed E_S , is a calculation



R^2	H	Me	<i>i</i> Pr	<i>t</i> Bu
E_s	1.24	0.00	-0.47	-1.54

small ←-----→ *large*

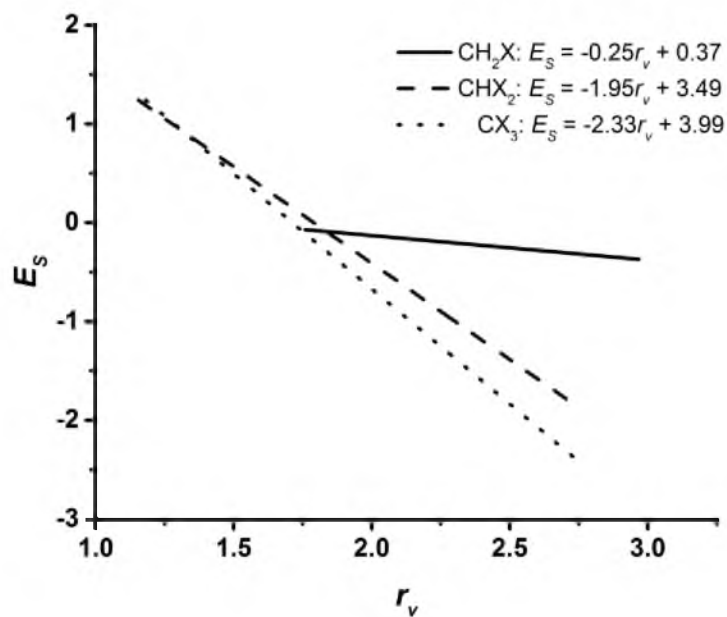
Figure 1.5. Depiction of the acid-catalyzed hydrolysis of methyl esters employed to measure the steric bulk of R^2 . The resultant steric descriptor, E_s , is a measure of hydrolysis rates relative to the hydrolysis of methyl acetate ($\text{R}^2 = \text{Me}$).

of the rate of hydrolysis relative to the rate when R² is methyl (Eq. 1.13).

$$\log(k_x/k_{Me}) = E_S \quad \text{Eq. 1.13}$$

In developing a measurement of steric bulk that can be generalized to describe steric influences in a variety of reactions, it is important that the measure describes only the desired steric feature and is not muddled by other contributions, such as electronic effects. The electronic influences of R² groups on the rate of hydrolysis was minimized to negligibility by measuring rates under acid-catalyzed conditions. In this scenario, the species immediately preceding and following hydrolysis are positively charged, and there is no net change in charge through the transition state. Indeed, the Hammett ρ value for the acid-catalyzed hydrolysis of *meta*- and *para*-substituted ethyl benzoates is essentially zero, indicating that no charge stabilization/destabilization is observed with varying arene substitution.¹¹

To further validate the claim that E_S values solely measure steric bulk, Charton used linear regression modelling to determine the contributions of σ_I , inductive effect; σ_R , resonance effect; and r_v , minimum van der Waals radius, on E_S (Eq. 1.14).¹³ Regression was performed on three symmetry-defined substituent sets: methylene (CH₂X), methine (CHX₂), and quaternary (CX₃) carbon substituents. Charton found that only one of the three terms—van der Waals radius, r_v —correlated to E_S values (Figure 1.6). Taft's values were, indeed, measuring an isolated steric effect. Charton furthered his examination of the relationship between relative rates of acid-catalyzed methyl ester hydrolysis and van der Waals radius by developing a new parameter, v , calculated according to Eq. 1.15.¹⁴ This



CH₂X	E_S	CHX₂	E_S	CX₃	E_S
CH ₂ CH ₃	-0.07	CHMe ₂	-0.47	CMe ₃	-1.54
CH ₂ OMe	-0.19	CHF ₂	-0.67	CF ₃	-1.16
CH ₂ F	-0.24	CHCl ₂	-1.54	CCl ₃	-2.06
CH ₂ Cl	-0.24	CHBr ₂	-1.86	CBr ₃	-2.43
CH ₂ Br	-0.27	H	1.24	Me	0.00
CH ₂ SMe	-0.34			H	1.24
CH ₂ I	-0.37				

Figure 1.6. Charton's correlation of symmetry-grouped substituents' Taft E_S values to van der Waals radii, r_v . Minimum van der Waals radii were used for substituents of the form CX_3 .

equation, which originated in the rates of acid-catalyzed methyl ester hydrolysis, allows the steric bulk of any substituent to be calculated.

$$E_S = \alpha\sigma_I + \beta\sigma_R + \psi r_v + h \quad \text{Eq. 1.14}$$

$$v_x = r_{vx} - r_{vH} \quad \text{Eq. 1.15}$$

Applying Charton v and Hammett σ to NHK Asymmetric Propargylation

Charton values have since been used in LFER analyses to investigate and identify the origin of selectivity in asymmetric catalytic reactions.¹⁵⁻¹⁹ An example of Charton analysis and a key extension of one-dimensional LFER comes from the work of Dr. Kaid Harper, a former graduate student in the Sigman group. Dr. Harper demonstrated the simultaneous modelling of electronic and steric effects in a Nozaki-Hiyama-Kishi (NHK) asymmetric propargylation of acetophenone using Hammett σ values and Charton v values (Figure 1.7).²⁰ In a quinoline-pyrrolidine-based ligand, two sites affecting changes in enantioselective propargylation were observed: **E**, modulating the electronic nature and, thus, coordination capacity of quinolone, and **S**, a site where steric changes impact enantioselection.

Once these sensitive features were identified, they were perturbed in a systematic manner. **E**, to be described by Hammett σ values, was assessed at three levels that span a range electronically compatible with the reaction's conditions: methoxy, hydrogen, and trifluoromethyl. Variation in the **S** dimension was accomplished by spanning a broad range of steric bulk, as quantitated by Charton v values: methyl, *tert*-butyl, and 3-ethyl pentyl (Figure 1.7a). Combinatorial analysis of both dimensions at three levels per descriptor

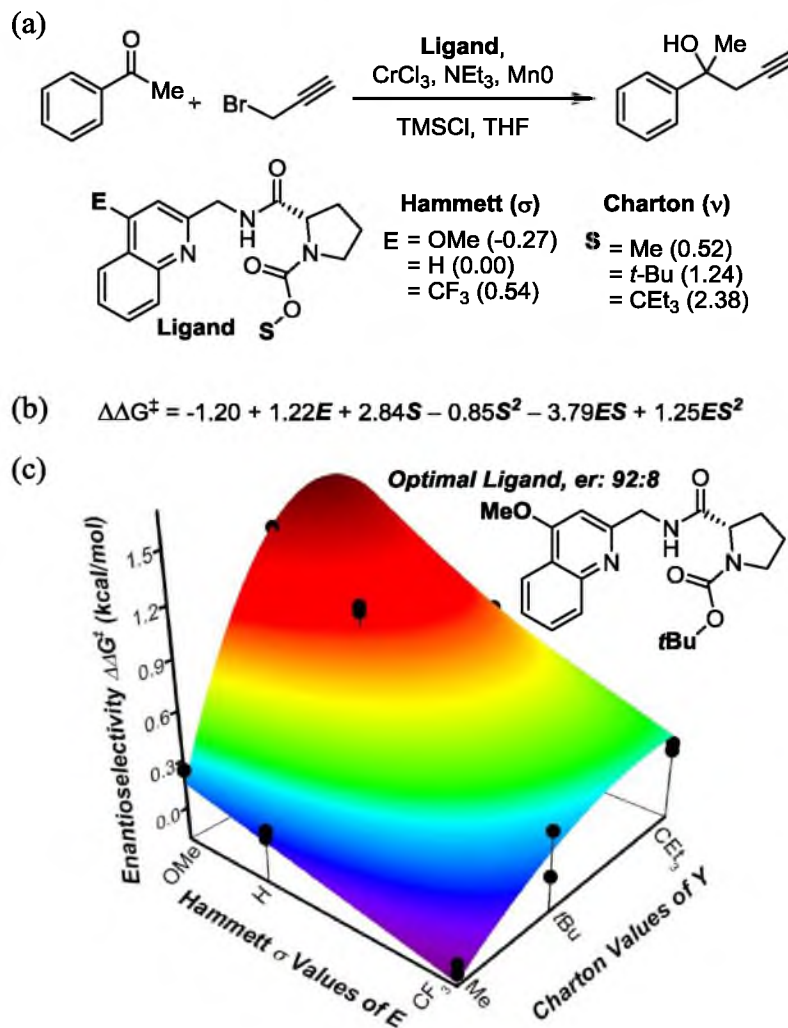


Figure 1.7. Multidimensional LFER analysis of NHK asymmetric propargylation of acetophenone. (a) NHK propargylation reaction scheme and perturbations to ligand steric (**S**) and electronic (**E**) features. (b) LFER model describing enantioselectivity of propargylation. (c) Graphical representation of LFER model and the model-dictated optimal ligand.

corresponds to a nine-membered library of catalysts. This library was assessed under the NHK propargylation conditions to afford enantioselectivities for each catalyst's reaction with acetophenone.

From this data set, regression modelling was performed to afford the model in Figure 1.7b, which depicts the synergistic impact that steric and electronic effects have on enantioselectivity ($\Delta\Delta G^\ddagger$). This equation was subsequently optimized to identify the synthetically accessible combination of ligand substituents at **E** (methoxy) and **S** (*tert*-butyl) that yield the highest enantioselectivity (Figure 1.7c).

Broadening the Scope of Free-Energy Relationships

While additional applications of LFER in the context of asymmetric catalysis have been demonstrated,^{15,16} in the course of numerous investigations of differential transition state free-energy as related to selectivity, the Sigman group has identified limitations to the application of the classical Hammett and Charton LFER parameters. In Chapter 2, the descriptive capabilities of Charton values are discussed and alternative steric parameters are introduced. In this example, a peptide-catalyzed desymmetrization of bisphenols is examined, and shortcomings of Charton values are highlighted in the demonstration of their inability to globally describe the observed trends in enantioselective bisphenol acylation.^{17,21} This failure proved to be an important turning point in the types of parameters that Sigman and colleagues used to develop free-energy relationships. Namely, the use of nonclassical (not relative rate-derived) LFER parameters began to be explored. Chapters 2–4 exemplify the selection and application of a diverse set of novel parameters for free-energy relationship mathematical modelling.

Infrared (IR) vibrations are one such parameter that has significantly expanded the number of reactions where steric and electronic effects can be mathematically described. While Hammett and Charton values were derived to measure isolated electronic and steric effects, respectively, the reactions characterizing modern synthetic organic chemistry often involve multiple synergistic effects, which cannot be independently assessed. Of note, Hammett values are only used for *meta*- and *para*-substituted arenes because *ortho*-substituted benzoic acids influence ionization rates through not only electronic effects but also steric effects.² Alternatively, within IR vibrational frequency and intensity are integrated steric and electronic features, enabling this parameter type to be widely applied to investigate reaction systems with entwined steric and electronic influences. In Chapters 2–4, the use of IR vibrations to describe a variety of reactions is extensively discussed and demonstrated.

Quantitative Structure-Activity Relationships

Relating multiple nonclassical LFER parameters to experimentally measured reaction outcomes is reminiscent of quantitative structure-activity relationship (QSAR) studies.²² The development of QSAR models involves relating a measured, often physiological, response to various chemical descriptors that are relevant to the investigated process. QSAR models have been useful tools for probing the nature of enzyme active sites, barriers to molecule absorption, toxicity effects of chemical species, metabolism, and other processes and interactions that are difficult to directly evaluate.²³ Hansch pioneered this now widely applied method when he related Hammett σ values and partition coefficients of molecules to the molecules' ability to induce plant growth.²⁴ From this

model, inferences could be made about the properties of the chemical species that allow its permeation to the site of its biological activity, while simultaneously considering the influence of Hammett electronic effects.

To develop descriptive models able to represent the complex interactions present in biological systems, many experimental data points are first gathered where structural changes to a molecule affect differences in measurable system outcomes. Second, a large set of potentially relevant parameters is collected, often using QSAR software packages, which contain many tabulated parameters or the capacity to compute parameters that are specific to a particular molecule.²⁵ With data and descriptor sets in hand, various modelling algorithms can be performed, e.g., linear regression, partial least squares regression, multivariate regression, and neural networks. These algorithms afford models that are validated via cross validation methods such as leave-*k*-out (where developed models are fit with new coefficients in the absence of *k* data points) and external validation (where the result of subjecting a new molecule to the system is predicted and compared to experimental data to measure the agreement between the two values).²⁶

While there are a few published examples of multivariate, QSAR-type modelling of asymmetric catalytic reactions²⁷⁻³³ (and a review of these examples was recently published²²), the Sigman group developed an alternative approach where models are developed using much smaller parameter sets and fewer data points. This simplification offers several advantages, not inconsequential of which is the mechanistic insight that can be drawn from models with few descriptive terms.

Development of Multidimensional Free-Energy Relationship Models

To permit robust multidimensional models to be developed from the fewest number of data points, two specifications must be met. First, information sufficient to intelligently form a mechanistic hypothesis of the origin of enantioselection is required. Second, Design of Experiments (DoE) logic is used to determine the most efficient manner of evenly perturbing the reaction's features that are hypothesized to modulate enantioselectivity. Various applications and failures of these precepts, as applied to enantio- and site-selective reactions, are explored in Chapters 2–4.

The selectivities resulting from the DoE-outlined experiments and the corresponding parameters that presumably describe aspects that engender selectivity are termed the training set. This training set is subjected to MATLAB's stepwise linear regression algorithms.³⁴ Stepwise regression is a method for identifying which parameters amongst those in the training set are statistically significant predictors of the observed trends in reaction outcomes. The selection process is performed by assessing the *p*-value for each parameter, i.e., the percent error that a parameter is determined to be a significant predictor of reaction outcomes when it is actually not significant. Through stepwise regression, various combinations of the originally hypothesized descriptors are assessed. The models resulting from this analysis are assessed for their validity in the same manner as described for QSAR models: leave-*k*-out (where *k* is one) cross validation and external validation.

Models determined to be robust are considered for their mechanistic value. Analogous to the mechanistic interpretations that can be gleaned from Hammett LFER, model terms that are capable of identifying trends in selectivity are presumed to be

describing aspects of the reaction's selectivity-determining steps. In the following chapters investigating model development, various means are explored to interpret the physical interactions that a parameter mathematically represents. From such analyses, systems are optimized to afford desired selectivity levels.

When developed models fail the tests of robustness, the process described (and outlined in Figure 1.8) must be iterated, reassessing the hypothesized origin of selectivity, the set of putatively descriptive parameters, and, if necessary, performing additional experiments to appropriately sample the refined experimental space. This process continues, refining mechanistic hypotheses until a robust, predictive model is afforded.

This model development process resulted through the successes and failures of the models described herein. What follows is a narrative presented in the context of three case studies describing how and why each step of this model development is necessary. Chapter 2 focuses on the implications of incorrect hypotheses guiding training set development and how this is remedied through iterative hypothesis refinement. Beginning in Chapter 2 and extended in Chapter 3, considerations for exploring novel reaction parameters are set forth. Through the use of nonclassical LFER parameters, models describing selectivity trends are developed, which would have been unattainable in the absence of a broadened perspective regarding suitable parameters for model development. Application of Design of Experiments precepts is initiated in Chapter 2 and is progressively refined through Chapter 4, where a rigorous application of DoE concepts is put forth for the construction of scope libraries. In Chapter 5, the outlook and further applications of these modelling concepts are examined.

Through each case-study presented, various aspects of successful modelling are

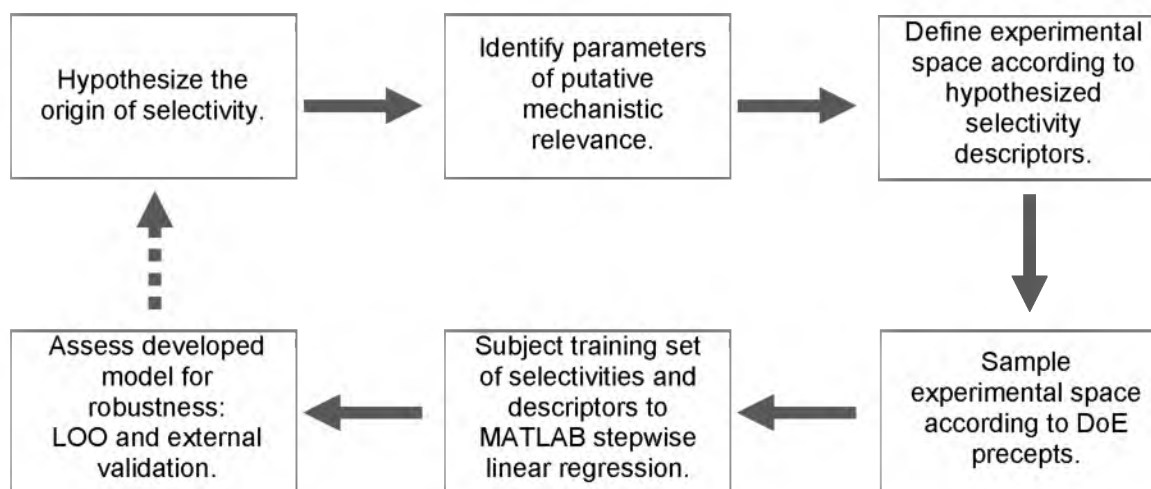


Figure 1.8. Flow chart describing the model development process.

explored and developed. What results is a structure for model development, with guidelines defining the construction of efficient, effective mathematical equations. These constructs provide a vantage point for gleaning mechanistic information about selectivity determination and guide the further development and applications of both the reactions studied and the process of mathematical model development.

References

1. Brown, A. C.; Fraser, T. R. On the Connection Between Chemical Constitution and Physiological Action; With Special Reference to the Physiological Action of the Salts of the Ammonium Bases Derived from Strychnia, Brucia, Thebaia, Codeia, Morphia, and Nicotia. *J. Anat. Physiol.* **1868**, *2*, 224–42.
2. Hammett, L. P. Some Relations between Reaction Rates and Equilibrium Constants. *Chem. Rev.* **1935**, *17*, 125–136.
3. Hammett, L. P. The Effect of Structure upon the Reactions of Organic Compounds. Benzene Derivatives. *J. Am. Chem. Soc.* **1937**, *59*, 96–103.
4. Halpern, J. Mechanism and Stereoselectivity of Asymmetric Hydrogenation. *Science* **1982**, *217*, 401–407.
5. Jacobsen, E. N.; Zhang, W.; Guler, M. L. Electronic Tuning of Asymmetric Catalysts. *J. Am. Chem. Soc.* **1991**, *113*, 6703–6704.
6. Palucki, M.; Finney, N. S.; Pospisil, P. J.; Güler, M. L.; Ishida, T.; Jacobsen, E. N. The Mechanistic Basis for Electronic Effects on Enantioselectivity in the (salen)Mn(III)-Catalyzed Epoxidation Reaction. *J. Am. Chem. Soc.* **1998**, *120*, 948–954.
7. Hammond, G. S. A Correlation of Reaction Rates. *J. Am. Chem. Soc.* **1955**, *77*, 334–338.
8. Wells, P. R. Linear Free Energy Relationships. *Chem. Rev.* **1963**, *63*, 171–219.
9. Shorter, J. The Separation of Polar, Steric, and Resonance Effects in Organic Reactions by the Use of Linear Free Energy Relationships. *Chem. Soc. Rev.* **1970**, *24*, 433–453.
10. Hansch, C.; Leo, A.; Taft, R. W. A Survey of Hammett Substituent Constants and Resonance and Field Parameters. *Chem. Rev.* **1991**, *91*, 165–195.
11. Taft, R. W. Polar and Steric Substituent Constants for Aliphatic and o-Benzoate Groups from Rates of Esterification and Hydrolysis of Esters. *J. Am. Chem. Soc.* **1952**, *74*, 3120–3128.
12. Taft, R. W. Linear Steric Energy Relationships. *J. Am. Chem. Soc.* **1953**, *75*, 4538–4539.
13. Charton, M. Nature of the Ortho Effect. II. Composition of the Taft Steric Parameters. *J. Am. Chem. Soc.* **1969**, *91*, 615–618.
14. Charton, M. Steric Effects. I. Esterification and Acid-Catalyzed Hydrolysis of Esters. *J. Am. Chem. Soc.* **1975**, *97*, 1552–1556.

15. Bess, E. N.; Sigman, M. S., Linear Free Energy Relationships (LFERs) in Asymmetric Catalysis. In *Asymmetric Synthesis II: More Methods and Applications*, Christmann, M.; Bräse, S., Eds. Wiley-VCH Verlag GmbH & Co. KGaA: Weinheim, 2012.
16. Harper, K. C.; Sigman, M. S. Using Physical Organic Parameters To Correlate Asymmetric Catalyst Performance. *J. Org. Chem.* **2013**, *78*, 2813–2818.
17. Gustafson, J. L.; Sigman, M. S.; Miller, S. J. Linear Free-Energy Relationship Analysis of a Catalytic Desymmetrization Reaction of a Diarylmethane-bis(phenol). *Org. Lett.* **2010**, *12*, 2794–2797.
18. Sigman, M. S.; Miller, J. J. Examination of the Role of Taft-Type Steric Parameters in Asymmetric Catalysis. *J. Org. Chem.* **2009**, *74*, 7633–7643.
19. Miller, J. J.; Sigman, M. S. Quantitatively Correlating the Effect of Ligand-Substituent Size in Asymmetric Catalysis Using Linear Free Energy Relationships. *Angew. Chem. Int. Ed.* **2008**, *47*, 771–774.
20. Harper, K. C.; Sigman, M. S. Three-Dimensional Correlation of Steric and Electronic Free Energy Relationships Guides Asymmetric Propargylation. *Science* **2011**, *333*, 1875–1878.
21. Harper, K. C.; Bess, E. N.; Sigman, M. S. Multidimensional Steric Parameters in the Analysis of Asymmetric Catalytic Reactions. *Nat. Chem.* **2012**, *4*, 366–374.
22. Milo, A.; Sigman, M. S., Applying Mathematical Modeling to the Analysis of Catalytic Reaction Outcomes: A Historical Perspective. In *Seminars in Organic Synthesis: XXXIX “A. Corbella” International Summer School*, SCI: 2014; pp 15–35.
23. Hansch, C.; Leo, A., *Exploring QSAR: Fundamentals and Applications in Chemistry and Biology*. American Chemical Society: Washington, D.C., 1995.
24. Hansch, C.; Maloney, P. P.; Fujita, T.; Muir, R. M. Correlation of Biological Activity of Phenoxyacetic Acids with Hammett Substituent Constants and Partition Coefficients. *Nature* **1962**, *194*, 178–180.
25. Verma, J.; Khedkar, V. M.; Coutinho, E. C. 3D-QSAR in Drug Design—A Review. *Curr. Top. Med. Chem.* **2010**, *10*, 95–115.
26. Arlot, S.; Celisse, A. A Survey of Cross-Validation Procedures for Model Selection. *Statist. Surv.* **2010**, *4*, 40–79.
27. Denmark, S. E.; Gould, N. D.; Wolf, L. M. A Systematic Investigation of Quaternary Ammonium Ions as Asymmetric Phase-Transfer Catalysts. Synthesis of Catalyst Libraries and Evaluation of Catalyst Activity. *J. Org. Chem.* **2011**, *76*, 4260–4336.

28. Denmark, S. E.; Gould, N. D.; Wolf, L. M. A Systematic Investigation of Quaternary Ammonium Ions as Asymmetric Phase-Transfer Catalysts. Application of Quantitative Structure Activity/Selectivity Relationships. *J. Org. Chem.* **2011**, *76*, 4337–4357.
29. Kozlowski, M. C.; Dixon, S. L.; Panda, M.; Lauri, G. Quantum Mechanical Models Correlating Structure with Selectivity: Predicting the Enantioselectivity of β -Amino Alcohol Catalysts in Aldehyde Alkylation. *J. Am. Chem. Soc.* **2003**, *125*, 6614–6615.
30. Phuan, P.-W.; Ianni, J. C.; Kozlowski, M. C. Is the A-Ring of Sparteine Essential for High Enantioselectivity in the Asymmetric Lithiation–Substitution of N-Boc-pyrrolidine? *J. Am. Chem. Soc.* **2004**, *126*, 15473–15479.
31. Huang, J.; Ianni, J. C.; Antoline, J. E.; Hsung, R. P.; Kozlowski, M. C. De Novo Chiral Amino Alcohols in Catalyzing Asymmetric Additions to Aryl Aldehydes. *Org. Lett.* **2006**, *8*, 1565–1568.
32. Ianni, J. C.; Annamalai, V.; Phuan, P.-W.; Panda, M.; Kozlowski, M. C. A Priori Theoretical Prediction of Selectivity in Asymmetric Catalysis: Design of Chiral Catalysts by Using Quantum Molecular Interaction Fields. *Angew. Chem. Int. Ed.* **2006**, *45*, 5502–5505.
33. Kozlowski, M. C.; Ianni, J. C. Quantum Molecular Interaction Field Models of Substrate Enantioselection in Asymmetric Processes. *J. Mol. Catal. A: Chem.* **2010**, *324*, 141–145.
34. MATLAB, *version 8.1.0.604 (R2013a)*. The MathWorks, Inc.: Natick, MA, 2013.

CHAPTER 2

IDENTIFYING MECHANISTICALLY RELEVANT CHEMICAL DESCRIPTORS FOR LINEAR REGRESSION MODELLING*

Introduction

Behind every reaction lies fundamental chemical principles that govern the process and its outcomes. While the combination of such principles and the magnitude of their importance is unique for each reaction, Chapter 1 reviewed how the identification and quantification of some of these effects has been achieved through linear free-energy relationship (LFER) analysis. Despite the successes and advancements in LFER, there are still many instances in which the parameters required to adequately describe a chemical transformation are lacking. In the Sigman group, we have used these apparent outliers as opportunities to further understand the capabilities and limitations of available chemical descriptors. Shortcomings in classical LFER-type parameters have also led us to explore the application of descriptors novel to LFER analysis, significantly expanding the types of processes that can be quantitatively modelled and investigated via linear regression analysis.

* This chapter is based on the author's work that has been reported in three publications,^{1,7,49} some content of which is herein reproduced with permission from Bess, E. N.; Sigman, M. S. Distinctive *Meta*-Directing Group Effect for Iridium-Catalyzed 1,1-Diarylalkene Enantioselective Hydrogenation. *Org. Lett.* **2013**, *15*, 646–649. Copyright 2013 American Chemical Society.

In this chapter, two case studies are presented where limitations in a descriptor set, manifested as data outliers, led to new parameters for free-energy relationship model development. The results discussed in this chapter demonstrate the iterative process of effective model development and present a template for further expanding the parameters that can be used for mechanistic investigations.

Selecting Suitable Chemical Descriptors

Uncovering underlying relationships in data relies on the selection of parameters that accurately describe changes imposed on a system. This critical concept was highlighted while exploring a peptide-catalyzed asymmetric acylation of bisphenols (Figure 2.1a).¹ Gustafson, Sigman, and Miller had identified a linear free-energy relationship² between Charton descriptors (derived from substituents' minimum van der Waals' radii) of R and the differential free-energy of enantioselection, $\Delta\Delta G^\ddagger$ (Figure 2.1b), for a set of sterically varied substituents.³ However, upon expanding the set of R groups examined, the identified model failed to provide a correlation between predicted and measured enantioselectivities (red data points, Figure 2.1b). Two possible conclusions that may be drawn from this failed correlation were 1) not all R-substituted bisphenols undergo the peptide-catalyzed reaction via the same mechanistic pathway, causing the break in the LFER plot, or 2) Charton values do not adequately describe the diversity in the R groups investigated.

Intrigued by the latter of these scenarios, comparisons were drawn between the two substituent types, i.e., the R groups modelled according to Charton values and the outliers that could not be modelled. It is noted that the R groups well-described by Charton values

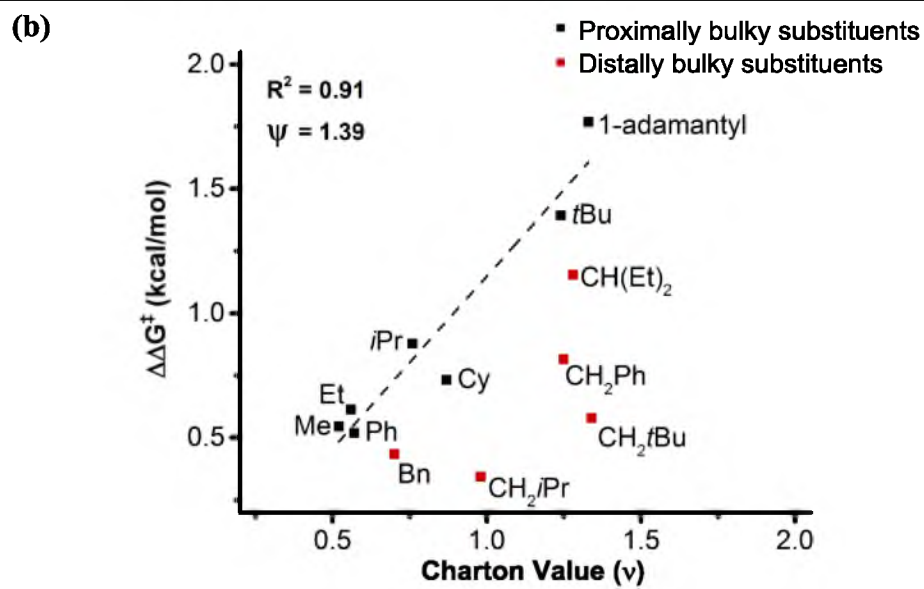
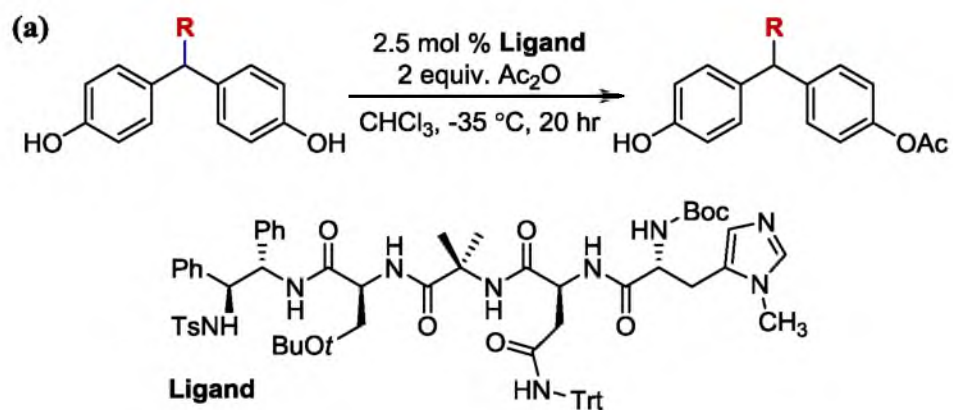


Figure 2.1. Peptide-catalyzed bisphenol desymmetrization. (a) Reaction scheme. (b) Charton LFER presented as ■. Distally bulky outliers are presented as ■.

bear their steric bulk proximal to the bisphenol methine, while the outliers bear their steric bulk more distal from this position. To account for this discrepancy, it was necessary to apply a descriptor capable of capturing the differences in spatial distribution of steric bulk.

Exploring alternative steric descriptors led to a relatively obscure steric parameter: Sterimol values. The Sterimol system (Figure 2.2a) describes a chemical group's steric size in a multidimensional manner: B_1 (minimum radius), B_5 (maximum radius), L (length).⁴⁻⁶ Detailing sterics in this way permitted a relationship to be identified (Figure 2.2b) that effectively relates B_1 and L to enantioselectivity for the entire set of R groups evaluated. This correlation demonstrates the effectiveness of the Sterimol parameter system for differentiating between steric bulk that resides proximal or distal to the prostereogenic methine. Additionally, this Sterimol-derived model points to an important lesson: the failure of the initial Charton correlation was due to Charton values' inadequacy for describing R-group variation. The reaction is likely invoking the same intermolecular interactions and following the same mechanistic path for all R-group-varied bisphenols that were evaluated.

Encouraged by this successful analysis, which was enabled by the unique application of descriptive parameters, an analogous investigation of the challenging iridium-catalyzed asymmetric hydrogenation of 1,1-diarylalkenes was envisioned.⁷ For several years, we and others have taken a keen interest in accessing the biologically relevant 1,1-diarylmethine scaffold.⁸⁻¹⁴ Although several methods exist for effectively accessing these molecules,¹⁵⁻¹⁹ approaches to their enantioselective synthesis have been limited.^{16,20-27} Notably, Jarvo and coworkers have developed a nickel-catalyzed stereospecific cross-coupling reaction, whereby enantiomerically enriched 1,1-diarylethers

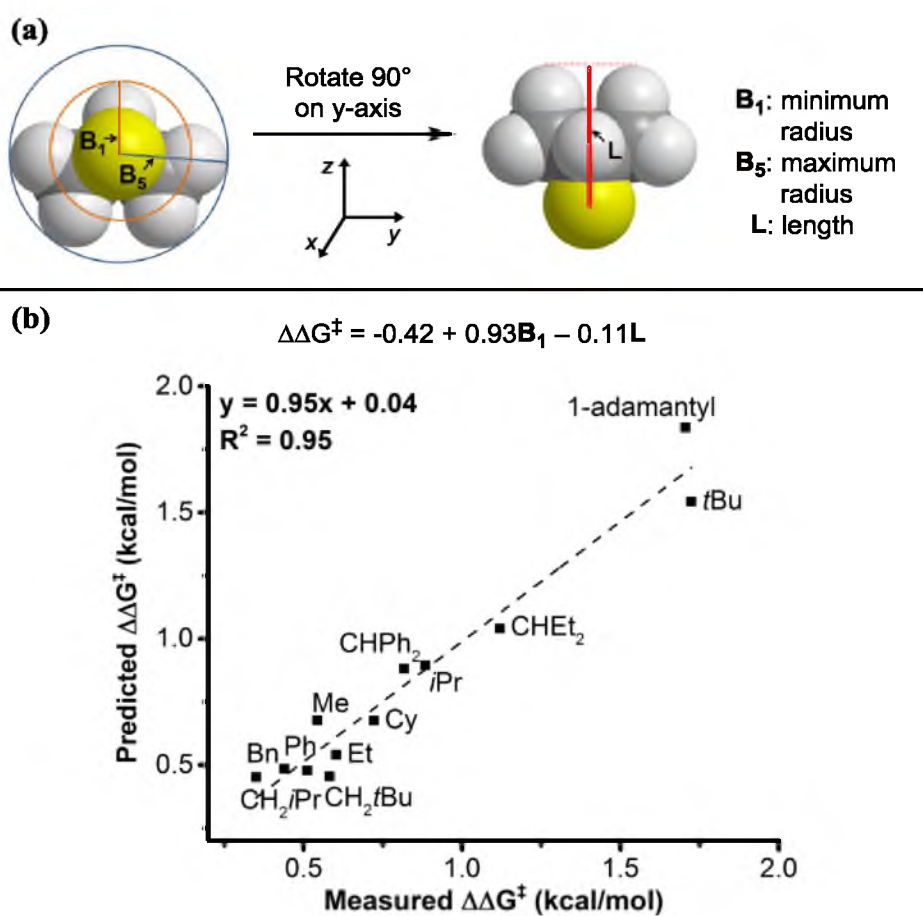


Figure 2.2. Sterimol analysis of peptide-catalyzed bisphenol desymmetrization reaction. (a) Sterimol values, depicted for an *isopropyl* substituent. (b) Free-energy analysis using Sterimol parameters.

undergo inversion of configuration to afford similarly enriched 1,1-diarylmethines.^{20,21}

Another attractive approach was reported by Carreira and coworkers where enantiomerically enriched β,β -diarylpropionaldehydes are converted to 1,1-diarylmethines using a stereoretentive rhodium-catalyzed decarbonylation protocol.²³ A complementary method for accessing this important pharmacophore was envisioned wherein the stereocenter is set in the key bond forming event. Specifically, an enantioselective hydrogenation of 1,1-diarylalkenes was desired, as this approach would be operationally simple and the substrates are easily accessed. Embarking upon enantioselective hydrogenation of this substrate class also represents an important challenge in the hydrogenation literature. Few examples of high enantioselectivity have been reported for the hydrogenation of 1,1-diarylalkenes.

In general, rhodium-, ruthenium-, and iridium-catalyzed asymmetric hydrogenation reactions can be divided into two broad classes: those that require coordination of a Lewis basic functional group in order to achieve high enantioselectivity and those that require no such coordination that is auxiliary to the alkene. Of these two classes, ruthenium- and rhodium-catalyzed hydrogenations typically fall into the former category, and iridium-catalyzed hydrogenation is associated with the latter.²⁸⁻³⁰ When considering the asymmetric hydrogenation of 1,1-diarylalkenes, the auxiliary coordination requirement of rhodium- and ruthenium-catalyzed systems constrains the potential substrate scope to those with Lewis basic groups at the *ortho* position on the aryl ring, which has been accomplished using oxygen directing groups.²² While this coordination constraint does not exist for iridium-catalyzed systems, a steric bias at an *ortho*-position has been required to achieve excellent enantioselectivity in the hydrogenation of 1,1-diarylalkenes. In the absence of

such bulk proximal to the prochiral site, enantioselectivity dramatically erodes, with the best reported enantiomeric ratio (er) of 82.5:17.5.^{31,32}

With Rh- and Ru-based catalytic hydrogenations requiring a coordinating group near the alkene in order to achieve high enantiomeric excess (ee), this reaction class suffered for 30 years from the inability to asymmetrically hydrogenate unfunctionalized alkenes. In the late 1990s, Pfaltz made significant progress towards alleviating this deficiency when he demonstrated iridium (Ir)-phosphorous/nitrogen (P/N) ligand complexes capable of high degrees of facial discrimination in the reaction of unfunctionalized olefins (Figure 2.3a).³³ P/N ligands have since emerged as a privileged ligand class, enabling these Ir-catalyzed hydrogenations to proceed with high levels of enantioselectivity.^{29,31,34,35}

Within the realm of unfunctionalized-alkene hydrogenation, terminal alkenes represent a particularly challenging substrate class due to the potential ease with which alkene substituents may exchange positions in the chiral environment (Figure 2.3b).³¹ This is in stark contrast to more obviously confined coordination environments of tri- and tetra-substituted alkenes (Figure 2.3c).³⁶ Despite this complication, important advances have been made for the hydrogenation of this substrate class. Specifically, terminal alkenes with substitution patterns of 1,1-aryl-alkyl and 1,1-diaryl (with proximal aryl ring substitution) have been hydrogenated highly enantioselectively (Figures 2.4a, b).³² Conversely, a related substrate scaffold that has seen only moderate ee's is the 1,1-diaryl alkene with distal aryl-ring substitution. To date, Andersson and coworkers have reported the highest ee for this substrate class: 65% ee as given in Figure 2.4c.³²

Although this ee is modest, it is quite remarkable when considered in context. The

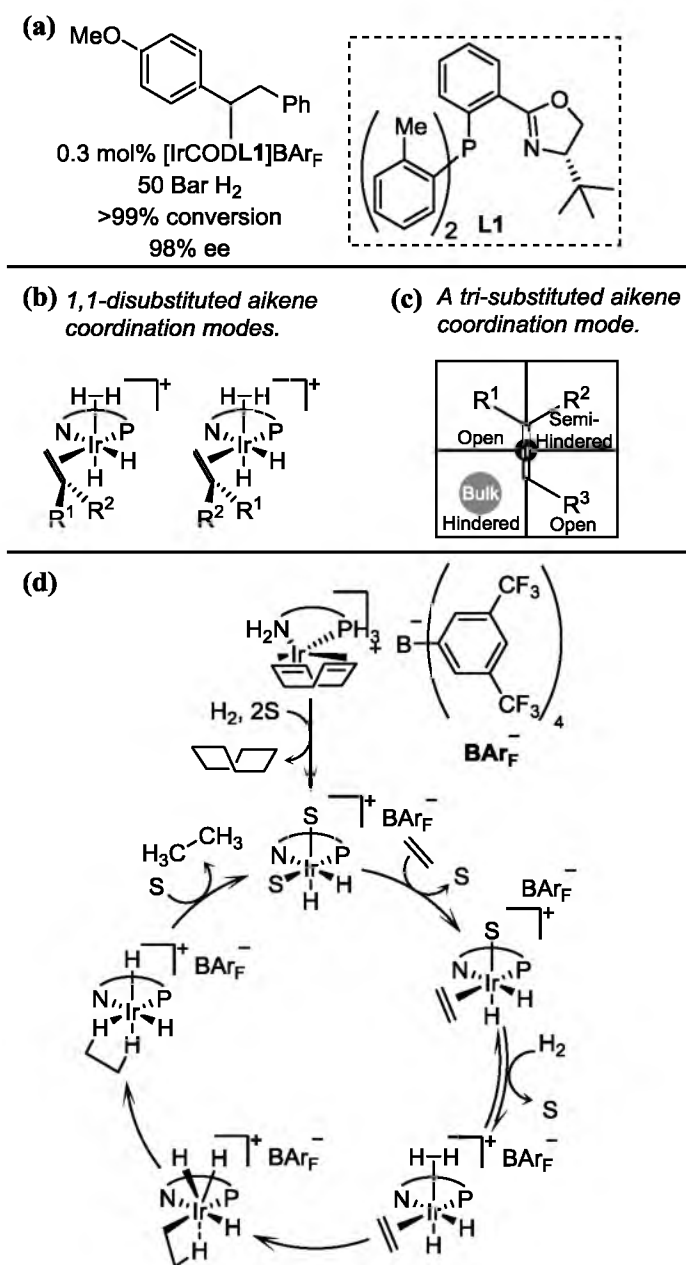


Figure 2.3. Ir-P/N-catalyzed asymmetric hydrogenation. (a) Work of Pfaltz and coworkers demonstrating high degrees of facial discrimination for unfunctionalized olefins. (b) Coordination modes of 1,1-disubstituted terminal alkenes and (c) tri-substituted alkenes to Ir-P/N complexes. (d) Proposed catalytic cycle of iridium-catalyzed hydrogenation.

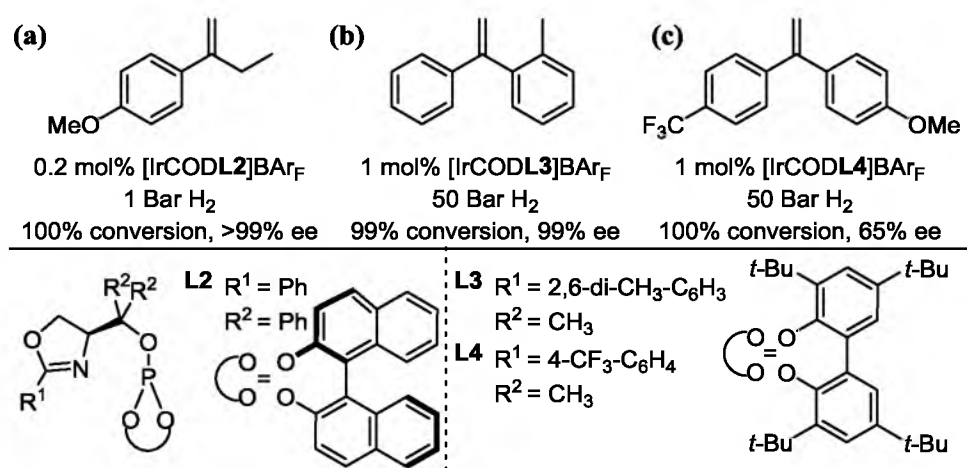


Figure 2.4. Results representative of highest substrate-class enantiomeric excesses (ee's) for 1,1-disubstituted terminal alkene classes: (a) 1,1-aryl-alkyl alkene; (b) 1,1-diaryl alkene with proximal arene substitution; (c) 1,1-diaryl alkene with distal arene substitution.

substrate scaffold is arguably one of the most difficult for this reaction type, with the substrate's high degree of structural symmetry breaking down only at positions distal from the prochiral site of hydrogenation. The similarities in steric bulk between the trifluoromethyl and methoxy substituents would suggest that the electronic dichotomy of these groups is, at least in part, responsible for enantioselection. While this 65% ee is relatively impressive, there is still much to be improved upon within the class of 1,1-terminal alkene asymmetric hydrogenation.

With an interest in developing a hydrogenation system capable of yielding highly enantioenriched 1,1-diarylmethine products from substrates lacking *ortho*-directing groups, we investigated the use of a new class of modular phosphoramidite ligands. The origin of this new ligand's design is the use of an aminooxazoline core structure with a proline-derived pyrrolidine as a key element for imparting rigidity. Synthesis of this ligand proceeds through standard amino alcohol/amino acid coupling, followed by cyclization to form the oxazoline, and *N*-pyrrolidine deprotection, all of which proceed in good yields and were performed according to previously published procedures (Figure 2.5).³⁷⁻⁴⁰ The phosphite moiety, a standard element in many iridium-based hydrogenation catalysts, is incorporated to afford the phosphoramidite ligand **PhosPrOx**.⁴¹ Stirring **PhosPrOx** with [IrCODCl]₂ yields the precatalyst [IrCOD**PhosPrOx**]BA_{TF}, although in poor yield.⁴²

We evaluated this new catalyst's performance in the hydrogenation of **1** (Figure 2.6). (Details regarding the optimization of reaction conditions is provided in the "Experimental Information" section.) Excitingly, hydrogenation using this unique catalyst complex affords the product in 92:8 er. To the best of our knowledge, this result represents the highest reported er for an iridium-catalyzed hydrogenation of this substrate type (i.e.,

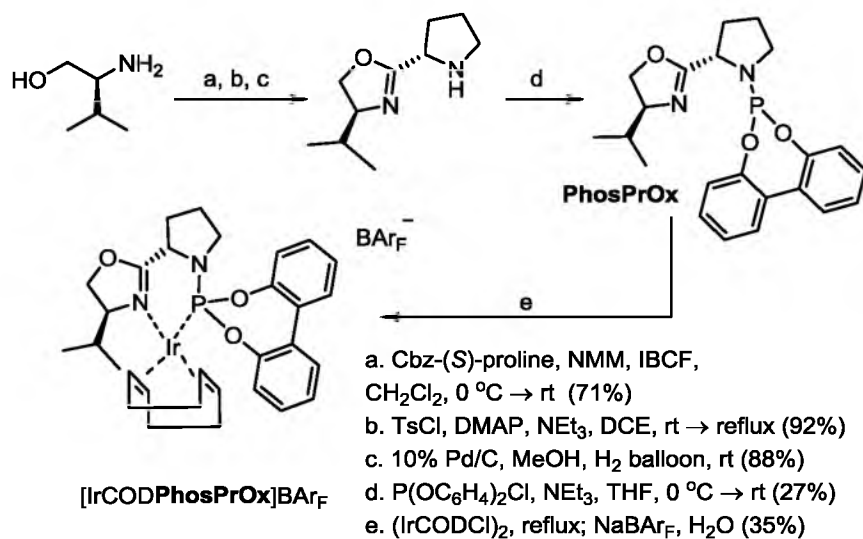


Figure 2.5. Synthetic route to novel iridium-phosphoramidite complex.

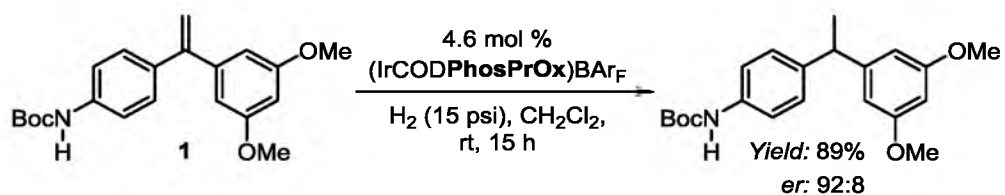


Figure 2.6. Initial evaluation of the novel catalyst, PhosPrOx.

non-*ortho*-substituted 1,1-diarylalkenes). As this substrate has two rings displaying unique functional groups, we desired to systematically evaluate the effects of each in order to determine the potential structural origin for face selection.

Due to the Lewis basic nature of **1**'s carbamate (and its potential catalyst-coordinating ability), it was hypothesized that steric bulk at this position may play a role in the reaction's mode of asymmetric induction. Modulating the electronic nature of the substrate by varying the geminal arene's 3,5-dimethoxy substitution pattern was also hypothesized to influence the substrates' reactivity, conceivably via its conjugative impact on the alkene functional group. Altering the relative electron density residing in the alkene π -system was postulated to play a role in facial selection similar to that observed for Andersson's catalyst system, where only electronic features differentiate the two arenes (Figure 2.4c). Because the dimethoxy substituents in **1** reside at the *meta*-positions and are less Lewis basic than the carbamate, their associated steric bulk (distal to the prochiral site) was predicted to play a negligible role in enantioselection.

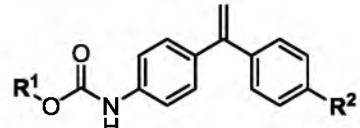
Application of Design of Experiments Principles

To systematically probe these steric and electronic features, with the goal of developing a mathematical equation relating electronic and steric parameters to $\Delta\Delta G^\ddagger$, we turned to Design of Experiments (DoE) principles.^{43,44} DoE principles dictate that an experimental system can be best understood when the system is systematically evaluated over a defined range of experimental interest. Furthermore, in order to develop a mathematical model that best relates these systematic perturbations to a measured outcome, the perturbations must be described by independent variables, i.e., variables where

variation in one does not cause variation in another.⁴³

Using substrate **1** as a template, electronic perturbation at **R**² (Figure 2.7), according to DoE principles, was a straightforward substituent-selection process when considered in terms of Hammett values (σ). Hammett values—derived from the equilibrium constants (K_{eq}) for ionization of substituted benzoic acids relative to unsubstituted benzoic acid—describe each substituent with one value.^{45,46} This single-value descriptor allows for facile selection of electronically disparate substituents that evenly span a relevant electronic space (with the caveat that the substituents are also synthetically feasible and compatible with the reaction conditions). These considerations led to the selection of three electronically varied 4-position substituents: methoxy, hydrogen, and trifluoromethyl (Figure 2.7).

Applying DoE principles to select substituents that represent systematic steric variation proved to be a more complex task. Given the demonstrated effectiveness of Sterimol values for depicting the steric effects in bisphenol desymmetrization,^{1,4,6,47} this descriptor system was considered for its ability to describe the steric effects in the iridium-catalyzed hydrogenation under investigation. However, with the increased descriptive specificity that this three-faceted parameter system affords also comes two additional challenges to experimental design and model development. One hurdle is the lack of independence amongst the three descriptor values, B_1 , B_5 , and L . In general, increases in substituent lengths (L) are necessary to accommodate increases in maximum radial bulk (B_5). This lack of parameter independence can confound effective linear regression (*vide supra*). Secondly, three descriptor values per substituent increases the difficulty of systematically sampling the multivariate steric space. In the case of parameterization using



The chemical structure shows a 1,1-diaryllalkene core. One phenyl ring is substituted with an amide group (-NH-C(=O)-OR¹) at the para position. The other phenyl ring is substituted with a substituent R² at the para position. The two phenyl rings are connected to a central carbon atom via a double bond.

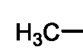
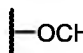
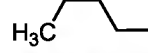
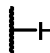
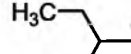
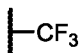
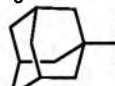
Steric Perturbation (R ¹)	Sterimol		Electronic Perturbation (R ²)	Hammett σ
	PC ₁	PC ₂		
	-2.76	0.06		-0.27
	1.29	-0.74		0.00
	-0.11	0.03		0.54
	1.05	1.14		

Figure 2.7. DoE-founded analysis of 1,1-diaryllalkene steric and electronic effects.

single-value parameters, such as the Hammett values, sequential ordering of the synthetically accessible substituents allows for ready identification of those that evenly span a relevant variable range. With three values describing each substituent, this selection scenario becomes complicated.

Principal Component Analysis (PCA) to Streamline DoE Application

We hypothesized that both of these obstacles could be simultaneously addressed through Principal Component Analysis (PCA)-guided application of DoE (Figure 2.8).⁴³ PCA is a mathematical technique that, from n dependent variables, yields n principal components (PCs), which represent new, independent (orthogonal) variables, composed of linear combinations of the n dependent variables (Figure 2.8a). Each PC is also rank-ordered according to its eigenvalue, which indicates the portion of variation in the data that the respective PC represents. Specifically, the PC that accounts for the greatest variation in the data is PC₁; the PC representing the second greatest data variation is PC₂, and so on.

Because the PCs generated from PCA are orthogonal variables, modeling diastereomeric transition states with these PCs meets the linear regression requirement of independent variables. Thus, PCA was applied to the Sterimol parameters by first identifying the steric space of interest at the carbamate's **R**² position, which space can be visualized with the substituent tree in Figure 2.8b. A matrix of the Sterimol values for each substituent in the tree was submitted to the MATLAB PCA algorithm, which yielded three PCs: Eq. 2.1 (eigenvalue: 0.98; variance represented: 68%), Eq. 2.2 (eigenvalue: 0.24; variance represented: 17%), Eq. 2.3 (eigenvalue: 0.22; variance represented: 15%).⁴⁸

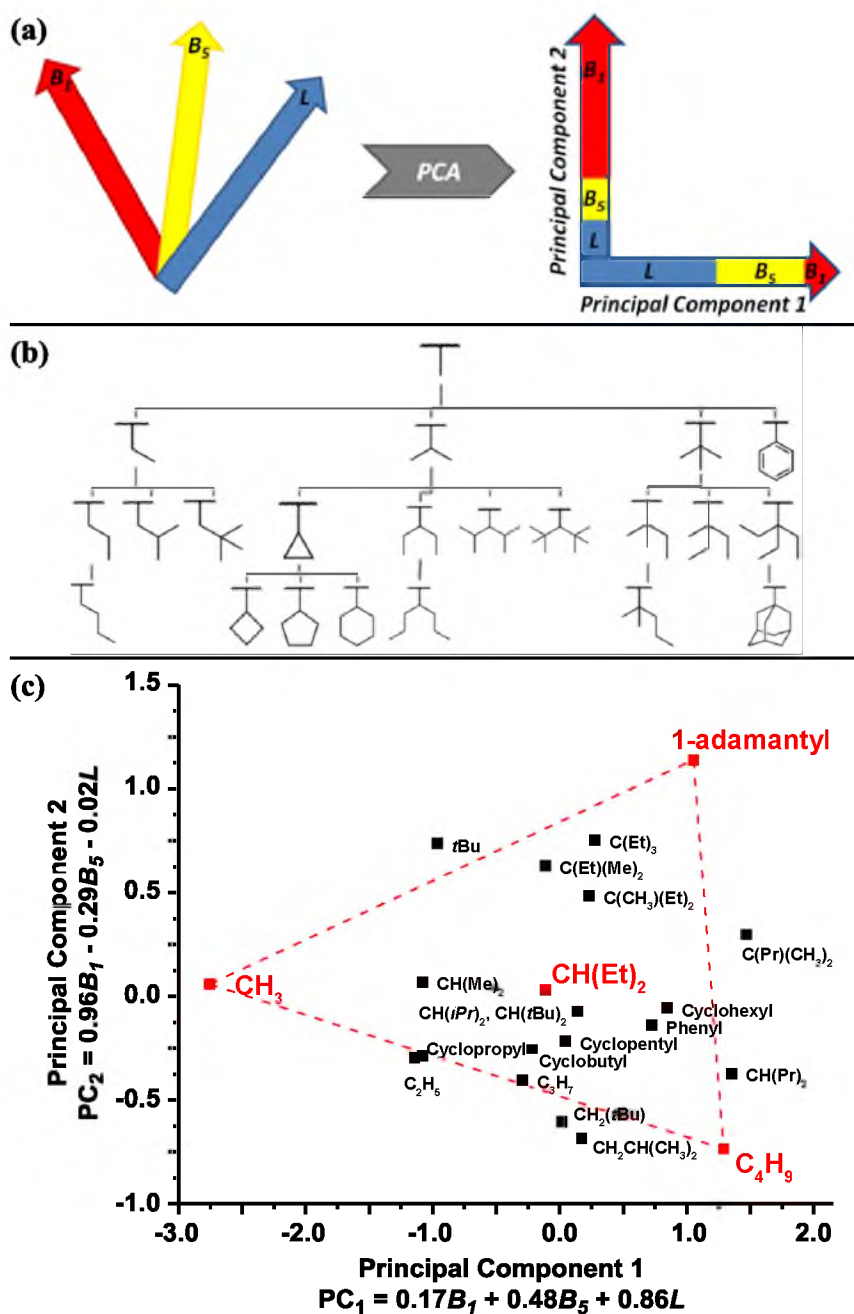


Figure 2.8. Principal Component Analysis (PCA) and its applications to Sterimol parameters. (a) Schematic depicting the PCA concept. (b) Steric space of the terminal alkene template's R^2 position. (c) Experimental space of R^2 steric effects transformed according to PCA.

$$PC_1 = 0.17B_1 + 0.48B_5 + 0.86L \quad \text{Eq. 2.1}$$

$$PC_2 = 0.96B_1 - 0.29B_5 - 0.02L \quad \text{Eq. 2.2}$$

$$PC_3 = -0.24B_1 - 0.82B_5 + 0.51L \quad \text{Eq. 2.3}$$

Comparison of the PC coefficients' relative magnitudes indicates that PC₁ is predominantly a representation of substituents' maximum radii (B₅) and lengths (L). This weighting of B₅ and L within PC₁ is in line with the aforementioned observation that increases in substituent lengths are necessary in order to accommodate increases in maximum radial bulk. PC₁'s eigenvalue of 0.98 corresponds to PC₁ capturing 68% (relative to the sum of all three eigenvalues) of the variation within the described steric space of interest. Additional consideration of PC₂, which is most descriptive of minimum radius (B₁), cumulatively represents 85% of the potential steric variability at the carbamate. With PC₃ corresponding to the least amount of variation in the data, it is hypothesized that PC₁ and PC₂ adequately represented the three Sterimol subparameters and their variation in the steric space. If this hypothesis proves accurate, the challenge of selecting sterically varied substituents that evenly span the steric space would be greatly simplified by allowing for consideration of only two, rather than three, descriptors. Additionally, describing steric bulk variation in two independent, rather than three dependent, descriptors facilitates model development using linear regression techniques.

The graph of PC₁ versus PC₂ (Figure 2.8c) evidences the simplification of substituent selection. This plot shows that methyl, *n*butyl, and 1-adamantyl define a triangle that almost entirely encompasses the PCA-interpreted steric space. To complete the selection of evenly distributed substituents, the substituent at the point nearest the triangle's

center, CH(Et)₂, was also selected.

With four substituents to probe steric modulation at the carbamate and three substituents to assess electronic variation on the adjacent arene, synthesis of every combination of these perturbations yielded a 12-membered substrate library (Figure 2.7). After measuring the resultant *er* and calculating the $\Delta\Delta G^\ddagger$ for each substrate in its [IrCODPhosPrOx]BARF-mediated hydrogenation, the ultimate goal of this library was mathematically interpreting the influence of steric and electronic effects on enantioselection, in a model of the form given in Eq. 2.4.

$$\Delta\Delta G^\ddagger = z_0 + a(PC_1) + b(PC_2) + c(\sigma) + d(PC_1*PC_2) + f(PC_1*\sigma) + g(PC_2*\sigma) \quad \text{Eq. 2.4}$$

Unfortunately, when this library of substrates was subjected to hydrogenation conditions, none of the reactions reached full conversion of alkene starting material to reduced alkane product. Conversions ranged from 0% to 65%, despite **1** proceeding in >95% conversion. Increasing the reaction time for related substrates did not increase the percentage of conversion.

The dominance of asymmetric hydrogenation catalysis as a means for synthesizing chiral compounds can be attributed, at least in part, to the reaction's 100% atom economy and a corresponding absence of side products.²⁹ With the substrates of the 12-membered library not achieving full conversion to reduced product, this reaction class's atom economy-advantage becomes irrelevant, particularly since starting material and product are not easily separable via common column chromatography techniques. In an effort to understand these unexpected results, which were surprising given the apparent similarities

between substrate **1** and the 12 library substrates, attempts were made at relating changes in steric bulk and electronics to the substrates' varied yields. No model could be generated with any degree of confidence, which may be an indication of the many modes by which yield can be influenced.

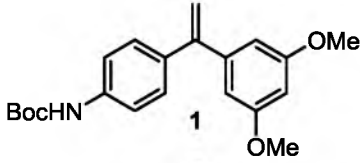
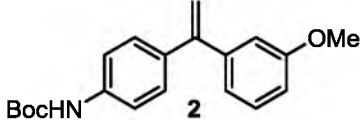
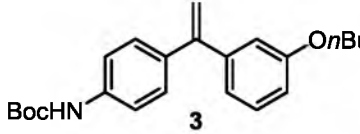
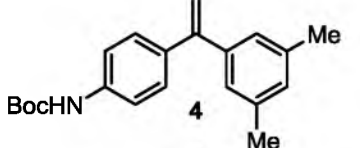
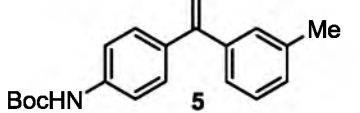
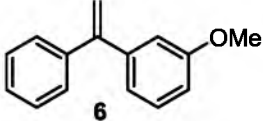
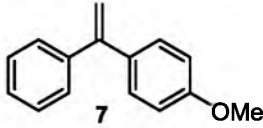
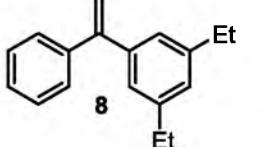
Although no quantitative conclusions could be drawn about the nature of the catalyst/substrate interaction from the results of this library study, the experiment's foundational DoE approach allowed for an important conclusion to be drawn: the results of the 12-membered library are not the outliers in this reaction system; they are the norm. Instead, these point to the uniqueness of **1**. It appears that we serendipitously identified an intriguing relationship between **1** and the **Ir-PhosPrOx** catalyst. Without applying DoE principles to systematically explore the steric and electronic aspects of derivatives of **1**, this same conclusion may have been realized. However, it likely would have required more time and experiments to be confident in the singular high enantioselectivity afforded with **1**, given the unanticipated nature of the library's results. The systematic DoE-guided approach streamlined this process.

A Qualitative DoE Approach

To understand the unique interaction between **Ir-PhosPrOx** and **1** that leads to high levels of enantioselection, the importance of each ring was systematically evaluated, using a qualitative DoE approach, to determine its mechanistic relevance. As a first experiment, removal of one methoxy substituent, as in substrate **2** (Table 2.1), led to a significant reduction in enantioselectivity upon hydrogenation (Table 2.1, entry 2, er = 74:26). Changing this group further to 3-*n*butoxy (**3**) had a negligible effect (Table 2.1, entry 3, er

Table 2.1. Exploration of substrate *meta*-directing group effects.

$$\text{Ar}^1\text{C}(\text{CH}_3)=\text{Ar}^2 \xrightarrow[\text{CH}_2\text{Cl}_2, \text{rt, 15 h}]{\text{4.6 mol \% (IrCODPhosPrOx)BAR}_F, \text{H}_2 (15 \text{ psi})} \text{Ar}^1\text{CH}(\text{CH}_3)\text{Ar}^2$$

entry	alkene	conversion (%) ^a	er ^b
1		89%	92:8
2		59%	74:26
3		66%	75:25
4		70%	63:37
5		54%	48.5:51.5
6		>95%	74:26
7		>95%	53:47
8		>95%	49:51

^aConversions, measured by ¹H NMR, are an average of two reactions.

^bEr, determined by SFC or HPLC instruments fitted with chiral stationary phases, represents average of two reactions.

= 75:25).

These preliminary results suggest that 3,5-substitution on the aryl ring is required for enhanced enantioselection. To probe whether this is a purely steric effect or if the Lewis basic substituents are required, 3,5-dimethoxy aryl was replaced by the 3,5-dimethyl variant. This change led to a considerable lowering of *er* (Table 2.1, entry 4, *er* = 63:37), suggesting the importance of the Lewis basic group. Interestingly, elimination of one of the methyl groups results in a system wherein the catalyst had no alkene facial preference (Table 2.1, entry 5). This combination of results is consistent with high enantioselectivity resulting from a strongly influential Lewis base substituent effect, which is augmented by the steric effect of substituents at both the 3- and 5-positions.

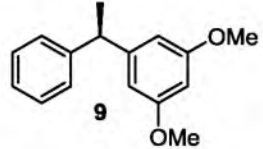
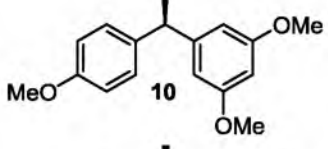
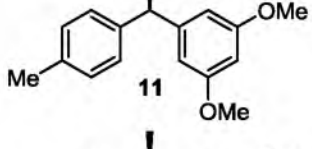
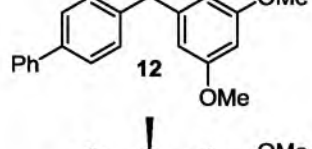
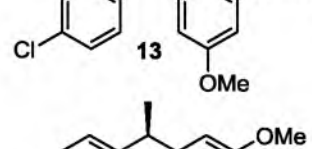
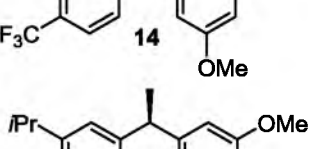
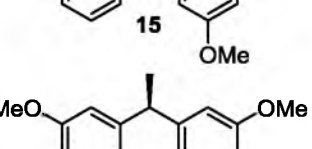
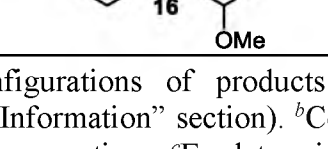
As support for this hypothesis, the other aryl ring should not have a major influence on the outcome of the reaction. Evaluation of a substrate in which the *N*-Boc is truncated leads to an excellent result, wherein very similar enantioselectivity is observed (Table 2.2, entry 1, *er* = 92.5:7.5). Again, removal of one of the *meta*-substituted methoxy groups (**6**) leads to a significant reduction in enantioselectivity, and evaluation of the corresponding *para*-methoxy-substituted substrate **7** leads to a nearly racemic hydrogenation.

While we had gathered considerable evidence indicating the importance of etheric aryl substituents, there remained a possibility that the steric bulk of the 3,5-dimethoxy substituents was the crucial feature for enantioselection. To assess this possibility, **8** was synthesized, incorporating 3,5-diethyl substitution as a steric bulk surrogate to 3,5-dimethoxy. In poignant support of our hypothesis, **8** (Table 2.1) was hydrogenated to yield a racemic product mixture.

Returning to the requisite 3,5-dimethoxy substitution pattern on one aryl ring, we

Table 2.2. Substrate scope for iridium(PhosPrOx)-catalyzed hydrogenation.

$$\text{Ar}^1\text{C}=\text{C}\text{Ar}^2 \xrightarrow[\text{CH}_2\text{Cl}_2, \text{rt, 15 h}]{\text{4.6 mol \% (IrCODPhosPrOx)BAR}_F, \text{H}_2 (15 \text{ psi})} \text{Ar}^1\text{CH}(\text{Me})\text{CH}_2\text{Ar}^2$$

entry	product	conversion (%) ^a	er ^b
1		>95%	92.5:7.5
2		>95%	91.5:8.5
3		>95%	88.5:11.5
4		>95%	89:11
5		>95%	96:4
6		>95% ^d	96.5:3.5
7		>95%	85.5:14.4
8 ^e		>95%	71:29

^aAbsolute configurations of products were assigned by analogy (see “Experimental Information” section). ^bConversion, measured by ¹H NMR, is an average of two reactions. ^cEr, determined by an SFC instrument fitted with a chiral stationary phase, represents an average of two reactions. ^dReactions performed using 10 mol % catalyst to achieve >95% conversion. ^eThe same sense of stereoselection is assumed, although not confirmed.

evaluated the reaction's enantioselective robustness to variation in the geminal aryl ring. Installing an electron-donating methoxy substituent at the 4-position (**10**) afforded the reduced product with very little change in er (Table 2.2, entry 2, er = 91.5: 8.5). Incorporating a 4-methyl substituent into the substrate (Table 2.2, entry 3) resulted in a slightly diminished er (88.5:11.5). However, a negligible effect on er is observed upon modification of 4-position steric bulk from methyl (**11**) to phenyl (**12**, Table 2.2, entry 4, er = 89:11).

The influence of electron-poor substituents on enantioselection was evaluated via 4-chloro (**13**) and 4-trifluoromethyl (**14**) substrates, which were hydrogenated in 96:4 er (Table 2.2, entry 5) and 96.5:3.5 er (Table 2.2, entry 6), respectively. These er's represent a significant improvement in enantioselectivity over the best previously reported er (82.5:17.5) obtained via an iridium-catalyzed hydrogenation of a 1,1-diaryllalkene that contains aryl substitution only at positions distal (*meta* and *para*) from the prochiral site.^{6b}

Convinced of the system's enantioselective robustness to 4-position steric bulk and electronic variation, we next investigated the effect of 3-position variation. Hydrogenation of substrate **15** (Table 2.2), bearing the bulky and electron-rich 3-*iso*-propyl substitution, yielded the corresponding diarylmethine in 85.5:14.5 er, representing only a slight decrease in enantioselection from 4-substituted substrates.

Finally, to challenge the 3,5-dimethoxy substitution pattern's capacity for directing facial selection in the presence of other potential directing groups, we evaluated the hydrogenation of **16** (Table 2.2), wherein the 3,5-dimethoxys remain intact on one ring, and 3-methoxy substitution is instituted on the geminal ring. In this scenario, the substitution patterns in both rings are each, in the absence of the other, capable of inducing

facial discrimination, although to a lesser extent for 3-methoxy than for 3,5-dimethoxy substitution. Interestingly, **16** was reduced in a 71:29 er, nearly identical to that seen for substrates **2** and **6** (Table 2.1, er = 74:26 and 74:26, respectively), which bear 3-methoxy substitution. We hypothesize that 3,5-dimethoxy substitution still acts as the dominate force in this transformation's enantiodetermining step, while the observed er erosion is a result of introducing another group (3-methoxy) with competing directing group capabilities.

A Quantitative Model from a Qualitatively Developed DoE Library

This systematic probing of the distally substituted 1,1-diaryl alkene scaffold supports the curious hypothesis that not only is a 3,5-dimethoxy motif on one aryl ring necessary for high levels of asymmetric induction, but the oxygen's Lewis basicity appears to be the enantiodetermining feature. To better detail this unprecedented selectivity, enantioselectivities for the library of substrates in Figure 2.9 were measured, with the objective of using the training set to develop a mathematical model that quantitatively illuminates the features of mechanistic significance to the modes of asymmetric induction. As it was unclear what parameters might be relevant for describing this reaction's outcomes, a quantitative DoE library design was not feasible. Instead, the library was constructed based on systematic sampling of observed enantioselectivities from a collection of analyzed substrates, as well as based on variation according to fundamental chemistry principles of steric and electronic effects.

Successful modeling analysis of this study's data required looking beyond the scope of typically employed molecular parameters, as classic parameters were inadequate

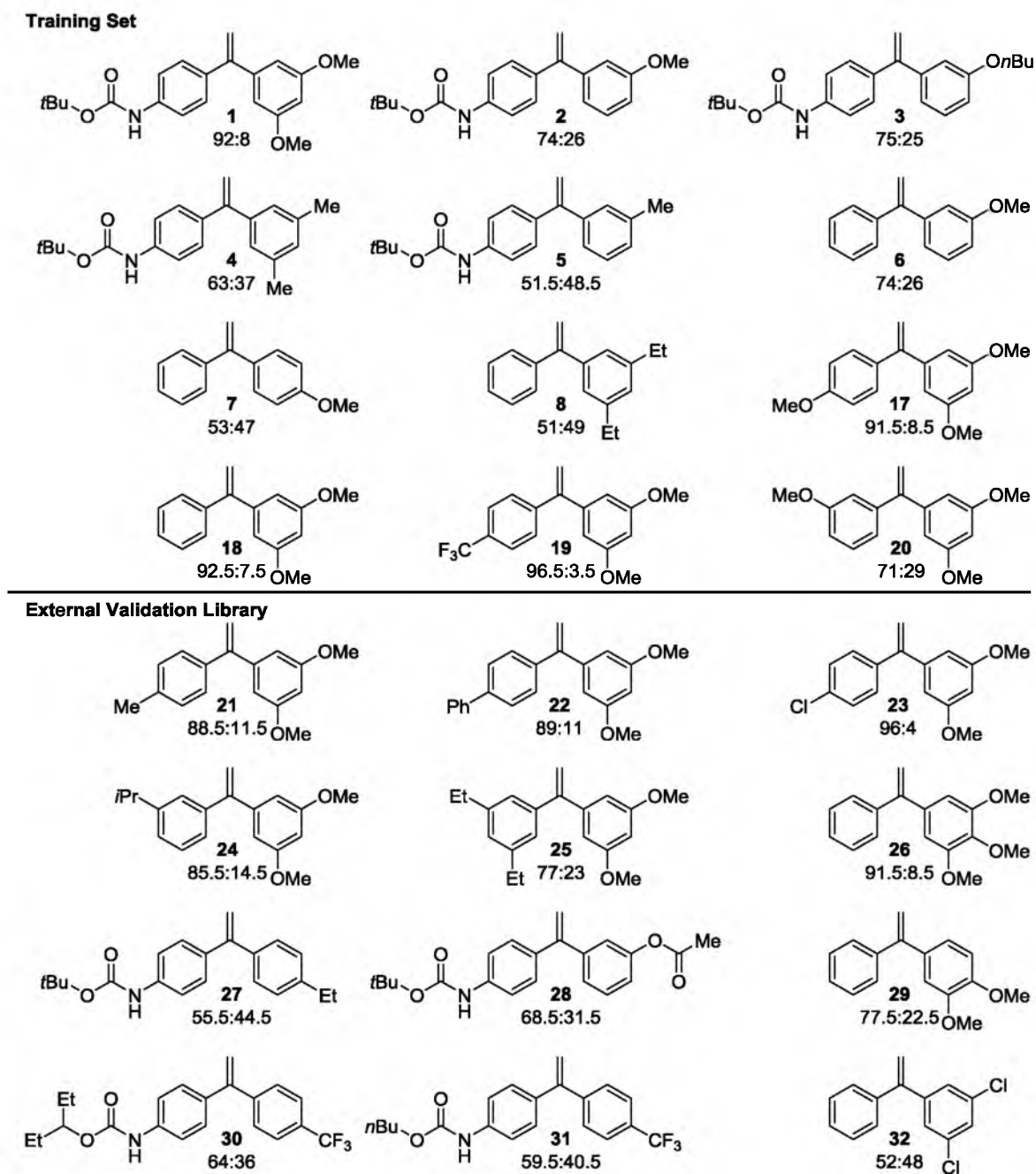


Figure 2.9. Substrate libraries used for the development (training set) and assessment (external validation library) of a mathematical model describing Ir-PhosPrOx-catalyzed hydrogenation.

for describing the substrates' variation. In collaboration with postdoctoral fellow Dr. Anat Milo, energy-minimization and frequency computational calculations were performed by Dr. Milo for the training set of substrates in Figure 2.9. *In silico* assessment of these molecules led to a set of molecular vibrations and a torsion measurement (descriptive parameters) that were hypothesized to numerically describe the steric and electronic effects of the alkene substrates that were important for imparting high enantiomeric excess in their iridium-catalyzed reduction.⁴⁹ This parameter set is defined by the frequencies and intensities of three alkene vibrations, as the alkene functional group is the site of reaction, and six arene C=C bond vibrations (three for each ring), which values change with changes to ring substitution. Given the possible role played by conjugation between each arene and the alkene, two additional vibrations displaying simultaneous, synchronized movement between both arenes were included. Tabulation of these vibrational frequencies and intensities and torsion measurements is given in the "Experimental Information" section.

From the precise delineation of the alkenes' properties that density functional theory (DFT) calculations afforded, Dr. Milo identified a robust mathematic relationship (Figure 2.10). Model development was carried out based on MATLAB stepwise linear regression algorithms. This is a procedure whereby *p*-values are calculated for each parameter of putative mechanistic significance, which value quantifies a parameter's likelihood of effectively describing the patterns in reaction outcomes. As defined by the stepwise algorithm, parameters with calculated *p*-values less than 0.05 are included in the regression model; those with *p*-values greater than 0.10 are removed from the model. Through such an iterative process, a descriptive model was developed (Figure 2.10a).

Prior to interpreting the model's mechanistic clues, this quantitative construct of

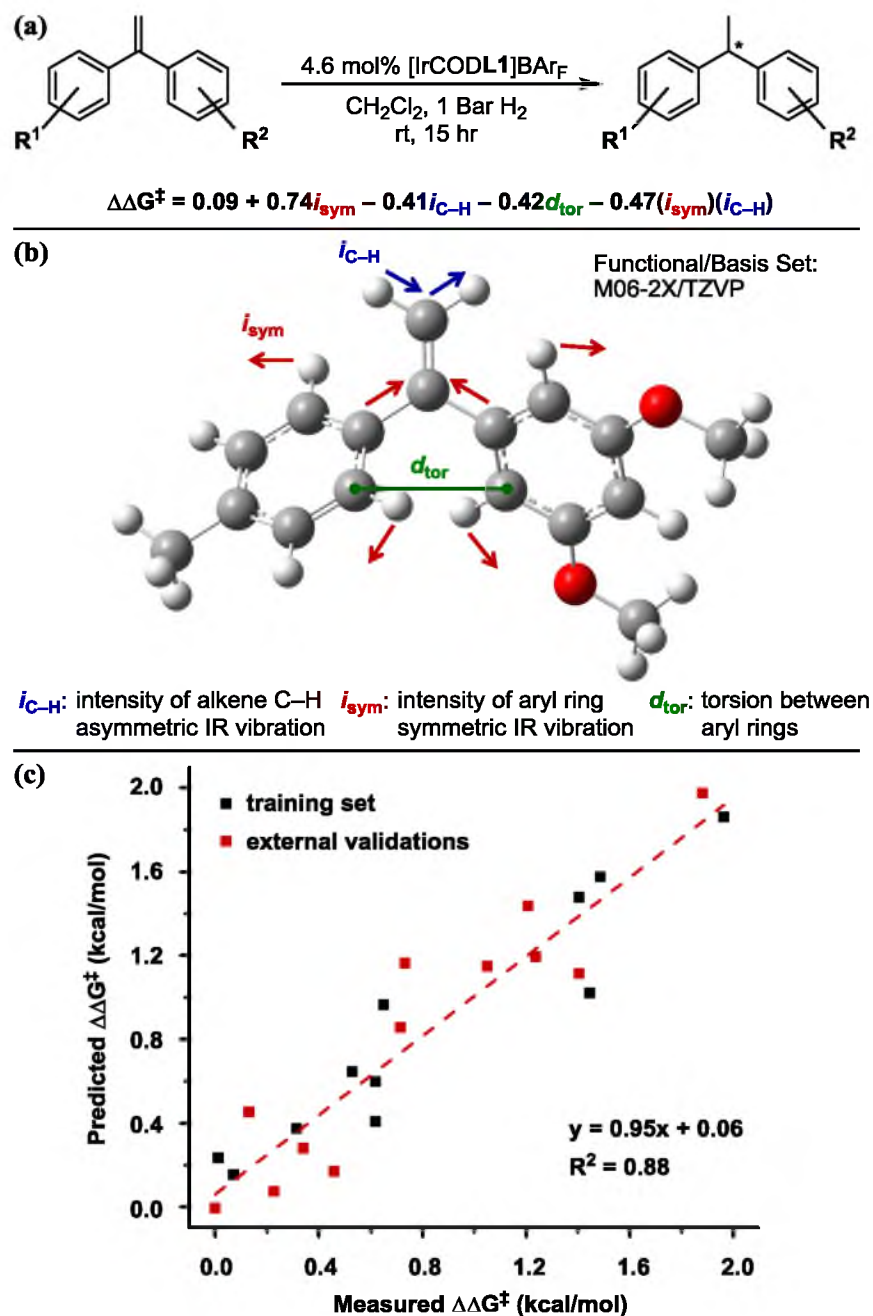


Figure 2.10. Mathematical analysis of Ir-PhosPrOx-catalyzed asymmetric hydrogenation. (a) Free-energy model for the reaction scheme given. (b) Depiction of parameters that are relevant descriptors of the chemical system's modes of asymmetric induction. (c) Graphical representation of the model, with predictive and descriptive robustness illustrated through effective external validation.

the reaction's enantiodetermining step was assessed for its accuracy and precision. Model validation was performed by subjecting a set of substrates that was not used for model development (the external validation set, Figure 2.9) to hydrogenation conditions. The agreement between model-predicted $\Delta\Delta G^\ddagger$ values and experimentally measured $\Delta\Delta G^\ddagger$ values was assessed via the plot in Figure 2.10c. This predicted versus measured $\Delta\Delta G^\ddagger$ plot's slope and R^2 values near unity demonstrate the generality and robustness of the model for describing steric and electronic substrate features that influence enantioselectivity.

With a mathematical demonstration of the model's correctness, the model was assessed from a perspective of fundamental chemical principles and logic. All descriptors in the identified model emphasize the differences between the two rings: vibrational intensities, i_{sym} and $i_{\text{C-H}}$, which differentially describe bond vibrations at the fusion of the two aryl rings, and the torsion measure, d_{tor} , that likely depicts the degree to which one aryl ring is better oriented than the other for engagement with the catalyst (Figure 2.10b). This emphasis of each arene's distinctiveness is in line with the model's ultimate objective of quantitating the catalyst's capacity for alkene facial discrimination. As a direct result of the compositional differences between each ring, the mathematical model describes the substrate features that are singularly interpreted by the catalyst for enantiodetermination.

It was supposed that the wealth of mechanistic information contained within the multifaceted vibration terms could be better understood by grouping substrates according to simple chemical patterns: substrates with *para* position variation and those with varied *meta* substituents. For each library, a micromodel was developed from the set of terms identified in the initial model. Interestingly, Hammett σ values were inadequate as a sole

description of *para* position variation (Figure 2.11). Instead, description of the *para*-substituted series was accomplished with two terms: the asymmetric stretching intensity of the alkene's C–H bonds ($i_{\text{C-H}}$) and the torsion measurement, d_{tor} (Figure 2.11b). The torsion term suggests that gross substrate conformation impacts the enantioselectivity of reduction. Yet, the more impactful predictor of selectivity (larger coefficient in the normalized model, Figure 2.11b) is $i_{\text{C-H}}$. The implications of this term are intriguing. By definition, as a vibrational intensity, this term represents the difference in dipole moment (dependent on bond length and atomic charges across the bond) between the compressed and elongated bond. Bonded atoms exhibiting greater vibrational intensity correspondingly are displaced a greater distance and occupy a greater net area over the course of a vibration. It follows that, in the context of $i_{\text{C-H}}$, alkenyl C–H bonds with larger intensity values effectively occupy a greater volume of space than do C–H bonds with less vibrational intensity.

Interpreting the relevance of $i_{\text{C-H}}$ as a steric effect, where larger values erode enantioselectivity (equation in Figure 2.11b), this term may be describing the closeness with which substrates may coordinate to the iridium catalyst. With substrates that exhibit smaller $i_{\text{C-H}}$ values and a smaller net displacement of the hydrogen atom upon vibration, coordination may be more facile, leading to higher levels of asymmetric induction—consistent with the developed micromodel for *para*-substituted substrate series.

Despite the disparate nature of *meta* substitution patterns in the *meta* micromodel set, they are unified by the single term, i_{sym} (Figure 2.12). As given in the developed model, increases in i_{sym} correspond to increases in enantioselection. This vibrational intensity, which importantly manifests as a simultaneous movement of the geminal arenes towards the alkene, is rationalized to quantitatively represent the electronic differences between the

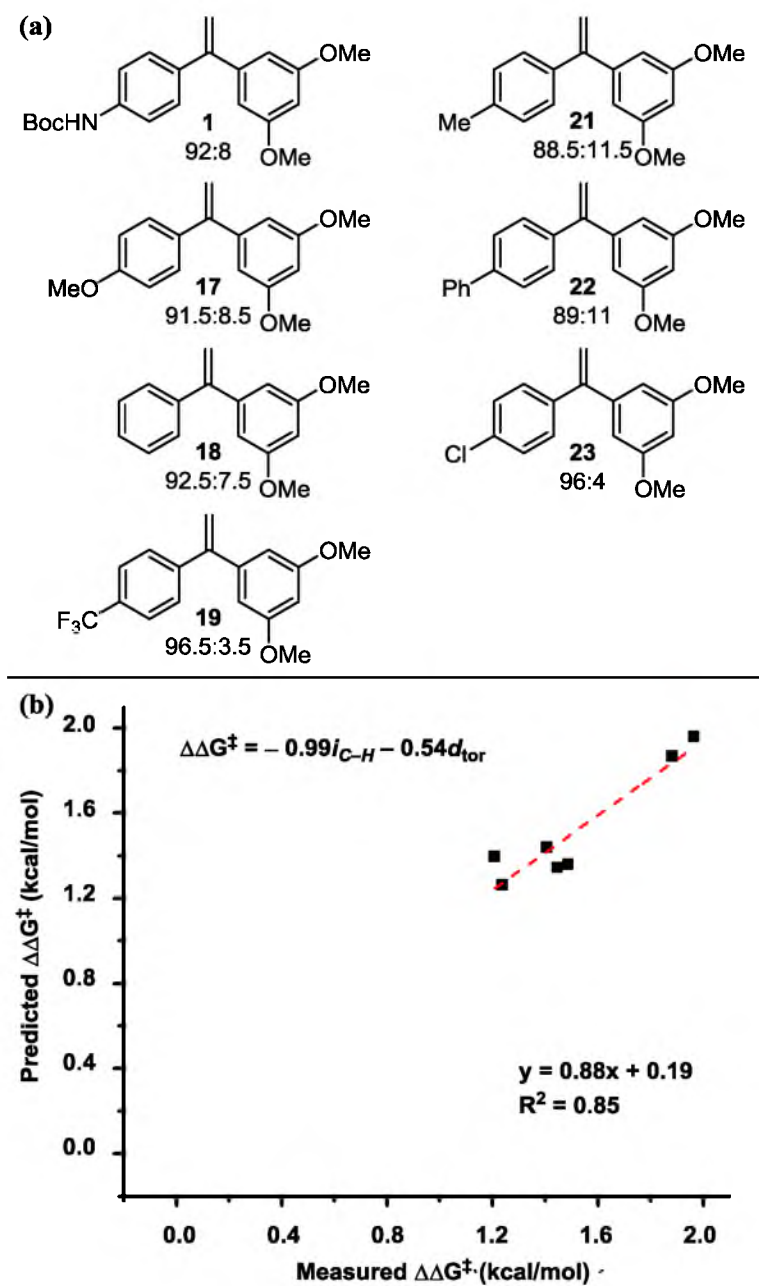


Figure 2.11. Micro analysis of *para* modulated substrates. (a) Library of *para* position variation and (b) its normalized descriptive model.

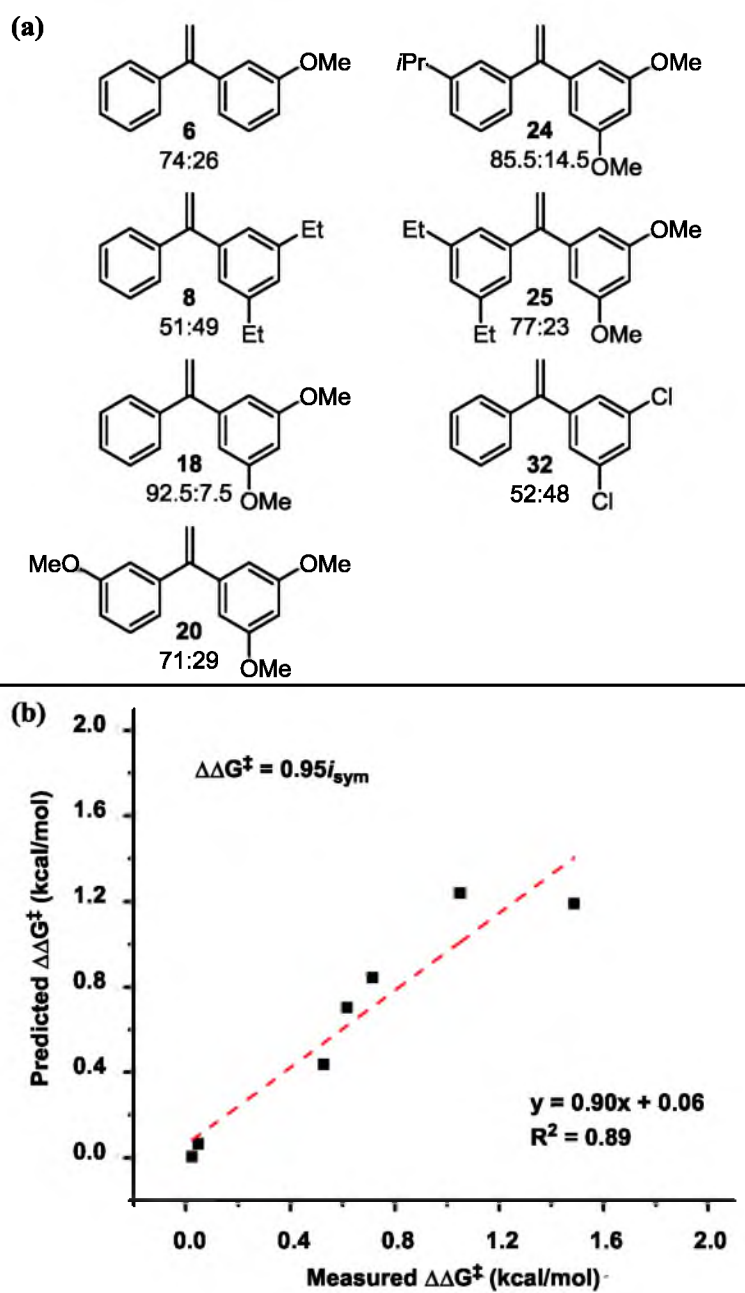


Figure 2.12. Micro analysis of *meta* modulated substrates. (a) Library of *meta* position variation and (b) its normalized descriptive model.

two rings and, thereby, their capacity for precoordination. This interpretation is supported by qualitative observations (*vide supra*) that led to the previously described hypothesis that Lewis basic groups at the *meta* position allow for advantageous substrate precoordination.

The inadequacy of the exclusive use of σ values combined with the importance of the torsion term suggest that asymmetric induction does not rely exclusively on electron-donating or -withdrawing features of the substrate. Instead, the degree of torsion, also ultimately of an electron-density origin, is a key factor that influences the substrate-catalyst interaction. Gross substrate structure playing prominently in enantioselection informs interpretation of the model developed from the *meta*-substituted series of substrates (Figure 2.12b). Described by the intensity of two arenes' vibrating toward and away from each other in tandem, i_{sym} seems to be representative of how each arene responds relative to the other, reminiscent of the role that torsion plays in the *para* model.

The terms of the full model, as well as the *meta* and *para* micromodels, and the qualitative conclusions drawn from the systematic changes made to aryl substitution, support the hypothesis that the 3,5-dimethoxy motif provokes an ideal degree of ring torsion that orients a methoxy oxygen to precoordinate to the catalyst. Precoordination may orchestrate the enantioselectivity-determining transition state to deliver the key hydride with high levels of facial precision.

Conclusions

Demonstrating the process of evolving descriptors to a set that can represent the reaction outcomes under investigation is a central facet of successful model development. The work presented in this chapter exemplifies this process and the results that led to

expanding the parameter scope from the useful, yet limited, Sterimol parameters to information-rich vibrations. The demonstration of vibration-derived descriptors' powerful ability to quantitate the nuances of IrPhosPrOx-catalyzed hydrogenation of diarylalkenes has provided a platform from which a variety of other reactions, not amenable to description by classic linear free-energy relationship analyses, may be investigated. The following two chapters demonstrate further unique applications of this unconventional, powerful free-energy modelling tool.

The novel application of the Design of Experiments (DoE) concept that was explored in this chapter inspired additional investigation of this principle. In Chapters 3 and 4, approaches are developed for the quantitative implementation of DoE for effective reaction analysis, augmenting the robustness of developed mathematical models for rich mechanistic gain.

Experimental Information

General Information

All glassware was dried in a 120 °C oven or flame-dried and cooled under nitrogen or vacuum, unless otherwise noted. All reactions were performed under nitrogen, with stirring, unless otherwise noted. Tetrahydrofuran (THF), dichloromethane, and toluene were passed through an activated alumina column, under a nitrogen atmosphere, prior to use. Methanol was distilled from magnesium methoxide. Triethylamine was distilled from CaH₂. PCl₃ was purified via simple distillation. All other reagents were from commercial sources and were used as received, unless otherwise noted.

Thin-layer chromatography was performed using silica gel 60 F₂₅₄ and the eluents

indicated, then visualized via a 254 nm UV lamp and/or stained with phosphomolybdic acid, potassium permanganate, ninhydrin, or vanillin. SiliaFlash® F60 40–63 μm silica gel or basic, activated alumina, Brockmann I (GFS Chemicals) was used for flash column chromatography, as designated. ^1H , ^{13}C , ^{19}F , and ^{31}P NMR spectra were acquired on a Varian Unity spectrometer at the MHz specified. Spectral referencing was performed relative to the CHCl_3 7.26 ppm singlet (^1H NMR), the center of the CH_2Cl_2 5.32 ppm resonance (^1H NMR), the center of the CH_3OH 3.31 ppm resonance (^1H NMR), the center peak of the CHCl_3 77.16 ppm triplet (^{13}C NMR), the center peak of the CH_2Cl_2 53.84 ppm pentet (^{13}C NMR), the center of the 49.0 CH_3OH ppm septet (^{13}C NMR), the H_3PO_4 0 ppm singlet (^{31}P NMR, external standard), or the CF_3COOD -78.5 ppm singlet (^{19}F NMR, external standard). All multiplicities reported are apparent. Abbreviations s, d, t, q, p, sex, sep, dd, ddd, td, bs, and m represent the resonance multiplicities singlet, doublet, triplet, quartet, pentet, sextet, septet, doublet of doublets, doublet of doublets of doublets, triplet of doublets, broad singlet, and multiplet, respectively. Infrared (IR) spectroscopy data were obtained using a Nicolet 380 FT-IR instrument. High-resolution mass spectrometry (HRMS) data were obtained using an Agilent LCTOF. Melting points were measured using a Thomas Hoover Unimelt capillary melting point apparatus. All melting points are uncorrected. Super critical fluid chromatography (SFC) analysis was performed using a Thar instrument under the conditions indicated. High Performance Liquid Chromatography (HPLC) analysis was performed using a Hewlett-Packard S1100 instrument under the conditions indicated. Specific rotations were determined using a PerkinElmer 343 Polarimeter, the 589 nm wavelength (sodium D line), and a 1 dm cell path length, with concentrations given in g/100 mL.

Synthetic Methods: Catalyst

The catalyst was synthesized according to previously published procedures (Figure 2.13).^{37-42,50}

(S)-2-((S)-1-(dibenzo[d,f][1,3,2]dioxaphosphepin-6-yl)pyrrolidin-2-yl)-4-isopropyl-4,5-dihydrooxazole (PhosPrOx). Oxazoline A (Figure 2.13) (2.244 mmol, 1.1 equiv.) was dissolved in THF (4.4 mL). After addition of NEt₃ (4.487 mmol, 2.2 equiv.), the solution was cooled to 0 °C, and the chlorophosphite (2.04 mL of a 1.0 M solution in THF, 1.0 equiv.) was added dropwise. The reaction was then allowed to warm to room temperature and stirred overnight. The phosphoramidite product was purified by flash silica-gel column chromatography (25% ethyl acetate in hexanes with 1% triethylamine) to afford 27% yield, 0.176 g (0.443 mmol), of the clear, pale yellow, viscous oil **PhosPrOx**. TLC (30% ethyl acetate in hexanes) R_f = 0.33. ¹H NMR (300 MHz, CDCl₃) δ: 0.86–1.01 (m, 6H), 1.64–1.94 (m, 3H), 1.96–2.18 (m, 2H), 2.92–3.05 (m, 1H), 3.16–3.30 (m, 1H), 3.91–4.11 (m, 2H), 4.25–4.35 (m, 1H), 4.47–4.55 (m, 1H), 7.14–7.25 (m, 4H), 7.28–7.38 (m, 2H), 7.42–7.44 (m, 1H), 7.44–7.47 (m, 1H). ¹³C NMR (75 MHz, CDCl₃) δ: 18.0 (s), 18.1 (s), 18.7 (s), 18.8 (s), 25.2 (s), 31.0 (d, *J* = 5.0 Hz), 32.6 (s), 45.1 (s), 55.3 (s), 55.7 (s), 70.4 (s), 71.9 (s), 122.0 (s), 122.2 (s), 124.5 (s), 124.6 (s), 129.2 (s), 129.7 (s), 129.8 (s), 131.3 (d, *J* = 2.6 Hz), 131.5 (d, *J* = 3.5 Hz), 151.7 (d, *J* = 4.1 Hz), 152.1 (d, *J* = 5.5 Hz), 168.6 (d, *J* = 1.5 Hz). ³¹P NMR (121 MHz, CDCl₃, H₃PO₄ external standard) δ: [150.8 (s) and 150.6 (s)] ratio 4.5:1. IR: 2957, 2872, 2361, 1665, 1600, 1567, 1497, 1474, 1434, 1384, 1365, 1270, 1247, 1207, 1190, 1128, 1077, 1010, 979, 883, 868, 847, 764, 745, 731, 681, 645, 597, 547 cm⁻¹. HRMS C₂₂H₂₆N₂O₃P [M+H]⁺ calculated 397.1681, observed 397.1687. [α]_D²⁰ = -49.9 (c 2.50, CHCl₃).

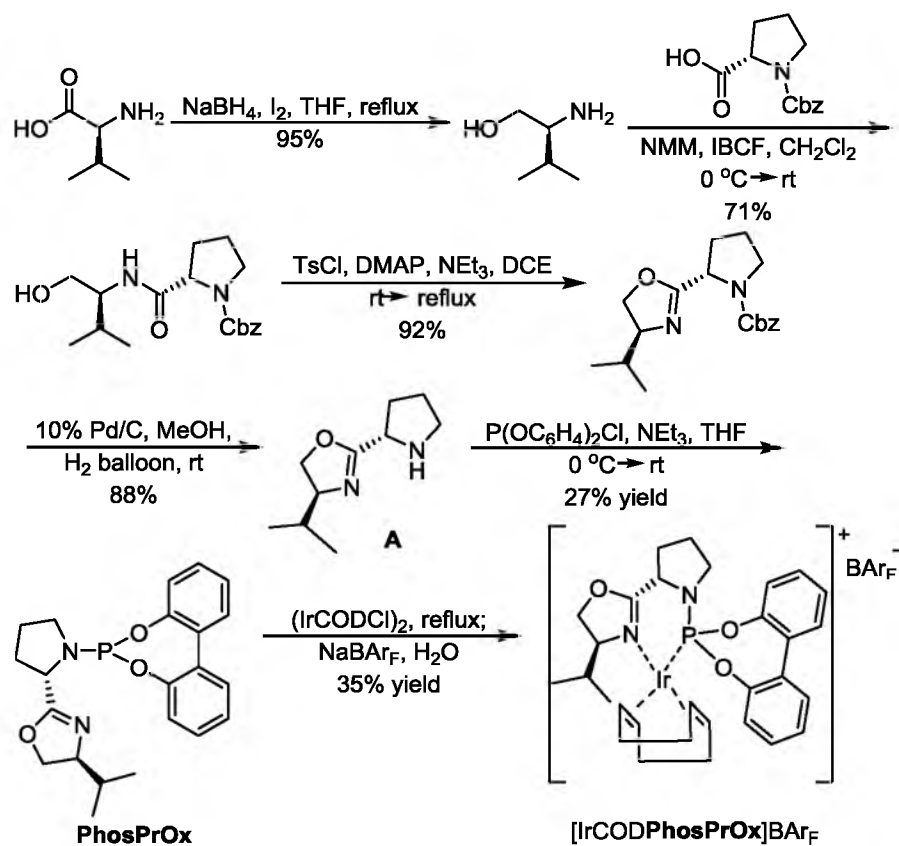


Figure 2.13. Schematic of synthetic route to [IrCODPhosPrOx]BAR_F.

[IrCODPhosPrOx]BAr_F. To an oven-dried Schlenk tube under nitrogen atmosphere was added **PhosPrOx** (0.399 mmol, 1 equiv.) and CH₂Cl₂ (8.3 mL). To this stirring solution, (IrCODCl)₂ (0.200 mmol, 0.5 equiv.) was added. The Schlenk tube was sealed, and the vessel was heated to 48 °C and stirred for 2 hrs. Next, the reaction mixture was cooled to room temperature, and NaBAr_F (0.519 mmol, 1.3 equiv.) was added. After stirring approximately 10 minutes, 8 mL of water was added, and the mixture was stirred vigorously for about 30 mins. Then, the organic layer was extracted, washed twice with brine, and dried with Na₂SO₄. **[IrCODPhosPrOx]BAr_F** was purified by flash silica-gel column chromatography (using 66% ethyl acetate in dichloromethane with 1% triethylamine) to give 35% yield, 0.111 g (0.071 mmol). TLC (66% ethyl acetate in dichloromethane) R_f = 0.25. M.P.: 67–70 °C. ¹H NMR (300 MHz, CDCl₃) δ: 0.90–1.06 (m, 6H), 1.55–1.76 (m, 2H), 1.76–1.91 (m, 2H), 1.91–2.20 (m, 5H), 2.23–2.47 (m, 4H), 2.71–2.92 (m, 1H), 3.06–3.15 (m, 1H), 3.15–3.27 (m, 1H), 3.69–3.82 (m, 1H), 3.98–4.11 (m, 1H), 4.39 (t, *J* = 9.82 Hz, 1H), 4.50–4.63 (m, 1H), 4.83–4.95 (m, 1H), 5.08–5.23 (m, 1H), 5.26–5.39 (m, 1H), 7.17–7.24 (m, 2H), 7.30–7.53 (m, 6H), 7.55 (s, 4H), 7.73 (s, 8H). ¹³C NMR (75 MHz, CDCl₃) δ: 14.7 (s), 17.9 (s), 26.1 (s), 26.1 (s), 26.5 (d, *J* = 3.0 Hz), 27.2 (s), 27.3 (s), 29.5 (s), 31.3 (d, *J* = 2.0 Hz), 32.9 (s), 35.4 (s), 35.5 (s), 46.8 (d, *J* = 5.0 Hz), 56.5 (s), 56.8 (s), 63.3 (d, *J* = 2.0 Hz), 65.8 (s), 69.8 (s), 71.8 (s), 101.8 (s), 102.0 (s), 104.7 (s), 104.9 (s), 117.6 (m), 119.3 (s), 120.9 (d, *J* = 3.0 Hz), 121.7 (d, *J* = 3.5 Hz), 122.9 (s), 126.5 (s), 126.6 (s), 127.0 (s), 128.8 (m), 129.2 (m), 109.7 (d, *J* = 2.0 Hz), 130.1 (s), 130.1 (s), 130.4 (s), 130.5 (s), 134.9 (s), 148.7 (s), 148.8 (s), 150.2 (s), 150.4 (s), 160.9 (s), 161.5 (s), 162.2 (s), 162.8 (s), 174.9 (s), 175.0 (s). ¹⁹F NMR (282 MHz, CDCl₃) δ: -63 (s). ³¹P NMR (121 MHz, CDCl₃) δ: 104.6 (s). IR (thin film): 2964, 2361, 2338, 1611, 1501, 1478,

1436, 1390, 1353, 1274, 1119, 1096, 1045, 943, 914, 886, 839, 776, 735, 713, 682, 669, 614, 556 cm^{-1} . HRMS $\text{C}_{30}\text{H}_{37}\text{N}_2\text{O}_3\text{PIr} [\text{M}]^+$ calculated 697.2171, observed 697.2176. $[\alpha]_D^{20} = -55.0$ (c 0.20, CHCl_3).

Synthetic Methods: Substrates

***Tert*-butyl (4-acetylphenyl)carbamate.** This carbamate was synthesized according to a published literature procedure, the schematic for which is given in Figure 2.14.⁵¹ Purity was assessed by comparison to published characterization data.⁵²

General Method A: 1,1-terminal alkene synthesis. This synthetic route is depicted in Figure 2.15. A round-bottom flask was charged with the corresponding bromobenzene (10.6 mmol, 2.5 equiv.), all of which were commercially available and used as received, with the exception of 3-bromophenyl 4-methylbenzenesulfonate and (3-bromophenoxy)(*tert*-butyl)diphenylsilane (*vide infra*). Under a nitrogen atmosphere, dry THF (24 mL) was added, and the reaction mixture was cooled to $-78\text{ }^\circ\text{C}$, followed by dropwise addition of *n*BuLi (10.6 mmol, 2.5 equiv.). After stirring at $-78\text{ }^\circ\text{C}$ for approximately 45 min., a solution of the corresponding acetophenone (4.250 mmol, 1 equiv.) in dry THF (9 mL) was added dropwise to the reaction mixture, which continued stirring at $-78\text{ }^\circ\text{C}$ for approximately 4 hrs. The reaction mixture was then quenched with H_2O . The organic phase was removed, and the aqueous phase was washed with EtOAc. The combined organic phases were dried with Na_2SO_4 and concentrated *in vacuo*. A solution of this product in 20 mL of CH_2Cl_2 (not dried) and 2 drops of concentrated HCl was stirred overnight. Next, H_2O was added to this solution, and the organic phase was extracted and subsequently washed with brine. Then, the combined aqueous phases were

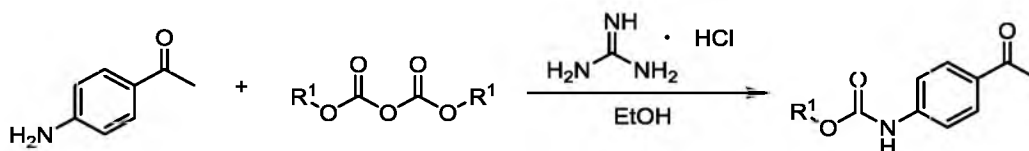


Figure 2.14. Carbamate synthesis reaction scheme.

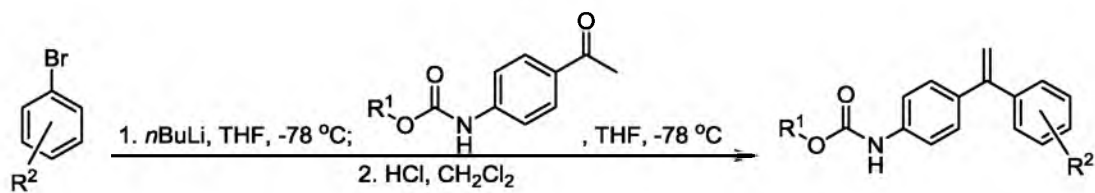


Figure 2.15. 1,1-terminal alkene synthesis via General Method A.

washed with CH_2Cl_2 . The organic phase was dried with Na_2SO_4 , concentrated *in vacuo*, and purified via flash-column chromatography.

General Method B: 1,1-terminal alkene synthesis. This synthetic route is depicted in Figure 2.16. Mg turnings (13.2 mmol, 1.38 equiv) were ground with mortar and pestle until shiny and added to an oven-dried round-bottom flask. Under a nitrogen atmosphere, 3 mL of THF (distilled from sodium benzophenone) were added, and the heterogeneous mixture stirred for 5 min at room temperature. After 2 drops of 1,2-dibromoethane (passed through a plug of activated, basic alumina prior to use) were added to the flask, the reaction mixture stirred for 10 min. Then, the respective bromobenzene derivative (12.0 mmol, 1.25 equiv) in THF (2 mL) was added all at once. After stirring 10 min at room temperature, 7 mL more of THF were added. The reaction mixture was stirred for approximately 2 h, at which time the respective acetophenone derivative (9.6 mmol, 1 equiv) in 10 mL of THF was added at room temperature, resulting in an exothermic reaction. After stirring overnight, the reaction mixture was quenched with H_2O , and EtOAc was added. The organic phase was removed and subsequently washed twice with saturated $\text{NH}_4\text{Cl}_{(\text{aq})}$ and once with brine. The resulting organic phase was dried with Na_2SO_4 and concentrated *in vacuo*. A solution of this product in 20 mL of CH_2Cl_2 (not dried prior to use) and 3 drops of concentrated HCl was stirred for 15–200 hours, as specified. Next, H_2O was added to this solution, and the organic phase was extracted and subsequently washed with brine. Then, the combined aqueous phases were washed with CH_2Cl_2 . The organic phase was dried with Na_2SO_4 , concentrated *in vacuo*. The crude product was purified via flash-column chromatography.

General Method C: 1,1-terminal alkene synthesis. This synthetic route is

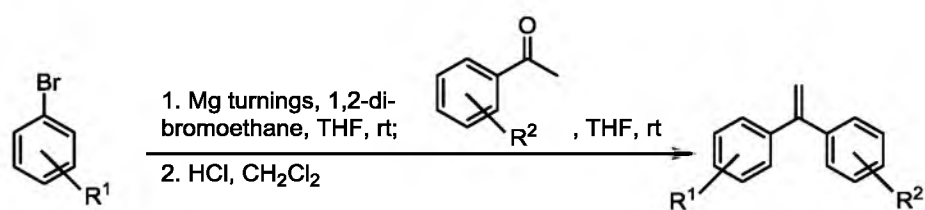


Figure 2.16. 1,1-terminal alkene synthesis via General Method B.

depicted in Figure 2.16. Mg turnings (13.2 mmol, 1.38 equiv) were ground with mortar and pestle until shiny and added to an oven-dried round-bottom flask. Under a nitrogen atmosphere, 3 mL of THF were added, and the heterogeneous mixture stirred for 5 min. at room temperature. After 2 drops of 1,2-dibromoethane (passed through a plug of activated, basic alumina prior to use) were added to the flask, the reaction mixture stirred for 10 minutes. Then, the respective bromobenzene derivative (12.0 mmol, 1.25 equiv) in THF (2 mL) was added all at once. After stirring 10 minutes at room temperature, 7 mL more of THF were added. The reaction mixture was stirred for approximately 2 hours, at which time the respective acetophenone derivative (9.6 mmol, 1 equiv) in 10 mL of THF was added at room temperature, resulting in an exothermic reaction. After stirring overnight, the reaction mixture was quenched with H₂O, and EtOAc was added. The organic phase was removed and subsequently washed twice with saturated NH₄Cl_(aq) and once with brine. The resulting organic phase was dried with Na₂SO₄, concentrated *in vacuo*, and passed through a silica column (using the same eluent as used for the final purification, unless otherwise noted) to remove the bulk of impurities. A solution of the resultant crude product in 20 mL of CH₂Cl₂ (not dried prior to use) and 3 drops of concentrated HCl was stirred for 15–96 hours, as specified. Next, H₂O was added to this solution, and the organic phase was extracted and subsequently washed with brine. Then, the combined aqueous phases were washed with CH₂Cl₂. The organic phase was dried with Na₂SO₄, concentrated *in vacuo*. The crude product was purified via flash-column chromatography.

1-bromo-3-butoxybenzene. To a round-bottom flask was added 3-bromophenol (11.560 mmol, 1 equiv.), 1-bromobutane (17.340 mmol, 1.5 equiv.), 4.6 mL of ethanol (200 proof), 0.46 mL deionized H₂O, and potassium carbonate (16.180 mmol, 1.4 equiv.).

After heating the reaction mixture to reflux for 20 hours, the reaction mixture was cooled, and the solvent was removed *in vacuo*. Diethyl ether was added to the remaining residue, followed by sequential washings with 1 M HCl (10 mL), H₂O (20 mL), 1 M NaOH (10 mL), and H₂O (20 mL). The organic phase was dried with Na₂SO₄. The solvent was removed and the product concentrated *in vacuo* to afford **S2**, a pale yellow liquid, in 45% isolated yield, 1.201 g (5.241 mmol). TLC (10% ethyl acetate in hexanes) R_f = 0.70. ¹H NMR (300 MHz, CDCl₃) δ: 0.98 (t, *J* = 7.41 Hz, 3H), 1.42–1.56 (m, 2H), 1.70–1.82 (m, 2H), 3.94 (t, *J* = 6.52 Hz, 2H), 6.80–6.86 (m, 1H), 7.03–7.09 (m, 2H), 7.09–7.17 (m, 1H). ¹³C NMR (126 MHz, CDCl₃) δ: 14.0 (s), 19.3 (s), 31.3 (s), 68.0 (s), 113.7 (s), 117.8 (s), 122.9 (s), 123.6 (s), 130.6 (s), 160.1 (s). IR (thin film): 2958, 2933, 2872, 2360, 1589, 1572, 1466, 1424, 1389, 1324, 1304, 1283, 1242, 1226, 1167, 1157, 1124, 1091, 1065, 1027, 1010, 991, 974, 909, 890, 856, 841, 762, 737, 679, 601 cm⁻¹. HRMS C₁₀H₁₄OBr [M+H]⁺: calculated 229.0228, observed 229.0225.

(3-bromophenoxy)(tert-butyl)diphenylsilane. This aryl bromide was synthesized according to a previously reported procedure,⁵³ which is depicted in Figure 2.17, and purified by flash silica gel column chromatography (10% ethyl acetate in hexanes with 1% triethylamine) to afford a clear, colorless oil in 80% isolated yield, 5.916 g (14.380 mmol). TLC (100% hexanes) R_f = 0.30; ¹H NMR (500 MHz, CD₂Cl₂): δ 1.17 (s, 9H), 6.72 (ddd, *J* = 8.30 Hz, 2.44 Hz, 0.98 Hz, 1H), 6.97 (t, *J* = 8.30 Hz, 1H), 7.04–7.08 (m, 1H), 7.08–7.12 (m, 1H), 7.41–7.47 (m, 4H), 7.47–7.53 (m, 2H), 7.76–7.81 (m, 4H); ¹³C NMR (126 MHz, CD₂Cl₂): δ 19.7, 26.6, 118.9, 122.6, 123.6, 124.6, 128.3, 130.5, 130.6, 132.7, 135.9, 156.9; IR (thin film): 3071, 2958, 2931, 2893, 2858, 1586, 1568, 1472, 1427, 1391, 1362, 1269, 1236, 1190, 1158, 1113, 1086, 1063, 996, 934, 861, 822, 771, 738, 699, 680, 665, 654, 613

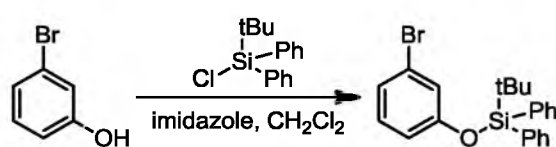


Figure 2.17. Schematic for the silylation of 3-bromophenol.

cm⁻¹; HRMS C₂₂H₂₃BrOSiK [M+K]⁺ calculated 449.0339, observed 449.0344.

***Tert*-butyl (4-(1-(3,5-dimethoxyphenyl)vinyl)phenyl)carbamate (1).** Alkene **1** was synthesized according to General Method A from 4.250 mmol of the corresponding acetophenone and purified via flash silica-gel column chromatography (using 30% ethyl acetate in hexanes) to afford isolated product, a white solid, in 78% yield, 1.178 g (3.315 mmol). TLC (20% ethyl acetate in hexanes) R_f = 0.36. M.P.: 76–79 °C ¹H NMR (300 MHz, CDCl₃) δ: 1.52 (s, 9H), 3.76 (s, 6H), 5.38 (d, *J* = 1.24 Hz, 1H), 5.41 (d, *J* = 1.24 Hz, 1H), 6.42–6.45 (m, 1H), 6.48 (d, *J* = 2.33 Hz, 2H), 6.50 (bs, 1H), 7.27–7.35 (m, 4H). ¹³C NMR (75 MHz, CDCl₃) δ: 28.4 (s), 55.4 (s), 80.7 (s), 100.0 (s), 106.7 (s), 113.6 (s), 118.2 (s), 128.9 (s), 135.9 (s), 138.1 (s), 143.9 (s), 149.5 (s), 152.8 (s), 160.6 (s). IR (thin film): 3333, 2976, 2837, 2360, 1728, 1701, 1589, 1521, 1456, 1422, 1406, 1392, 1366, 1348, 1314, 1230, 1204, 1154, 1051, 1027, 1015, 901, 840, 771, 731, 688, 668, 610 cm⁻¹. HRMS C₂₁H₂₅NO₄Na [M+Na]⁺ calculated 378.1681, observed 378.1690.

***Tert*-butyl (4-(1-(3-methoxyphenyl)vinyl)phenyl)carbamate (2).** Alkene **2** was synthesized according to General Method A from 3.190 mmol of the corresponding acetophenone and purified via flash silica-gel column chromatography (using 20% ethyl acetate in hexanes with 1% triethylamine) to afford isolated product, a clear, pale yellow liquid, in 14% yield, 0.149 g (0.459 mmol). TLC (30% ethyl acetate in hexanes) R_f = 0.56. ¹H NMR (300 MHz, CDCl₃) δ: 1.53 (s, 9H), 3.79 (s, 3H), 5.39 (d, *J* = 1.24 Hz, 1H), 5.42 (d, *J* = 1.24 Hz, 1H), 6.52 (bs, 1H), 6.83–6.96 (m, 3H), 7.20–7.36 (m, 5H). ¹³C NMR (126 MHz, CDCl₃) δ: 28.5 (s), 55.4 (s), 80.8 (s), 113.4 (s), 113.7 (s), 114.0 (s), 118.3 (s), 121.1 (s), 129.0 (s), 129.2 (s), 136.2 (s), 138.1 (s), 143.2 (s), 149.5 (s), 152.8 (s), 159.6 (s). IR (thin film): 3331, 2976, 2360, 1727, 1700, 1608, 1584, 1519, 1454, 1429, 1404, 1392,

1367, 1313, 1285, 1228, 1155, 1049, 1015, 897, 841, 784, 745, 715, 684, 589 cm^{-1} . HRMS $\text{C}_{20}\text{H}_{23}\text{NO}_3\text{Na}$ $[\text{M}+\text{Na}]^+$ calculated 348.1576, observed 348.1575.

***Tert*-butyl (4-(1-(3-butoxyphenyl)vinyl)phenyl)carbamate (3).** Alkene **3** was synthesized according to the General Method A from 1.920 mmol of the corresponding acetophenone and purified via flash silica-gel column chromatography (using 10% ethyl acetate in hexanes) to afford isolated product, a clear, colorless liquid, in 33% yield, 0.236 g (0.642 mmol). TLC (20% ethyl acetate in hexanes) $R_f = 0.54$. ^1H NMR (500 MHz, CDCl_3) δ : 0.96 (t, $J = 7.33$, 3H), 1.45–1.51 (m, 2H), 1.53 (s, 9H), 1.71–1.78 (m, 2H), 3.94 (t, $J = 6.60$ Hz, 2H), 5.38 (d, $J = 1.47$, 1H), 5.40 (d, $J = 1.47$, 1H), 6.51 (bs, 1H), 6.84–6.88 (m, 2H), 6.88–6.92 (m, 1H), 7.22 (t, $J = 7.82$, 1H), 7.26–7.30 (m, 2H), 7.32 (d, $J = 8.31$, 2H). ^{13}C NMR (126 MHz, CDCl_3) δ : 14.0 (s), 19.4 (s), 28.5 (s), 31.5 (s), 67.8 (s), 80.8 (s), 113.6 (s), 113.9 (s), 114.7 (s), 118.3 (s), 120.9 (s), 129.0 (s), 129.2 (s), 136.3 (s), 138.1 (s), 143.1 (s), 149.5 (s), 152.8 (s), 159.1 (s). IR (thin film): 3333, 2959, 2932, 2871, 1729, 1700, 1584, 1518, 1435, 1404, 1392, 1366, 1313, 1285, 1224, 1153, 1050, 1027, 1014, 980, 933, 900, 840, 781, 733, 714, 683, 581 cm^{-1} . HRMS $\text{C}_{23}\text{H}_{29}\text{NO}_3\text{Na}$ $[\text{M}+\text{Na}]^+$ calculated 390.2045, observed 390.2048.

***Tert*-butyl (4-(1-(3,5-dimethylphenyl)vinyl)phenyl)carbamate (4).** Alkene **4** was synthesized according to General Method A from 3.190 mmol of the corresponding acetophenone and purified via flash silica-gel column chromatography (using 15% ethyl acetate in hexanes) to afford isolated product, a white solid, in 95% yield, 0.978 g (3.023 mmol). TLC (20% ethyl acetate in hexanes) $R_f = 0.52$. M.P.: 98–101 $^\circ\text{C}$. ^1H NMR (500 MHz, CDCl_3) δ : 1.54 (s, 9H), 2.31 (s, 6H), 5.36 (d, $J = 1.47$ Hz, 1H), 5.38 (d, $J = 1.47$ Hz, 1H), 6.55 (bs, 1H), 6.93–6.99 (m, 3H), 7.26–7.31 (m, 2H), 7.33 (d, $J = 8.79$ Hz, 2H). ^{13}C

NMR (500 MHz, CDCl₃) δ : 21.4 (s), 28.5 (s), 80.7 (s), 113.3 (s), 118.3 (s), 126.3 (s), 129.0 (s), 129.5 (s), 136.6 (s), 137.7 (s), 138.0 (s), 141.7 (s), 149.8 (s), 152.9 (s). IR (thin film): 3329, 2977, 2918, 2360, 1730, 1701, 1610, 1593, 1518, 1455, 1405, 1392, 1367, 1336, 1313, 1292, 1230, 1156, 1091, 1052, 1027, 1015, 894, 842, 771, 731, 686, 610, 542 cm⁻¹. HRMS C₂₁H₂₅NO₂Na [M+Na]⁺ calculated 346.1783, observed 346.1779.

***Tert*-butyl (4-(1-(*m*-tolyl)vinyl)phenyl)carbamate (5).** Alkene **5** was synthesized according to General Method A from 3.190 mmol of the corresponding acetophenone and purified via flash silica-gel column chromatography (using 15% ethyl acetate in hexanes) to afford isolated product, a yellow-white solid, in 80% yield, 0.788 g (2.546 mmol). TLC (20% ethyl acetate in hexanes) R_f = 0.52. M.P.: 93–94 °C. ¹H NMR (500 MHz, CDCl₃) δ : 1.54 (s, 9H), 2.35 (s, 3H), 5.37 (d, *J* = 1.47 Hz, 1H), 5.40 (d, *J* = 1.47 Hz, 1H), 6.53 (bs, 1H), 7.12–7.14 (m, 1H), 7.14–7.16 (m, 2H), 7.20–7.25 (m, 1H), 7.26–7.28 (m, 1H), 7.28–7.30 (m, 1H), 7.33 (d, *J* = 8.79 Hz, 2H). ¹³C NMR (126 MHz, CDCl₃) δ : 21.6 (s), 28.5 (s), 80.8 (s), 113.4 (s), 118.3 (s), 125.6 (s), 128.2 (s), 128.6 (s), 129.0 (s), 129.1 (s), 136.5 (s), 137.8 (s), 138.0 (s), 141.7 (s), 149.7 (s), 152.9 (s). IR (thin film): 3329, 2977, 2929, 1729, 1699, 1610, 1585, 1518, 1454, 1403, 1392, 1367, 1313, 1290, 1231, 1155, 1052, 1027, 1015, 893, 841, 791. 744, 715, 683, 595 cm⁻¹. HRMS C₂₀H₂₃NO₂Na [M+Na]⁺ calculated 332.1626, observed 332.1622.

1-methoxy-3-(1-phenylvinyl)benzene (6). Alkene **6** was synthesized according to General Method C from 9.6 mmol of 1-(3-methoxyphenyl)ethanone, stirring with HCl for 96 hours, and purified via flash silica-gel column chromatography (using 15% ethyl acetate in hexanes), affording isolated product, a clear, colorless oil, in 42% yield, 0.853 g (4.058 mmol). TLC (20% ethyl acetate in hexanes) R_f = 0.55. ¹H NMR (300 MHz, CDCl₃) δ : 3.80

(s, 3H), 5.47 (s, 2H), 6.85–6.91 (m, 2H), 6.91–6.96 (m, 1H), 7.23–7.29 (m, 1H), 7.30–7.38 (m, 5H). ^{13}C NMR (126 MHz, CDCl_3) δ : 55.4 (s), 113.3 (s), 114.1 (s), 114.6 (s), 121.0 (s), 127.9 (s), 128.3 (s), 128.4 (s), 129.3 (s), 141.5 (s), 143.1 (s), 150.1 (s), 159.6 (s). IR (thin film): 3055, 3027, 2937, 2833, 2359, 2340, 1597, 1575, 1487, 1463, 1447, 1431, 1329, 1285, 1240, 1183, 1159, 1133, 1047, 898, 863, 777, 723, 699, 591, 549 cm^{-1} . HRMS $\text{C}_{15}\text{H}_{15}\text{O}$ $[\text{M}+\text{H}]^+$ calculated 211.1123, observed 211.1122.

1-methoxy-4-(1-phenylvinyl)benzene (7). Alkene **7** was synthesized according to General Method C from 9.6 mmol of 1-(4-methoxyphenyl)ethanone, stirring with HCl for 65 hours, and purified via flash silica-gel column chromatography (using 15% ethyl acetate in hexanes), affording isolated product, a white solid, in 19% yield, 0.379 g (1.801 mmol). TLC (20% ethyl acetate in hexanes) $R_f = 0.53$. M.P.: 68–72 °C. ^1H NMR (300 MHz, CDCl_3) δ : 3.84 (s, 3H), 5.37 (d, $J = 1.24$ Hz, 1H), 5.41 (d, $J = 1.23$ Hz, 1H), 6.85–6.88 (m, 1H), 6.88–6.91 (m, 1H), 7.26–7.40 (m, 7H). ^{13}C NMR (126 MHz, CDCl_3) δ : 55.4 (s), 113.1 (s), 113.6 (s), 127.8 (s), 128.3 (s), 128.4 (s), 129.5 (s), 134.1 (s), 141.9 (s), 149.6 (s), 159.5 (s). IR (thin film): 3093, 3031, 3005, 2951, 2904, 2835, 2536, 2359, 2341, 2029, 1967, 1907, 1811, 1781, 1715, 1663, 1601, 1572, 1506, 1491, 1456, 1441, 1415, 1328, 1314, 1288, 1245, 1178, 1161, 1151, 1116, 1082, 1069, 1027, 975, 963, 901, 841, 784, 747, 707, 681, 650, 625, 612, 580, 551 cm^{-1} . HRMS $\text{C}_{15}\text{H}_{15}\text{O}$ $[\text{M}+\text{H}]^+$ calculated 211.1123, observed 211.1124.

1,3-diethyl-5-(1-phenylvinyl)benzene (8). Alkene **8** was synthesized according to General Method C (except THF was distilled from sodium benzophenone) from 9.6 mmol of acetophenone (passed through a plug of activated, basic alumina prior to use), stirring with HCl for 40 hours, and purified via flash silica-gel column chromatography (using 15%

ethyl acetate in hexanes for removal of bulk impurities prior to stirring in HCl and 100% hexanes for final purification), affording isolated product, a clear, colorless liquid, in 62% yield, 1.411 g (5.970 mmol). TLC (100% hexanes) $R_f = 0.30$. ^1H NMR (300 MHz, CDCl_3) δ : 1.25 (t, $J = 7.55$ Hz, 6H), 2.64 (q, $J = 7.60$ Hz, 4H), 5.45–5.49 (m, 2H), 7.03 (s, 3H), 7.32–7.43 (m, 5H). ^{13}C NMR (126 MHz, CDCl_3) δ : 15.8 (s), 29.0 (s), 114.1 (s), 125.5 (s), 127.1 (s), 127.7 (s), 128.2 (s), 128.4 (s), 141.6 (s), 141.9 (s), 144.2 (s), 150.5 (s). IR (thin film): 3022, 2962, 2930, 2871, 2360, 2340, 1792, 1700, 1653, 1594, 1575, 1493, 1457, 1443, 1374, 1347, 1318, 1237, 1144, 1095, 1072, 1027, 893, 872, 776, 726, 699, 668, 613 cm^{-1} . HRMS $\text{C}_{18}\text{H}_{21}$ $[\text{M}+\text{H}]^+$ calculated 237.1643, observed 237.1639.

1,3-dimethoxy-5-(1-(4-methoxyphenyl)vinyl)benzene (17). This alkene was synthesized according to General Method C from 9.6 mmol of 1-(4-methoxyphenyl)ethanone, stirring with HCl for 96 hours, and purified via flash silica-gel column chromatography (using 15% ethyl acetate in hexanes), affording isolated product, a clear, colorless liquid, in 39% yield, 1.021 g (3.777 mmol). TLC (15% ethyl acetate in hexanes) $R_f = 0.28$. ^1H NMR (300 MHz, CDCl_3) δ : 3.78 (s, 6H), 3.83 (s, 3H), 5.36–5.39 (m, 1H), 5.40–5.42 (m, 1H), 6.44–6.48 (m, 1H), 6.49–6.54 (m, 2H), 6.84–6.91 (m, 2H), 7.28–7.34 (m, 2H). ^{13}C NMR (126 MHz, CDCl_3) δ : 55.4 (s), 55.5 (s), 99.9 (s), 106.7 (s), 113.1 (s), 113.6 (s), 129.5 (s), 133.8 (s), 144.1 (s), 149.6 (s), 159.5 (s), 160.6 (s). IR (thin film): 2999, 2935, 2835, 2359, 1588, 1509, 1453, 1421, 1344, 1317, 1293, 1265, 1246, 1203, 1177, 1153, 1132, 1113, 1087, 1063, 1049, 1033, 992, 935, 896, 835, 813, 721, 689, 668, 595, 539 cm^{-1} . HRMS $\text{C}_{17}\text{H}_{19}\text{O}_3$ $[\text{M}+\text{H}]^+$ calculated 271.1334, observed 271.1331.

1,3-dimethoxy-5-(1-phenylvinyl)benzene (18). This alkene was synthesized according to General Method B from 9.6 mmol of acetophenone (passed through a plug of

activated, basic alumina prior to use), stirring with HCl overnight, and purified via flash silica-gel column chromatography (using 2% acetone in hexanes), followed by bulb-to-bulb vacuum distillation with heating, distilling off a lower-boiling impurity and affording a clear, yellow liquid in 15% isolated yield, 0.350 g (1.455 mmol). TLC (20% ethyl acetate in hexanes) $R_f = 0.51$. $^1\text{H NMR}$ (500 MHz, CDCl_3) δ : 3.79 (s, 6H), 5.49 (s, 2H), 6.48 (t, $J = 2.44$ Hz, 1H), 6.53 (d, $J = 1.95$ Hz, 2H), 7.31–7.40 (m, 5H). $^{13}\text{C NMR}$ (126 MHz, CDCl_3) δ : 55.5 (s), 99.9 (s), 106.7 (s), 114.5 (s), 127.9 (s), 128.3 (s), 128.3 (s), 141.3 (s), 143.8 (s), 150.1 (s), 160.7 (s). IR (thin film): 2999, 2935, 2836, 1587, 1493, 1452, 1421, 1342, 1288, 1266, 1203, 1151, 1091, 1062, 1047, 1027, 992, 934, 899, 835, 777, 726, 697, 643, 615, 538 cm^{-1} . HRMS $\text{C}_{16}\text{H}_{17}\text{O}_2$ $[\text{M}+\text{H}]^+$ calculated 241.1229 observed 241.1225.

1,3-dimethoxy-5-(1-(4-(trifluoromethyl)phenyl)vinyl)benzene (19). This alkene was synthesized according to General Method C from 9.6 mmol of 1-(4-(trifluoromethyl)phenyl)ethanone, stirring in HCl approximately 10 days, and purified via flash silica-gel column chromatography (using 15% ethyl acetate in hexanes), affording isolated product, a clear, yellow liquid, in 4% yield, 0.117 g (0.379 mmol). TLC (15% ethyl acetate in hexanes) $R_f = 0.37$. $^1\text{H NMR}$ (300 MHz, CDCl_3) δ : 3.79 (s, 6H), 5.53 (d, $J = 0.83$ Hz, 1H), 5.59 (d, $J = 0.82$ Hz, 1H), 6.47–6.51 (m, 3H), 7.48 (d, $J = 8.65$ Hz, 2H), 7.61 (dd, $J = 8.10$ Hz, 0.55 Hz, 2H). $^{13}\text{C NMR}$ (126 MHz, CDCl_3) δ : 55.5 (s), 100.1 (s), 106.7 (s), 116.2 (s), 124.4 (q, $J = 272.8$ Hz), 125.3 (q, $J = 3.78$ Hz), 128.7 (s), 129.9 (q, $J = 32.3$ Hz), 142.9 (s), 144.9 (s), 149.0 (s), 160.9 (s). $^{19}\text{F NMR}$ (282 MHz, CDCl_3) δ : -63. IR (thin film): 2938, 2839, 2360, 2341, 1591, 1457, 1423, 1324, 1268, 1206, 1157, 1124, 1089, 1065, 1016, 908, 849, 744, 689, 668, 648 cm^{-1} . HRMS $\text{C}_{17}\text{H}_{16}\text{O}_2\text{F}_3$ $[\text{M}+\text{H}]^+$ calculated 309.1102, observed 309.1100.

1,3-dimethoxy-5-(1-(3-methoxyphenyl)vinyl)benzene (20). This alkene was synthesized according to General Method C from 9.6 mmol of 1-(3,5-dimethoxyphenyl)ethanone, stirring with HCl for 44 hours, and purified via flash silica-gel column chromatography (using 15% ethyl acetate in hexanes), affording isolated product, a clear, colorless liquid, in 62% yield, 1.606 g (5.941 mmol). TLC (15% ethyl acetate in hexanes) $R_f = 0.36$. ^1H NMR (300 MHz, CDCl_3) δ : 3.77 (s, 6H), 3.80 (s, 3H), 5.46 (s, 2H), 6.42–6.45 (m, 1H), 6.49 (d, $J = 2.33$ Hz, 2H), 6.84–6.96 (m, 3H), 7.21–7.28 (m, 1H). ^{13}C NMR (75 MHz, CDCl_3) δ : 55.3 (s), 55.5 (s), 100.0 (s), 106.7 (s), 113.3 (s), 114.0 (s), 114.7 (s), 120.9 (s), 129.2 (s), 142.7 (s), 143.6 (s), 150.0 (s), 159.5 (s), 160.6 (s). IR (thin film): 2999, 2937, 2835, 1586, 1486, 1453, 1422, 1346, 1317, 1284, 1249, 1227, 1203, 1153, 1063, 1046, 993, 940, 926, 904, 882, 838, 786, 730, 706, 688, 630 cm^{-1} . HRMS $\text{C}_{17}\text{H}_{19}\text{O}_3$ $[\text{M}+\text{H}]^+$ calculated 271.1334, observed 271.1328.

1,3-dimethoxy-5-(1-(*p*-tolyl)vinyl)benzene (21). This alkene was synthesized according to General Method C (with the exception that THF distilled from sodium benzophenone was used) from 9.6 mmol of 1-(*p*-tolyl)ethanone, stirring with HCl for 40 hours, and purified via flash silica-gel column chromatography (using 15% ethyl acetate in hexanes), affording isolated product, a clear, faintly yellow liquid, in 21% yield, 0.514 g (2.020 mmol). TLC (15% ethyl acetate in hexanes) $R_f = 0.44$. ^1H NMR (500 MHz, CDCl_3) δ : 2.38 (s, 3H), 3.78 (s, 6H), 5.42 (d, $J = 1.02$ Hz, 1H), 5.44 (d, $J = 0.98$ Hz, 1H), 6.44–6.46 (m, 1H), 6.51 (d, $J = 1.96$ Hz, 2H), 7.15 (d, $J = 8.31$ Hz, 2H), 7.24–7.28 (m, 2H). ^{13}C NMR (126 MHz, CDCl_3) δ : 21.3 (s), 55.5 (s), 99.9 (s), 106.8 (s), 113.9 (s), 128.2 (s), 129.0 (s), 137.7 (s), 138.4 (s), 144.0 (s), 150.0 (s), 160.6 (s). IR (thin film): 2998, 2935, 2836, 2360, 1588, 1510, 1452, 1421, 1341, 1317, 1307, 1263, 1203, 1152, 1086, 1063,

1048, 1019, 992, 934, 899, 824, 730, 687, 646, 593, 538 cm^{-1} . HRMS $\text{C}_{17}\text{H}_{19}\text{O}_2$ $[\text{M}+\text{H}]^+$ calculated 255.1385, observed 255.1389.

4-(1-(3,5-dimethoxyphenyl)vinyl)-1,1'-biphenyl (22). This alkene was synthesized according to General Method C from 9.6 mmol of 1-(3,5-dimethoxyphenyl)ethanone, stirring with HCl for 100 hours, and purified via flash silica-gel column chromatography (using 15% ethyl acetate in hexanes), affording isolated product, a white solid, in 52% yield, 1.580 g (4.995 mmol). TLC (10% ethyl acetate in hexanes) $R_f = 0.32$. M.P.: 73–75 °C. ^1H NMR (300 MHz, CDCl_3) δ : 3.79 (s, 6H), 5.49 (d, $J = 1.24$ Hz, 1H), 5.54 (d, $J = 1.23$ Hz, 1H), 6.46–6.49 (m, 1H), 6.54 (d, $J = 2.33$ Hz, 2H), 7.32–7.40 (m, 1H), 7.42–7.49 (m, 4H), 7.55–7.65 (m, 4H). ^{13}C NMR (126 MHz, CDCl_3) δ : 55.5 (s), 100.0 (s), 106.8 (s), 114.6 (s), 127.0 (s), 127.2 (s), 127.5 (s), 128.7 (s), 128.9 (s), 140.2 (s), 140.7 (s), 140.9 (s), 143.8 (s), 149.7 (s), 160.7 (s). IR (thin film): 3028, 2999, 2935, 2836, 2361, 2338, 1589, 1486, 1453, 1422, 1350, 1307, 1272, 1259, 1204, 1154, 1064, 1049, 1007, 935, 902, 846, 794, 771, 742, 718, 697, 668, 617 cm^{-1} . HRMS $\text{C}_{22}\text{H}_{21}\text{O}_2$ $[\text{M}+\text{H}]^+$ calculated 317.1542, observed 317.1540.

1-(1-(4-chlorophenyl)vinyl)-3,5-dimethoxybenzene (23). This alkene was synthesized according to Method B from 9.6 mmol of 1-(4-chlorophenyl)ethanone, stirring with HCl for 100 hours, and purified via flash silica-gel column chromatography (using 15% ethyl acetate in hexanes), affording isolated product, a clear, pale yellow liquid, in 43% yield, 1.144 g (4.165 mmol). TLC (10% ethyl acetate in hexanes) $R_f = 0.37$. ^1H NMR (300 MHz, CDCl_3) δ : 3.77 (s, 6H), 5.44 (d, $J = 1.10$ Hz, 1H), 5.47 (d, $J = 1.10$ Hz, 1H), 6.46 (s, 3H), 7.27–7.33 (m, 4H). ^{13}C NMR (126 MHz, CDCl_3) δ : 55.5 (s), 100.1 (s), 106.7 (s), 114.9 (s), 128.5 (s), 129.7 (s), 133.8 (s), 139.8 (s), 143.3 (s), 149.0 (s), 160.7 (s). IR

(thin film): 3000, 2936, 2837, 2362, 2338, 1589, 1489, 1454, 1422, 1350, 1275, 1204, 1155, 1093, 1064, 1050, 1013, 935, 903, 835, 787, 717, 688, 668 cm^{-1} . HRMS $\text{C}_{16}\text{H}_{16}\text{O}_2\text{Cl}$ $[\text{M}+\text{H}]^+$ calculated 275.0839, observed 275.0836.

1-(1-(3-isopropylphenyl)vinyl)-3,5-dimethoxybenzene (24). This alkene was synthesized according to General Method C from 9.6 mmol of 1-(3,5-dimethoxyphenyl)ethanone, stirring with HCl for 44 hours, and purified via flash silica-gel column chromatography (using 15% ethyl acetate in hexanes), affording isolated product, a clear, yellow liquid, in 54% yield, 1.477 g (5.229 mmol). TLC (15% ethyl acetate in hexanes) $R_f = 0.49$. ^1H NMR (300 MHz, CDCl_3) δ : 1.25 (d, $J = 6.87$ Hz, 6H), 2.90 (sep, $J = 6.86$ Hz, 1H), 3.77 (s, 6H), 5.46 (s, 2H), 6.44–6.47 (m, 1H), 6.50–6.54 (m, 2H), 7.14–7.21 (m, 2H), 7.21–7.29 (m, 2H). ^{13}C NMR (75 MHz, CDCl_3) δ : 24.2 (s), 34.2 (s), 55.5 (s), 100.0 (s), 106.7 (s), 114.4 (s), 125.9 (s), 126.0 (s), 126.6 (s), 128.2 (s), 141.1 (s), 143.9 (s), 148.8 (s), 150.3 (s), 160.6 (s). IR (thin film): 2959, 2837, 2175, 1980, 1591, 1455, 1422, 1351, 1279, 1204, 1156, 1065, 1050, 897, 836, 802, 707, 636 cm^{-1} . HRMS $\text{C}_{19}\text{H}_{23}\text{O}_2$ $[\text{M}+\text{H}]^+$ calculated 283.1698, observed 283.1695.

1-(1-(3,5-diethylphenyl)vinyl)-3,5-dimethoxybenzene (25). This alkene was synthesized according to General Method B from 9.6 mmol of 1-(3,5-dimethoxyphenyl)ethanone and stirred with HCl for 4.5 days. The product was purified via flash silica gel column chromatography (15% ethyl acetate in hexanes, to remove the majority of impurities prior to stirring in HCl, and 15% ethyl acetate in hexanes for purification of alkene) to afford isolated product, a clear, colorless oil, in 58% yield, 1.507 g (5.575 mmol). TLC (10% ethyl acetate in hexanes) $R_f = 0.39$. ^1H NMR (300 MHz, CDCl_3) δ : 1.24 (t, $J = 7.55$ Hz, 6H), 2.63 (q, $J = 7.60$ Hz, 4H), 3.78 (s, 6H), 5.45 (d, $J =$

1.24 Hz, 1H), 5.46 (d, $J = 1.23$ Hz, 1H), 6.45–6.48 (m, 1H), 6.53 (d, $J = 2.33$ Hz, 2H), 7.02 (s, 3H); ^{13}C NMR (126 MHz, CDCl_3) δ : 15.9, 29.0, 55.5, 100.0, 106.7, 114.2, 125.4, 127.2, 141.2, 144.1, 144.2, 150.4, 160.6; IR (thin film): 2962, 2933, 2872, 2837, 2361, 2338, 1591, 1455, 1422, 1354, 1329, 1279, 1204, 1155, 1065, 940, 873, 837, 711, 687, 668 cm^{-1} . HRMS $\text{C}_{20}\text{H}_{25}\text{O}_2$ $[\text{M}+\text{H}]^+$ calculated 297.1855, observed 297.1852.

1,2,3-trimethoxy-5-(1-phenylvinyl)benzene (26). This alkene was synthesized according to General Method C (with the exception that the magnesium turnings, 1,2-dibromoethane, and THF were heated with a heat gun and then stirred for 5 hours) from 9.6 mmol of acetophenone (in 4.5 mL of THF) and stirred with HCl overnight. The product was purified via flash silica gel column chromatography (2% acetone in hexanes, to remove the majority of impurities prior to stirring in HCl, and 15% ethyl acetate in hexanes for purification of alkene), followed by bulb-to-bulb distillation to remove remaining low boiling impurities, to afford isolated product, a clear, pale yellow oil, in 17% yield, 0.439 g (1.625 mmol). TLC (20% ethyl acetate in hexanes) $R_f = 0.36$. ^1H NMR (300 MHz, CDCl_3) δ : 3.81 (s, 6H), 3.88 (s, 3H), 5.42 (d, $J = 1.24$ Hz, 1H), 5.45 (d, $J = 1.23$ Hz, 1H), 6.55 (s, 2H), 7.31–7.40 (m, 5H). ^{13}C NMR (126 MHz, CDCl_3) δ : 56.3, 61.1, 105.8, 114.1, 128.0, 128.3, 128.4, 137.4, 138.0, 141.3, 150.2, 153.0. IR (thin film): 2936, 2834, 2360, 2340, 1700, 1653, 1578, 1503, 1462, 1409, 1347, 1267, 1234, 1182, 1123, 1026, 1006, 945, 898, 843, 779, 738, 700, 669, 622, 580 cm^{-1} . HRMS $\text{C}_{17}\text{H}_{19}\text{O}_3$ $[\text{M}+\text{H}]^+$ calculated 271.1334, observed 271.1327.

***Tert*-butyl (4-(1-(4-ethylphenyl)vinyl)phenyl)carbamate (27).** This alkene was synthesized according to General Method A from 3.19 mmol of *tert*-butyl (4-acetylphenyl)carbamate and purified by flash silica-gel column chromatography (10%

ethyl acetate in hexanes) to afford isolated product in 49% yield, 0.509 g (1.574 mmol). M.P.: 105–107 °C. TLC (20% ethyl acetate in hexanes) $R_f = 0.54$. ^1H NMR (300 MHz, CDCl_3) δ : 1.26 (t, $J = 7.62$ Hz, 3H), 1.53 (s, 9H), 2.67 (q, $J = 7.60$ Hz, 2H), 5.37 (s, 2H), 6.50 (bs, 1H), 7.16 (d, $J = 7.96$ Hz, 2H), 7.23–7.36 (m, 6H). ^{13}C NMR (126 MHz, CDCl_3) δ : 15.64, 28.49, 28.70, 80.74, 112.97, 118.28, 127.76, 128.37, 129.08, 136.59, 137.99, 139.00, 143.99, 149.46, 152.85. IR (thin film): 3327, 2967, 2931, 1730, 1699, 1609, 1587, 1520, 1455, 1406, 1392, 1367, 1313, 1231, 1158, 1121, 1076, 1052, 1016, 895, 839, 772, 740, 668, 617, 582 cm^{-1} . HRMS $\text{C}_{21}\text{H}_{25}\text{NO}_2\text{Na}$ $[\text{M}+\text{Na}]^+$ calculated 346.1783, observed 346.1791.

***Tert*-butyl (4-(1-(3-((*tert*-butyldiphenylsilyl)oxy)phenyl)vinyl)phenyl)carbamate.** This alkene was synthesized according to General Method A from 4.894 mmol of *tert*-butyl (4-acetylphenyl)carbamate and purified via flash silica gel column chromatography (10% ethyl acetate in hexanes) to afford isolated product, a clear, pale yellow, viscous oil, in 26% yield, 0.694 g (1.263 mmol). TLC (20% ethyl acetate in hexanes) $R_f = 0.49$. ^1H NMR (500 MHz, CDCl_3) δ : 1.10 (s, 9H), 1.54 (s, 9H), 5.15 (d, $J = 0.98$ Hz), 5.27 (d, $J = 0.98$, 1H), 6.48 (bs, 1H), 6.67–6.73 (m, 1H), 6.77 (t, $J = 1.96$ Hz, 1H), 6.78–6.84 (m, 1H), 6.98–7.06 (m, 1H), 7.02 (t, $J = 7.82$ Hz, 1H), 7.13–7.17 (m, 2H), 7.23–7.29 (m, 1H), 7.33–7.39 (m, 4H), 7.39–7.45 (m, 2H), 7.68–7.72 (m, 4H); ^{13}C NMR (126 MHz, CDCl_3) δ : 19.6, 26.7, 28.5, 80.7, 113.4, 118.2, 119.2, 120.0, 121.4, 127.9, 128.9, 130.0, 133.1, 135.0, 135.7, 136.2, 137.9, 142.8, 149.2, 155.6. IR (thin film): 3330, 2975, 2931, 2858, 1711, 1576, 1518, 1500, 1482, 1427, 1404, 1392, 1367, 1313, 1267, 1232, 1155, 1112, 1051, 1015, 1027, 1001, 966, 906, 843, 822, 774, 791, 730, 699, 648, 611 cm^{-1} . HRMS $\text{C}_{35}\text{H}_{39}\text{NO}_3\text{SiNa}$ $[\text{M}+\text{Na}]^+$ calculated 572.2597, observed 572.2610.

3-(1-(4-((*tert*-butoxycarbonyl)amino)phenyl)vinyl)phenyl acetate (28). This alkene was afforded by subjecting *tert*-butyl (4-(1-(3-((*tert*-butyldiphenylsilyl)oxy)phenyl)vinyl)phenyl)carbamate (0.61 mmol) to a desilylation protocol,⁵⁴ resulting in 0.180 g (0.579 mmol) phenolic alkene, which was added to a flame-dried 10 mL round bottom flask, followed by addition of CH₂Cl₂ (1.16 mL), triethylamine (1.2 equiv, 0.695 mmol), and distilled acetic anhydride (1.2 equiv, 0.695 mmol). After stirring the reaction mixture at room temperature overnight, the solvent was removed and the resulting material was dissolved in ethyl acetate, washed with 1 M NaOH and brine, dried with Na₂SO₄, and concentrated. Following purification via column chromatography (ethyl acetate in hexanes), the product, a white-peach solid, was afforded in 78% isolated yield, 0.160 g (0.454 mmol). M.P.: 118–121 °C. TLC (30% ethyl acetate in hexanes) R_f = 0.47. ¹H NMR (500 MHz, CDCl₃) δ: 1.52 (s, 9H), 2.28 (s, 3H), 5.41 (s, 1H), 5.43 (s, 1H), 6.51 (bs, 1H), 7.02–7.06 (m, 2H), 7.22 (dd, *J* = 7.82 Hz, 0.98 Hz, 1H), 7.24–7.29 (m, 2H), 7.31–7.36 (m, 3H). ¹³C NMR (126 MHz, CDCl₃) δ: 21.3, 28.5, 80.8, 114.3, 118.4, 121.0, 121.6, 125.9, 129.1, 129.2, 135.8, 138.2, 143.2, 148.6, 150.7, 152.8, 169.6. IR (thin film): 3345, 2977, 2928, 1766, 1726, 1610, 1586, 1520, 1455, 1433, 1405, 1392, 1367, 1314, 1290, 1226, 1195, 1156, 1131, 1051, 1015, 945, 894, 843, 804, 787, 733, 709, 597 cm⁻¹. HRMS C₂₁H₂₃NO₄Na [M+Na]⁺ calculated 376.1525, observed 376.1531.

1,2-dimethoxy-4-(1-phenylvinyl)benzene (29). The alkene was synthesized according to General Method C (with the exception that the magnesium turnings, 1,2-dibromoethane, and THF were heated with a heat gun and then stirred for 5 hours) from 9.6 mmol of acetophenone (in 4.5 mL of THF) and stirred with HCl for overnight. The product was purified via flash silica gel column chromatography (2% acetone in hexanes,

to remove the majority of impurities prior to stirring in HCl, and 15% ethyl acetate in hexanes for purification of alkene) to afford isolated product, a white solid, in 23% yield, 0.521 g (2.169 mmol). M.P.: 78–85 °C. TLC (20% ethyl acetate in hexanes) $R_f = 0.33$. ^1H NMR (300 MHz, CDCl_3) δ : 3.84 (s, 3H), 3.91 (s, 3H), 5.39 (d, $J = 1.24$ Hz, 1H), 5.42 (d, $J = 1.24$ Hz, 1H), 6.81–6.86 (m, 1H), 6.87–6.93 (m, 2H), 7.31–7.40 (m, 5H). ^{13}C NMR (126 MHz, CDCl_3) δ : 55.9, 56.0, 110.9, 111.6, 113.3, 121.0, 127.8, 128.2, 128.4, 134.4, 141.7, 148.7, 148.9, 149.8. IR (thin film): 3091, 3062, 3027, 2995, 2955, 2836, 2574, 2361, 2340, 1612, 1599, 1577, 1510, 1467, 1441, 1414, 1319, 1308, 1274, 1252, 1228, 1177, 1143, 1133, 1084, 1027, 925, 896, 867, 825, 819, 777, 763, 709, 697, 662, 626, 581 cm^{-1} . HRMS $\text{C}_{16}\text{H}_{17}\text{O}_2$ $[\text{M}+\text{H}]^+$ calculated 241.1229, observed 241.1225.

Pentan-3-yl (4-(1-(4-(trifluoromethyl)phenyl)vinyl)phenyl)carbamate (30).

The alkene was synthesized according to previously published procedure⁷ from 1.20 mmol of pentan-3-yl (4-acetylphenyl)carbamate and purified via flash silica-gel column chromatography (using 100% dichloromethane) to afford isolated product in 26% yield, 0.091 g (0.242 mmol). M.P.: 82–86 °C. TLC (30% acetone in hexanes) $R_f = 0.62$. ^1H NMR (500 MHz, CDCl_3) δ : 0.95 (t, $J = 7.57$ Hz, 6H), 1.56–1.70 (m, 4H), 4.76 (q, $J = 6.23$ Hz, 1H), 5.44 (d, $J = 0.98$ Hz, 1H), 5.52 (s, 1H), 6.72 (bs, 1H), 7.24–7.28 (m, 2H), 7.40 (d, $J = 8.31$ Hz, 2H), 7.44 (d, $J = 8.30$ Hz, 2H), 7.59 (d, $J = 7.82$ Hz, 2H). ^{13}C NMR (126 MHz, CDCl_3) δ : 9.7, 26.8, 78.2, 115.2, 118.4, 124.4 (q, $J = 272.8$ Hz), 125.3 (q, $J = 4.1$ Hz), 128.7, 129.0, 129.9 (q, $J = 32.4$ Hz), 135.6, 138.3, 145.3 (app d, $J = 1.5$ Hz), 148.5, 153.8. ^{19}F NMR (282 MHz, CDCl_3) δ : -63.2. IR (thin film): 3317, 2969, 2880, 2361, 1697, 1611, 1590, 1522, 1463, 1408, 1320, 1220, 1165, 1122, 1076, 1062, 1016, 930, 903, 847, 770, 739, 706, 652, 619 cm^{-1} . HRMS $\text{C}_{21}\text{H}_{22}\text{NO}_2\text{F}_3\text{Na}$ $[\text{M}+\text{Na}]^+$ calculated 400.1500, observed

400.1507.

Pentan-3-yl (4-acetylphenyl)carbamate. To a solution of 4-acetylphenyl isocyanate (31.025 mmol, 1 equiv) in CH₂Cl₂ (155 mL) and under nitrogen atmosphere was added DMAP (3.723 mmol, 0.12 equiv), NEt₃ (62.050 mmol, 2 equiv), and pentan-3-ol (31.025 mmol, 1.2 equiv). After the reaction mixture was stirred for 5 hours at room temperature and then refluxed overnight, the solvent was removed by rotary evaporation and purified by flash-column chromatography (50% ethyl acetate in dichloromethane with 1% triethylamine) to afford isolated product, a white solid, in 70% yield, 5.389 g (21.614 mmol). M.P.: 123–124 °C. TLC (5% methanol in dichloromethane) R_f = 0.71. ¹H NMR (300 MHz, CDCl₃) δ: 0.93 (t, *J* = 12.47 Hz, 6H), 1.56–1.69 (m, 4H), 2.57 (s, 3H), 4.75 (p, *J* = 6.18 Hz, 1H), 6.89 (bs, 1H), 7.49 (d, *J* = 14.42 Hz, 2H), 7.89–7.96 (m, 2H). ¹³C NMR (126 MHz, CDCl₃) δ: 9.7, 26.6, 26.7, 78.6, 117.6, 130.0, 132.1, 142.8, 153.3, 197.0. IR (thin film): 3302, 2968, 2938, 2879, 2362, 1730, 1708, 1665, 1589, 1529, 1462, 1410, 1359, 1312, 1272, 1216, 1179, 1119, 1078, 1051, 959, 929, 840, 770, 706, 592 cm⁻¹. HRMS C₁₄H₁₉NO₃Na [M+Na]⁺ calculated 272.1263, observed 272.1260.

Butyl (4-(1-(4-(trifluoromethyl)phenyl)vinyl)phenyl)carbamate (31). This alkene was synthesized according to the schematic in Figure 2.18. A dry round-bottom flask was charged with the corresponding benzenaminium chloride (2.4 mmol, 1 equiv). Under a nitrogen atmosphere, 12 mL CH₂Cl₂ was added, followed by pyridine (5.536 mmol, 2.3 equiv), which was passed through a plug of activated, basic alumina prior to use. After stirring 5 min. at room temperature, the solution was cooled to 0 °C, and corresponding chloroformate (2.888 mmol, 1.2 equiv) was added. The reaction mixture continued stirring at 0 °C for 2 hr. Then, the mixture was warmed to room temperature and

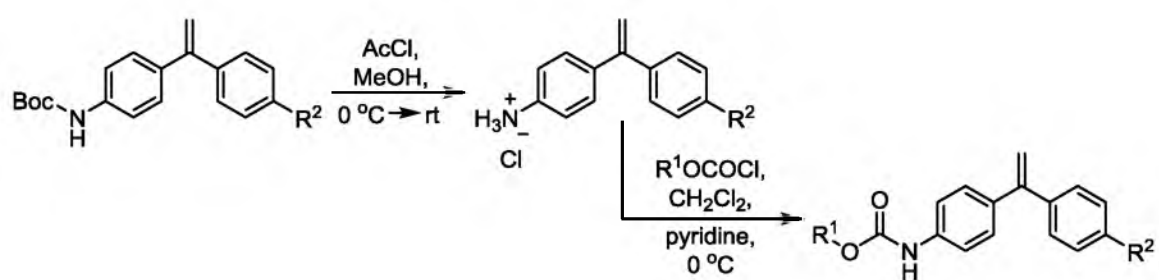


Figure 2.18. Schematic for the synthesis of butyl (4-(1-(4-(trifluoromethyl)phenyl)vinyl)phenyl)carbamate.

purified via silica-gel column chromatography (using 100% dichloromethane) to afford isolated product in 54% yield, 0.461 g (1.268 mmol). M.P.: 86–88 °C. TLC (100% dichloromethane) $R_f = 0.52$. ^1H NMR (500 MHz, CDCl_3) δ : 0.96 (t, $J = 7.33$ Hz, 3H), 1.42 (sex, 2H, $J = 7.42$ Hz), 1.67 (m, 2H), 4.18 (t, $J = 6.60$ Hz, 2H), 5.44 (s, 1H), 5.52 (s, 1H), 6.70 (bs, 1H), 7.25 (d, $J = 8.79$ Hz, 2H), 7.37 (d, $J = 7.82$ Hz, 2H), 7.44 (d, $J = 7.82$ Hz, 2H), 7.58 (d, $J = 8.31$ Hz, 2H). ^{13}C NMR (126 MHz, CDCl_3): δ 13.8, 19.2, 31.1, 65.40, 115.3, 118.5, 124.34 (q, $J = 272.5$ Hz), 125.3 (q, $J = 3.8$ Hz), 128.7, 129.0, 129.9 (q, $J = 32.6$ Hz), 135.7, 138.1, 145.3, 148.4, 153.8. ^{19}F NMR (282 MHz, CDCl_3): δ -63.2; IR (thin film): 3319, 2960, 2875, 2361, 1702, 1610, 1589, 1523, 1467, 1408, 1320, 1218, 1163, 1110, 1076, 1062, 1015, 960, 903, 841, 769, 734, 708, 651, 618, 600 cm^{-1} . HRMS $\text{C}_{20}\text{H}_{20}\text{NO}_2\text{F}_3\text{Na}$ $[\text{M}+\text{Na}]^+$ calculated 386.1344, observed 386.1343.

***Tert*-butyl (4-(1-(4-(trifluoromethyl)phenyl)vinyl)phenyl)carbamate.** The alkene was synthesized according to General Method A from 8.5 mmol of *tert*-butyl (4-acetylphenyl)carbamate and purified via flash silica-gel column chromatography (using 100% dichloromethane) to afford isolated product in 54% yield, 1.663 g (4.578 mmol). M.P.: 119–122 °C. TLC (5% acetone in hexanes) $R_f = 0.17$. ^1H NMR (300 MHz, CDCl_3): δ 1.54 (s, 9H), 5.44 (s, 1H), 5.52 (d, $J = 0.83$ Hz, 1H), 6.55 (bs, 1H), 7.25 (m, 2H), 7.36 (d, $J = 7.96$ Hz, 2H), 7.45 (d, $J = 7.96$ Hz, 2H), 7.59 (d, $J = 8.1$ Hz, 2H). ^{13}C NMR (75 MHz, CDCl_3) δ : 28.5, 80.9, 115.2, 118.4, 124.4 (q, $J = 272.8$ Hz), 125.28 (q, $J = 3.8$ Hz), 128.7, 129.0, 129.87 (q, $J = 32.4$ Hz), 135.5, 138.4, 145.3, 148.5, 152.8. ^{19}F NMR (282 MHz, CDCl_3) δ : -63.20. IR (thin film): 3328, 2979, 2361, 1699, 1612, 1587, 1521, 1456, 1406, 1368, 1322, 1231, 1157, 1123, 1076, 1062, 1015, 902, 842, 771, 740, 701, 651, 620, 563 cm^{-1} . HRMS $\text{C}_{20}\text{H}_{20}\text{NO}_2\text{F}_3\text{Na}$ $[\text{M}+\text{Na}]^+$ calculated 386.1344, observed 386.1354.

4-(1-(4-(trifluoromethyl)phenyl)vinyl)benzenaminium chloride. To a dry round-bottom flask, under nitrogen atmosphere, was added methanol (5.2 mL), which solution was cooled to 0 °C. Acetyl chloride (41.487 mmol, 15 equiv) was added dropwise, and the solution stirred 10 min. before a solution of *tert*-butyl 4-(1-(4-(trifluoromethyl)phenyl)vinyl)phenyl)carbamate (2.690 mmol, 1 equiv) in methanol (10 mL) was slowly added. The resulting reaction mixture was warmed to room temperature and stirred for 3 hrs. After the solvent was removed *in vacuo*, CH₂Cl₂ was added, followed by addition of hexanes until the solution became cloudy. The solvent was again removed *in vacuo* to afford a solid. The solid was washed with diethyl ether, and residual solvent was removed *in vacuo* to give the crude product in 53% yield, 0.426 g (1.422 mmol). The crude product was directly carried on to react with the appropriate chloroformate.

Synthetic Methods: Alkene Reduction

Asymmetric hydrogenation was carried out according to Method C or D, as noted for each product. For characterization purposes, pure product samples were obtained and characterized according to one of the below procedures: Method C, Method D, or the General Racemic Hydrogenation Procedure.

General Method D: Asymmetric hydrogenation procedure. To a 5 mL oven-dried, screw-top vial, equipped with a stirbar and cooled under nitrogen, was added (IrCODL)BA_{rF} (0.003 mmol, 0.046 equiv). The vial was fitted with a screw-cap septum and placed under a nitrogen atmosphere. A solution of the corresponding alkene (0.056 mmol, 1 equiv) in CH₂Cl₂ (2 mL) was added. The nitrogen inlet was removed and replaced with a needle open to the atmosphere. After placing the vial in a high-pressure reactor

vessel, the vessel was evacuated and refilled with hydrogen gas to 15 psi three to five times. Then, the reaction was allowed to stir for 15 hours at room temperature, at which time the pressure in the vessel was slowly released. The solvent was evaporated, and then 1:1 diethyl ether:pentane was added. This solution was passed through a short silica column, to remove the catalyst, and concentrated *in vacuo*. Conversion of starting material to product was then measured by ^1H NMR, and enantiomeric excess was measured by SFC or HPLC, as indicated.

General Method E: Asymmetric hydrogenation procedure. To a 5 mL oven-dried, screw-top vial, equipped with a stirbar and cooled under nitrogen, was added the corresponding alkene substrate (0.056 mmol, 1 equiv). The vial was fitted with a screw-cap septum and placed under a nitrogen atmosphere. 2 mL of a standard solution of (IrCODL)BAr_F in CH₂Cl₂ (0.001 M) was added. The nitrogen inlet was removed and replaced with a needle, open to the atmosphere. After placing the vial in a high-pressure reactor vessel, the vessel was evacuated and refilled with hydrogen gas to 15 psi three to five times. Then, the reaction was allowed to stir for 15 hours at room temperature, at which time the pressure in the vessel was slowly released. The solvent was evaporated, and then 1:1 diethyl ether:pentane was added. This solution was passed through a short silica column, to remove the catalyst, and concentrated *in vacuo*. Conversion of starting material to product was then measured by ^1H NMR, and enantiomeric excess was measured by SFC or HPLC, as indicated.

General Method F: Racemic hydrogenation procedure. To an oven-dried round bottom flask, equipped with a stirbar and cooled nitrogen, was added 10% Pd/C (0.011 mmol, 0.2 equiv). After bringing the flask under nitrogen atmosphere, the corresponding

alkene (0.056 mmol, 1 equiv) in 0.3 mL of ethyl acetate was added to the flask. Using a hydrogen-filled balloon, the flask was subsequently evacuated and refilled with hydrogen three times, and the reaction was stirred, under balloon-pressure of hydrogen, overnight. Finally, the solvent was evaporated, and the remaining residue was taken up in 1:1 diethyl ether:pentane, passed through a short silica column, and concentrated *in vacuo*.

Assignment of absolute configuration. Absolute configurations were assigned by analogy to the known absolute configuration of (*R*)-(+)-4-(1-(3,5-dimethoxyphenyl)ethyl)-1,1'-biphenyl.²⁰

(*R*)-(+)-*tert*-butyl 4-(1-(3,5-dimethoxyphenyl)ethyl)phenylcarbamate.

Reduction was carried out according to General Method D to afford ¹H NMR conversions of 88% (run 1) and 89% (run 2), and er's of 92:8 and 92:8, respectively. Absolute configuration was assigned by analogy (*vide supra*). $[\alpha]_D^{20} = +2.8$ (*c* 0.84, CHCl₃). The product's purity was assessed by comparison to published characterization data.¹⁹ Enantiomers were separated by SFC on a Chiralpak AD-H column (4.6 mm x 250 mm, 5 μm particle size) under the following conditions: 38 °C, 20% isopropyl alcohol, 2 mL min⁻¹, 160 Bar. R_T = 12.05 min, 13.77 min.

***Tert*-butyl 4-(1-(3-methoxyphenyl)ethyl)phenylcarbamate.** The diarylmethine was synthesized according to General Method D to afford ¹H NMR conversions of 64% (run 1) and 54% (run 2), and er's of 74:26 and 74:26, respectively. TLC (20% ethyl acetate in hexanes) R_f = 0.44. M.P.: 76–79 °C. ¹H NMR (500 MHz, CDCl₃) δ: 1.51 (s, 9H), 1.59 (d, *J* = 7.33 Hz, 3H), 3.77 (s, 3H), 4.07 (q, *J* = 7.33 Hz, 1H), 6.41 (bs, 1H), 6.72 (ddd, *J* = 8.30 Hz, 2.44 Hz, 0.97 Hz, 1H), 6.75 (t, *J* = 2.20 Hz, 1H), 6.79 (dt, *J* = 8.31 Hz, 0.98 Hz, 1H), 7.14 (d, *J* = 8.79 Hz, 2H), 7.19 (t, *J* = 7.82 Hz, 1H), 7.24–7.28 (m, 2H). ¹³C NMR

(126 MHz, CDCl₃) δ : 22.0, 28.5, 44.3, 55.3, 80.5, 111.1, 113.8, 118.8, 120.2, 128.2, 129.4, 136.4, 141.1, 148.3, 153.0, 159.7. IR (thin film): 3334, 2969, 2931, 2359, 1699, 1594, 1520, 1486, 1454, 1435, 1410, 1392, 1366, 1313, 1231, 1155, 1051, 1016, 900, 836, 777, 741, 696 cm⁻¹. HRMS C₂₀H₂₅NO₃Na [M+Na]⁺ calculated 350.1732, observed 350.1732. Enantiomers were separated by HPLC on a Chiralpak AD-H column (4.6 mm x 250 mm, 5 μ m particle size) under the following conditions: ambient temperature, 10% isopropyl alcohol in hexanes, 0.9 mL min⁻¹. R_T = 9.76 min, 10.69 min.

***Tert*-butyl (4-(1-(3-butoxyphenyl)ethyl)phenyl)carbamate.** The diarylmethine was synthesized according to General Method D to afford ¹H NMR conversions of 66% (run 1) and 66% (run 2) and er's of 75:25 and 75:25, respectively. TLC (20% ethyl acetate in hexanes) R_f = 0.48. ¹H NMR (500 MHz, CDCl₃) δ : 0.96 (t, *J* = 7.33 Hz, 3H), 1.45–1.53 (m, 11H), 1.59 (d, *J* = 7.33 Hz, 3H), 1.69–1.79 (m, 2H), 3.91 (t, *J* = 6.35 Hz, 2H), 4.06 (q, *J* = 7.33 Hz, 1H), 6.41 (bs, 1H), 6.70 (dd, *J* = 8.31 Hz, 2.45 Hz, 1H), 6.73–6.79 (m, 2H), 7.11–7.19 (m, 3H), 7.22–7.29 (m, 2H). ¹³C NMR (126 MHz, CDCl₃) δ : 14.0 (s), 19.4 (s), 22.0 (s), 28.5 (s), 31.5 (s), 44.3 (s), 67.7 (s), 80.5 (s), 111.6 (s), 114.4 (s), 118.8 (s), 120.0 (s), 128.2 (s), 129.3 (s), 136.4 (s), 141.2 (s), 148.2 (s), 153.0 (s), 159.3 (s). IR (thin film): 3335, 2962, 2931, 2872, 2359, 1727, 1699, 1594, 1520, 1486, 1453, 1410, 1391, 1367, 1313, 1228, 1155, 1052, 1028, 1016, 974, 904, 835, 775, 740, 696 cm⁻¹. HRMS C₂₃H₃₁NO₃Na [M+Na]⁺ calculated 392.2202, observed 392.2210. Enantiomers were separated by HPLC on a Chiralpak AD-H column (4.6 mm x 250 mm, 5 μ m particle size) under the following conditions: ambient temperature, 5% isopropyl alcohol in hexanes, 0.9 mL min⁻¹. R_T = 9.74 min, 10.51 min.

***Tert*-butyl (4-(1-(3,5-dimethylphenyl)ethyl)phenyl)carbamate.** The

diarylmethine was synthesized according to General Method D to afford ^1H NMR conversions of 71% (run 1) and 68% (run 2) and er's of 64:36 and 62:38, respectively. TLC (20% ethyl acetate in hexanes) $R_f = 0.53$. ^1H NMR (500 MHz, CDCl_3) δ : 1.51 (s, 9H), 1.58 (d, $J = 7.33$ Hz, 3H), 2.27 (s, 6H), 4.02 (q, $J = 7.33$ Hz, 1H), 6.40 (bs, 1H), 6.81 (s, 3H), 7.12–7.18 (m, 2H), 7.26 (d, $J = 8.31$ Hz, 2H). ^{13}C NMR (126 MHz, CDCl_3) δ : 21.5 (s), 22.1 (s), 28.5 (s), 44.2 (s), 80.5 (s), 118.8 (s), 125.5 (s), 127.8 (s), 128.2 (s), 136.3 (s), 137.9 (s), 141.5 (s), 146.6 (s), 153.0 (s). IR (thin film): 3334, 2969, 2929, 2360, 2167, 1728, 1700, 1596, 1521, 1455, 1410, 1392, 1367, 1313, 1232, 1159, 1051, 1028, 1017, 901, 835, 771, 702, 543 cm^{-1} . HRMS $\text{C}_{21}\text{H}_{27}\text{NO}_2\text{Na}$ $[\text{M}+\text{Na}]^+$ calculated 348.1939, observed 348.1946. Enantiomers were separated by SFC on a Chiralcel OD column (4.6 mm x 250 mm) under the following conditions: 28 $^\circ\text{C}$, 10% isopropyl alcohol, 3 mL min^{-1} . $R_T = 4.36$ min, 14.58 min.

***Tert*-butyl (4-(1-(*m*-tolyl)ethyl)phenyl)carbamate.** The diarylmethine was synthesized according to General Method D to afford ^1H NMR conversions of 57% (run 1) and 50% (run 2) and er's of 49:51 and 52:48, respectively. TLC (20% ethyl acetate in hexanes) $R_f = 0.54$. ^1H NMR (500 MHz, CDCl_3) δ : 1.51 (s, 9H), 1.60 (d, $J = 7.33$ Hz, 3H), 2.31 (s, 3H), 4.07 (q, $J = 7.33$ Hz, 1H), 6.41 (bs, 1H), 6.97–7.03 (m, 3H), 7.12–7.19 (m, 3H), 7.23–7.29 (m, 2H). ^{13}C NMR (126 MHz, CDCl_3) δ : 21.6 (s), 22.1 (s), 28.5 (s), 44.2 (s), 80.5 (s), 118.8 (s), 124.7 (s), 126.9 (s), 128.2 (s), 128.4 (s), 128.5 (s), 136.4 (s), 138.0 (s), 141.4 (s), 146.6 (s), 153.0 (s). IR (thin film): 3334, 2972, 2929, 2362, 1728, 1699, 1594, 1521, 1455, 1410, 1392, 1367, 1314, 1233, 1158, 1054, 1017, 902, 837, 779, 741, 703, 552 cm^{-1} . HRMS $\text{C}_{20}\text{H}_{25}\text{NO}_2\text{Na}$ $[\text{M}+\text{Na}]^+$ calculated 334.1783, observed 334.1784. Enantiomers for run 1 were separated by HPLC on a Chiralpak AD-H column (4.6 mm x

250 mm, 5 μm particle size) under the following conditions: ambient temperature, 3% isopropyl alcohol in hexanes, 0.9 mL min^{-1} . $R_T = 10.39$ min, 11.40 min. Enantiomers for run 2 were separated by SFC on a Chiralcel OZ-H column (4.6 mm x 250 mm, 5 μm particle size) under the following conditions: 40 $^\circ\text{C}$, 5% isopropyl alcohol, 2 mL min^{-1} . $R_T = 9.66$ min, 11.01 min.

1-methoxy-3-(1-phenylethyl)benzene. The diarylmethine, a previously reported molecule,⁵⁵ was synthesized according to General Method E to afford ^1H NMR conversions of >95% (run 1) and >95% (run 2) and er's of 73:27 and 75:25, respectively. Enantiomers were separated by SFC on a Chiralcel OJ-H column (4.6 mm x 250 mm) under the following conditions: 40 $^\circ\text{C}$, 1% methanol, 4 mL min^{-1} . $R_T = 10.71$ min, 11.66 min.

1-methoxy-4-(1-phenylethyl)benzene. The diarylmethine, a previously reported molecule,²⁰ was synthesized according to General Method E to afford ^1H NMR conversions of >95% (run 1) and >95% (run 2) and er's of 52:48 and 54:46, respectively. Enantiomers were separated by SFC on a Chiralcel OJ-H column (4.6 mm x 250 mm) under the following conditions: 40 $^\circ\text{C}$, 1% methanol, 4 mL min^{-1} . $R_T = 10.71$ min, 11.66 min.

1,3-diethyl-5-(1-phenylvinyl)benzene. The diarylmethine was synthesized according to General Method E to afford ^1H NMR conversions of >95% (run 1) and >95% (run 2) and er's of 49:51 and 48:52, respectively. TLC (10% ethyl acetate in hexanes) $R_f = 0.63$. ^1H NMR (300 MHz, CDCl_3) δ : 1.21 (t, $J = 7.62$ Hz, 6H), 1.63 (d, $J = 7.28$ Hz, 3H), 2.59 (q, $J = 7.60$ Hz, 4H), 4.11 (q, $J = 7.19$ Hz, 1H), 6.88 (s, 3H), 7.14–7.32 (m, 5H). ^{13}C NMR (126 MHz, CDCl_3) δ : 15.8 (s), 22.2 (s), 29.0 (s), 45.0 (s), 124.7 (s), 125.3 (s), 126.0 (s), 127.8 (s), 128.4 (s), 144.3 (s), 146.4 (s), 146.8 (s). IR (thin film): 3024, 2964, 2931, 2872, 2359, 2341, 1599, 1495, 1458, 1373, 1319, 1067, 1030, 868, 762, 711, 699,

668 cm^{-1} . HRMS $\text{C}_{18}\text{H}_{22}\text{Ag}$ $[\text{M}+\text{Ag}]^+$ calculated 345.0772, observed 345.0797. Enantiomers were separated by SFC on a Chiralcel OJ-H column (4.6 mm x 250 mm) under the following conditions: 40 °C, 0% cosolvent, 2 mL min^{-1} . $R_T = 5.75$ min, 6.21 min.

(R)-(-)-1,3-diethyl-5-(1-phenylethyl)benzene (9). The diarylmethine was synthesized according to General Method E to afford ^1H NMR conversions of >95% (run 1) and >95% (run 2) and er's of 92:8 and 93:7, respectively. Absolute configuration was assigned by analogy (*vide supra*). TLC (10% ethyl acetate in hexanes) $R_f = 0.33$. ^1H NMR (500 MHz, CDCl_3) δ : 1.63 (d, $J = 7.33$ Hz, 3H), 3.76 (s, 6H), 4.09 (q, $J = 7.33$ Hz, 1H), 6.31 (t, $J = 2.44$ Hz, 1H), 6.40 (d, $J = 2.45$ Hz, 2H), 7.19 (t, $J = 7.33$ Hz, 1H), 7.24 (d, $J = 7.33$ Hz, 2H), 7.27–7.31 (m, 2H). ^{13}C NMR (126 MHz, CDCl_3) δ : 21.9 (s), 45.1 (s), 55.4 (s), 97.8 (s), 106.2 (s), 126.2 (s), 127.7 (s), 128.5 (s), 146.2 (s), 149.0 (s), 160.9 (s). IR (thin film): 2964, 2934, 2836, 2359, 1594, 1495, 1457, 1427, 1345, 1322, 1289, 1204, 1153, 1070, 1042, 1029, 990, 927, 834, 764, 703, 668, 540 cm^{-1} . HRMS $\text{C}_{16}\text{H}_{19}\text{O}_2$ $[\text{M}+\text{H}]^+$ calculated 243.1385, observed 243.1388. $[\alpha]_D^{20} = -2.5$ (c 0.40, CHCl_3). Enantiomers were separated by SFC on a Chiralpak AD-H column (4.6 mm x 250 mm, 5 μm particle size) under the following conditions: 32 °C, gradient 5%–50% methanol over 10 min., 3 mL min^{-1} . $R_T = 2.92$ min, 3.36 min.

(R)-(+)-1,3-dimethoxy-5-(1-(4-methoxyphenyl)ethyl)benzene (10). The diarylmethine was synthesized according to General Method E to afford ^1H NMR conversions of >95% (run 1) and >95% (run 2) and er's of 91:9 and 92:8, respectively. Absolute configuration was assigned by analogy (*vide supra*). TLC (10% ethyl acetate in hexanes) $R_f = 0.24$. ^1H NMR (300 MHz, CDCl_3) δ : 1.59 (d, $J = 7.14$ Hz, 3H), 3.75 (s, 6H), 3.78 (s, 3H), 4.03 (q, $J = 7.23$ Hz, 1H), 6.27–6.31 (m, 1H), 6.34–6.39 (m, 2H), 6.79–6.85

(m, 2H), 7.11–7.18 (m, 2H). ^{13}C NMR (126 MHz, CDCl_3) δ : 22.1 (s), 44.3 (s), 55.4 (s), 97.7 (s), 106.0 (s), 113.9 (s), 128.6 (s), 138.3 (s), 149.4 (s), 158.0 (s), 160.8 (s). IR (thin film): 2962, 2934, 2835, 2360, 2341, 1653, 1606, 1595, 1540, 1559, 1540, 1511, 1458, 1428, 1373, 1302, 1247, 1204, 1179, 1154, 1117, 1074, 1035, 927, 831, 810, 695, 668 cm^{-1} . HRMS $\text{C}_{17}\text{H}_{21}\text{O}_3$ $[\text{M}+\text{H}]^+$ calculated 273.1491, observed 273.1483. $[\alpha]_D^{20} = +5.0$ (c 0.48, CHCl_3). Enantiomers were separated by SFC on a Chiralcel OJ-H column (4.6 mm x 250 mm) under the following conditions: 40 °C, 3% methanol, 4 mL min^{-1} . $R_T = 5.66$ min, 6.37 min.

(R)-(+)-1,3-dimethoxy-5-(1-(*p*-tolyl)ethyl)benzene (11). The diarylmethine was synthesized according to General Method E to afford ^1H NMR conversions of >95% (run 1) and >95% (run 2) and er's of 88:12 and 89:11, respectively. Absolute configuration was assigned by analogy (*vide supra*). TLC (10% ethyl acetate in hexanes) $R_f = 0.35$. ^1H NMR (300 MHz, CDCl_3) δ : 1.60 (d, $J = 7.28$ Hz, 3H), 2.31 (s, 3H), 3.76 (s, 6H), 4.05 (q, $J = 7.19$ Hz, 1H), 6.29–6.32 (m, 1H), 6.38–6.42 (m, 2H), 7.07–7.16 (m, 4H). ^{13}C NMR (126 MHz, CDCl_3) δ : 21.1 (s), 22.0 (s), 44.8 (s), 55.4 (s), 97.7 (s), 106.1 (s), 127.5 (s), 129.2 (s), 135.7 (s), 143.2 (s), 149.2 (s), 160.8 (s). IR (thin film): 2964, 2933, 2836, 2360, 1595, 1513, 1458, 1427, 1344, 1289, 1204, 1155, 1076, 1043, 1021, 991, 927, 818, 740, 695, 668, 544 cm^{-1} . HRMS $\text{C}_{17}\text{H}_{21}\text{O}_2$ $[\text{M}+\text{H}]^+$ calculated 257.1542, observed 257.1536. $[\alpha]_D^{20} = +0.9$ (c 0.55, CHCl_3). Enantiomers were separated by SFC on a Chiralcel OJ-H column (4.6 mm x 250 mm) under the following conditions: 40 °C, 3% methanol, 4 mL min^{-1} . $R_T = 4.45$ min, 4.99 min.

(R)-(+)-4-(1-(3,5-dimethoxyphenyl)ethyl)-1,1'-biphenyl (12). The diarylmethine was synthesized according to General Method E to afford ^1H NMR conversions of >95%

(run 1) and >95% (run 2) and er's of 89:11 and 89:11, respectively. Absolute configuration previously reported (*vide supra*). TLC (10% ethyl acetate in hexanes) $R_f = 0.33$. ^1H NMR (300 MHz, CDCl_3) δ : 1.66 (d, $J = 7.14$ Hz, 3H), 3.77 (s, 6H), 4.13 (q, $J = 7.23$ Hz, 1H), 6.31–6.34 (m, 1H), 6.44 (d, $J = 2.33$ Hz, 2H), 7.28–7.37 (m, 3H), 7.38–7.47 (m, 2H), 7.48–7.61 (m, 4H). ^{13}C NMR (126 MHz, CDCl_3) δ : 21.9 (s), 44.9 (s), 55.4 (s), 97.8 (s), 106.2 (s), 127.2 (s), 127.2 (s), 127.3 (s), 128.1 (s), 128.8 (s), 139.1 (s), 141.1 (s), 145.3 (s), 148.9 (s), 160.9 (s). IR (thin film): 3027, 2964, 2933, 2835, 2361, 2338, 2210, 2176, 2159, 1595, 1486, 1458, 1427, 1345, 1288, 1204, 1154, 1076, 1045, 1008, 927, 835, 767, 738, 697, 668, 549 cm^{-1} . HRMS $\text{C}_{22}\text{H}_{23}\text{O}_2$ $[\text{M}+\text{H}]^+$ calculated 319.1698, observed 319.1706. $[\alpha]_D^{20} = +11.4$ (c 0.57, CHCl_3). Enantiomers were separated by SFC on a Chiralcel AY-H column (4.6 mm x 250 mm, 5 μm particle size) under the following conditions: 40 $^\circ\text{C}$, gradient 5%–50% methanol over 10 min., 3 mL min^{-1} . $R_T = 5.40$ min, 6.12 min.

(*R*)-(+)-1-(1-(4-chlorophenyl)ethyl)-3,5-dimethoxybenzene (13). The diarylmethine was synthesized according to General Method E to afford ^1H NMR conversions of >95% (run 1) and >95% (run 2) and er's of 96:4 and 96:4, respectively. Absolute configuration was assigned by analogy (*vide supra*). TLC (10% ethyl acetate in hexanes) $R_f = 0.39$. ^1H NMR (300 MHz, CDCl_3) δ : 1.59 (d, $J = 7.28$ Hz, 3H), 3.76 (s, 6H), 4.05 (q, $J = 7.23$ Hz, 1H), 6.31–6.34 (m, 1H), 6.33–3.37 (m, 2H), 7.12–7.18 (m, 2H), 7.21–7.27 (m, 2H). ^{13}C NMR (126 MHz, CDCl_3) δ : 21.8 (s), 44.5 (s), 55.4 (s), 97.9 (s), 106.1 (s), 128.6 (s), 129.0 (s), 131.9 (s), 144.7 (s), 148.4 (s), 160.9 (s). IR (thin film): 2965, 2934, 2836, 2361, 2337, 1595, 1491, 1458, 1427, 1407, 1344, 1288, 1204, 1155, 1092, 1075, 1042, 1014, 928, 829, 782, 730, 697, 668 cm^{-1} . HRMS $\text{C}_{16}\text{H}_{17}\text{ClO}_2$ $[\text{M}+\text{H}]^+$ calculated 277.0995, observed 277.0995. $[\alpha]_D^{20} = +4.5$ (c 0.71, CHCl_3). Enantiomers were separated

by SFC on a Chiralpak AD-H column (4.6 mm x 250 mm, 5 μ m particle size) under the following conditions: 40 °C, 3% methanol, 4 mL min⁻¹. R_T = 3.16 min, 5.89 min.

(R)-(-)-1,3-dimethoxy-5-(1-(4-(trifluoromethyl)phenyl)ethyl)benzene (14). The diarylmethine was synthesized according to General Method E to afford ¹H NMR conversions of >95% (run 1) and >95% (run 2) and er's of 96:4 and 97:3, respectively. Absolute configuration was assigned by analogy (*vide supra*). TLC (15% ethyl acetate in hexanes) R_f = 0.43. ¹H NMR (300 MHz, CDCl₃) δ : 1.63 (d, *J* = 7.28 Hz, 3H), 3.76 (s, 6H), 4.13 (q, *J* = 7.28 Hz, 1H), 6.31–6.34 (m, 1H), 6.34–6.37 (m, 2H), 7.33 (dd, *J* = 8.10 Hz, 0.69 Hz, 2H), 7.53 (d, *J* = 8.10 Hz, 2H). ¹³C NMR (126 MHz, CDCl₃) δ : 21.6 (s), 45.0 (s), 55.4 (s), 98.0 (s), 106.2 (s), 124.4 (q, *J* = 272.5 Hz), 125.5 (q, *J* = 3.8 Hz), 128.0 (s), 128.5 (q, *J* = 32.4 Hz), 147.8 (s), 150.3 (m), 161.0 (s). ¹⁹F NMR (282 MHz, CDCl₃) δ : -63. IR (thin film): 2967, 2839, 2360, 1596, 1459, 1429, 1325, 1205, 1159, 1118, 1068, 1043, 1017, 928, 841, 742, 698, 668, 611 cm⁻¹. HRMS C₁₇H₁₈O₂F₃ [M+H]⁺ calculated 311.1259, observed 311.1253. $[\alpha]_D^{20}$ = -2.6 (*c* 0.69, CHCl₃). Enantiomers were separated by SFC on a Chiralpak AD-H column (4.6 mm x 250 mm) under the following conditions: 40 °C, 2% methanol, 2 mL min⁻¹, 160 Bar. R_T = 3.65 min, 4.62 min.

(R)-(-)-1-(1-(3-isopropylphenyl)ethyl)-3,5-dimethoxybenzene (15). The diarylmethine was synthesized according to General Method E to afford ¹H NMR conversions of >95% (run 1) and >95% (run 2) and er's of 85:15 and 86:14, respectively. Absolute configuration was assigned by analogy (*vide supra*). TLC (15% ethyl acetate in hexanes) R_f = 0.50. ¹H NMR (300 MHz, CDCl₃) δ : 1.24 (d, *J* = 6.87 Hz, 6H), 1.62 (d, *J* = 7.28 Hz, 3H), 2.88 (sep, *J* = 6.91 Hz, 1H), 3.76 (s, 6H), 4.07 (q, *J* = 7.23 Hz, 1H), 6.30 (t, *J* = 2.20 Hz, 1H), 6.41 (dd, *J* = 2.33 Hz, 0.55 Hz, 2H), 7.02–7.09 (m, 2H), 7.09–7.12 (m,

1H), 7.18–7.25 (m, 1H). ¹³C NMR (75 MHz, CDCl₃) δ: 22.0 (s), 24.2 (s), 24.2 (s), 34.3 (s), 45.2 (s), 55.4 (s), 97.7 (s), 106.1 (s), 124.1 (s), 125.1 (s), 126.1 (s), 128.4 (s), 146.0 (s), 149.0 (s), 149.2 (s), 160.8 (s). IR (thin film): 2960, 2836, 2364, 1596, 1459, 1427, 1345, 1289, 1204, 1154, 1071, 1043, 928, 832, 796, 707, 668 cm⁻¹. HRMS C₁₉H₂₅O₂ [M+H]⁺ calculated 285.1855, observed 285.1862. $[\alpha]_D^{20} = -3.1$ (c 0.70, CHCl₃). Enantiomers were separated by SFC on a Chiralcel OJ-H column (4.6 mm x 250 mm) under the following conditions: 27 °C, 0% cosolvent, 4 mL min⁻¹. R_T = 3.21 min, 3.76 min.

(R)-(-)-1,3-dimethoxy-5-(1-(3-methoxyphenyl)ethyl)benzene (16). The diarylmethine was synthesized according to General Method E to afford ¹H NMR conversions of >95% (run 1) and >95% (run 2) and er's of 71:29 and 71:29, respectively. Absolute configuration was assigned by analogy (*vide supra*). TLC (15% ethyl acetate in hexanes) R_f = 0.38. ¹H NMR (300 MHz, CDCl₃) δ: 1.60 (d, *J* = 7.14 Hz, 3H), 3.75 (s, 6H), 3.78 (s, 3H), 4.05 (q, *J* = 7.14 Hz, 1H), 6.29–6.31 (m, 1H), 6.39 (d, *J* = 2.33 Hz, 2H), 6.73 (ddd, *J* = 8.17 Hz, 2.54 Hz, 0.96 Hz, 1H), 6.76–6.80 (m, 1H), 6.83 (dt, *J* = 7.69 Hz, 0.82 Hz, 1H), 7.17–7.23 (m, 1H). ¹³C NMR (75 MHz, CDCl₃) δ: 21.8 (s), 45.1 (s), 55.3 (s), 55.4 (s), 97.8 (s), 106.1 (s), 111.1 (s), 113.8 (s), 120.1 (s), 129.4 (s), 147.8 (s), 148.8 (s), 159.7 (s), 160.8 (s). IR (thin film): 2964, 2835, 2362, 1595, 1486, 1458, 1428, 1318, 1287, 1263, 1204, 1154, 1040, 928, 834, 782, 735, 708 cm⁻¹. HRMS C₁₇H₂₁O₃ [M+H]⁺ calculated 273.1491, observed 273.1503. $[\alpha]_D^{20} = -1.3$ (c 0.61, CHCl₃). Enantiomers were separated by SFC on a Chiralcel OJ-H column (4.6 mm x 250 mm) under the following conditions: 24 °C, 0% cosolvent, 2 mL min⁻¹. R_T = 15.55 min, 17.48 min.

1-(1-(3,5-diethylphenyl)ethyl)-3,5-dimethoxybenzene. The diarylmethine was synthesized according to General Method E to afford ¹H NMR conversions of >95% (run

1) and >95% (run 2) and er's of 78.5:21.5 and 76.2:23.8, respectively. TLC (10% ethyl acetate in hexanes) $R_f = 0.41$. ^1H NMR (300 MHz, CDCl_3) δ : 1.22 (t, $J = 7.62$ Hz, 6H), 1.61 (d, $J = 7.28$ Hz, 3H), 2.60 (q, $J = 7.60$ Hz, 4H), 3.77 (s, 6H), 4.03 (q, $J = 7.28$ Hz, 1H), 6.30 (t, $J = 2.33$ Hz, 1H), 6.41 (d, $J = 2.33$ Hz, 2H), 6.86–6.92 (m, 3H). ^{13}C NMR (126 MHz, CDCl_3) δ : 15.8, 22.1, 29.0, 45.2, 55.4, 97.7, 106.2, 124.6, 125.4, 144.3, 146.0, 149.3, 160.8; IR (thin film): 2963, 2932, 2872, 2836, 2361, 2339, 2024, 1595, 1458, 1427, 1373, 1325, 1204, 1155, 1045, 928, 869, 832, 724, 699, 668 cm^{-1} . HRMS $\text{C}_{20}\text{H}_{27}\text{O}_2$ $[\text{M}+\text{H}]^+$ calculated 299.2011, observed 299.2005. Enantiomers were separated by SFC on a Chiralcel OZ-H column (4.6 mm x 250 mm, 5 μm particle size) under the following conditions: 27 $^\circ\text{C}$, 1% isopropyl alcohol, 2 mL min^{-1} , 160 Bar. $R_T = 12.35$ min, 13.57 min.

1,2,3-trimethoxy-5-(1-phenylethyl)benzene. The diarylmethine was synthesized according to General Method E to afford ^1H NMR conversions of 59% (run 1) and 66% (run 2) and er's of 92.0:8.0 and 91.0:9.0, respectively. TLC (15% ethyl acetate in hexanes) $R_f = 0.22$. ^1H NMR (300 MHz, CDCl_3) δ : 1.63 (d, $J = 7.14$ Hz, 3H), 3.82 (s, 6H), 3.82 (s, 3H), 4.09 (q, $J = 7.32$ Hz, 1H), 6.44 (s, 2H), 7.16–7.34 (m, 5H). ^{13}C NMR (126 MHz, CDCl_3) δ : 22.1, 45.1, 56.2, 60.9, 104.8, 126.2, 127.6, 128.5, 136.3, 142.1, 146.3, 153.2. IR (thin film): 2964, 2934, 2835, 2360, 1588, 1507, 1458, 1418, 1328, 1234, 1183, 1125, 1009, 920, 835, 780, 702, 661, 614 cm^{-1} . HRMS $\text{C}_{17}\text{H}_{20}\text{O}_3\text{Na}$ $[\text{M}+\text{Na}]^+$ calculated 295.1310, observed 295.1313. Enantiomers were separated by HPLC on a Chiralpak AD-H column (4.6 mm x 250 mm, 5 μm particle size) under the following conditions: ambient temperature, 1% isopropyl alcohol in hexanes, 1 mL min^{-1} . $R_T = 11.29$ min, 12.75 min.

***Tert*-butyl (4-(1-(4-ethylphenyl)ethyl)phenyl)carbamate.** The diarylmethine was synthesized according to General Method D to afford a ^1H NMR conversion of 49% and

er of 55.9:44.1 and General Method E to afford a ^1H NMR conversion of 54% and er of 55.3:44.7. M.P.: 87–91 °C. TLC (15% ethyl acetate in hexanes) $R_f = 0.42$. ^1H NMR (500 MHz, CDCl_3) δ : 1.22 (t, $J = 7.57$ Hz, 3H), 1.51 (s, 9H), 1.60 (d, $J = 7.33$ Hz, 3H), 2.61 (q, $J = 7.49$ Hz, 2H), 4.08 (q, $J = 7.33$ Hz, 1H), 6.40 (bs, 1H), 7.11 (s, 4H), 7.12–7.16 (m, 2H), 7.24–7.29 (m, 2H). ^{13}C NMR (126 MHz, CDCl_3) δ : 15.7, 22.1, 28.5, 28.5, 43.9, 80.5, 118.8, 127.6, 127.9, 128.2, 136.3, 141.5, 141.9, 143.9, 153.0. IR (thin film): 3336, 2966, 2930, 2873, 2361, 1728, 1700, 1614, 1594, 1521, 1454, 1410, 1392, 1367, 1313, 1233, 1159, 1055, 1016, 902, 831, 773, 604, 550 cm^{-1} . HRMS $\text{C}_{21}\text{H}_{27}\text{NO}_2\text{Na}$ $[\text{M}+\text{Na}]^+$ calculated 348.1939, observed 348.1938. Enantiomers were separated by HPLC on a Chiralpak AD-H column (4.6 mm x 250 mm, 5 μm particle size) under the following conditions: ambient temperature, 3% isopropyl alcohol in hexanes, 0.9 mL min^{-1} . $R_T = 10.93$ min, 12.90 min.

3-(1-(4-((*tert*-butoxycarbonyl)amino)phenyl)ethyl)phenyl acetate. The diarylmethine was synthesized according to General Method E to afford ^1H NMR conversions of 13% (run 1) and 28% (run 2) and er's of 67.8:32.2 and 68.6:31.4, respectively. M.P.: 66–71 °C. TLC (20% ethyl acetate in hexanes) $R_f = 0.25$. ^1H NMR (300 MHz, CDCl_3) δ : 1.51 (s, 9H), 1.59 (d, $J = 7.28$ Hz, 3H), 2.27 (s, 3H), 4.10 (q, $J = 7.23$ Hz, 1H), 6.43 (bs, 1H), 6.87–6.94 (m, 2H), 7.03–7.09 (m, 1H), 7.09–7.16 (m, 2H), 7.21–7.32 (m, 3H). ^{13}C NMR (126 MHz, CDCl_3) δ : 21.3, 22.0, 28.5, 44.0, 80.6, 118.9, 119.3, 120.8, 125.3, 128.3, 129.3, 136.6, 140.6, 148.4, 150.8, 153.0, 169.6. IR (thin film): 3348, 2972, 2930, 2359, 1765, 1724, 1594, 1522, 1486, 1455, 1411, 1392, 1367, 1314, 1205, 1158, 1052, 1016, 938, 903, 886, 837, 796, 775, 697 cm^{-1} . HRMS $\text{C}_{21}\text{H}_{25}\text{NO}_4\text{Na}$ $[\text{M}+\text{Na}]^+$ calculated 378.1681, observed 378.1686. Enantiomers were separated by SFC on a Chiralpak AD-H column (4.6 mm x 250 mm, 5 μm particle size) under the following

conditions: 41 °C, 20% isopropyl alcohol, 2 mL min⁻¹, 160 Bar. R_T = 8.13 min, 9.86 min.

1,2-dimethoxy-4-(1-phenylethyl)benzene. The diarylmethine was synthesized according to General Method E to afford er's of 77.0:23.0 (run 1) and 78.0:22.0 (run 2), respectively. This molecule was previously reported.⁵⁶ Enantiomers were separated by HPLC on a Chiralcel OJ-H column (4.6 mm x 250 mm, 5 μm particle size) under the following conditions: ambient temperature, 0.5% isopropyl alcohol in hexanes, 2 mL min⁻¹. R_T = 40.48 min, 54.13 min.

Pentan-3-yl (4-(1-(4-(trifluoromethyl)phenyl)ethyl)phenyl)carbamate. The diarylmethine was synthesized according to General Method E to afford ¹H NMR conversions of 24% (run 1) and 24% (run 2) and er's of 61.8:38.2 and 62.2:37.8, respectively. TLC (100% dichloromethane) R_f = 0.50. ¹H NMR (500 MHz, CDCl₃) δ: 0.93 (t, *J* = 7.57 Hz, 6H), 1.55–1.66 (m, 7H), 4.16 (q, *J* = 7.16 Hz, 1H), 4.73 (p, *J* = 6.23 Hz, 1H), 6.54 (bs, 1H), 7.11–7.16 (m, 2H), 7.28–7.36 (m, 4H), 7.52 (d, *J* = 7.82 Hz, 2H). ¹³C NMR (126 MHz, CD₂Cl₂): δ 9.8, 21.8, 27.0, 44.4, 78.0, 119.0, 124.9 (q, *J* = 272.3 Hz), 125.6 (q, *J* = 3.8 Hz), 128.3, 128.4 (q, *J* = 32.1 Hz), 128.4, 137.2, 140.5, 151.4, 154.0. ¹⁹F NMR (282 MHz, CDCl₃) δ: -63.0. IR (thin film): 3323, 2970, 2937, 2880, 2361, 2339, 2164, 2049, 1699, 1617, 1597, 1526, 1459, 1414, 1325, 1226, 1164, 1123, 1070, 1016, 931, 837, 769, 668 cm⁻¹. HRMS C₂₁H₂₄NO₂F₃Na [M+Na]⁺ calculated 402.1657, observed 402.1661. Enantiomers were separated by SFC on a Chiralpak AD-H column (4.6 mm x 250 mm, 5 μm particle size) under the following conditions: 42 °C, 7% isopropyl alcohol, 4 mL min⁻¹, 160 Bar. R_T = 10.35 min, 12.01 min.

Butyl (4-(1-(4-(trifluoromethyl)phenyl)ethyl)phenyl)carbamate. The diarylmethine was synthesized according to General Method E to afford ¹H NMR

conversions of 18% (run 1) and 18% (run 2) and er's of 58.8:41.2 and 60.1:39.9, respectively. M.P.: 70–72 °C. TLC (100% dichloromethane) $R_f = 0.45$. ^1H NMR (500 MHz, CDCl_3) δ : 0.95 (t, $J = 7.33$ Hz, 3H), 1.37–1.45 (m, 2H), 1.61–1.69 (m, 5H), 4.13–4.19 (m, 3H), 6.55 (bs, 1H), 7.13 (d, $J = 8.80$ Hz, 2H), 7.30 (d, $J = 7.82$ Hz, 4H), 7.52 (d, $J = 8.80$ Hz, 2H). ^{13}C NMR (126 MHz, CD_2Cl_2) δ : 13.9, 19.5, 21.8, 31.4, 44.5, 65.4, 119.2, 124.9 (q, $J = 272.3$ Hz), 125.7 (q, $J = 3.8$ Hz), 128.3, 128.4 (q, $J = 32.4$ Hz), 128.5, 137.0, 140.7, 151.3, 154.1. ^{19}F NMR (282 MHz, CDCl_3) δ : -63.0. IR (thin film): 3321, 2964, 2875, 2361, 2338, 2176, 2160, 2136, 2040, 2012, 1977, 1703, 1617, 1598, 1531, 1457, 1415, 1326, 1223, 1164, 1122, 1070, 1016, 837, 770, 668, 545 cm^{-1} . HRMS $\text{C}_{20}\text{H}_{22}\text{NO}_2\text{F}_3\text{Na}$ $[\text{M}+\text{Na}]^+$ calculated 388.1500, observed 388.1512. Enantiomers were separated by SFC on a Chiralpak AD-H column (4.6 mm x 250 mm, 5 μm particle size) under the following conditions: 27 °C, 15% isopropyl alcohol, 2 mL min^{-1} , 160 Bar. $R_T = 11.66$ min, 13.42 min.

1,3-dichloro-5-(1-phenylethyl)benzene. The diarylmethine was synthesized according to General Method E to afford ^1H NMR conversions of 18% (run 1) and 22% (run 2) and er's of 50.4:49.6 and 53.6:46.4, respectively. The racemic sample was synthesized according to a previously published hydroarylation procedure using boronic ester 2-(3,5-dichlorophenyl)-1,3,2-dioxaborolane.¹⁸ TLC (hexanes) $R_f = 0.58$. ^1H NMR (500 MHz, CD_2Cl_2) δ : 1.62 (d, $J = 7.22$ Hz, 3H), 4.13 (q, $J = 7.17$ Hz, 1H), 7.04–7.55 (m, 8H). ^{13}C NMR (126 MHz, CD_2Cl_2) δ : 21.75, 44.98, 124.1, 125.6, 126.8, 127.9, 128.1, 133.98, 144.12, 149.43. IR (thin film): 2967, 2925, 2850, 1586, 1565, 1495, 1451, 1377, 1118, 1104, 1029, 1009, 856, 800, 777, 759, 700, 687, 668 cm^{-1} . MS $\text{C}_{14}\text{H}_{12}\text{Cl}_2$ $[\text{M}]^+$ calculated 250.0, observed 250.0. Enantiomers were separated by SFC on a Chiralpak

OJ-H column (4.6 mm x 250 mm) under the following conditions: 40 °C, 0% cosolvent, 2 mL min⁻¹, 100 Bar. R_T = 19.56 min, 21.23 min.

2-(3,5-dichlorophenyl)-1,3,2-dioxaborolane. To an oven-dried round bottom flask fitted with a condenser was added (3,5-dichlorophenyl)boronic acid (7.86 mmol, 1.0 equiv). After bringing the flask under a nitrogen atmosphere, 60 mL of benzene was added. The reaction mixture was heated to 55 °C and stirred for 1 hour, then heated to reflux and stirred for an additional 45 minutes. To the suspension of boronic acid in benzene was added ethylene glycol (11.4 mmol, 1.45 equiv), and the reaction mixture continued stirring at refluxing temperature for another 15 minutes, affording a homogeneous reaction mixture. After cooling to room temperature, MgSO₄ was added until there was no clumping of the drying agent upon addition, and the slurry was stirred for 10 minutes, followed by filtration and concentration, *in vacuo*, to afford product as a white solid in quantitative yield. TLC (30% ethyl acetate in hexanes) R_f = 0.48; M.P.: 57–58 °C; ¹H-NMR (500 MHz, CDCl₃): δ 4.38 (s, 4H), 7.44 (t, *J* = 0.49 Hz, 1H), 7.64 (d, *J* = 0.49 Hz, 2H); ¹³C-NMR (126 MHz, CDCl₃): δ 66.4, 131.5, 132.9, 134.9; IR (thin film): 3074, 2981, 2914, 1820, 1556, 1482, 1454, 1443, 1421, 1404, 1369, 1357, 1326, 1255, 1244, 1226, 1134, 1113, 1100, 1003, 992, 941, 894, 874, 832, 792, 715, 702, 694, 642 cm⁻¹; HRMS C₁₇H₂₀O₃-C₂H₃O₂ [M+AcO]⁺ calculated 275.0049, observed 275.0059.

Optimization of Hydrogenation Conditions

Design of Experiments (DoE) principles were employed to identify the optimal conditions under which the (IrCODPhosPrOx)BA_{TF}-catalyzed hydrogenations were performed. DoE principles indicate that by systematically varying experimental conditions across a range of interest and evaluating these changes' influence on some measureable

outcome, the relationship between conditions' variations and outcome can be mathematically related.⁵⁷ From such a mathematical relationship, the optimal combination of assessed variables could be predicted.

With this foundation, quantifiable, modifiable conditions—catalyst loading, concentration, and pressure—to optimize enantiomeric excess (ee) were identified. Next, the range of experimental interest was identified for each variable based upon conditions typical of iridium-catalyzed hydrogenations reported in the literature: 1.1 mol% to 4.6 mol% catalyst loading, 0.03 M to 0.5 M in CH₂Cl₂, 1 to 50 bar H₂ pressure.³² To understand the effect of variation across each of these ranges, a third point was incorporated into the experimental design at the center of each variable's range, resulting in a 3x3x3 matrix.

While simultaneous optimization of each variable would be facilitated by evaluating each variable combination, this results in 27 experiments (Figure 2.19a), some of which provide redundant information. Instead, by selecting an appropriate experimental design matrix, the number of experiments performed was reduced while still gathering sufficient information to model the relationship between the modified variables and ee. Applying a face-centered cubic (FCC) design matrix to the 3x3x3 matrix reduced the number of experiments performed, from 27 to 15 experiments (Figure 2.19b). The results of these 15 experiments, performed on substrate **1**, are reported in Table 2.3.

Performing standard stepwise regression analysis (using MATLAB) to relate ee to catalyst loading, concentration, and pressure yielded Eq. 2.5.⁴⁸ According to *p*-value test, catalyst loading was a statistically insignificant variable to the model. Through assessment of Eq. 2.5 and its graphical representation in Figure 2.20, it is readily apparent that ee values increase as concentration and pressure decrease. The lowest pressure and

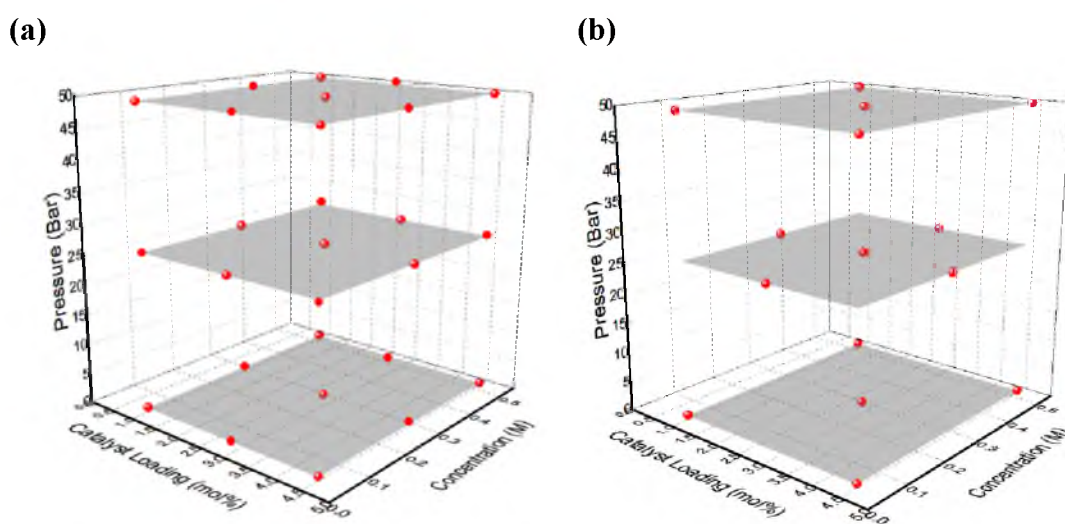


Figure 2.19. Design of Experiments (DoE) matrices. (a) Full experimental matrix. (b) Face-centered-cubic (FCC) reduction matrix.

Table 2.3. Design of Experiments matrix for optimization of reaction conditions.

Entry	Catalyst Loading	Concentration (M)	H ₂ (Bar)	Conv. ^a	ee ^b
1	1.1	0.028	1.4	57%	80%
2	4.6	0.028	1.4	>95%	81%
3	2.9	0.270	1.4	76%	77%
4	1.1	0.500	1.4	31%	65%
5	4.6	0.500	1.4	67%	69%
6	2.9	0.028	27	91%	74%
7	1.1	0.270	27	77%	37%
8	2.9	0.270	27	>95%	38%
9	4.6	0.270	27	>95%	41%
10	2.9	0.500	27	>95%	28%
11	1.1	0.028	50	59%	37%
12	4.6	0.028	50	>95%	59%
13	2.9	0.270	50	>95%	28%
14	1.1	0.500	50	>95%	20%
15	4.6	0.500	50	>95%	31%

^aConversions are representative of one experiment and measured by ¹H NMR. ^bee's were measured by SFC fitted with a chiral stationary phase.

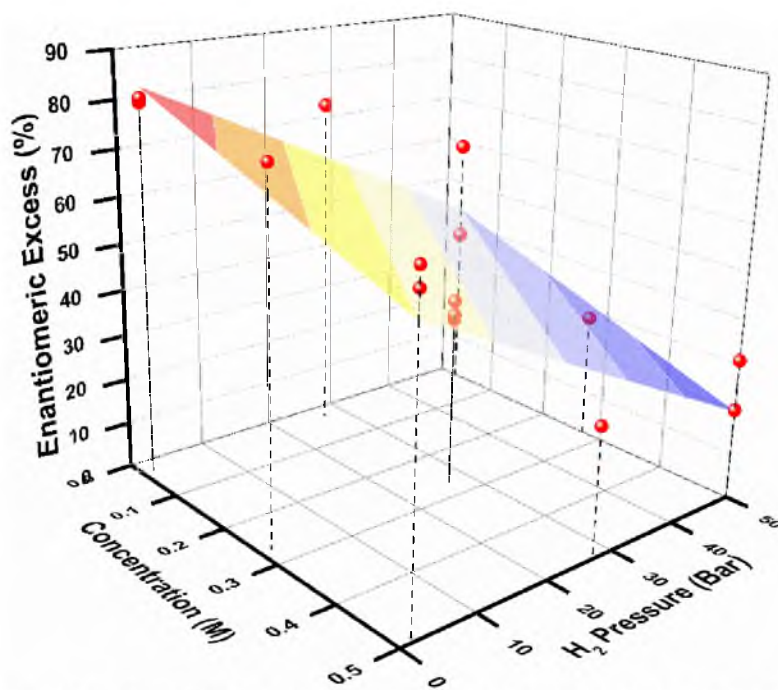


Figure 2.20. Graphical depiction of the mathematical model in Eq. 2.5.

concentration evaluated were 1.4 bar (20 psi) and 0.03 M in CH₂Cl₂, respectively. While catalyst loading had no statistically significant impact on ee, it did influence conversion of starting material to product. This influence is highlighted in the comparison of Table 2.3, entries 1 and 2, wherein concentration is 0.03 M, pressure is 1.4 bar, and catalyst loading is 1.1 mol% and 4.6 mol%, respectively. Of these two condition sets, only the latter afforded >95% conversion of starting material. Based on the results of this experiment, we performed further hydrogenation experiments under the conditions of 1 bar H₂, 0.03 M in CH₂Cl₂, and 4.6 mol% catalyst loading.

$$ee\% = 86 - 50\textit{Concentration} - 0.82\textit{Pressure} \quad R^2=0.81 \quad \text{Eq. 2.5}$$

Computational Methods

For computationally derived molecular distances and IR vibration values, all studied substrates were geometrically optimized and their frequencies were calculated using Gaussian 09 software.⁵⁸ The functional used for DFT calculation is M06-2x, which was previously benchmarked for thermodynamic and kinetic accuracy.^{59,60} A triple zeta potential basis-set (TZVP^{61,62}) was chosen based on the evaluation of the M06-2x functional for organic molecules, as triple zeta quality basis sets generally lead to quantitative correlations.⁵⁹ As it was our intention to seek correlations, we opted not to incorporate scaling factors for vibrational terms.⁶³ This simplification was justified by the assumption that a constant scaling factor would neither change the descriptive parameters identified, nor the relationship between them. The parameters used for modelling reaction enantioselectivities are given in Table 2.4.

Table 2.4. Parameter set used for descriptive modelling.

Substrate	ν_{ASYM}	i_{ASYM}	ν_{SYM}	i_{SYM}	sp² C=C ring stretch (1 of 6)	sp² C=C ring stretch (2 of 6)
1	1112.51	108.83	1170.95	34.12	1526.87	1574.32
2	1111.3	105.06	1176.48	17.42	1535.57	1573.29
3	1105.06	65.6577	1176.24	34.5517	1540.45	1573.85
4	1100.54	78.0479	1181.66	8.5951	1526.91	1577.00
5	1103.68	72.185	1177.85	6.6118	1540.04	1576.43
6	1104.44	21.26	1174.67	26.33	1534.45	1543.70
7	1100.06	17.09	1188.76	4.99	1542.57	1565.82
8	1128.95	1.1394	1180.28	3.1238	1507.90	1542.92
17	1106.09	84.24	1170.24	53.11	1526.88	1566.10
18	1105.06	30.13	1168.7	42.65	1526.75	1543.81
19	1104.78	18.78	1169.06	30.42	1527.42	1568.14
20	1112.18	92.28	1161.49	17.42	1526.63	1535.71
21	1109.1	41.14	1169.27	41.54	1526.55	1564.10
22	1109.63	47.86	1170.21	39.98	1527.00	1570.46
23	1106.65	37.5	1168.3	37.18	1526.96	1541.65
24	1115.22	40.05	1166.28	44.24	1526.77	1535.42
25	1123.17	22.22	1171.87	31.03	1507.62	1527.33
26	1106.14	7.42	1159.12	18.23	1542.85	1550.21
27	1106.17	11.228	1190.66	1.3051	1560.70	1569.89
28	1111.84	37	1171.52	2.59	1533.43	1573.68
29	1110.95	18.3333	1168.27	42.36	1542.19	1565.42
30	1102.35	46.76	1190.62	7.65	1565.92	1571.19
31	1103.58	42.5697	1190.85	4.1342	1567.79	1577.22
32	1108.65	1.606	1152.75	5.074	1486.56	1544.35

Table 2.4. Continued.

sp ² C=C ring stretch (3 of 6)	sp ² C=C ring stretch (4 of 6)	sp ² C=C ring stretch (5 of 6)	sp ² C=C ring stretch (5 of 6)	v _{C=C}	i _{C=C}	v _{C-H(sym)}
1649.33	1655.84	1681.75	1686.93	1708.09	12.07	3179.75
1648.73	1649.95	1683.19	1686.51	1707.21	20.54	3180.03
1647.73	1649.95	1681.73	1687.44	1708.65	11.947	3180.52
1648.73	1668.60	1671.73	1687.16	1707.59	16.4215	3179.13
1648.72	1654.33	1677.33	1686.07	1707.70	15.49	3178.88
1647.98	1649.22	1676.18	1682.42	1709.76	14.1	3180.24
1642.65	1647.91	1675.98	1686.17	1707.31	19.67	3180.24
1648.86	1667.79	1670.20	1675.83	1707.63	14.0959	3177.50
1643.01	1655.57	1681.71	1686.67	1710.07	11.4	3178.23
1647.80	1654.69	1676.62	1682.11	1709.57	7.48	3180.29
1646.81	1656.25	1681.86	1690.76	1712.15	5.9	3180.13
1649.52	1654.90	1680.88	1684.86	1710.87	4.15	3179.97
1637.64	1655.32	1682.23	1687.20	1711.06	9.38	3177.20
1623.06	1655.40	1681.41	1685.21	1708.84	9.26	3179.57
1637.62	1656.12	1668.98	1681.26	1710.57	8.78	3179.94
1652.90	1655.52	1674.64	1683.01	1711.78	6.07	3179.14
1656.39	1667.58	1670.75	1682.57	1710.42	4.29	3179.77
1641.96	1647.95	1675.84	1677.57	1709.08	13.081	3180.63
1635.08	1644.12	1685.04	1687.25	1706.03	23.788	3180.01
1648.81	1653.36	1677.73	1686.33	1709.09	16.29	3179.61
1643.20	1648.01	1675.92	1681.00	1706.58	17.88	3179.13
1643.93	1646.25	1686.17	1691.01	1708.74	16.97	3180.80
1645.46	1647.99	1687.29	1691.39	1707.67	14.2139	3180.28
1631.41	1649.10	1659.66	1677.00	1709.73	8.7745	3180.82

Table 2.4. Continued.

$i_{\text{C-H(sym)}}$	$\nu_{\text{C-H(asym)}}$	$i_{\text{C-H(asym)}}$	d_{TOR}	Enantiomeric Ratio		$\Delta\Delta G^\ddagger$
1.13	3267.81	7.54	3.19708	92	8	1.446177
1.04	3267.78	7.37	3.20511	74	26	0.619345
1.0752	3268.31	7.5377	3.19805	75	25	0.650517
0.796	3267.01	7.7972	3.20392	63	37	0.315139
0.8118	3266.79	7.136	3.20569	48.5	51.5	0.035538
0.81	3268.65	5.97	3.21196	74	26	0.619345
0.82	3268.37	7.11	3.20651	53	47	0.071141
0.88	3265.46	7.0901	3.21072	49	51	0.023688
1.11	3266.53	7.18	3.19756	91.5	8.5	1.407053
0.92	3268.75	6.27	3.20356	92.5	7.5	1.487601
0.56	3268.93	5.1	3.20073	96.5	3.5	1.963951
0.88	3268.8	6.17	3.20488	71	29	0.53018
1.16	3265.56	6.66	3.20094	88.5	11.5	1.208325
0.9	3267.93	6.9	3.20169	89	11	1.237982
0.74	3268.60	5.85	3.19816	96	4	1.881808
0.82	3267.46	7.1	3.20151	85.5	14.5	1.050649
0.9	3268.51	7.01	3.2032	77	23	0.715472
0.7799	3268.68	6.47	3.19694	91.5	8.5	1.407053
0.77	3267.69	7.6418	3.20196	44.5	55.5	0.130797
0.39	3267.46	5.97	3.20351	68.5	31.5	0.459991
0.81	3266.81	7.02	3.20167	77.5	22.5	0.732319
0.37	3268.82	5.57	3.20495	36	64	0.340688
0.3575	3268.72	5.8222	3.20583	40.5	59.5	0.227776
0.35	3269.43	4.7812	3.20669	52	48	0.047395

References

1. Harper, K. C.; Bess, E. N.; Sigman, M. S. Multidimensional Steric Parameters in the Analysis of Asymmetric Catalytic Reactions. *Nat. Chem.* **2012**, *4*, 366–374.
2. Bess, E. N.; Sigman, M. S. Linear Free Energy Relationships (LFERs) in Asymmetric Catalysis. In *Asymmetric Synthesis II: More Methods and Applications*, Christmann, M.; Bräse, S., Eds. Wiley-VCH Verlag GmbH & Co. KGaA: Weinheim, 2012.
3. Gustafson, J. L.; Sigman, M. S.; Miller, S. J. Linear Free-Energy Relationship Analysis of a Catalytic Desymmetrization Reaction of a Diarylmethane-bis(phenol). *Org. Lett.* **2010**, *12*, 2794–2797.
4. Verloop, A.; Hoogenstraaten, W.; Tipker, J. Development and Application of New Steric Substituent Parameters in Drug Design. In *Drug Design*, Ariens, E. J., Ed. Academic Press: New York, 1976; Vol. VII, pp 165–207.
5. Verloop, A.; Tipker, J. A Comparative Study of New Steric Parameters in Drug Design. *Pharmacochem. Libr.* **1977**, *2*, 63–81.
6. Verloop, A.; Tipker, J. Physical Basis of STERIMOL and Related Steric Constants. In *QSAR in Drug Design and Toxicology*, Hadzi, D.; Jerman-Blazic, B., Eds. Elsevier: Amsterdam, 1986; Vol. 10, p 97.
7. Bess, E. N.; Sigman, M. S. Distinctive Meta-Directing Group Effect for Iridium-Catalyzed 1,1-Diarylalkene Enantioselective Hydrogenation. *Org. Lett.* **2013**, *15*, 646–649.
8. Messaoudi, S.; Hamze, A.; Provot, O.; Tréguier, B.; Rodrigo De Losada, J.; Bignon, J.; Liu, J.-M.; Wdzieczak-Bakala, J.; Thoret, S.; Dubois, J., et al. Discovery of Isoerianin Analogues as Promising Anticancer Agents. *ChemMedChem* **2011**, *6*, 488–497.
9. Moree, W. J.; Li, B.-F.; Zamani-Kord, S.; Yu, J.; Coon, T.; Huang, C.; Marinkovic, D.; Tucci, F. C.; Malany, S.; Bradbury, M. J., et al. Identification of a Novel Selective H1-Antihistamine with Optimized Pharmacokinetic Properties for Clinical Evaluation in the Treatment of Insomnia. *Bioorg. Med. Chem. Lett.* **2010**, *20*, 5874–5878.
10. Liang, H.; Wu, X.; Yalowich, J. C.; Hasinoff, B. B. A Three-Dimensional Quantitative Structure-Activity Analysis of a New Class of Bisphenol Topoisomerase II α Inhibitors. *Mol. Pharmacol.* **2008**, *73*, 686–696.
11. Moriconi, A.; Cesta, M. C.; Cervellera, M. N.; Aramini, A.; Coniglio, S.; Colagioia, S.; Beccari, A. R.; Bizzarri, C.; Cavicchia, M. R.; Locati, M., et al. Design of Noncompetitive Interleukin-8 Inhibitors Acting on CXCR1 and CXCR2. *J. Med. Chem.* **2007**, *50*, 3984–4002.

12. Barda, D. A.; Wang, Z.-Q.; Britton, T. C.; Henry, S. S.; Jagdmann, G. E.; Coleman, D. S.; Johnson, M. P.; Andis, S. L.; Schoepp, D. D. SAR Study of a Subtype Selective Allosteric Potentiator of Metabotropic Glutamate 2 Receptor, N-(4-phenoxyphenyl)-N-(3-Pyridinylmethyl)ethanesulfonamide. *Bioorg. Med. Chem. Lett.* **2004**, *14*, 3099–3102.
13. Cheltsov, A. V.; Aoyagi, M.; Aleshin, A.; Yu, E. C.-W.; Gilliland, T.; Zhai, D.; Bobkov, A. A.; Reed, J. C.; Liddington, R. C.; Abagyan, R. Vaccinia Virus Virulence Factor NIL is a Novel Promising Target for Antiviral Therapeutic Intervention. *J. Med. Chem.* **2010**, *53*, 3899–3906.
14. Gligorich, K.; Vaden, R.; Shelton, D.; Wang, G.; Matsen, C.; Looper, R.; Sigman, M.; Welm, B. Development of a Screen to Identify Selective Small Molecules Active Against Patient-Derived Metastatic and Chemoresistant Breast Cancer Cells. *Breast Cancer Res.* **2013**, *15*, R58.
15. Pathak, T. P.; Sigman, M. S. Palladium-Catalyzed Hydrofunctionalization of Vinyl Phenol Derivatives with Heteroaromatics. *Org. Lett.* **2011**, *13*, 2774–2777.
16. Podhajsky, S. M.; Iwai, Y.; Cook-Sneathen, A.; Sigman, M. S. Asymmetric Palladium-Catalyzed Hydroarylation of Styrenes and Dienes. *Tetrahedron* **2011**, *67*, 4435–4441.
17. Gligorich, K. M.; Iwai, Y.; Cummings, S. A.; Sigman, M. S. A New Approach to Carbon–Carbon Bond Formation: Development of Aerobic Pd-Catalyzed Reductive Coupling Reactions of Organometallic Reagents and Styrenes. *Tetrahedron* **2009**, *65*, 5074–5083.
18. Iwai, Y.; Gligorich, K. M.; Sigman, M. S. Aerobic Alcohol Oxidation Coupled to Palladium-Catalyzed Alkene Hydroarylation with Boronic Esters. *Angew. Chem. Int. Ed.* **2008**, *47*, 3219–3222.
19. Gligorich, K. M.; Cummings, S. A.; Sigman, M. S. Palladium-Catalyzed Reductive Coupling of Styrenes and Organostannanes under Aerobic Conditions. *J. Am. Chem. Soc.* **2007**, *129*, 14193–14195.
20. Greene, M. A.; Yonova, I. M.; Williams, F. J.; Jarvo, E. R. Traceless Directing Group for Stereospecific Nickel-Catalyzed Alkyl–Alkyl Cross-Coupling Reactions. *Org. Lett.* **2012**, *14*, 4293–4296.
21. Taylor, B. L. H.; Swift, E. C.; Waetzig, J. D.; Jarvo, E. R. Stereospecific Nickel-Catalyzed Cross-Coupling Reactions of Alkyl Ethers: Enantioselective Synthesis of Diarylethanes. *J. Am. Chem. Soc.* **2010**, *133*, 389–391.
22. Wang, X.; Guram, A.; Caille, S.; Hu, J.; Preston, J. P.; Ronk, M.; Walker, S. Highly Enantioselective Hydrogenation of Styrenes Directed by 2'-Hydroxyl Groups. *Org. Lett.* **2011**, *13*, 1881–1883.

23. Fessard, T. C.; Andrews, S. P.; Motoyoshi, H.; Carreira, E. M. Enantioselective Preparation of 1,1-Diarylethanes: Aldehydes as Removable Steering Groups for Asymmetric Synthesis. *Angew. Chem. Int. Ed.* **2007**, *46*, 9331–9334.
24. Wilkinson, J. A.; Rossington, S. B.; Ducki, S.; Leonard, J.; Hussain, N. Asymmetric Alkylation of Diarylmethane Derivatives. *Tetrahedron* **2006**, *62*, 1833–1844.
25. Wilkinson, J. A.; Rossington, S. B.; Ducki, S.; Leonard, J.; Hussain, N. Asymmetric Alkylation of N-pivaloyl-o-benzylaniline. *Tetrahedron: Asymmetry* **2004**, *15*, 3011–3013.
26. Prat, L.; Dupas, G.; Duflos, J.; Quéguiner, G.; Bourguignon, J.; Levacher, V. Deracemization of Alkyl Diarylmethanes Using (–)-Sparteine or a Chiral Proton Source. *Tetrahedron Lett.* **2001**, *42*, 4515–4518.
27. Hatanaka, Y.; Hiyama, T. Stereochemistry of the Cross-Coupling Reaction of Chiral Alkylsilanes with Aryl Triflates: A Novel Approach to Optically Active Compounds. *J. Am. Chem. Soc.* **1990**, *112*, 7793–7794.
28. Gridnev, I. D.; Imamoto, T. On the Mechanism of Stereoselection in Rh-Catalyzed Asymmetric Hydrogenation: A General Approach for Predicting the Sense of Enantioselectivity. *Acc. Chem. Res.* **2004**, *37*, 633–644.
29. Roseblade, S. J.; Pfaltz, A. Iridium-Catalyzed Asymmetric Hydrogenation of Olefins. *Acc. Chem. Res.* **2007**, *40*, 1402–1411.
30. Church, T. L.; Andersson, P. G. Iridium Catalysts for the Asymmetric Hydrogenation of Olefins with Nontraditional Functional Substituents. *Coord. Chem. Rev.* **2008**, *252*, 513–531.
31. Pàmies, O.; Andersson, P. G.; Diéguez, M. Asymmetric Hydrogenation of Minimally Functionalised Terminal Olefins: An Alternative Sustainable and Direct Strategy for Preparing Enantioenriched Hydrocarbons. *Chem. Eur. J.* **2010**, *16*, 14232–14240.
32. Mazuela, J.; Verendel, J. J.; Coll, M.; Schäffner, B. n.; Börner, A.; Andersson, P. G.; Pàmies, O.; Diéguez, M. Iridium Phosphite–Oxazoline Catalysts for the Highly Enantioselective Hydrogenation of Terminal Alkenes. *J. Am. Chem. Soc.* **2009**, *131*, 12344–12353.
33. Lightfoot, A.; Schnider, P.; Pfaltz, A. Enantioselective Hydrogenation of Olefins with Iridium–Phosphanodihydrooxazole Catalysts. *Angew. Chem. Int. Ed.* **1998**, *37*, 2897–2899.
34. Källström, K.; Munslow, I.; Andersson, P. G. Ir-Catalysed Asymmetric Hydrogenation: Ligands, Substrates and Mechanism. *Chem. Eur. J.* **2006**, *12*, 3194–3200.

35. Pfaltz, A.; Blankenstein, J.; Hilgraf, R.; Hörmann, E.; McIntyre, S.; Menges, F.; Schönleber, M.; Smidt, S. P.; Wüstenberg, B.; Zimmermann, N. Iridium-Catalyzed Enantioselective Hydrogenation of Olefins. *Adv. Synth. Catal.* **2003**, *345*, 33–43.
36. Tolstoy, P.; Engman, M.; Paptchikhine, A.; Bergquist, J.; Church, T. L.; Leung, A. W. M.; Andersson, P. G. Iridium-Catalyzed Asymmetric Hydrogenation Yielding Chiral Diarylmethines with Weakly Coordinating or Noncoordinating Substituents. *J. Am. Chem. Soc.* **2009**, *131*, 8855–8860.
37. McKennon, M. J.; Meyers, A. I.; Drauz, K.; Schwarm, M. A Convenient Reduction of Amino Acids and Their Derivatives. *J. Org. Chem.* **1993**, *58*, 3568–3571.
38. Miller, J. J.; Sigman, M. S. Design and Synthesis of Modular Oxazoline Ligands for the Enantioselective Chromium-Catalyzed Addition of Allyl Bromide to Ketones. *J. Am. Chem. Soc.* **2007**, *129*, 2752–2753.
39. Rajaram, S.; Sigman, M. S. Design of Hydrogen Bond Catalysts Based on a Modular Oxazoline Template: Application to an Enantioselective Hetero Diels–Alder Reaction. *Org. Lett.* **2005**, *7*, 5473–5475.
40. Jensen, K. H.; Sigman, M. S. Systematically Probing the Effect of Catalyst Acidity in a Hydrogen-Bond-Catalyzed Enantioselective Reaction. *Angew. Chem. Int. Ed.* **2007**, *46*, 4748–4750.
41. Bernsmann, H.; van den Berg, M.; Hoen, R.; Minnaard, A. J.; Mehler, G.; Reetz, M. T.; De Vries, J. G.; Feringa, B. L. PipPhos and MorfPhos: Privileged Monodentate Phosphoramidite Ligands for Rhodium-Catalyzed Asymmetric Hydrogenation. *J. Org. Chem.* **2005**, *70*, 943–951.
42. Smidt, S. P.; Menges, F.; Pfaltz, A. SimplePHOX, a Readily Available Chiral Ligand System for Iridium-Catalyzed Asymmetric Hydrogenation. *Org. Lett.* **2004**, *6*, 2023–2026.
43. Carlson, R. *Design and Optimization in Organic Synthesis*. Elsevier: Amsterdam, 1992; Vol. 8.
44. Deming, S. N.; Morgan, S. L. *Experimental Design: A Chemometric Approach*. Elsevier: Amsterdam, 1993; Vol. 11.
45. Hammett, L. P. Some Relations between Reaction Rates and Equilibrium Constants. *Chem. Rev.* **1935**, *17*, 125–136.
46. Hammett, L. P. The Effect of Structure upon the Reactions of Organic Compounds. Benzene Derivatives. *J. Am. Chem. Soc.* **1937**, *59*, 96–103.
47. Verloop, A.; Tipker, J. A Comparative Study of New Steric Parameters in Drug Design. In *Biological Activity and Chemical Structure*, Buisman, J. A. K., Ed. Elsevier: Amsterdam, 1977.

48. MATLAB. *version 8.1.0.604 (R2013a)*. The MathWorks, Inc.: Natick, MA, 2013.
49. Milo, A.; Bess, E. N.; Sigman, M. S. Interrogating Selectivity in Catalysis Using Molecular Vibrations. *Nature* **2014**, *507*, 210–214.
50. Yakelis, N. A.; Bergman, R. G. Safe Preparation and Purification of Sodium Tetrakis[(3,5-trifluoromethyl)phenyl]borate (NaBArF₂₄): Reliable and Sensitive Analysis of Water in Solutions of Fluorinated Tetraarylborates. *Organometallics* **2005**, *24*, 3579–3581.
51. Jahani, F.; Tajbakhsh, M.; Golchoubian, H.; Khaksar, S. Guanidine Hydrochloride as an Organocatalyst for N-Boc Protection of Amino Groups. *Tetrahedron Lett.* **2011**, *52*, 1260–1264.
52. Li, J. J.; Li, J. J.; Li, J.; Trehan, A. K.; Wong, H. S.; Krishnananthan, S.; Kennedy, L. J.; Gao, Q.; Ng, A.; Robl, J. A., et al. A Synthesis of N-Bridged 5,6-Bicyclic Pyridines via A Mild Cyclodehydration Using the Burgess Reagent and Discovery of A Novel Carbamylsulfonylation Reaction. *Org. Lett.* **2008**, *10*, 2897–2900.
53. Shimizu, M.; Mochida, K.; Hiyama, T. Modular Approach to Silicon-Bridged Biaryls: Palladium-Catalyzed Intramolecular Coupling of 2-(Arylsilyl)aryl Triflates. *Angew. Chem. Int. Ed.* **2008**, *47*, 9760–9764.
54. Gerstenberger, B. S.; Konopelski, J. P. *tert*-Butyldiphenylsilylethyl (“TBDPSE”): A Practical Protecting Group for Phenols. *J. Org. Chem.* **2005**, *70*, 1467–1470.
55. López-Pérez, A.; Adrio, J.; Carretero, J. C. Palladium-Catalyzed Cross-Coupling Reaction of Secondary Benzylic Bromides with Grignard Reagents. *Org. Lett.* **2009**, *11*, 5514–5517.
56. Murali, A.; Puppala, M.; Varghese, B.; Baskaran, S. A Lewis Acid Mediated Schmidt Reaction of Benzylic Azide: Synthesis of Sterically Crowded Aromatic Tertiary Amines. *Eur. J. Org. Chem.* **2011**, *2011*, 5297–5302.
57. Carlson, R. *Design and Optimization in Organic Synthesis*. Elsevier: Amsterdam, 1992.
58. Frisch, M. J.; Trucks, G. W.; Schlegel, H. B.; Scuseria, G. E.; Robb, M. A.; Cheeseman, J. R.; Scalmani, G.; Barone, V.; Mennucci, B.; Petersson, G. A., et al. *Gaussian 09, Revision C.01*, Gaussian, Inc.: Wallingford, CT, 2009.
59. Zhao, Y.; Truhlar, D. G. The M06 Suite of Density Functionals for Main Group Thermochemistry, Thermochemical Kinetics, Noncovalent Interactions, Excited States, and Transition Elements: Two New Functionals and Systematic Testing of Four M06-Class Functionals and 12 Other Functionals. *Theor. Chem. Acc.* **2007**, *120*, 215–241.
60. Valero, R.; Gomes, J. R. B.; Truhlar, D. G.; Illas, F. Good Performance of the M06

- Family of Hybrid Meta Generalized Gradient Approximation Density Functionals on a Difficult Case: CO Adsorption on MgO(001). *J. Chem. Phys.* **2008**, *129*, 124710.
61. Schäfer, A.; Horn, H.; Ahlrichs, R. Fully Optimized Contracted Gaussian Basis Sets for Atoms Li to Kr. *J. Chem. Phys.* **1992**, *97*, 2571.
 62. Schäfer, A.; Huber, C.; Ahlrichs, R. Fully Optimized Contracted Gaussian Basis Sets of Triple Zeta Valence Quality for Atoms Li to Kr. *J. Chem. Phys.* **1994**, *100*, 5829.
 63. Merrick, J. P.; Moran, D.; Radom, L. An Evaluation of Harmonic Vibrational Frequency Scale Factors. *J. Phys. Chem. A* **2007**, *111*, 11683–11700.

CHAPTER 3

A DESIGN OF EXPERIMENTS-GUIDED APPROACH TO THE INVESTIGATION OF RHODIUM-CATALYZED C–H AMINATION SITE SELECTIVITY*

Introduction

Our approach to exploring and evaluating unique, appropriately descriptive parameters, which is discussed in Chapter 2, represents a common thread in the mathematical analyses of chemical systems described in this and the following chapter. From such a foundation of chemically relevant descriptors, model development proceeds most effectively when Design of Experiments (DoE) principles are applied to reaction investigation.^{1,2} Described in this chapter is an unconventional application of DoE precepts, by which a predictive mathematical model describing a Rh-catalyzed reaction's site-selectivity was developed. Examination of this model allowed for the design of a new reagent that affords improved site-selective outcomes for the reaction investigated. The synthetic results reported in this chapter are primarily the work of Dr. Ryan DeLuca, with contributions made by Dr. Martins Oderinde and Daniel Tindall. The computational

* This chapter is based on the author's reported work that is herein reproduced with permission from Bess, E. N.; DeLuca, R. J.; Tindall, D. J.; Oderinde, M. S.; Roizen, J. L.; Du Bois, J.; Sigman, M. S. Analyzing Site Selectivity in Rh₂(esp)₂-Catalyzed Intermolecular C–H Amination Reactions. *J. Am. Chem. Soc.* **2014**, *136*, 5783–5789. Copyright 2014 American Chemical Society.

energy minimizations and frequency calculations, experimental design, and linear regression model development are the author's work.

Discriminate control over product selectivity in carbon-hydrogen (C–H) bond functionalization reactions represents one of the great challenges in modern synthetic chemistry.³ The high energy barriers to C–H bond cleavage (on the order of 98 kcal mol⁻¹) contrast the small energetic differences that bias enantio- and chemoselective C–H bond functionalization ($\Delta\Delta G^\ddagger$ of ~2 kcal mol⁻¹ for >20:1 selectivity). Given the small differences in transition state free energies that modulate isomeric product ratios, it is often difficult to distinguish the steric and electronic factors that influence reaction selectivity. Identification of the dominant influences on reaction outcome can prove invaluable for tailoring catalyst and reagent structures to afford greater control over reaction outcomes.

The Du Bois group recently reported an intermolecular Rh-catalyzed C–H amination protocol⁴ and demonstrated that oxidation of isoamylbenzene **a** results in benzylic-to-tertiary (B:T) product ratios that are dependent upon the choice of sulfamate ester **b** (Figure 3.1).⁵ The relationships between steric and electronic factors that contribute to these disparate outcomes are not obvious from the trends in selectivity. Specifically, sulfamate ester **b1**, R = CH₂CCl₃, yielded the highest degree of B:T selectivity (8:1), while substitution to R = CH₂*t*-Bu (**b2**), a steric homolog, resulted in reduced benzylic selectivity (4:1). An equally intriguing result was obtained from the evaluation of sulfamate ester **b3**, R = CH(CF₃)₂, which yields equimolar amounts of the two products. Similar losses in selectivity were observed for both electron-poor (**b4**, R = 2,6-F₂C₆H₃, 1.5:1) and electron-rich (**b5**, 4-*t*-BuC₆H₄, 1:1) aryl sulfamate esters.

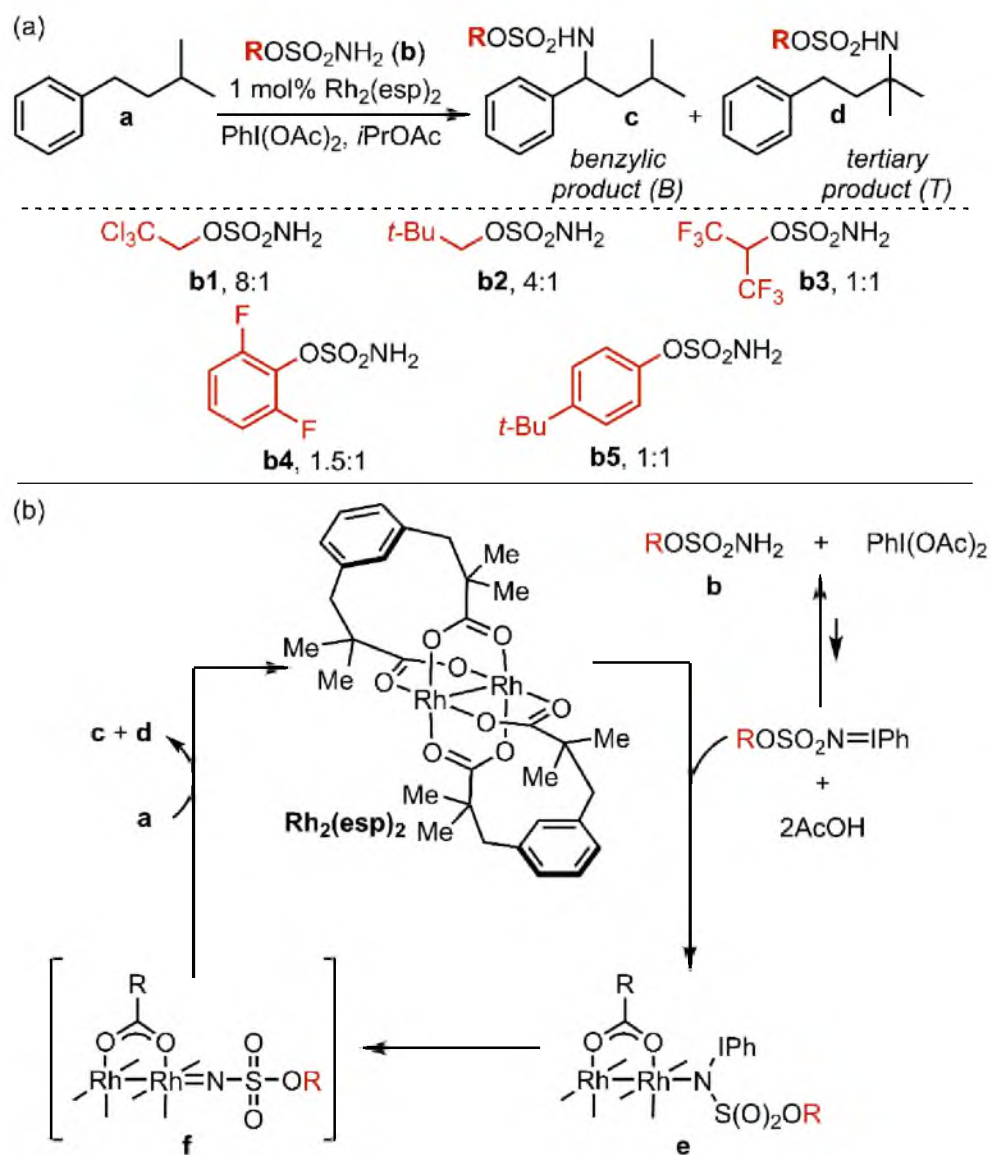


Figure 3.1. $\text{Rh}_2(\text{esp})_2$ -catalyzed C–H amination of isoamylbenzene. (a) Varying the sulfamate ester evokes changes in site selectivity, demonstrating the sensitivity of the reaction. (b) Proposed catalytic cycle of this amination reaction.

An archetypical physical organic technique for identifying features that influence product selectivity as a function of substituent changes is linear free-energy relationship (LFER) analysis.^{6,7} Pioneered by Hammett for electronic analysis of *meta*- or *para*-substituted benzene rings^{8,9} and adopted by Taft^{10,11} and, later, Charton¹² for steric effect analyses, these techniques have been broadly applied to interrogate reaction outcomes.¹³⁻¹⁹ While these classic LFER parameters have been instrumental in a variety of contexts, often illuminating mechanistic details by relating $\log(K)$ to empirically derived electronic or steric constants (where K may represent relative rate and equilibrium constants, ratios of enantiomers and constitutional isomers, etc.), LFERs also bear significant limitations.^{20,21} Namely, a modest number of reactions can be successfully modeled using Hammett or Taft/Charton parameters alone.^{21,22-24}

As discussed in Chapter 2, over the last several years, the Sigman laboratory has investigated the use of discretely measured molecular parameters (*vide infra*) as opposed to those derived from relative-rate experiments (e.g., Hammett and Taft values) for nonclassic free-energy relationship analysis, relating these parameters to $\Delta\Delta G^\ddagger$ for differential transition state interrogation.^{21,25} As the data from the Rh-catalyzed C–H amination lack obvious explanation, commonly employed free-energy relationships are not likely capable of delineating the entangled effects of the sulfamate ester on site selectivity. Therefore, we turned to our recent discovery that specific infrared (IR) molecular vibrations represent a broadly applicable, yet uniquely descriptive, parameter set, which was discussed in Chapter 2 in the context of iridium-catalyzed hydrogenation.²² IR vibrations can be computationally calculated for any molecule, the result of which is a tailored parameter set that is capable of describing the distinct nature

of each reactive species.

Herein, we exploit the intrinsic ability of IR vibrations to describe the inherent molecular properties of sulfamate ester nitrene precursors in selective Rh₂(esp)₂-catalyzed amination of benzylic versus tertiary C–H bonds. Using IR-derived descriptors to quantitate steric and electronic selectivity determinants, we apply linear regression modeling to identify the sulfamate ester features responsible for differential benzylic-to-tertiary functionalization. Insights garnered from this free-energy model have led us to design a new sulfamate ester, which yields the highest selectivity ratio (9.5:1, B:T) reported, to date, for this C–H amination process.

Investigating the Reaction

Through the Du Bois group's investigation of intermolecular oxidation reactions (a proposed mechanism of which is depicted in Figure 3.1b),⁴ an interesting relationship was noted between the steric and electronic structure of the sulfamate ester **b** and the B:T ratio in the oxidation of isoamylbenzene **a** (Figure 3.1a).⁵ The results of these investigations were ascribed principally to steric differences between sulfamate reagents, but the influence of electronic substituent effects could not be discounted.

Accordingly, a sulfamate ester library was designed to more thoroughly probe the interplay of steric and electronic perturbations on the selectivity dependence of this system (Figure 3.2). Library construction was based on two features inspired by the original results: 1) the exploration of chain-length and halogenation (**2a–2l**) and 2) the evaluation of branching and steric bulk distal to the α -carbon of the sulfamate (**2m–2t**). The sulfamate esters depicted in Figure 3.2 were synthesized and evaluated in the

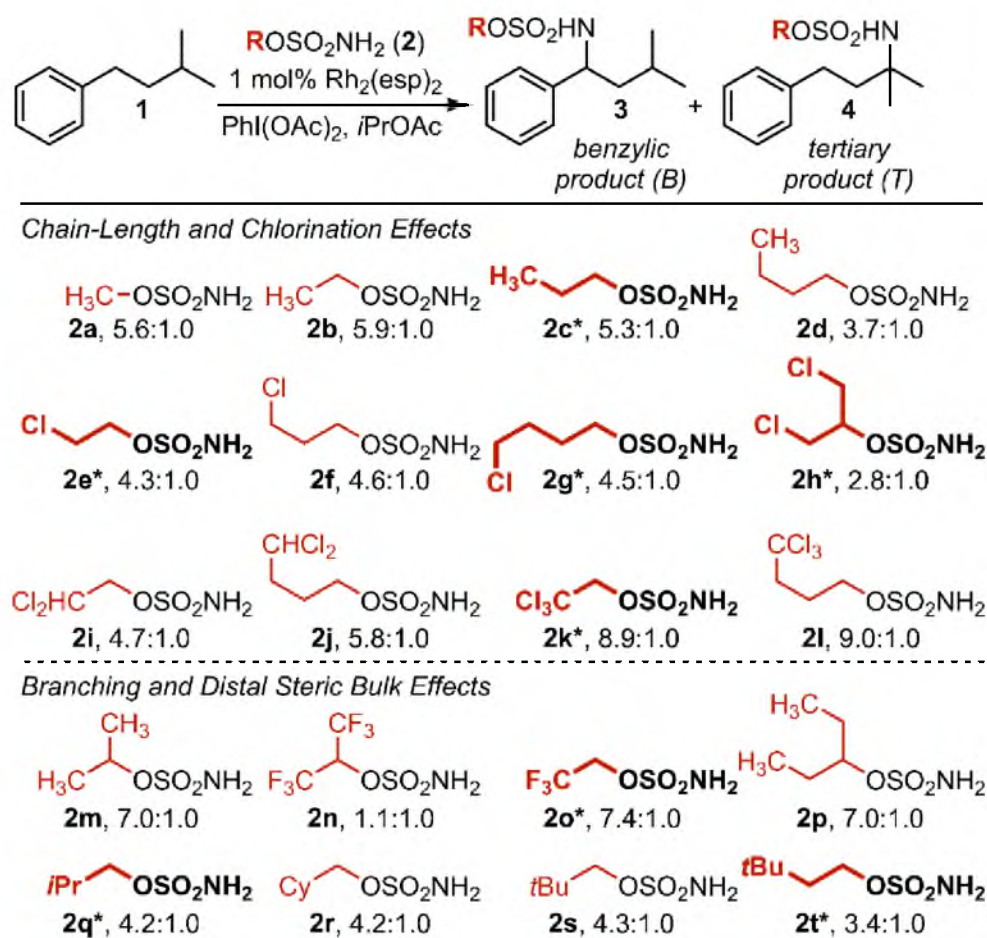


Figure 3.2. Twenty-membered sulfamate ester library used to probe the rhodium-catalyzed reaction's site-selection sensitivity. Ratios, determined by GC analysis, are averaged over three experimental runs. Bolded and asterisked sulfamate ester structures represent the DoE-defined subset of nitrene sources.

Rh₂(esp)₂-catalyzed amination of **1**. Of particular interest, chlorine substitution (**2e–2l**) has a pronounced effect on product selectivity with trichloromethyl sulfamate esters (**2k, 2l**) yielding B:T ratios of ~9:1, regardless of the proximity of this group to the -SO₂NH₂ moiety. Relative to R = *n*Bu (**2d**), this same trend is maintained for di- and monochloromethyl substrates, where B:T ratios average 5.3:1 (**2i, 2j**) and 4.5:1 (**2e–2g**), respectively.

The insensitivity of B:T selectivity to chain length is a general trend observed throughout the data set. The influence of steric effects on selectivity becomes apparent when the sulfamate ester bears a branched α -carbon (i.e., sulfamates prepared from secondary alcohols). Specifically, selectivity for the benzylic insertion product increases for *i*PrOSO₂NH₂ (**2m**, 7.0:1) relative to EtOSO₂NH₂ (**2b**, 5.9:1). A marked change in the product ratio is noted when halogen substituents are introduced in these secondary alcohol-derived sulfamate esters (**2h, 2n**). For example, a reaction performed with (CF₃)₂CHOSO₂NH₂ yields nearly equal amounts of the benzylic and tertiary products. However, replacing one CF₃ group with H (**2o**, 7.4:1), to eliminate the branching pattern, rescues selectivity.

Parameter Selection

Collectively, the data portrayed in Figure 3.2 reflect an ill-defined role for steric and electronic modulation of the sulfamate ester on product selectivity. Steric influences manifest principally in the narrow dimension of branched versus nonbranched sulfamate groups. Additionally, while inclusion of electronegative halogen atoms clearly alters product selectivity, the effect cannot be ascribed entirely to electronic differences in

nitrenoid reactivity. These general features of the amination reaction significantly complicate quantitative free-energy modeling of selectivity. Classic steric parameters, such as Taft^{10,11} and Charton¹² values and Winstein-Holness (A) values²⁶—derived from relative-rate and conformation equilibration experiments, respectively—treat substituent steric bulk as a spherical unit.²¹ Therefore, this treatment has the disadvantage of averaging the nuances of substituent asymmetry and width-to-length ratios into a single-value representation of steric effects.

In the development of free-energy relationships describing selectivity, it is precisely these subtleties that are responsible for the differential transition state energies leading to isomeric product ratios, as predicated by the Curtin-Hammett principle.²⁷ Verloop innovatively approached this deficiency in the description of steric effects through the development of Sterimol parameters (Figure 3.3).²⁸⁻³⁰ As demonstrated in the Sterimol analysis of bisphenol desymmetrization (Chapter 2), this parameter set lends dimensional specificity to the description of steric bulk through its three subparameters: B₁, substituent minimum radius; B₅, substituent maximum radius; and L, substituent length.

While the effectiveness of Sterimol parameters in various contexts has been successfully demonstrated,^{21,22,25} this steric descriptor still lacks information about the position along L at which steric bulk resides. For example, as depicted in Figure 3.3, Sterimol measures of the -CH₂*t*-Bu substituent are 1.52 (B₁), 4.18 (B₅), and 4.89 (L).³¹ Comparatively, the Sterimol system describes *n*Pr, a group with its own distinct apparent steric bulk, as nearly isosteric with CH₂*t*-Bu, measuring 1.52 (B₁), 3.49 (B₅), and 4.92 (L).

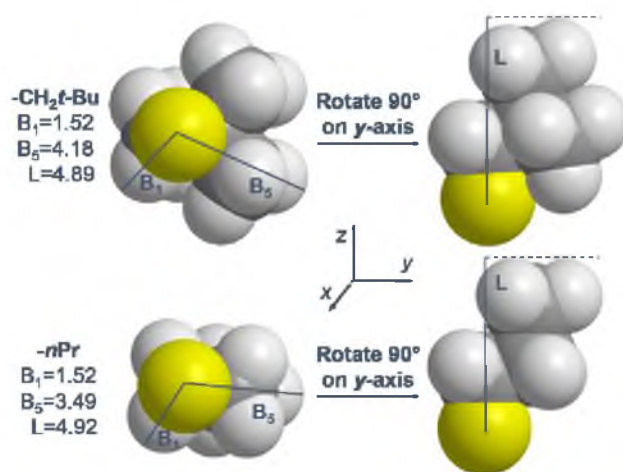


Figure 3.3. Schematics of the Sterimol parameter system, describing the subparameters B_1 (minimum radius), B_5 (maximum radius), and L (length). Comparisons of *n*Pr and CH₂*t*-Bu substituents' Sterimol parameters demonstrate a deficiency in the Sterimol parameters' description of bulk, where sterically distinct groups are similarly described.

A similar parameter deficiency is observed for electronic description. The presence of R-group chlorine atoms, particularly trichloromethyl, generally enhances selectivity (in the absence of branching), independent of the chlorine atom distance from the $-\text{NH}_2$ group of the sulfamate moiety. This observation cannot be explained through the use of the ubiquitous electronic descriptor, $\text{p}K_{\text{a}}$, or any descriptor of induction.³² These apparent limitations warrant a more sophisticated approach to characterize the underlying selectivity trends in C–H amination. Thus, we have turned to IR molecular vibrations, which were successfully demonstrated to model the differential free-energy of enantioselection in the iridium-catalyzed asymmetric hydrogenation assessed in Chapter 2.²² Derived from the unique vibrational fingerprint of every molecule and representative of the fundamental energies, bond strengths, and dipole moments contained therein, IR stretches were computationally calculated for each sulfamate ester using the computational method M06-2X/TZVP.³³⁻³⁷

While the reactive oxidant believed to be involved in the selectivity-defining step of the Rh-catalyzed amination is a Rh-nitrene (**f**, Figure 3.1b), the computed vibrational data are from the sulfamate ester and not the nitrenoid. As noted above, the differential energy between nitrenoid transition states ($\Delta\Delta G^\ddagger$) is responsible for benzylic-to-tertiary amination ratios. The working hypothesis, for which supporting evidence is provided, is that modifications to the nitrene precursor (i.e., sulfamate ester) commensurately impact molecular properties of the selectivity-defining transition states (*vide infra*).²⁷ This is an important qualification, which allows ground state IR frequencies and intensities to be computed for the simplest of these species, the sulfamate ester. This approach significantly reduces the computational effort, making

the methodology tractable.

In order to proceed with free-energy relationship model development, it is necessary to identify IR vibrations that are hypothesized to be potential selectivity descriptors. From such a set, stepwise linear regression analysis is performed, whereby the descriptors are statistically whittled down to a subset of parameters that best mathematically relates features of the sulfamate ester to $\Delta\Delta G^\ddagger$ (equating to $-RT \cdot \ln(\text{tertiary/benzylic})$, where R is the ideal gas constant and T is temperature). As each sulfamate ester is characterized with many disparate vibrational modes, the vibrations chosen are those that were consistently identified in the computed molecules (i.e., major vibrational modes) and presumed to significantly impact the putative Rh-nitrene selectivity profile.

Given these criteria, four vibrations were chosen as potential descriptors of selectivity: O–S–N asymmetric stretch (ν_{OSN}), C–O stretch (ν_{CO}), SO₂ symmetric stretch ($\nu_{\text{SO}_2\text{sym}}$), and SO₂ asymmetric stretch ($\nu_{\text{SO}_2\text{asym}}$). Figure 3.4 depicts a simulated IR spectrum for sulfamate ester **2a** (R = Me) and highlights both the calculated frequencies and intensities of these four vibrations, giving a total of eight vibration-derived descriptors that were used for regression analysis. While many other unique combinations of potential descriptors are possible, the set identified, based on chemical knowledge of foundational chemical principles, was carried forward to model development. Subsequently, the appropriateness of the identified descriptors for effectively describing and predicting reaction outcomes was assessed.

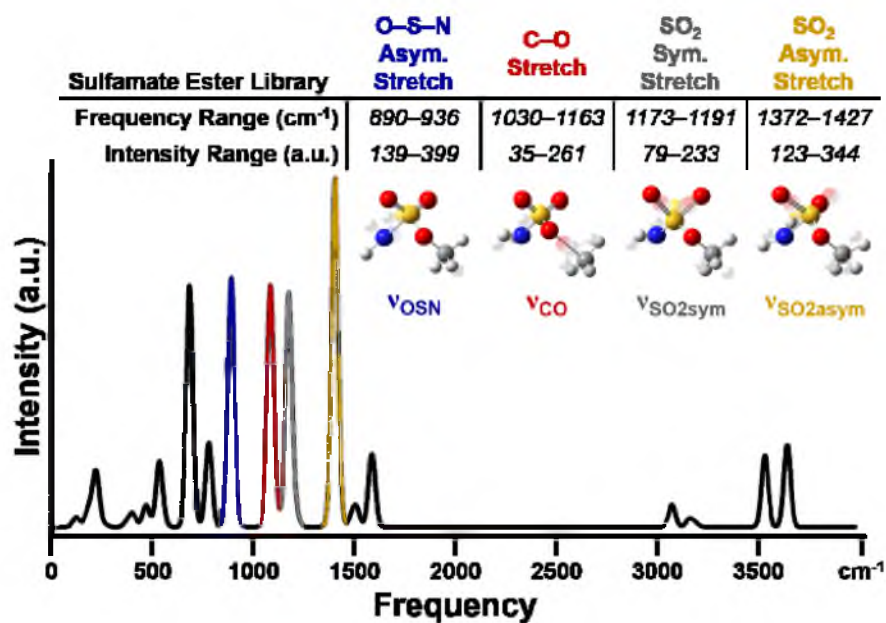


Figure 3.4. Computationally derived IR spectrum for sulfamate ester **2a**, MeOSO₂NH₂. Vibrations used as modeling parameters are color-coded, and graphical depictions approximating vibrational motions are presented. Vibrational frequency and intensity ranges for the 20-membered sulfamate ester library are presented.

Model Development

In Chapter 2, the initial application of Design of Experiments (DoE) precepts did not enable the development of a model descriptive of diarylalkene hydrogenation enantioselectivity. This is attributed to the initial 12-membered library design being founded upon a flawed hypothesis of the origin of enantioselection in the iridium-catalyzed reaction. Thus, prior to developing a mathematical relationship between selectivity and the identified vibrational frequencies and intensities, DoE principles were first applied to the 20-membered sulfamate ester library (Figure 3.2).^{1,2} This library was built to span the synthetically accessible experimental space of sulfamate esters, as this approach affords the greatest likelihood of probing the origin of site-selectivity. Thus, it was presumed that from a DoE-selected sample of this library, the features influencing site-selectivity could be identified and quantitated via linear regression-derived mathematical models. Correspondingly, eight sulfamate esters were selected (termed the DoE set and noted with asterisks and bolded in Figure 3.2) that quantitatively sample the observed range of B:T ratios and qualitatively represent a distribution of steric and electronic perturbations.

In addition to examining sulfamate substituent effects on B:T selectivity, the electronic structure of the isoamylbenzene substrate was also varied. After preparing a traditional Hammett series ($R' = \text{OMe}$ (**1a**), *t*-Bu (**1c**), H (**1**), Br (**1d**), CF_3 (**1c**)), this library was subjected to oxidation reactions with each of the eight DoE-set sulfamate esters. (See Figure 3.5 for a description of the two evaluations that did not yield measureable data.) The selectivity results of this analysis are presented in Figure 3.5 and are correlated to Hammett σ^+ values. As a measure of resonance stabilization,

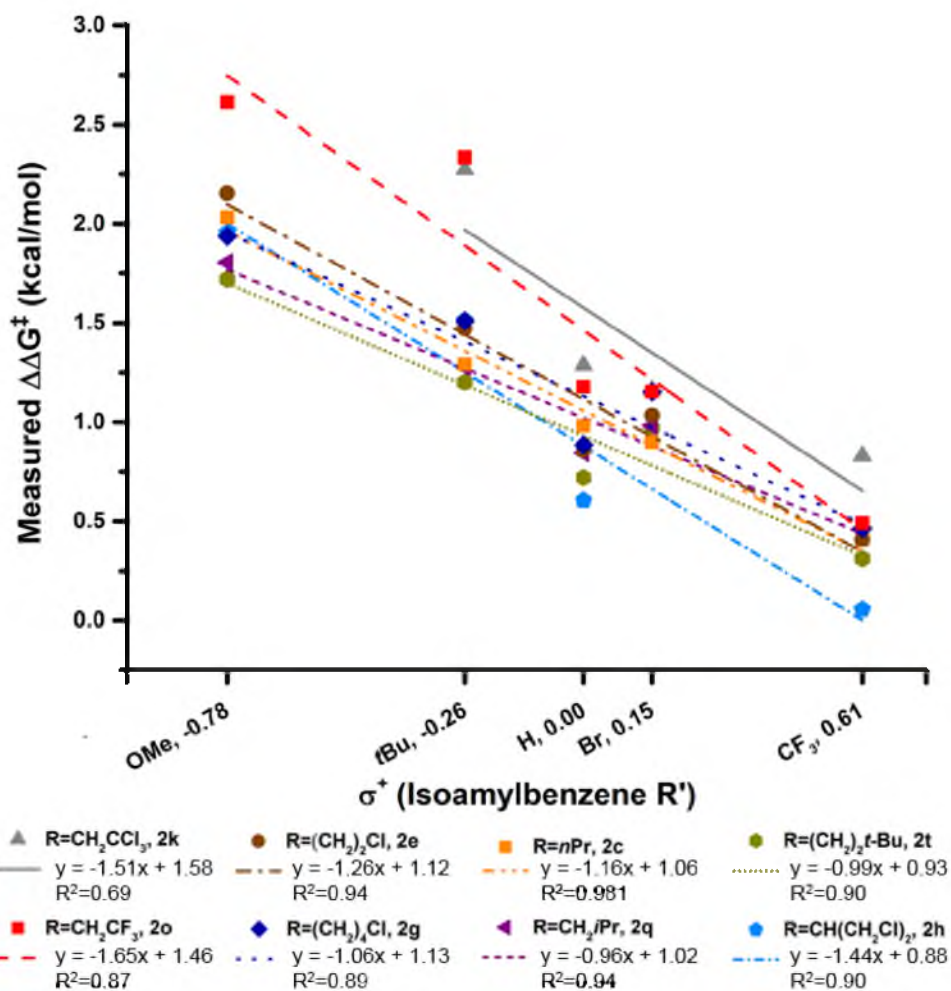


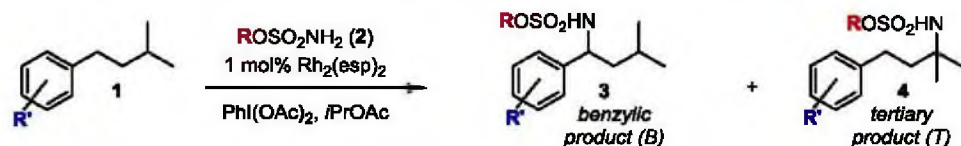
Figure 3.5. Plot of measured $\Delta\Delta G^\ddagger$ versus Hammett σ^+ for the DoE set of sulfamate esters evaluated in the isoamylbenzene substrate series $R' = \text{OMe}$ (**1a**), $t\text{-Bu}$ (**1c**), H (**1**), Br (**1d**), CF_3 (**1b**). $\Delta\Delta G^\ddagger = -RT\ln(\text{tertiary/benzylic})$, where T is 23 °C. Omitted from this plot are data points corresponding to $R = \text{CH}_2\text{CCl}_3$, $R' = \text{OMe}$ (benzylic-to-tertiary ratio >100:1) and $R = \text{CH}(\text{CH}_2\text{Cl})_2$, $R' = \text{Br}$ (no measurable products observed).

Hammett σ^+ values serve as a better descriptor of the observed selectivity trends across varying R' than do Hammett σ values.³⁸ The higher degree of correlation provided by σ^+ values is consistent with the electrophilic nature of the putative nitrenoid and developing σ^+ charge at the carbon center undergoing oxidation in the transition structure.^{39,40}

With data from reactions of the eight sulfamate esters (DoE set) and three isoamylbenzene-derived substrates ($R'=OMe$ (**1a**), H (**1**), CF_3 (**1b**)), the 23-membered training set (Table 3.1, see Figure 3.5 for an explanation of the data point omitted) was subjected to a standard stepwise linear regression algorithm, the details of which are described in the Experimental Information and Methods section.⁴¹ Using this algorithm, which facilitates statistical exploration of the relationship between vibrational parameters, σ^+ , and $\Delta\Delta G^\ddagger$, a descriptive equation was formulated and is depicted in Figure 3.6a.

To evaluate the accuracy of this model, predicted and measured $\Delta\Delta G^\ddagger$ values are compared in Figure 3.6b, which demonstrates a high level of correlation between experimental values and model predictions. Leave-one-out (LOO) analysis was also performed to evaluate the robustness of the model (Figure 3.6c). LOO is a cross-validation method wherein one data point is removed from a training set and the model is refit to the remaining data. Then, the model-predicted value of the omitted data point is compared to the experimental value. This process is iteratively carried out for each data point in the training set. The resulting LOO-derived model predictions are compared to the experimentally measured values, as is seen in Figure 3.6c.⁴² The slope and R^2 values, which are close to unity, are positive indicators of the model's accuracy.

Table 3.1. Training set (entries 1–23), external validations (entries 24–61), and predictions (entries 62–64).



R¹=4-OMe (1a), 4-H (1), 4-CF₃ (1b), 4-*t*-Bu (1c), 4-Br (1d), 3-Cl (1e), 4-Ph (1f), 3-*t*-Bu (1g)

Entry	R	R ¹	Pred. $\Delta\Delta G^\ddagger$ (kcal/moi)	Meas. $\Delta\Delta G^\ddagger$ (kcal/mol)	Meas. B/T	Entry	R	R ¹	Pred. $\Delta\Delta G^\ddagger$ (kcal/mol)	Meas. $\Delta\Delta G^\ddagger$ (kcal/mol)	Meas. B/T
1	CH ₂ CF ₃	OMe	2.32	2.61	85.0 ± 1.4	33	CH ₂ Cy	4-H	0.89	0.84	4.2 ± 0.1
2	<i>n</i> Pr	OMe	2.02	2.03	31.6 ± 0.1	34	<i>n</i> Bu	4-H	1.05	0.77	3.7 ± 0.1
3	(CH ₂) ₂ Cl	OMe	2.15	2.15	38.9 ± 0.9	35	CH(CF ₃) ₂	4-H	1.19	0.06	1.1 ± 0.1
4	(CH ₂) ₂ <i>t</i> -Bu	OMe	1.77	1.72	18.8 ± 0.3	36	CH ₂ CCl ₃	4- <i>t</i> -Bu	1.96	2.27	47.6 ± 0.3
5	CH(CH ₂ Cl) ₂	OMe	1.82	1.95	27.7 ± 1.3	37	CH ₂ CF ₃	4- <i>t</i> -Bu	1.61	2.33	52.8 ± 0.1
6	CH ₂ <i>i</i> Pr	OMe	1.70	1.81	21.5 ± 0.5	38	<i>n</i> Pr	4- <i>t</i> -Bu	1.38	1.29	9.0 ± 0.3
7	(CH ₂) ₄ Cl	OMe	1.86	1.94	26.9 ± 0.5	39	(CH ₂) ₂ Cl	4- <i>t</i> -Bu	1.44	1.47	12.2 ± 0.1
8	CH ₂ CCl ₃	H	1.58	1.29	8.9 ± 0.1	40	(CH ₂) ₂ <i>t</i> -Bu	4- <i>t</i> -Bu	1.21	1.20	7.7 ± 0.2
9	CH ₂ CF ₃	H	1.25	1.18	7.4 ± 0.2	41	CH(CH ₂ Cl) ₂	4- <i>t</i> -Bu	1.18	1.51	13.1 ± 0.1
10	<i>n</i> Pr	H	1.06	0.98	5.3 ± 0.3	42	CH ₂ <i>i</i> Pr	4- <i>t</i> -Bu	1.21	1.28	8.8 ± 0.5
11	(CH ₂) ₂ Cl	H	1.09	0.86	4.3 ± 0.1	43	(CH ₂) ₄ Cl	4- <i>t</i> -Bu	1.25	1.51	13.0 ± 0.5
12	(CH ₂) ₂ <i>t</i> -Bu	H	0.92	0.72	3.4 ± 0.2	44	CH ₂ CCl ₃	4-Br	1.37	1.16	7.2 ± 0.1
13	CH(CH ₂ Cl) ₂	H	0.86	0.61	2.8 ± 0.1	45	CH ₂ CF ₃	4-Br	1.04	1.15	7.1 ± 0.1
14	CH ₂ <i>i</i> Pr	H	0.96	0.84	4.2 ± 0.3	46	<i>n</i> Pr	4-Br	0.88	0.90	4.6 ± 0.3
15	(CH ₂) ₄ Cl	H	0.95	0.89	4.5 ± 0.1	47	(CH ₂) ₂ Cl	4-Br	0.88	1.03	5.8 ± 0.2
16	CH ₂ CCl ₃	CF ₃	0.70	0.83	4.1 ± 0.3	48	(CH ₂) ₂ <i>t</i> -Bu	4-Br	0.77	0.97	5.2 ± 0.2
17	CH ₂ CF ₃	CF ₃	0.41	0.49	2.3 ± 0.1	49	CH ₂ <i>i</i> Pr	4-Br	0.82	0.98	5.3 ± 0.4
18	<i>n</i> Pr	CF ₃	0.31	0.41	2.0 ± 0.2	50	(CH ₂) ₄ Cl	4-Br	0.77	1.15	7.1 ± 0.3
19	(CH ₂) ₂ Cl	CF ₃	0.26	0.41	2.0 ± 0.1	51	CH ₂ CHCl ₂	4-OMe	2.23	2.40	59.3 ± 0.4
20	(CH ₂) ₂ <i>t</i> -Bu	CF ₃	0.27	0.31	1.7 ± 0.1	52	(CH ₂) ₃ Cl	4-OMe	1.88	2.21	42.7 ± 0.5
21	CH(CH ₂ Cl) ₂	CF ₃	0.11	0.06	1.1 ± 0.1	53	<i>n</i> Bu	4-OMe	2.01	1.74	19.3 ± 0.5
22	CH ₂ <i>i</i> Pr	CF ₃	0.39	0.46	2.2 ± 0.1	54	<i>n</i> Bu	3-Cl	0.56	0.63	2.9 ± 0.2
23	(CH ₂) ₄ Cl	CF ₃	0.24	0.46	2.2 ± 0.2	55	(CH ₂) ₂ Cl	3-Cl	0.55	0.52	2.4 ± 0.1
24	(CH ₂) ₃ CCl ₃	4-H	1.05	1.29	9.0 ± 0.3	56	CH ₂ <i>i</i> Pr	3-Cl	0.59	0.49	2.3 ± 0.1
25	CH(Et) ₂	4-H	1.02	1.15	7.0 ± 0.3	57	(CH ₂) ₂ Cl	4-Ph	1.33	1.68	17.3 ± 0.2
26	<i>i</i> Pr	4-H	1.07	1.15	7.0 ± 0.1	58	<i>n</i> Bu	4-Ph	1.27	1.39	10.7 ± 0.2
27	Et	4-H	0.87	1.04	5.9 ± 0.1	59	CH ₂ CF ₃	3- <i>t</i> -Bu	1.33	1.41	10.9 ± 0.4
28	(CH ₂) ₃ CHCl ₂	4-H	1.02	1.03	5.8 ± 0.1	60	(CH ₂) ₂ Cl	3- <i>t</i> -Bu	1.17	0.92	4.8 ± 0.1
29	Me	4-H	1.01	1.01	5.6 ± 0.3	61	<i>n</i> Bu	3- <i>t</i> -Bu	1.12	0.79	3.8 ± 0.2
30	CH ₂ CHCl ₂	4-H	1.33	0.92	4.8 ± 0.1	62	CH ₂ CF ₂ CF ₃	4-H	1.38	1.32	9.5 ± 0.2
31	(CH ₂) ₃ Cl	4-H	0.99	0.90	4.6 ± 0.1	63	CH ₂ (CF ₂) ₂ CF ₃	4-H	1.43	1.26	8.5 ± 0.1
32	CH ₂ <i>t</i> -Bu	4-H	1.15	0.86	4.3 ± 0.3	64	CH ₂ C(Me) ₂ CH ₂ Cl	4-H	1.17	1.06	6.1 ± 0.1

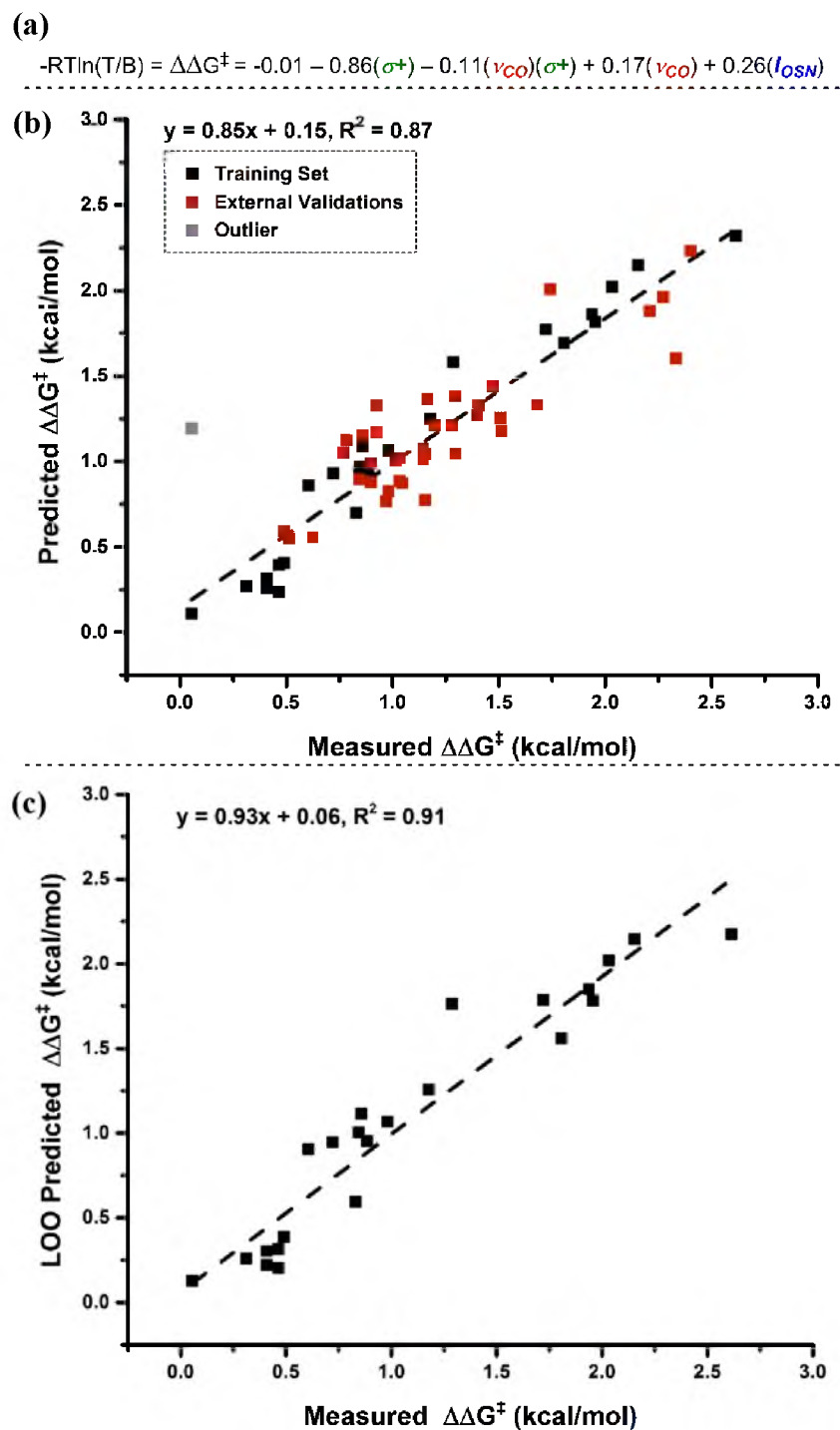


Figure 3.6. Descriptive model and its robustness measures. (a) Normalized mathematical relationship, derived from tabulated training set in Table 3.1, describing differential free energy of tertiary-to-benzylic (T/B) amination. R: ideal gas constant, T: 23 °C. (b) Predicted versus measured $\Delta\Delta G^\ddagger$ plot of training set and external validations. Grayed data point, designated as an outlier, represents R = CH(CF₃)₂, R' = H. (c) Leave-one-out (LOO) analysis.

Development of this robust model relied on iterative analyses of a large set of potential descriptors, including point charges, Sterimol values, pK_a , molecular weight, and IR vibrations. Terms that consistently failed to describe site-selectivity were whittled from the descriptor set. This paring has a subjective nature and, therefore, many possible outcomes. While the robustness of the developed model indicates its validity, it is only one of presumably many potential solutions.

Assessing Model Robustness via External Validation

A third measure of model strength was determined by externally validating the model with data points not part of the training set. Of the original 20-membered library, 12 sulfamate esters, which were not members of the DoE set, were evaluated with isoamylbenzene (**1**). The robustness of the model for describing substrate variation was evaluated with five isoamylbenzene derivatives: 1-(*t*-butyl)-4-isopentylbenzene (**1c**), 1-bromo-4-isopentylbenzene (**1d**), 1-Cl-3-isoamylbenzene (**1e**), 1-Ph-4-isoamylbenzene (**1f**), and 1-*t*-Bu-3-isoamylbenzene (**1g**). The complete external validation set is tabulated in Table 3.1. Graphical representation of this data (■, Figure 3.6b) demonstrates the overall good agreement between predicted $\Delta\Delta G^\ddagger$ values and experimental measurements.

An obvious outlier in the plot of predicted versus measured $\Delta\Delta G^\ddagger$ values occurs with sulfamate ester **2n**, $(CF_3)_2CHOSO_2NH_2$. It is hypothesized that this highly electron-deficient, sterically large sulfamate ester may be forced to adopt conformations not accessible to other nitrene sources in the defining C–N bond forming event. It is also possible that **2n** facilitates C–H amination through a mechanistic pathway that

differs from that of other sulfamate esters. Future investigations of reactions with **2n** are warranted, and use of this reagent was discontinued for the remainder of this study.

Analyzing and Interpreting the Model

Capitalizing on the robustness of the identified descriptive model for quantitating features of mechanistic relevance, steric and electronic features of the nitrene source were optimized, thereby informing the synthesis of new sulfamate structures that display a higher propensity towards benzylic C–H insertion. As the relationship in Figure 3.6a is a normalized equation, the magnitude of the coefficients yield information about the relative influence of each parameter on selectivity. Notably, the overriding selectivity determinant, σ^+ , is associated with the strength of the benzylic C–H bond (*vide supra*). Perhaps unsurprisingly, the C–O frequency (ν_{CO}) of the sulfamate ester also plays a prominent role in this model. Included as a single term and, again, within a cross-term, ν_{CO} is the shortest conduit from the O-alkyl substituent to the sulfamate moiety. As such, the vibrational frequency of the C–O bond will reflect changes in the substituent groups on the alkyl chain, which alter the force constant and/or reduced mass (components of vibrational modes).

It is particularly intriguing to find that the C–O stretching vibration is coupled with the Hammett descriptor, σ^+ , in the optimized selectivity model. This result suggests a synergistic relationship between the nitrenoid and the isoamylbenzene substrate, indicative of a defined intermolecular interaction between these two species. While the precise nature of this interaction is unclear, it was considered that the origin of ν_{CO} trends may be illuminated by assessing sulfamate esters according to increasing C–O

frequency (Figure 3.7a). Qualitatively, it is observed that the more halogenated sulfamate esters showed greater ν_{CO} values. In accordance with this trend, more polarized bonds vibrate with energetically higher frequencies. Greater differential electronegativity across a bond increases the bond force constant and, thus, its vibrational frequency.⁴³

Patterning in a similar manner the analysis of the other vibration-related parameter, I_{OSN} , revealed in the model, Figure 3.7b was constructed, which displays sulfamate ester R groups according to increasing O–S–N asymmetric stretch intensities. Organizing the data in this manner, it is observed that variation in I_{OSN} is primarily characterized by increases in distal steric bulk and by halogenation. These qualitative trends served to inform our use of the developed model as a tool for predicting new sulfamate esters that yield improved B:T ratios.

Predicting an Improved Sulfamate Ester

We have computationally evaluated several sulfamate derivatives that included electronegative atoms and variation in chain-length; most of these, however, were not predicted to afford improved site selection. In contrast, sulfamate esters **2u** (R = CH₂CF₂CF₃) and **2v** (R = CH₂(CF₂)₂CF₃) were identified using our model, as these two reagents were expected to give enhanced levels of the benzylic oxidation product. In practice, the predicted selectivities closely matched those measured, with sulfamate ester **2u** effecting the highest degree of site-selection observed for amination of isoamylbenzene (**1**) (Figure 3.8a). The enhancement of selectivity achieved by changing the sulfamate from CCl₃CH₂OSO₂NH₂ (**2k**) to CF₃CF₂CH₂OSO₂NH₂ (**2u**),

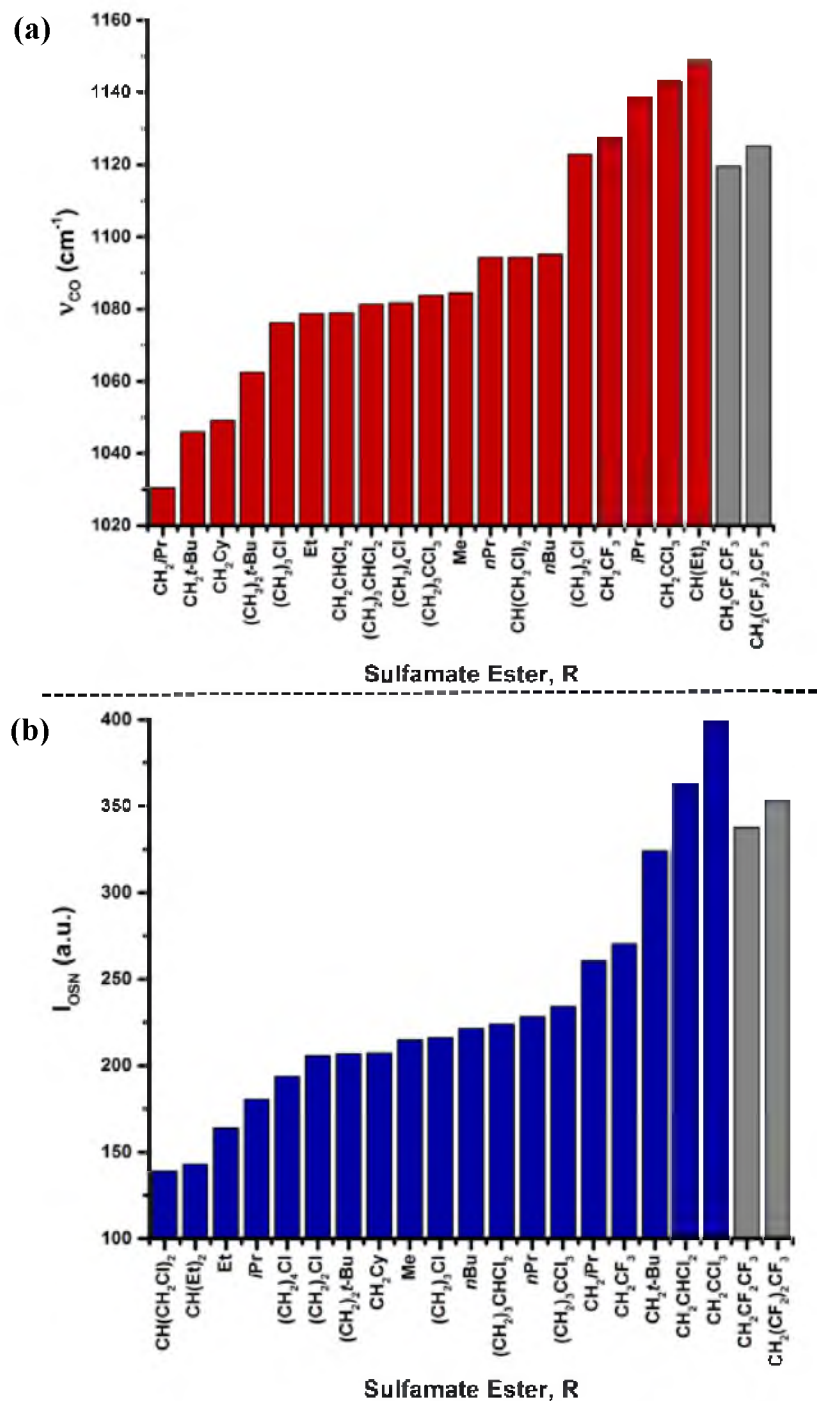


Figure 3.7. Analysis of vibration-derived parameters. (a) Representation of increasing C–O stretch frequency (ν_{CO}) versus sulfamate ester R group. (b) Representation of increasing intensity of O–S–N asymmetric stretch (I_{OSN}) versus sulfamate ester R group. Grayed columns highlight model-informed predictions **2u** (R = $\text{CH}_2\text{CF}_2\text{CF}_3$) and **2v** (R = $\text{CH}_2(\text{CF}_2)_2\text{CF}_3$).

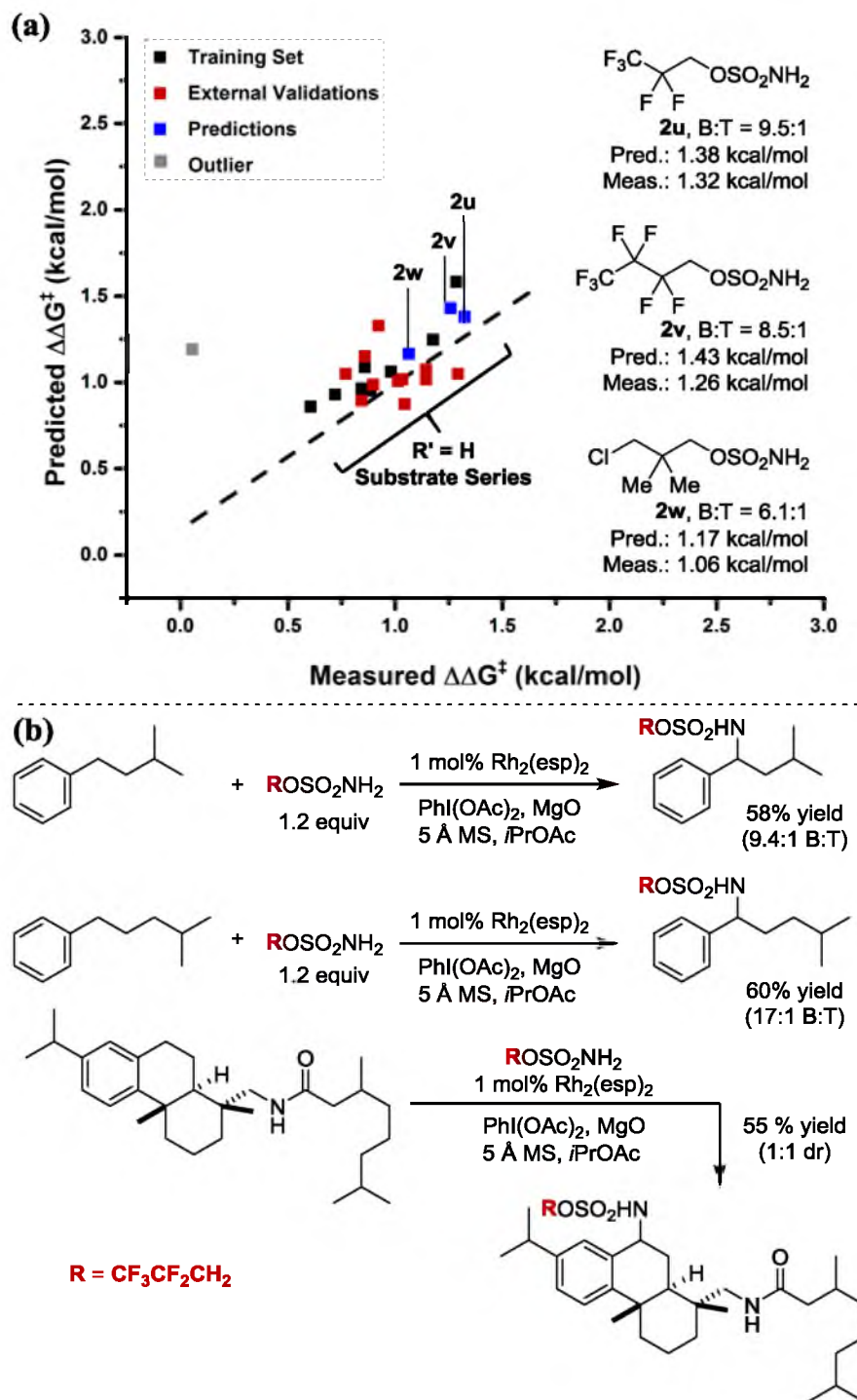


Figure 3.8. Prediction and assessment of new sulfamate esters. (a) Plot of predicted versus measured $\Delta\Delta G^\ddagger$ for amination of isoamylbenzene, **1**. A mathematical model correlating differential reaction free energy ($\Delta\Delta G^\ddagger$) with IR vibrational data and Hammett σ^+ parameters informed the design of new sulfamate esters. Sulfamate ester **2u** affords the highest B:T selectivity reported, to date, for Rh-catalyzed amination of isoamylbenzene. (b) Preparative scale (0.5 mmol) reactions using sulfamate ester **2u**.

albeit modest, is striking given the apparent electronic similarities and steric differences between these two reagents.

The identification of **2u** and **2v** by consideration of both ν_{CO} and I_{OSN} (grey columns, Figure 3.7) highlights the predictive utility of the developed model. Of note, the calculated IR frequencies and intensities of these nitrene sources do not represent the highest observed values in the sulfamate ester library. This is rationalized by considering the interdependency of the terms derived from vibrational modes since these are intrinsically linked. Thus, maximizing the value of ν_{CO} alone does not guarantee proportionate increases in $\Delta\Delta G^\ddagger$ values. This underscores the balance that is achieved in the developed model (see equation in Figure 3.6a) between the selectivity-enhancing effects of the ν_{CO} and I_{OSN} parameters (positive coefficients) and the deleterious effect on site selection of the $(\nu_{CO})(\sigma^+)$ cross term (negative coefficient).

As a final step, the performance of sulfamate ester **2u** was evaluated on a preparative scale (0.5 mmol) with isoamylbenzene, **1** (Figure 3.8b). The benzylic product from this reaction was obtained in 58% yield with the same level of B:T site-selectivity (9.4:1) that was noted in the original evaluation process (0.3 mmol scale). The reaction of **2u** with substrate **5** shows even higher levels of site selectivity in favor of the benzylic amine product (60% yield). Finally, oxidation of a more sophisticated polycyclic substrate, **6**, is demonstrated to give exclusively the product of secondary, benzylic oxidation in 55% yield.

Conclusions

In summary, the subtle interplay of steric and electronic effects in the $\text{Rh}_2(\text{esp})_2$ -catalyzed C–H amination of isoamylbenzenes has been evaluated with a wide-range of sulfamate esters. Product selectivity in these reactions can be effectively modeled using a combination of a classical Hammett parameter and computed IR vibrational data. Of particular interest is the ability to deconstruct the model and use this information to extrapolate to new sulfamate esters, one of which offers the highest performance, to date, for this intermolecular Rh-catalyzed C–H amination reaction.

Efforts are currently underway in the Du Bois group (Dr. Martins Oderinde) to computationally model the reaction's putative Rh-nitrene species. There is particular interest in distinguishing the reactive nitrene as a singlet or triplet, and we envision mathematical models playing a key role in this determination. By tabulating two parameter sets, one per species, we hypothesize that one of these will afford more robust models, lending key mechanistic support for the associated nitrene being the active species engaging in selective C–H amination.

This work demonstrating the capability of mathematical models for informing approaches for catalyst/reagent optimization foreshadows the power of such an approach in the analysis of substrate scope. Chapter 4 explores the quantitative application of design of experiments principles and establishes a protocol for its implementation in substrate scope libraries for the mechanistic investigation of reactions.

Experimental Information

DFT Calculations

Using Gaussian 09 software, sulfamate esters were energy-minimized and IR vibrations were computed according to the M06-2X functional and TZVP basis set, a combination that has been benchmarked for IR calculations³³⁻³⁷. As there are several conformations of local energetic minima available to each sulfamate ester, we built our vibrational parameter set upon those molecular conformations displaying the highest degrees of conformational similarity. Where multiple conformations exist for a molecule, beyond the realm of the conformationally conserved framework, we tabulated vibrations for the conformation in which the net molecular dipole was also minimized.

Model Development

Models were developed using the Statistics Toolbox of MATLAB[®] R2013a software.⁴¹ Four algorithms were used to identify models. Each algorithm begins the modeling process by starting from a prescribed set of starting terms. Linear (x_1 , x_2 , x_3 , etc.), interaction ($x_1:x_2$, $x_1:x_3$, etc.), and squared (x_1^2 , x_2^2 , x_3^2 , etc.) terms are added or removed from each model according to a p -value test. For a term to enter a model, its p -value is <0.05 . For a term to exit a model, its p -value is >0.1 . The four algorithms used to identify potential models are as follows, with the nature of the starting model described.

`LinearModel.stepwise(X, y)` performs stepwise linear regression from a starting model bearing no variable terms. `LinearModel.stepwise(X, y, 'linear')` performs stepwise linear regression from a starting model of linear terms.

LinearModel.stepwise(X, y, 'interactions') performs stepwise linear regression from a starting model of linear and interaction terms. LinearModel.stepwise(X, y, 'purequadratic') performs stepwise linear regression from a starting model of linear terms and squared terms. Resultant models were evaluated by leave-one-out (LOO) analysis and external validation.⁴² Training, external validation, and prediction raw data sets are given in Table 3.2. The combined three data sets were normalized prior to model development. After normalization was performed on the entire data set (combined training, external validation, and prediction sets), the training set was subjected to the four above-mentioned stepwise regression algorithms. The linear regression models, LOO analyses, and external validation analyses resulting from the models generated by each algorithm are presented below. For external validation analysis, the training set and external validation data are plotted. All R^2 values presented are adjusted R^2 values.

Using the MATLAB command “LinearModel.stepwise(X, y),” the model in Eq. 3.1 was afforded.

$$y = -0.03 - 0.82(\sigma^+) + 0.31(v_{SO2asym}) \quad \text{Eq. 3.1}$$

The statistical robustness of this model was assessed via LOO and external validation analyses, which are presented in Figures 3.9a–b. The command “LinearModel.stepwise(X, y, 'linear’)” afforded Eq. 3.2, and robustness measures are given in Figures 3.9c–d.

$$y = -0.01 - 0.86(\sigma^+) - 0.11(\sigma^+)(v_{CO}) + 0.17(v_{CO}) + 0.26(v_{OSN}) \quad \text{Eq. 3}$$

Table 3.2. Training, external validation, and prediction data sets for model development.

R	R'	$\Delta\Delta G^\ddagger$ (kcal/mol)	σ^+	v_{OSN}	I_{OSN}	v_{CO}	I_{CO}	$v_{\text{SO}_2\text{sym}}$	$I_{\text{SO}_2\text{sym}}$	$v_{\text{SO}_2\text{asym}}$	$I_{\text{SO}_2\text{asym}}$
Training Set											
CH ₂ CF ₃	4-OMe	2.61455	-0.78	908.67	270.3053	1127.39	261.4782	1183.37	174.7465	1417.39	279.8990
<i>n</i> Pr	4-OMe	2.032222	-0.78	904.49	228.3224	1094.3	93.3049	1174.28	167.8645	1399.31	272.7238
(CH ₂) ₂ Cl	4-OMe	2.154536	-0.78	936.37	205.8182	1122.95	118.2498	1180.85	221.4151	1402.29	277.0106
(CH ₂) ₂ <i>t</i> -Bu	4-OMe	1.720313	-0.78	928.06	206.9872	1062.47	34.5064	1173.15	190.8933	1394.28	251.6505
CH(CH ₂ Cl) ₂	4-OMe	1.9547	-0.78	902.80	138.9470	1094.31	66.4699	1176.68	186.8029	1381.02	344.0420
CH ₂ <i>i</i> Pr	4-OMe	1.805584	-0.78	906.68	260.5564	1030.49	234.7518	1176.96	210.3368	1400.21	254.2135
(CH ₂) ₄ Cl	4-OMe	1.937453	-0.78	901.08	193.7590	1081.69	156.7322	1175.43	208.1870	1401.16	267.4892
CH ₂ CCl ₃	4-H	1.286516	0.00	909.04	399.1987	1143.06	117.4317	1183.25	210.1953	1411.41	266.7582
CH ₂ CF ₃	4-H	1.177893	0.00	908.67	270.3053	1127.39	261.4782	1183.37	174.7465	1417.39	279.8990
<i>n</i> Pr	4-H	0.981464	0.00	904.49	228.3224	1094.3	93.3049	1174.28	167.8645	1399.31	272.7238
(CH ₂) ₂ Cl	4-H	0.858411	0.00	936.37	205.8182	1122.95	118.2498	1180.85	221.4151	1402.29	277.0106
(CH ₂) ₂ <i>t</i> -Bu	4-H	0.720206	0.00	928.06	206.9872	1062.47	34.5064	1173.15	190.8933	1394.28	251.6505
CH(CH ₂ Cl) ₂	4-H	0.605943	0.00	902.8	138.9470	1094.31	66.4699	1176.68	186.8029	1381.02	344.0420
CH ₂ <i>i</i> Pr	4-H	0.844563	0.00	906.68	260.5564	1030.49	234.7518	1176.96	210.3368	1400.21	254.2135
(CH ₂) ₄ Cl	4-H	0.885166	0.00	901.08	193.7590	1081.69	156.7322	1175.43	208.1870	1401.16	267.4892
CH ₂ CCl ₃	4-CF ₃	0.830382	0.61	909.04	399.1987	1143.06	117.4317	1183.25	210.1953	1411.41	266.7582
CH ₂ CF ₃	4-CF ₃	0.490176	0.61	908.67	270.3053	1127.39	261.4782	1183.37	174.7465	1417.39	279.8990
<i>n</i> Pr	4-CF ₃	0.407925	0.61	904.49	228.3224	1094.3	93.3049	1174.28	167.8645	1399.31	272.7238
(CH ₂) ₂ Cl	4-CF ₃	0.407925	0.61	936.37	205.8182	1122.95	118.2498	1180.85	221.4151	1402.29	277.0106
(CH ₂) ₂ <i>t</i> Bu	4-CF ₃	0.312281	0.61	928.06	206.9872	1062.47	34.5064	1173.15	190.8933	1394.28	251.6505
CH(CH ₂ Cl) ₂	4-CF ₃	0.056091	0.61	902.8	138.9470	1094.31	66.4699	1176.68	186.8029	1381.02	344.0420
CH ₂ <i>i</i> Pr	4-CF ₃	0.464016	0.61	906.68	260.5564	1030.49	234.7518	1176.96	210.3368	1400.21	254.2135
(CH ₂) ₄ Cl	4-CF ₃	0.464016	0.61	901.08	193.7590	1081.69	156.7322	1175.43	208.1870	1401.16	267.4892

Table 3.2. Continued.

R	R'	$\Delta\Delta G^\ddagger$ (kcal/mol)	σ^+	v_{OSN}	I_{OSN}	v_{CO}	I_{CO}	v_{SO2sym}	I_{SO2sym}	$v_{SO2asym}$	$I_{SO2asym}$
External Validation Set											
Me	4-H	1.013867	0.00	893.98	214.7984	1084.51	202.6777	1176.51	201.3258	1402.71	300.0244
Et	4-H	1.044579	0.00	889.97	163.7985	1078.76	194.6939	1178.06	184.1726	1398.99	247.0540
(CH ₂) ₃ Cl	4-H	0.898101	0.00	895.82	216.1081	1076.24	147.6745	1175.5	206.0898	1401.27	122.5614
CH ₂ CHCl ₂	4-H	0.923148	0.00	904.37	363.0072	1079.02	204.8069	1181.57	217.0065	1408.58	272.3191
CH(Et) ₂	4-H	1.14519	0.00	908.81	142.9984	1148.88	94.5522	1180.36	79.6382	1372.3	202.5934
<i>n</i> Bu	4-H	0.769969	0.00	920.95	221.3675	1095.19	95.3903	1172.97	153.3218	1398.5	267.9414
CH ₂ <i>t</i> -Bu	4-H	0.858411	0.00	912.12	324.1384	1045.96	193.4698	1176.15	220.7748	1399.14	265.8966
(CH ₂) ₃ CHCl ₂	4-H	1.034519	0.00	901.91	223.9915	1081.44	157.4553	1177.35	208.7615	1402.02	264.1869
CH ₂ Cy	4-H	0.844563	0.00	901.35	207.3514	1049.21	220.1915	1175.84	193.9566	1399.83	261.6535
CH(CF ₃) ₂	4-H	0.056091	0.00	912.71	204.4970	1162.56	109.7599	1190.80	232.5111	1427.02	161.8919
(CH ₂) ₃ CCl ₃	4-H	1.293091	0.00	904.54	234.2345	1083.86	167.3353	1177.2	201.5702	1403.22	260.6449
<i>i</i> Pr	4-H	1.14519	0.00	914.44	180.5888	1138.81	155.7580	1175.61	79.2804	1389.91	195.5056
CH ₂ CCl ₃	4- <i>t</i> -Bu	2.27332	-0.26	909.04	399.1987	1143.06	117.4317	1183.25	210.1953	1411.41	266.7582
CH ₂ CF ₃	4- <i>t</i> -Bu	2.334336	-0.26	908.67	270.3053	1127.39	261.4782	1183.37	174.7465	1417.39	279.8990
<i>n</i> Pr	4- <i>t</i> -Bu	1.293091	-0.26	904.49	228.3224	1094.3	93.3049	1174.28	167.8645	1399.31	272.7238
(CH ₂) ₂ Cl	4- <i>t</i> -Bu	1.472123	-0.26	936.37	205.8182	1122.95	118.2498	1180.85	221.4151	1402.29	277.0106
(CH ₂) ₂ <i>t</i> -Bu	4- <i>t</i> -Bu	1.201281	-0.26	928.06	206.9872	1062.47	34.5064	1173.15	190.8933	1394.28	251.6505
CH(CH ₂ Cl) ₂	4- <i>t</i> -Bu	1.514011	-0.26	902.8	138.9470	1094.31	66.4699	1176.68	186.8029	1381.02	344.0420
CH ₂ <i>i</i> Pr	4- <i>t</i> -Bu	1.279866	-0.26	906.68	260.5564	1030.49	234.7518	1176.96	210.3368	1400.21	254.2135
(CH ₂) ₄ Cl	4- <i>t</i> -Bu	1.509501	-0.26	901.08	193.7590	1081.69	156.7322	1175.43	208.1870	1401.16	267.4892
CH ₂ CCl ₃	4-Br	1.161769	0.15	909.04	399.1987	1143.06	117.4317	1183.25	210.1953	1411.41	266.7582
CH ₂ CF ₃	4-Br	1.153538	0.15	908.67	270.3053	1127.39	261.4782	1183.37	174.7465	1417.39	279.8990
<i>n</i> Pr	4-Br	0.898101	0.15	904.49	228.3224	1094.3	93.3049	1174.28	167.8645	1399.31	272.7238
(CH ₂) ₂ Cl	4-Br	1.034519	0.15	936.37	205.8182	1122.95	118.2498	1180.85	221.4151	1402.29	277.0106

Table 3.2. Continued.

R	R'	$\Delta\Delta G^\ddagger$ (kcal/mol)	σ^+	v_{OSN}	I_{OSN}	v_{CO}	I_{CO}	v_{SO2sym}	I_{SO2sym}	v_{SO2asym}	I_{SO2asym}
External Validation Set (continued)											
(CH ₂) ₂ <i>t</i> -Bu	4-Br	0.970254	0.15	928.06	206.9872	1062.47	34.5064	1173.15	190.8933	1394.28	251.6505
CH ₂ <i>i</i> Pr	4-Br	0.981464	0.15	906.68	260.5564	1030.49	234.7518	1176.96	210.3368	1400.21	254.2135
(CH ₂) ₄ Cl	4-Br	1.153538	0.15	901.08	193.7590	1081.69	156.7322	1175.43	208.1870	1401.16	267.4892
(CH ₂) ₃ Cl	4-OMe	2.209388	-0.78	895.82	216.1081	1076.24	147.6745	1175.5	206.0898	1401.27	122.5614
<i>n</i> Bu	4-OMe	1.742055	-0.78	920.95	221.3675	1095.19	95.3903	1172.97	153.3218	1398.5	267.9414
CH ₂ CHCl ₂	4-OMe	2.402661	-0.78	904.37	363.0072	1079.02	204.8069	1181.57	217.0065	1408.58	272.3191
CH ₂ <i>i</i> Pr	3-Cl Ph	0.490176	0.4	906.68	260.5564	1030.49	234.7518	1176.96	210.3368	1400.21	254.2135
<i>n</i> Bu	3-Cl Ph	0.626594	0.4	920.95	221.3675	1095.19	95.3903	1172.97	153.3218	1398.5	267.9414
(CH ₂) ₂ Cl	3-Cl Ph	0.515223	0.4	936.37	205.8182	1122.95	118.2498	1180.85	221.4151	1402.29	277.0106
<i>n</i> Bu	4-Ph Ph	1.394915	-0.18	920.95	221.3675	1095.19	95.3903	1172.97	153.3218	1398.5	267.9414
(CH ₂) ₂ Cl	4-Ph Ph	1.677673	-0.18	936.37	205.8182	1122.95	118.2498	1180.85	221.4151	1402.29	277.0106
CH ₂ CF ₃	3- <i>t</i> -Bu Ph	1.405814	-0.06	908.67	270.3053	1127.39	261.4782	1183.37	174.7465	1417.39	279.8990
<i>n</i> Bu	3- <i>t</i> -Bu Ph	0.785663	-0.06	920.95	221.3675	1095.19	95.3903	1172.97	153.3218	1398.5	267.9414
(CH ₂) ₂ Cl	3- <i>t</i> -Bu Ph	0.923148	-0.06	936.37	205.8182	1122.95	118.2498	1180.85	221.4151	1402.29	277.0106
Prediction Set											
CH ₂ CF ₂ CF ₃	4-H	1.32491	0.00	901.04	337.5706	1119.53	178.7140	1184.8	217.6569	1418.82	264.0398
CH ₂ (CF ₂) ₂ CF ₃	4-H	1.259453	0.00	898.81	352.9919	1125.2	154.5898	1184.13	317.1686	1418.64	281.0195
CH ₂ C(CH ₃) ₂ - CH ₂ Cl	4-H	1.064198	0.00	911.67	302.5492	1069.78	243.9570	1176.02	202.0502	1402.17	262.2446

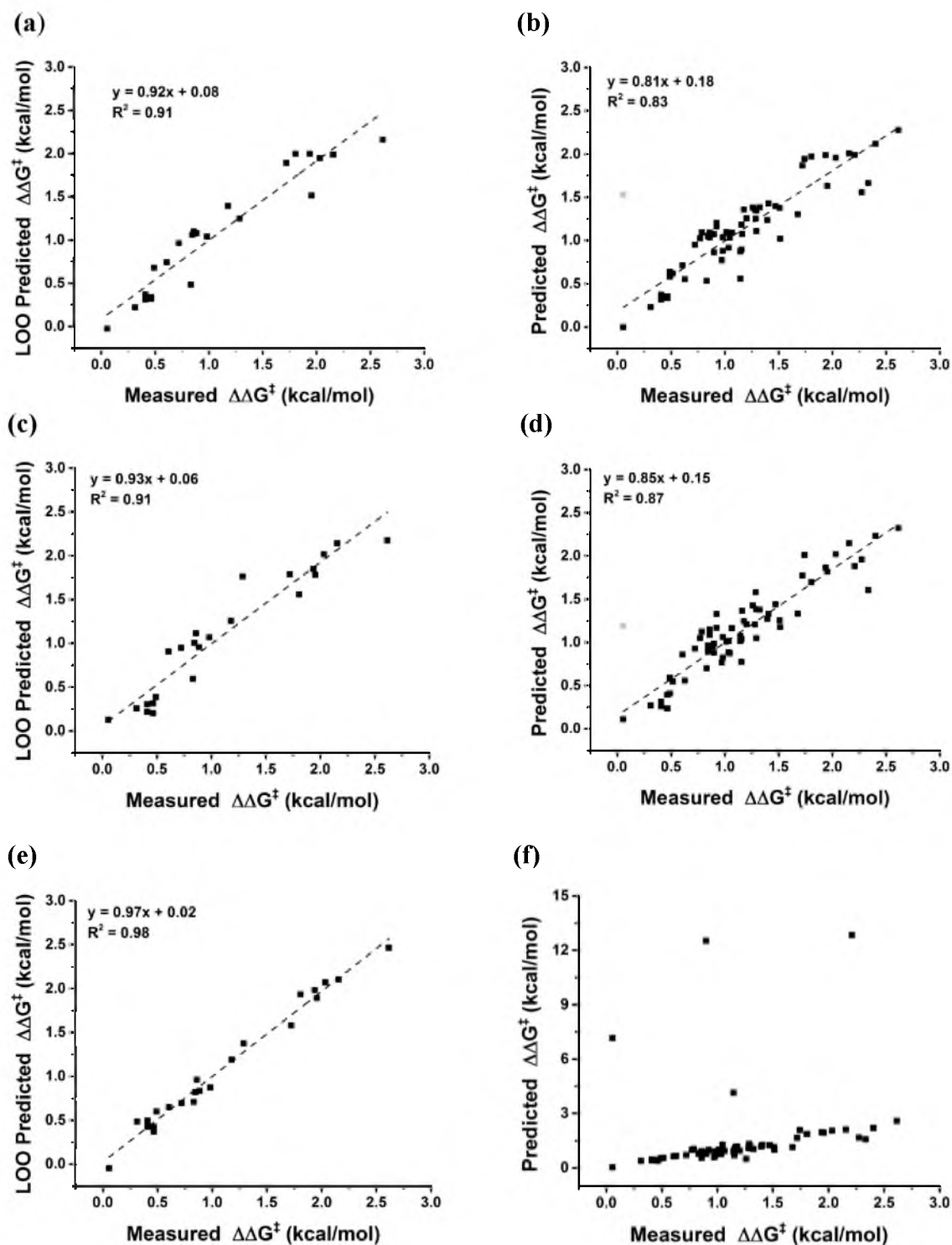


Figure 3.9. Model development analyses. (a) Leave-one-out (LOO) and (b) external validation analyses of the model in Eq. 3.1. (c) LOO and (d) external validation analyses of the model in Eq. 3.2. (e) LOO and (f) external validation analyses of the mode in Eq. 3.3. The greyed outliers in (b) and (d) correspond to $(\text{CF}_3)_2\text{CHOSO}_2\text{NH}_2$.

With the command “LinearModel.stepwise(X, y, 'interactions'),” the model in Eq. 3.1 was again afforded. “LinearModel.stepwise(X, y, 'purequadratic’)” produced Eq. 3.3.

$$\begin{aligned}
 y = & -0.12 - 0.76(\sigma^+) + 0.25(v_{CO}) - 0.25(v_{SO2sym}) + 0.80(v_{SO2sym}) & \text{Eq. 3.3} \\
 & - 1.05(v_{SO2asym}) - 0.11(\sigma^+)(v_{SO2asym}) - 0.19(\sigma^+)(v_{SO2asym}) \\
 & + 0.14(\sigma^+)^2 - 0.46(v_{SO2asym})^2 + 1.17(v_{SO2asym})^2
 \end{aligned}$$

Of the three unique models developed, Eq. 3.2 was determined to be the optimal model, with better LOO and external validation statistics than those for Eq. 3.1. In Eq. 3.3, the high number of model terms, the nearly perfect LOO model statistics, and the significant external validation outliers (shown in Figure 3.9e and 3.9f) suggest that Eq. 3.3 represents an overfit of the data, making it an inaccurate model.

General Experimental Information

MgO, 3 Å molecular sieves, and powdered 5 Å molecular sieves were activated by heating with a Bunsen burner while under vacuum. DMA, THF, ether, toluene, and acetonitrile were dried by passing through a column of activated alumina. Unless otherwise noted all chemicals were purchased from Aldrich, Acros, TCI, or Alfa Aesar and used without further purification. ^1H NMR spectra were obtained in CDCl_3 or $(\text{CD}_3)_2\text{CO}$ at 300 MHz, 400 MHz, or 500 MHz. Chemical shifts are reported in ppm and referenced to the CHCl_3 singlet at 7.26 ppm, or the center peak of the pentet from the residual ^1H resonance present in D_6 -acetone at 2.05 ppm. ^{13}C NMR spectra were obtained in CDCl_3 or $(\text{CD}_3)_2\text{CO}$ at 75 MHz, 100 MHz, or 125 MHz and referenced to

the center peak of the CDCl_3 triplet at 77.23 ppm or the center peak of the $(\text{CD}_3)_2\text{CO}$ septet at 29.84 ppm. The abbreviations s, d, t, p, sex, sept, dd, dt, tq, qt, and m stand for the resonance multiplicities singlet, doublet, triplet, pentet, sextet, septet, doublet of doublets, doublet of triplets, triplet of quartets, quartet of triplets, and multiplet, respectively. Thin-layer chromatography was performed with EMD silica gel 60 F₂₅₄ plates eluting with solvents indicated, visualized by a 254 nm UV lamp and stained with phosphomolybdic acid (PMA). Flash chromatography was performed using EM reagent silica 60 (230–400 mesh). All melting points are uncorrected and recorded on Thomas Hoover Unimelt capillary melting point apparatus. GC separations were performed with an HP6890 GC with a flame ionization detector equipped with a DB-5 column using a 50:1 split. IR spectra were recorded using a Thermo Nicolet FT-IR. HRMS data were obtained on a Waters LCP Premier XE instrument by ESI/TOF. LRG-MS data were obtained on an Agilent Technologies 5975c VL MSD instrument.

Preparation of Substrates

General procedure for Wittig olefination. The reaction scheme is presented in Figure 3.10. To a dry 100 mL round-bottom flask equipped with a stirbar under N_2 were added 6.00 g of isobutyltriphenylphosphonium bromide (15.0 mmol, 1.30 equiv) and 50 mL of toluene. To this solution, 1.68 g of $\text{KO}t\text{-Bu}$ (15.0 mmol, 1.30 equiv) in 10 mL of THF was added dropwise via cannulation. The reaction mixture was stirred for 4 h. The mixture was cooled to $-78\text{ }^\circ\text{C}$ and the aldehyde (11.6 mmol, 1.00 equiv) in 5.0 mL toluene was added dropwise via syringe. The mixture was allowed to warm to room temperature and was stirred for 3 h. Upon completion by TLC analysis, the

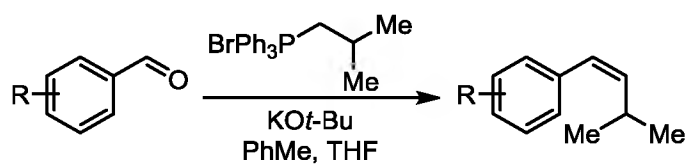


Figure 3.10. Wittig olefination reaction.

reaction was quenched with 10 mL of saturated aqueous NH_4Cl . The mixture was diluted with 100 mL of diethyl ether and washed with H_2O (2×10 mL) and brine (1×20 mL). The organic layer was dried over Na_2SO_4 , decanted, and concentrated *in vacuo*. The crude reaction mixture was purified by flash column chromatography.

(Z)-1-methoxy-4-(3-methylbut-1-en-1-yl)benzene. The general Wittig reaction procedure was followed using 1.58 g of 4-methoxybenzaldehyde (11.6 mmol). The crude mixture was purified by flash chromatography eluting with hexanes to afford the product as a colorless oil in 83% yield (1.70 g), $R_f = 0.2$ (hexanes). ^1H NMR (300 MHz, CDCl_3): δ 1.11 (d, $J = 6.6$ Hz, 6H), 2.89–3.05 (m, 1H), 3.85 (s, 3H), 5.45 (dd, $J = 11.6, 10.2$ Hz, 1H), 6.30 (d, $J = 11.6$ Hz, 1H), 6.92 (d, $J = 8.6$ Hz, 2H), 7.27 (d, $J = 8.6$ Hz, 2H). ^{13}C NMR (75 MHz, CDCl_3): δ 23.4, 27.3, 55.3, 113.7, 126.0, 130.0, 130.7, 139.2, 158.3. IR (neat): 2999, 2956, 2865, 2834, 1606, 1574, 1461, 1403, 1360, 1297, 1240, 1174, 1099, 1034, 929, 864, 830, 807, 760, 731, 707, 658, 625, 564 cm^{-1} . HRMS (EI^+ -TOF) m/z calculated for $\text{C}_{12}\text{H}_{16}\text{O}$ [M^{+}]: 176.1201, found 176.1201.

(Z)-1-(3-methylbut-1-en-1-yl)-4-(trifluoromethyl)benzene. The general Wittig reaction procedure was followed using 2.00 g of (4-(trifluoromethyl)benzaldehyde (11.6 mmol). The crude mixture was purified by flash chromatography eluting with hexanes to afford the product, an inseparable mixture of isomers [$Z:E = 10:1$], as a colorless oil in 85% yield (2.11 g), major isomer: $R_f = 0.8$ (hexanes). ^1H NMR (500 MHz, CDCl_3): δ 1.05 (d, $J = 6.5$ Hz, 6H), 2.80–2.88 (m, 1H), 5.58 (dd, $J = 11.5, 10.5$ Hz, 1H), 6.32 (d, $J = 12.0$ Hz, 1H), 7.35 (d, $J = 8.0$ Hz, 2H), 7.58 (d, $J = 8.0$ Hz, 2H). ^{13}C NMR (125 MHz, CDCl_3): δ 23.2, 27.5, 124.7 (q, $J_{\text{CF}} = 272.5$ Hz), 125.3 (q, $J_{\text{CF}} = 3.9$ Hz), 125.5, 126.3, 128.6 (q, $J_{\text{CF}} = 32.3$ Hz), 129.0, 142.6. IR (neat): 2962, 2869, 1616, 1465, 1402, 1363,

1321, 1161, 1120, 1105, 1064, 1016, 969, 927, 869, 839, 741, 633, 599, 565 cm^{-1} .

HRMS (EI⁺-TOF) m/z calculated for C₁₂H₁₃F₃ [M⁺]: 214.0969, found 214.0969.

(Z)-1-(tert-butyl)-4-(3-methylbut-1-en-1-yl)benzene. The general Wittig reaction procedure was followed using 1.88 g of 4-(tert-butyl)benzaldehyde (11.6 mmol). The crude mixture was purified by flash chromatography eluting with hexanes to afford the product as a colorless oil in 84% yield (1.97 g), $R_f = 0.8$ (hexanes). ¹H NMR (400 MHz, CDCl₃): δ 1.05 (d, $J = 6.0$ Hz, 6H), 1.33 (s, 9H), 2.85–3.00 (m, 1H), 5.43 (t, $J = 11.0$ Hz, 1H), 6.26 (d, $J = 11.6$ Hz, 1H), 7.22 (d, $J = 8.4$ Hz, 2H), 7.35 (d, $J = 8.4$ Hz, 2H). ¹³C NMR (100 MHz, CDCl₃): δ 23.5, 27.4, 31.6, 34.7, 125.3, 126.4, 128.6, 135.2, 140.1, 149.5. IR (neat): 2999, 2958, 2904, 2866, 1508, 1461, 1399, 1378, 1361, 1299, 1269, 1201, 1160, 1106, 1017, 928, 867, 833, 781, 732, 691, 640, 617, 576 cm^{-1} . HRMS (EI⁺-TOF) m/z calculated for C₁₅H₂₂ [M⁺]: 202.1722, found 202.1722.

(Z)-1-bromo-4-(3-methylbut-1-en-1-yl)benzene. The general Wittig reaction procedure was followed using 2.15 g of 4-bromobenzaldehyde (11.6 mmol). The crude mixture was purified by flash chromatography eluting with hexanes to afford the product, an inseparable mixture of isomers [$Z:E = 10:1$], as a colorless oil in 88% yield (2.30 g), major isomer: $R_f = 0.8$ (hexanes). ¹H NMR (300 MHz, CDCl₃): δ 1.06 (d, $J = 6.6$ Hz, 6H), 2.77–2.93 (m, 1H), 5.52 (dd, $J = 11.6, 10.3$ Hz, 1H), 6.24 (d, $J = 11.7$ Hz, 1H), 7.14 (d, $J = 8.4$ Hz, 2H), 7.46 (d, $J = 8.4$ Hz, 2H). ¹³C NMR (75 MHz, CDCl₃): δ 23.3, 27.4, 120.5, 125.5, 130.4, 131.4, 136.9, 141.3. IR (neat): 3003, 2957, 2924, 2865, 1899, 1642, 1586, 1484, 1463, 1413, 1391, 1361, 1324, 1162, 1124, 1071, 1009, 927, 863, 826, 774, 750, 715, 558 cm^{-1} . HRMS (EI⁺-TOF) m/z calculated for C₁₁H₁₃Br [M⁺]: 224.0201, found 224.0203.

(Z)-1-chloro-3-(3-methylbut-1-en-1-yl)benzene. The general Wittig reaction procedure was followed using 1.63 g of 3-chlorobenzaldehyde (11.6 mmol). The crude mixture was purified by flash chromatography eluting with hexanes to afford the product as a colorless oil in 97% yield (2.03 g), $R_f = 0.9$ (hexanes). ^1H NMR (300 MHz, CDCl_3): δ 1.08 (d, $J = 6.6$ Hz, 6H), 2.80–2.98 (m, 1H), 5.54 (dd, $J = 11.6, 10.3$ Hz, 1H), 6.27 (d, $J = 11.6$ Hz, 1H), 7.13–7.30 (m, 4H). ^{13}C NMR (75 MHz, CDCl_3): δ 23.3, 27.4, 125.4, 126.7, 127.0, 128.8, 129.6, 134.2, 139.9, 141.8. IR (neat): 3004, 2959, 2926, 2866, 1642, 1594, 1563, 1465, 1423, 1361, 1324, 1192, 1163, 1118, 1090, 1076, 989, 930, 886, 789, 746, 700, 684 cm^{-1} . HRMS (EI^+ -TOF) m/z calculated for $\text{C}_{11}\text{H}_{13}\text{Cl}$ [M^+]: 180.0706, found 180.0706.

(Z)-4-(3-methylbut-1-en-1-yl)-1,1'-biphenyl. The general Wittig reaction procedure was followed using 2.11 g of biphenyl-4-carboxaldehyde (11.6 mmol). The crude mixture was purified by flash chromatography eluting with hexanes to afford the product as a colorless oil in 97% yield (2.03 g), $R_f = 0.6$ (hexanes). ^1H NMR (300 MHz, CDCl_3): δ 1.18 (d, $J = 6.6$ Hz, 6H), 2.98–3.17 (m, 1H), 5.61 (dd, $J = 11.6, 10.5$ Hz, 1H), 6.43 (d, $J = 11.6$ Hz, 1H), 7.39–7.56 (m, 5H), 7.63–7.72 (m, 4H). ^{13}C NMR (75 MHz, CDCl_3): δ 23.4, 27.5, 126.2, 127.1, 127.2, 127.4, 129.0, 129.3, 137.1, 139.4, 140.9, 141.0. IR (neat): 3028, 2999, 2956, 2923, 2864, 1600, 1513, 1485, 1447, 1396, 1360, 1298, 1158, 1098, 1074, 1006, 927, 866, 838, 772, 740, 728, 694, 634, 579 cm^{-1} . HRMS (EI^+ -TOF) m/z calculated for $\text{C}_{17}\text{H}_{18}$ [M^+]: 222.1409, found 222.1408.

(Z)-1-(tert-butyl)-3-(3-methylbut-1-en-1-yl)benzene. The general Wittig reaction procedure was followed using 1.88 g of 3-(tert-butyl)benzaldehyde (11.6 mmol). The crude mixture was purified by flash chromatography eluting with hexanes

to afford the product as a colorless oil in 90% yield (2.11 g), $R_f = 0.8$ (hexanes). ^1H NMR (300 MHz, CDCl_3): δ 1.06 (d, $J = 6.6$ Hz, 6H), 1.33 (s, 9H), 2.78–3.03 (m, 1H), 5.46 (dd, $J = 11.6, 10.2$ Hz, 1H), 6.31 (d, $J = 11.6$ Hz, 1H), 7.07–7.13 (m, 1H), 7.24–7.31 (m, 3H). ^{13}C NMR (75 MHz, CDCl_3): δ 23.5, 27.5, 31.6, 34.8, 123.7, 125.9, 126.0, 127.3, 128.1, 137.7, 140.2, 151.0. IR (neat): 3000, 2958, 2865, 1599, 1578, 1483, 1461, 1393, 1361, 1269, 1191, 1160, 1089, 933, 897, 799, 750, 720, 702 cm^{-1} . HRMS (EI⁺-TOF) m/z calculated for $\text{C}_{15}\text{H}_{22}$ [M^+]: 202.1722, found 202.1722.

(Z)-(4-methylpent-1-en-1-yl)benzene. The general Wittig reaction procedure was followed using 1.23 g of benzaldehyde (11.6 mmol) and with the modification that 6.20 g of isopentyltriphenylphosphonium bromide (15.0 mmol) was used instead of isobutyltriphenylphosphonium bromide. The crude mixture was purified by flash chromatography eluting with hexanes to afford the product as a colorless oil in 92% yield (1.71 g). Analytical data match the literature.⁴⁴

General procedure for alkene hydrogenation. The reaction scheme is presented in Figure 3.11. To a dry 100 mL round-bottom flask equipped with a stirbar was added 50 mg of 10% palladium on carbon (10 mg / 1 mmol substrate). After bringing the flask under N_2 atmosphere, 25 mL of EtOAc and the corresponding alkene (5.00 mmol, 1.00 equiv) were added to the flask. Using a hydrogen-filled balloon, the flask was evacuated and refilled with hydrogen three times. The reaction was stirred for 3 h under balloon-pressure of hydrogen, after which time the reaction was passed through celite and concentrated *in vacuo*. The material was deemed pure and used without chromatographic purification.

1-isopentyl-4-methoxybenzene (1a). The general hydrogenation procedure was

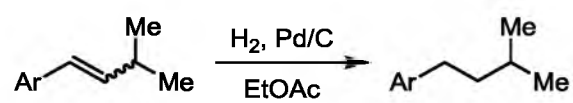


Figure 3.11. Alkene hydrogenation.

followed using 0.881 g of (*Z*)-1-methoxy-4-(3-methylbut-1-en-1-yl)benzene (5.00 mmol). The crude mixture was passed through celite and concentrated *in vacuo* to afford the product as a colorless oil in quantitative yield (0.891 g), $R_f = 0.3$ (hexanes). $^1\text{H NMR}$ (300 MHz, CDCl_3): δ 0.96 (d, $J = 6.3$ Hz, 6H), 1.45–1.67 (m, 3H), 2.58 (t, $J = 8.1$ Hz, 2H) 3.81 (s, 3H), 6.85 (d, $J = 8.6$ Hz, 2H), 7.13 (d, $J = 8.6$ Hz, 2H). $^{13}\text{C NMR}$ (75 MHz, CDCl_3): δ 22.8, 27.8, 33.0, 41.3, 55.4, 113.9, 129.4, 135.4, 157.7. IR (neat): 2952, 2931, 2867, 2833, 1611, 1589, 1510, 1464, 1441, 1383, 1365, 1299, 1242, 1175, 1117, 1038, 820, 742, 701, 555 cm^{-1} . HRMS (EI^+ -TOF) m/z calculated for $\text{C}_{12}\text{H}_{18}\text{O}$ [M^+]: 178.1358, found 178.1355.

1-isopentyl-4-(trifluoromethyl)benzene (1b). The general hydrogenation procedure was followed using 1.07 g of (*Z*)-1-(3-methylbut-1-en-1-yl)-4-(trifluoromethyl)benzene (5.00 mmol). The crude mixture was passed through celite and concentrated *in vacuo* to afford the product as a colorless oil in quantitative yield (1.09 g), $R_f = 0.8$ (hexanes). $^1\text{H NMR}$ (300 MHz, CDCl_3): δ 0.96 (d, $J = 6.3$ Hz, 6H), 1.48–1.68 (m, 3H), 2.68 (t, $J = 8.0$ Hz, 2H), 7.30 (d, $J = 8.0$ Hz, 2H), 7.54 (d, $J = 8.0$ Hz, 2H). $^{13}\text{C NMR}$ (75 MHz, CDCl_3): δ 22.7, 27.9, 33.9, 40.7, 124.7 (q, $J_{\text{CF}} = 270.0$ Hz), 125.4 (q, $J_{\text{CF}} = 3.8$ Hz), 128.2 (q, $J_{\text{CF}} = 32.0$ Hz), 128.8, 147.4. IR (neat): 2957, 2870, 1618, 1468, 1417, 1385, 1321, 1160, 1116, 1086, 1066, 1018, 950, 857, 822, 628, 595 cm^{-1} . HRMS (EI^+ -TOF) m/z calculated for $\text{C}_{12}\text{H}_{15}\text{F}_3$ [M^+]: 216.1126, found 216.1122.

1-(*tert*-butyl)-4-isopentylbenzene (1c). The general hydrogenation procedure was followed using 1.01 g of (*Z*)-1-(*tert*-butyl)-4-(3-methylbut-1-en-1-yl)benzene (5.00 mmol). The crude mixture was passed through celite and concentrated *in vacuo* to afford the product as a colorless oil in quantitative yield (1.02 g), $R_f = 0.8$ (hexanes). ^1H

NMR (500 MHz, CDCl₃): δ 0.94 (d, $J = 6.5$ Hz, 6H), 1.31 (s, 9H), 1.46–1.64 (m, 3H), 2.58 (t, $J = 8.0$ Hz, 2H), 7.12 (d, $J = 8.5$ Hz, 2H), 7.30 (d, $J = 8.5$ Hz, 2H). ¹³C NMR (125 MHz, CDCl₃): δ 22.8, 28.0, 31.7, 33.4, 34.5, 41.0, 125.3, 128.2, 140.2, 148.5. IR (neat): 2954, 2867, 1744, 1515, 1466, 1392, 1383, 1364, 1268, 1237, 1202, 1124, 1109, 1019, 929, 856, 840, 817, 566 cm⁻¹. HRMS (EI⁺-TOF) m/z calculated for C₁₅H₂₄ [M⁺]: 204.1817, found 204.1874.

1-bromo-4-isopentylbenzene (1d). The general hydrogenation procedure was followed using 1.13 g of (*Z*)-1-bromo-4-(3-methylbut-1-en-1-yl)benzene (5.00 mmol). The crude mixture was passed through celite and concentrated *in vacuo* to afford the product as a colorless oil in quantitative yield (1.14 g), $R_f = 0.8$ (hexanes). ¹H NMR (300 MHz, CDCl₃): δ 0.97 (d, $J = 6.3$ Hz, 6H), 1.46–1.68 (m, 3H), 2.59 (t, $J = 8.0$ Hz, 2H), 7.08 (d, $J = 8.4$ Hz, 2H), 7.41 (d, $J = 8.0$ Hz, 2H). ¹³C NMR (75 MHz, CDCl₃): δ 22.7, 27.8, 33.4, 40.8, 119.4, 130.3, 131.5, 142.2. IR (neat): 2953, 2867, 1590, 1486, 1466, 1403, 1383, 1366, 1168, 1071, 1010, 850, 805, 707, 630, 535 cm⁻¹. HRMS (EI⁺-TOF) m/z calculated for C₁₁H₁₅Br [M⁺]: 226.0357, found 226.0362.

1-chloro-3-isopentylbenzene (1e). The general hydrogenation procedure was followed using 0.905 g of (*Z*)-1-chloro-3-(3-methylbut-1-en-1-yl)benzene (5.00 mmol). The crude mixture was passed through celite and concentrated *in vacuo* to afford the product as a colorless oil in quantitative yield (0.915 g), $R_f = 0.9$ (hexanes). ¹H NMR (300 MHz, CDCl₃): δ 1.05 (d, $J = 6.3$ Hz, 6H), 1.53–1.75 (m, 3H), 2.67 (t, $J = 8.0$ Hz, 2H), 7.10–7.33 (m, 4H). ¹³C NMR (75 MHz, CDCl₃): δ 22.7, 27.9, 33.7, 40.8, 125.9, 126.7, 128.7, 129.6, 134.2, 145.2. IR (neat): 2954, 2868, 1598, 1572, 1467, 1427, 1384, 1366, 1204, 1165, 1089, 999, 969, 883, 865, 816, 778, 757, 694, 683 cm⁻¹. HRMS (EI⁺-

TOF) m/z calculated for $C_{11}H_{15}Cl$ [M^+]: 182.0862, found 182.0862.

4-isopentyl-1,1'-biphenyl (1f). The general hydrogenation procedure was followed using 1.11 g of (*Z*)-4-(3-methylbut-1-en-1-yl)-1,1'-biphenyl (5.00 mmol). The crude mixture was passed through celite and concentrated *in vacuo* to afford the product as a colorless oil in quantitative yield (1.12 g), $R_f = 0.6$ (hexanes). 1H NMR (300 MHz, $CDCl_3$): δ 1.17 (d, $J = 6.3$ Hz, 6H), 1.71–1.91 (m, 3H), 2.86 (t, $J = 8.0$ Hz, 2H), 7.45 (d, $J = 7.8$ Hz, 2H), 7.51 (t, $J = 6.6$ Hz, 1H), 7.61 (t, $J = 7.2$ Hz, 2H), 7.71 (d, $J = 8.1$ Hz, 2H), 7.78 (d, $J = 8.1$ Hz, 2H). ^{13}C NMR (75 MHz, $CDCl_3$): δ 22.8, 27.9, 33.6, 41.0, 127.1, 127.2 (2), 128.9, 129.0, 138.7, 141.4, 142.4. IR (neat): 3026, 2952, 2928, 2866, 1601, 1519, 1485, 1466, 1407, 1383, 1365, 1168, 1121, 1074, 1007, 910, 854, 822, 758, 728, 694, 599 cm^{-1} . HRMS (EI⁺-TOF) m/z calculated for $C_{17}H_{20}$ [M^+]: 224.1565, found 224.1565.

1-(*tert*-butyl)-3-isopentylbenzene (1g). The general hydrogenation procedure was followed using 1.01 g of (*Z*)-1-(*tert*-butyl)-3-(3-methylbut-1-en-1-yl)benzene (5.00 mmol). The crude mixture was passed through celite and concentrated *in vacuo* to afford the product as a colorless oil in quantitative yield (1.02 g), $R_f = 0.8$ (hexanes). 1H NMR (300 MHz, $CDCl_3$): δ 0.94 (d, $J = 6.3$ Hz, 6H), 1.32 (s, 9H), 1.46–1.68 (m, 3H), 2.61 (t, $J = 8.0$ Hz, 2H), 6.98–7.03 (m, 1H), 7.19–7.23 (m, 3H). ^{13}C NMR (75 MHz, $CDCl_3$): δ 22.8, 28.1, 31.7, 34.4, 34.8, 41.3, 122.7, 125.6 (2), 128.2, 142.9, 151.2. IR (neat): 3024, 2953, 2867, 1605, 1488, 1466, 1383, 1364, 1273, 1202, 1168, 1083, 1024, 883, 788, 759, 704 cm^{-1} . HRMS (EI⁺-TOF) m/z calculated for $C_{15}H_{24}$ [M^+]: 204.1878, found 204.1880.

(4-methylpentyl)benzene (5). The general hydrogenation procedure was

followed using 0.80 g of (*Z*)-(4-methylpent-1-en-1-yl)benzene (5.00 mmol). The crude mixture was passed through celite and concentrated *in vacuo* to afford the product as a colorless oil in quantitative yield (0.81 g). Analytical data match the literature.⁴⁵

General procedure for alcohol synthesis. This reaction scheme is presented in Figure 3.12. To a dry 250 mL round-bottom flask equipped with a stirbar under N₂ were added 1.79 g of CHCl₃ (15.0 mmol, 1.00 equiv) and 150 mL of THF, and the solution was cooled to -94 °C using a hexane/liquid N₂ bath. Then, 6.0 mL of a 2.5 M solution of *n*BuLi (15.0 mmol, 1.00 equiv) was added dropwise via syringe and allowed to stir for 1 h. Then, 0.871 g of oxetane (15.0 mmol, 1.00 equiv) was added in one portion, followed by dropwise addition of 2.13 g of BF₃•EtO₂ (15.0 mmol, 1.00 equiv). The resulting mixture was allowed to gradually warm to -60 °C over 1 h, then it was quenched with 20 mL of 1.0 M HCl. The aqueous layer was extracted with EtOAc (3 × 20 mL) and the combined organic layers were washed with brine (1 × 20 mL), dried over Na₂SO₄, decanted, and concentrated *in vacuo*. The product was purified by silica gel flash chromatography to give the desired alcohol product.

4,4,4-trichlorobutan-1-ol. This compound was prepared according to the general procedure for alcohol synthesis using 1.79 g of CHCl₃ (15.0 mmol). The product was purified by silica gel flash chromatography eluting with 20% EtOAc in hexanes to give the product as a colorless oil in 64% yield (1.70 g). Analytical data match the literature.⁴⁶

4,4-dichlorobutan-1-ol. This compound was prepared according to the general procedure for alcohol synthesis with the modification that 1.27 g of CH₂Cl₂ (15.0 mmol) was used instead of CHCl₃. The product was purified by silica gel flash

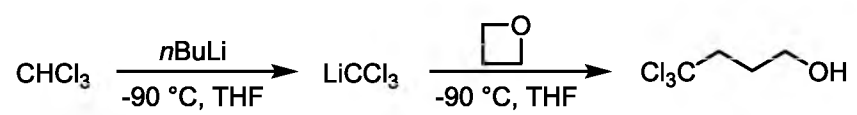


Figure 3.12. Formation of alcohols for eventual sulfamate ester synthesis.

chromatography eluting with 30% EtOAc in hexanes to give the product as a colorless oil in 55% yield (1.18 g). Analytical data match the literature.⁴⁶

***N*-(((1*R*,4*aS*,10*aR*)-7-Isopropyl-1,4*a*-dimethyl-1,2,3,4,4*a*,9,10,10*a*-octahydrophen-anthren-1-yl)methyl)-3,7-dimethyloctanamide (6).** To a stirred solution of 3,7-dimethyloctanoic acid (500 mg, 2.90 mmol) in 10 mL of CH₂Cl₂ was added solid *N,N'*-dicyclohexylcarbodiimide (659 mg, 3.19 mmol, 1.2 equiv) in a single portion. A solution of (+)-dehydroabietylamine (2.4 M in pyridine, 1.38 g, 2.90 mmol) in 5 mL of CH₂Cl₂ was then added dropwise via cannula. Transfer of this material was made quantitative with an additional 2 mL of CH₂Cl₂. After stirring for 18 h, the reaction mixture was transferred to a separatory funnel with 20 mL of CH₂Cl₂, and the solution washed successively with 1.0 M HCl (2 × 10 mL), saturated aqueous NaHCO₃ (1 × 10 mL), and brine (1 × 10 mL). The organic fraction was collected, dried over anhydrous MgSO₄, filtered, and concentrated under reduced pressure. Purification of this material by chromatography on silica gel eluting with 20% EtOAc in hexanes to afforded the desired amide as a viscous, colorless oil in 42% yield (536 mg), *R_f* = 0.20 (20% EtOAc in hexanes); ¹H NMR (400 MHz, CDCl₃) δ 0.84 (d, *J* = 6.4 Hz, 6H), 0.89 (d, *J* = 6.4 Hz, 3H), 0.93 (s, 3H), 1.08–1.14 (m, 2H), 1.21 (s, 3H), 1.22 (d, *J* = 7.6 Hz, 6H), 1.25–1.39 (m, 2H), 1.42 (d, *J* = 7.6 Hz, 3H), 1.43–1.55 (m, 2H), 1.64–1.80 (m, 4H), 1.86–1.94 (m, 4H), 2.10–2.19 (m, 1H), 2.29 (d, *J* = 13.6 Hz, 1H), 2.77–2.94 (m, 3H), 3.17 (d, *J* = 6.4 Hz, 2H), 5.34 (s, 1H), 6.89 (s, 1H), 6.99 (d, *J* = 8.4 Hz, 1H), 7.17 (d, *J* = 8.4 Hz, 1H). ¹³C NMR (100 MHz, CDCl₃) δ 18.6, 18.7, 18.9, 19.7, 22.6, 22.7, 23.9, 24.7, 25.3, 27.9, 30.2, 30.7, 33.4, 36.2, 36.9, 37.0, 37.3, 37.4, 38.3, 39.1, 44.8, 45.5, 49.8, 123.8, 124.1, 126.9, 134.7, 145.5, 147.1, 172.7. IR (thin film): 3303, 2955, 2926, 2867, 16421, 1551,

1497, 1460, 1382, 1365, 1307, 1231, 1186, 820 cm^{-1} . HRMS (ESI-TOF) m/z calculated for $\text{C}_{30}\text{H}_{50}\text{NO}$ $[\text{M}+\text{H}]^+$: 440.3892, found 440.3887.

General procedure for sulfamate ester synthesis. To a dry 25 mL round-bottom flask equipped with a stirbar under N_2 were added 8.0 mL of CH_3CN and 5.0 mL of chlorosulfonyl isocyanate (57.0 mmol, 2.20 equiv), and the solution was cooled to 0 °C. Next, 2.2 mL of formic acid (58.0 mmol, 2.24 equiv) was added dropwise via syringe, and gas evolution was observed immediately. The resulting mixture was allowed to stir at 0 °C for 30 min, then was diluted with 16 mL of CH_3CN and allowed to gradually warm to room temperature and stir for an additional 2 h. The mixture was then recooled to 0 °C and a solution of alcohol (25.9 mmol, 1.00 equiv) in 12.0 mL of DMA was added dropwise via cannula. Transfer of the alcohol was made quantitative with an additional 9.0 mL of DMA. After 10 min, the reaction was warmed to room temperature and stirred for 16 h. The reaction was quenched by the addition of 20 mL of H_2O and transferred to a separatory funnel. The aqueous layer was extracted with EtOAc (2×50 mL). The combined organic layers were washed successively with H_2O (3×20 mL) and brine (1×20 mL), dried over Na_2SO_4 , decanted, and concentrated *in vacuo*. The product was purified by silica gel flash chromatography to give the desired sulfamate ester product.

Methyl sulfamate (2a). This compound was prepared according to the general procedure for sulfamate ester synthesis using 0.830 g of methanol (25.9 mmol). The product was purified by silica gel flash chromatography eluting with 40% EtOAc in hexanes to give the product as a white solid in 78% yield (2.24 g). Analytical data match the literature.⁴⁷

Ethyl sulfamate (2b). This compound was prepared according to the general procedure for sulfamate ester synthesis using 1.19 g of ethanol (25.9 mmol). The product was purified by silica gel flash chromatography eluting with 30% EtOAc in hexanes to give the product as a white solid in 93% yield (3.02 g). Analytical data match the literature.⁴⁸

Propyl sulfamate (2c). This compound was prepared according to the general procedure for sulfamate ester synthesis using 1.56 g of propan-1-ol (25.9 mmol). The product was purified by silica gel flash chromatography eluting with 30% EtOAc in hexanes to give the product as a colorless oil in 83% yield (2.99 g). Analytical data match the literature.⁴⁷

Butyl sulfamate (2d): This compound was prepared according to the general procedure for sulfamate ester synthesis using 1.92 g of butan-1-ol (25.9 mmol). The crude mixture was purified by silica gel flash chromatography eluting with 30% EtOAc in hexanes to give the product as a colorless oil in 66% yield (2.62 g), $R_f = 0.3$ (30% EtOAc in hexanes). ¹H NMR (500 MHz, CDCl₃): δ 0.95 (t, $J = 7.4$ Hz, 3H), 1.44 (sex, $J = 7.5$ Hz, 2H), 1.73 (p, $J = 7.5$ Hz, 2H), 4.22 (t, $J = 6.5$ Hz, 2H), 4.87 (s, 2H). ¹³C NMR (125 MHz, CDCl₃): δ 13.7, 18.9, 30.9, 71.6. IR (neat): 3283, 2962, 2876, 1558, 1466, 1350, 1171, 1055, 1014, 995, 919, 882, 817, 792, 729, 667, 590, 550 cm⁻¹. HRMS (ESI-TOF) m/z calculated for C₄H₁₁NO₃NaS [M+Na]⁺: 176.0357, found 176.0360.

2-chloroethyl sulfamate (2e). This compound was prepared according to the general procedure for sulfamate ester synthesis using 2.09 g of 2-chloroethan-1-ol (25.9 mmol). The crude mixture was purified by silica gel flash chromatography eluting with 50% EtOAc in hexanes to give the product as a white solid in 51% yield (2.11 g), M.P.

= 43–45 °C, R_f = 0.3 (50% EtOAc in hexanes). ^1H NMR (500 MHz, CDCl_3): δ 3.78 (t, J = 5.8 Hz, 2H), 4.43 (t, J = 5.8 Hz, 2H), 4.91 (s, 2H). ^{13}C NMR (125 MHz, CDCl_3): δ 41.2, 70.2. IR (thin film): 3388, 3285, 1557, 1456, 1430, 1359, 1305, 1174, 1071, 1006, 925, 767, 668, 590, 551 cm^{-1} . HRMS (ESI-TOF) m/z calculated for $\text{C}_2\text{H}_5\text{ClINO}_3\text{S}$ [$\text{M}-\text{H}^+$]: 157.9679, found 157.9687.

3-chloropropyl sulfamate (2f). This compound was prepared according to the general procedure for sulfamate ester synthesis using 2.45 g of 3-chloropropan-1-ol (25.9 mmol). The product was purified by silica gel flash chromatography eluting with 40% EtOAc in hexanes to give the product as a yellow oil in 26% yield (1.17 g). Analytical data match the literature.⁴⁸

4-chlorobutyl sulfamate (2g). This compound was prepared according to the general procedure for sulfamate ester synthesis using 2.81 g of 4-chlorobutan-1-ol (25.9 mmol). The crude mixture was purified by silica gel flash chromatography eluting with 30% EtOAc in hexanes to give the product as a colorless oil in 46% yield (2.24 g), R_f = 0.2 (30% EtOAc in hexanes). ^1H NMR (500 MHz, CDCl_3): δ 1.91–1.95 (m, 4H), 3.59 (t, J = 6.0 Hz, 2H), 4.50 (t, J = 5.8 Hz, 2H), 4.93 (s, 2H). ^{13}C NMR (125 MHz, CDCl_3): δ 26.4, 28.7, 44.4, 70.7. IR (neat): 26.4, 28.7, 44.4, 70.7. IR (neat): 3382, 3281, 2963, 1552, 1444, 1352, 1280, 1171, 1075, 915, 808, 738, 645, 591, 549 cm^{-1} . HRMS (ESI-TOF) m/z calculated for $\text{C}_4\text{H}_{10}\text{ClINaO}_3\text{S}$ [$\text{M}+\text{Na}$] $^+$: 209.9968, found 209.9969.

1,3-dichloropropan-2-yl sulfamate (2h). This compound was prepared according to the general procedure for sulfamate ester synthesis using 3.34 g of 1,3-dichloropropan-2-ol (25.9 mmol). The crude mixture was purified by silica gel flash chromatography eluting with 30% EtOAc in hexanes to give the product as a white

solid in 63% yield (3.39 g), M.P. = 75–77 °C, R_f = 0.5 (30% EtOAc in hexanes). ^1H NMR (500 MHz, CDCl_3): δ 3.87 (t, J = 5.3 Hz, 4H), 4.87 (p, J = 5.3 Hz, 1H), 4.96 (s, 2H). ^{13}C NMR (125 MHz, CDCl_3): δ 42.6, 79.7. IR (thin film): 3853, 3743, 3628, 3392, 3287, 1733, 1716, 1699, 1683, 1652, 1616, 1558, 1506, 1429, 1363, 1296, 1177, 1009, 920, 864, 789, 753, 699, 667, 598, 555 cm^{-1} . HRMS (ESI-TOF) m/z calculated for $\text{C}_3\text{H}_6\text{Cl}_2\text{NO}_3\text{S}$ $[\text{M}-\text{H}^+]$: 205.9445, found 205.9452.

2,2-dichloroethyl sulfamate (2i). This compound was prepared according to the general procedure for sulfamate ester synthesis using 2.98 g of 2,2-dichloroethan-1-ol (25.9 mmol). The crude mixture was purified by silica gel flash chromatography eluting with 30% EtOAc in hexanes to give the product as a white solid in 69% yield (3.47 g), M.P. = 39–40 °C, R_f = 0.3 (30% EtOAc in hexanes). ^1H NMR (500 MHz, CDCl_3): δ 4.49 (d, J = 6.0 Hz, 2H), 5.06 (s, 2H), 5.90 (t, J = 6.0 Hz, 1H). ^{13}C NMR (125 MHz, CDCl_3): δ 67.6, 73.4. IR (thin film): 3738, 3628, 3394, 3293, 1761, 1699, 1652, 1558, 1506, 1455, 1370, 1294, 1182, 1062, 1004, 932, 839, 797, 756, 707, 667, 553 cm^{-1} . HRMS (ESI-TOF) m/z calculated for $\text{C}_2\text{H}_4\text{Cl}_2\text{NO}_3\text{S}$ $[\text{M}-\text{H}^+]$: 191.9289, found 191.9307.

4,4-dichlorobutyl sulfamate (2j). This compound was prepared according to the general procedure for sulfamate ester synthesis using 3.70 g of 4,4-dichlorobutan-1-ol (25.9 mmol). The crude mixture was purified by silica gel flash chromatography eluting with 30% EtOAc in hexanes to give the product as a white solid in 78% yield (4.49 g), M.P. = 44–46 °C, R_f = 0.3 (30% EtOAc in hexanes). ^1H NMR (500 MHz, CDCl_3): δ 2.01–2.09 (m, 2H), 2.32–2.39 (m, 2H), 4.29 (t, J = 6.0 Hz, 2H), 4.82 (s, 2H), 5.84 (t, J = 5.8 Hz, 1H). ^{13}C NMR (125 MHz, CDCl_3): δ 25.4, 39.7, 70.1, 72.7. IR (thin

film): 3853, 3734, 3628, 3386, 3285, 2967, 1699, 1652, 1558, 1506, 1471, 1444, 1361, 1178, 1078, 1017, 935, 890, 750, 667, 655, 594, 552 cm^{-1} . HRMS (ESI-TOF) m/z calculated for $\text{C}_4\text{H}_8\text{Cl}_2\text{NO}_3\text{S}$ $[\text{M}-\text{H}^+]^-$: 219.9602, found 219.9617.

2,2,2-trichloroethyl sulfamate (2k). This compound was prepared according to the general procedure for sulfamate ester synthesis using 3.87 g of 2,2,2-trichloroethan-1-ol (25.9 mmol). The product was purified by silica gel flash chromatography eluting with 30% EtOAc in hexanes to give the product as a white solid in 81% yield (4.79 g). Analytical data match the literature.⁴⁷

4,4,4-trichlorobutyl sulfamate (2l). This compound was prepared according to the general procedure for sulfamate ester synthesis using 4.60 g of 4,4,4-trichlorobutan-1-ol (25.9 mmol). The crude mixture was purified by silica gel flash chromatography eluting with 30% EtOAc in hexanes to give the product as a white solid in 82% yield (5.45 g), M.P. = 67–69 °C, R_f = 0.3 (30% EtOAc in hexanes). ^1H NMR (500 MHz, CDCl_3): δ 2.23–2.28 (m, 2H), 2.84–2.88 (m, 2H), 4.34 (t, J = 6.0 Hz, 2H), 4.90 (s, 2H). ^{13}C NMR (125 MHz, CDCl_3): δ 26.4, 51.6, 69.7, 99.1. IR (thin film): 3853, 3628, 3288, 2970, 1733, 1652, 1558, 1473, 1453, 1362, 1256, 1236, 1180, 1154, 1082, 1036, 936, 818, 746, 667, 660, 591, 552 cm^{-1} . HRMS (ESI-TOF) m/z calculated for $\text{C}_4\text{H}_7\text{Cl}_3\text{NO}_3\text{S}$ $[\text{M}-\text{H}^+]^-$: 253.9212, found 253.9218.

Isopropyl sulfamate (2m). This compound was prepared according to the general procedure for sulfamate ester synthesis using 1.56 g of propan-2-ol (25.9 mmol). The crude mixture was purified by silica gel flash chromatography eluting with 30% EtOAc in hexanes to give the product as a colorless oil in 62% yield (2.23 g), R_f = 0.4 (30% EtOAc in hexanes). ^1H NMR (500 MHz, CDCl_3): δ 1.41 (d, J = 6.0 Hz, 6H),

4.84 (sept, $J = 6.3$ Hz, 1H), 5.02 (s, 2H). ^{13}C NMR (125 MHz, CDCl_3): δ 22.8, 78.3. IR (neat): 3853, 3733, 3628, 3371, 3281, 2988, 1699, 1652, 1558, 1506, 1470, 1456, 1351, 1177, 1100, 919, 881, 767, 667, 590, 555 cm^{-1} . HRMS (ESI-TOF) m/z calculated for $\text{C}_3\text{H}_9\text{NO}_3\text{NaS}$ $[\text{M}+\text{Na}]^+$: 162.0201, found 162.0207.

1,1,1,3,3,3-hexafluoropropan-2-yl sulfamate (2n). This compound was prepared according to the general procedure for sulfamate ester synthesis using 4.35 g of 1,1,1,3,3,3-hexafluoropropan-2-ol (25.9 mmol). The product was purified by silica gel flash chromatography eluting with 30% EtOAc in hexanes to give the product as a white solid in 88% yield (5.63 g). Analytical data match the literature.⁵

2,2,2-trifluoroethyl sulfamate (2o). This compound was prepared according to the general procedure for sulfamate ester synthesis using 2.59 g of 2,2,2-trifluoroethanol (25.9 mmol). The product was purified by silica gel flash chromatography eluting with 40% EtOAc in hexanes to give the product as a white solid in 83% yield (3.85 g). Analytical data match the literature.⁴⁸

Pentan-3-yl sulfamate (2p). This compound was prepared according to the general procedure for sulfamate ester synthesis using 2.28 g of pentan-3-ol (25.9 mmol). The crude mixture was purified by silica gel flash chromatography eluting with 30% EtOAc in hexanes to give the product as a colorless oil in 49% yield (2.12 g). $R_f = 0.2$ (20% EtOAc in hexanes). ^1H NMR (500 MHz, CDCl_3): δ 0.97 (t, $J = 7.5$ Hz, 6H), 1.71–1.79 (m, 4H), 4.50 (p, $J = 6.0$ Hz, 1H), 4.87 (s, 2H). ^{13}C NMR (125 MHz, CDCl_3): δ 9.4, 26.5, 87.8. IR (neat): 3853, 3734, 3628, 3280, 2973, 2942, 2889, 1700, 1652, 1558, 1506, 1458, 1341, 1174, 1102, 1034, 901, 843, 777, 741, 667, 586, 552 cm^{-1} . HRMS (ESI-TOF) m/z calculated for $\text{C}_5\text{H}_{13}\text{NNaO}_3\text{S}$ $[\text{M}+\text{Na}]^+$: 190.0514, found

190.0515.

Isobutyl sulfamate (2q). This compound was prepared according to the general procedure for sulfamate ester synthesis using 1.92 g of 2-methylpropan-1-ol (25.9 mmol). The crude mixture was purified by silica gel flash chromatography eluting with 30% EtOAc in hexanes to give the product as a colorless oil in 79% yield (3.13 g), $R_f = 0.5$ (30% EtOAc in hexanes). $^1\text{H NMR}$ (500 MHz, CDCl_3): δ 0.97 (d, $J = 6.5$ Hz, 6H), 2.03 (nonet, $J = 6.8$ Hz, 1H), 3.97 (d, $J = 6.5$ Hz, 2H), 5.07 (s, 2H). $^{13}\text{C NMR}$ (125 MHz, CDCl_3): δ 18.8, 28.1, 77.4. IR (neat): 3374, 3280, 2965, 2877, 1557, 1470, 1353, 1171, 978, 919, 839, 814, 667, 583, 552 cm^{-1} . HRMS (ESI-TOF) m/z calculated for $\text{C}_4\text{H}_{11}\text{NO}_3\text{NaS}$ $[\text{M}+\text{Na}]^+$: 176.0357, found 176.0360.

Cyclohexylmethyl sulfamate (2r). This compound was prepared according to the general procedure for sulfamate ester synthesis using 2.96 g of cyclohexylmethanol (25.9 mmol). The product was purified by silica gel flash chromatography eluting with 30% EtOAc in hexanes to give the product as a white solid in 76% yield (3.80 g). Analytical data match the literature.⁴⁷

Neopentyl sulfamate (2s). This compound was prepared according to the general procedure for sulfamate ester synthesis using 2.28 g of 2,2-dimethylpropan-1-ol (25.9 mmol). The product was purified by silica gel flash chromatography eluting with 30% EtOAc in hexanes to give the product as a white solid in 80% yield (4.33 g), M.P. = 55–57 °C, $R_f = 0.5$ (30% EtOAc in hexanes). $^1\text{H NMR}$ (500 MHz, d^6 -acetone/TMS): δ 0.97 (s, 9H), 3.80 (s, 2H), 6.60 (s, 2H). $^{13}\text{C NMR}$ (125 MHz, d^6 -acetone/TMS): δ 25.7, 31.3, 78.6. IR (thin film): 3365, 3274, 2957, 1557, 1476, 1404, 1355, 1297, 1269, 1172, 1035, 977, 919, 831, 758, 667, 583, 557 cm^{-1} . HRMS (ESI-TOF) m/z calculated

for $C_5H_{13}NO_3NaS$ $[M+Na]^+$: 190.0514, found 190.0519.

3,3-dimethylbutyl sulfamate (2t). This compound was prepared according to the general procedure for sulfamate ester synthesis using 2.65 g of 3,3-dimethylbutan-1-ol (25.9 mmol). The crude mixture was purified by silica gel flash chromatography eluting with 30% EtOAc in hexanes to give the product as a white solid in 74% yield (3.50 g), M.P. = 47–48 °C, R_f = 0.5 (30% EtOAc in hexanes). 1H NMR (500 MHz, $CDCl_3$): δ 0.96 (s, 9H), 1.68 (t, J = 7.5 Hz, 2H), 4.26 (t, J = 7.5 Hz, 2H), 4.87 (s, 2H). ^{13}C NMR (125 MHz, $CDCl_3$): δ 29.7, 30.0, 42.0, 69.6. IR (thin film): 3853, 3628, 3374, 3289, 2956, 2870, 1700, 1652, 1558, 1475, 1365, 1177, 1080, 1018, 962, 928, 829, 775, 744, 667, 556 cm^{-1} . HRMS (ESI-TOF) m/z calculated for $C_6H_{15}NO_3NaS$ $[M+Na]^+$: 204.0670, found 204.0674.

2,2,3,3,3-pentafluoropropyl sulfamate (2u). This compound was prepared according to the general procedure for sulfamate ester synthesis using 3.89 g of 2,2,3,3,3-pentafluoropropan-1-ol (25.9 mmol). The crude mixture was purified by silica gel flash chromatography eluting with 30% EtOAc in hexanes to give the product as a colorless oil in 80% yield (4.74 g), R_f = 0.7 (30% EtOAc in hexanes). 1H NMR (500 MHz, d_6 -acetone/TMS): δ 4.68 (t, J = 12.8 Hz, 2H), 7.15 (s, 2H). ^{13}C NMR (125 MHz, d_6 -acetone/TMS): δ 65.2 (t, J_{CF} = 27.9 Hz), 113.7 (tq, J_{CF} = 253.4, 38.0 Hz), 120.2 (qt, J_{CF} = 283.6, 34.2 Hz). IR (neat): 3398, 3296, 1552, 1456, 1373, 1299, 1261, 1182, 1157, 1106, 1041, 1008 930, 818, 776, 717, 667, 622, 549 cm^{-1} . HRMS (ESI-TOF) m/z calculated for $C_3H_3F_5NO_3S$ $[M-H]^+$: 227.9754, found 227.9759.

2,2,3,3,4,4,4-heptafluorobutyl sulfamate (2v). This compound was prepared according to the general procedure for sulfamate ester synthesis using 5.18 g of

2,2,3,3,4,4,4-heptafluorobutan-1-ol (25.9 mmol). The crude mixture was purified by silica gel flash chromatography eluting with 30% EtOAc in hexanes to give the product as a low melting white solid in 90% yield (6.51 g), $R_f = 0.6$ (30% EtOAc in hexanes). ^1H NMR (500 MHz, d_6 -acetone/TMS): δ 4.75 (t, $J = 13.5$ Hz, 2H), 7.21 (s, 2H). ^{13}C NMR (125 MHz, d_6 -acetone/TMS): δ 63.4 (t, $J_{CF} = 27.0$ Hz), 106.8–112.5 (m), 113.7 (tt, $J_{CF} = 254.9, 30.5$ Hz), 117.4 (qt, $J_{CF} = 285.1, 33.4$ Hz). IR (neat): 3853, 3837, 3801, 3733, 3675, 3628, 3396, 3297, 1772, 1733, 1716, 1699, 1683, 1652, 1635, 1616, 1558, 1540, 1506, 1456, 1374, 1356, 1297, 1226, 1180, 1124, 1051, 1015, 958, 914, 819, 760, 724, 668, 649 cm^{-1} . HRMS (ESI-TOF) m/z calculated for $\text{C}_4\text{H}_3\text{F}_7\text{NO}_3\text{S}$ $[\text{M}-\text{H}]^-$: 277.9722, found 277.9727.

3-chloro-2,2-dimethylpropyl sulfamate (2w). This compound was prepared according to the general procedure for sulfamate ester synthesis using 3.18 g of 3-chloro-2,2-dimethylpropan-1-ol (25.9 mmol). The crude mixture was purified by silica gel flash chromatography eluting with 30% EtOAc in hexanes to give the product as a white solid in 77% yield (4.012 g), M.P. = 43–45 °C, $R_f = 0.5$ (30% EtOAc in hexanes). ^1H NMR (300 MHz, CDCl_3): δ 1.07 (s, 6H), 3.45 (s, 2H), 4.02 (s, 2H), 5.07 (s, 2H). ^{13}C NMR (75 MHz, CDCl_3): δ 22.5, 36.5, 51.4, 75.3. IR (thin film): 3859, 3792, 3628, 3384, 3289, 2971, 1733, 1716, 1699, 1683, 1652, 1558, 1506, 1472, 1436, 1356, 1305, 1267, 1175, 974, 920, 830, 775, 730, 702, 668, 585, 554 cm^{-1} . HRMS (ESI-TOF) m/z calculated for $\text{C}_5\text{H}_{11}\text{ClNO}_3\text{S}$ $[\text{M}-\text{H}]^-$: 200.0148, found 200.0149.

General C–H amination procedure A. This transformation is presented in Figure 3.13. Into a 1.5-dram vial equipped with a stirbar was added the sulfamate ester (0.30 mmol, 1.0 equiv). Then, 300 μL of a 2 mL standard solution (freshly prepared,

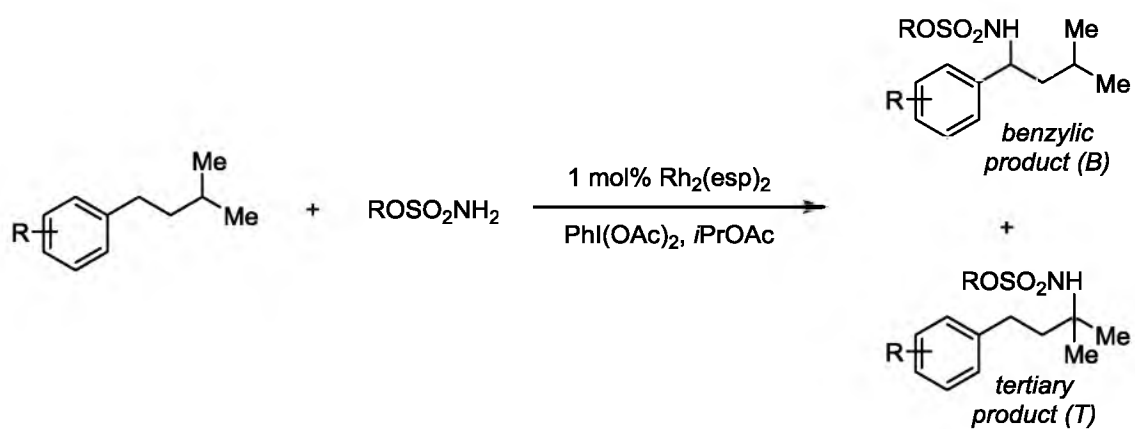


Figure 3.13. $\text{Rh}_2(\text{esp})_2$ -catalyzed C-H amination.

containing the isoamyl substrate (2.0 mmol), 50 μ L of tetradecane, 15 mg of Rh₂(esp)₂ (0.02 mmol, 0.01 equiv), and *i*PrOAc) were added to the vial. The vial was then sealed with a teflon-lined cap and stirred for 5 min, at which time the vial was uncapped and 193 mg of PhI(OAc)₂ (0.60 mmol, 2.0 equiv) was added in a single portion. The vial was then re-capped and allowed to stir for 16 h. (Note: the reaction changes color from green to red within 5 min of adding PhI(OAc)₂.) The reaction was then passed through celite and analyzed by GC and GC-MS.

General C–H amination procedure B. Into a 1.5-dram vial equipped with a stirbar were added the sulfamate ester (0.60 mmol, 1.2 equiv), 81 mg of freshly activated MgO (2.0 mmol, 4.0 equiv), and 100 mg of freshly activated 5 Å molecular sieves. Then, 500 μ L of a 2 mL standard solution (freshly prepared, containing the isoamyl substrate (2.0 mmol), 15 mg of Rh₂(esp)₂ (0.02 mmol, 0.01 equiv), and *i*PrOAc) were added to the vial. The vial was then sealed with a teflon-lined cap and stirred for 5 min, at which time the vial was uncapped and 322 mg of PhI(OAc)₂ (1.0 mmol, 2.0 equiv) was added in a single portion. The vial was then re-capped and allowed to stir for 16 h. The reaction was then passed through celite and concentrated *in vacuo*. The product was purified by silica gel flash chromatography to give the desired sulfamate ester product.

2,2,3,3,3-pentafluoropropyl (3-methyl-1-phenylbutyl)sulfamate (3u). The general C–H amination procedure B was followed using 137 mg of 2,2,3,3,3-pentafluoropropyl sulfamate (**2u**) (0.60 mmol). The crude mixture was purified by silica gel flash chromatography eluting with 20% diethyl ether in hexanes to give the product as a white solid in 58% yield (109 mg), M.P. = 47-48 °C, R_f = 0.4 (20% ether

in hexanes). ^1H NMR (500 MHz, CDCl_3): δ 0.93 (d, $J = 6.5$ Hz, 6H), 1.53 (sept, $J = 6.5$ Hz, 1H), 1.66(dt, $J = 13.9, 7.1$ Hz, 1H), 1.77 (dt, $J = 14.0, 7.1$ Hz, 1H), 3.99 (q, $J = 12.2$ Hz, 1H), 4.07 (q, $J = 12.2$ Hz, 1H), 4.50 (t, $J = 7.7$ Hz, 1H), 5.20 (s, 1H), 7.25–7.34 (m, 3H), 7.35–7.40 (m, 2H). ^{13}C NMR (125 MHz, CDCl_3): δ 22.3, 22.5, 24.9, 46.2, 58.1, 63.9 (t, $J_{\text{CF}} = 27.9$ Hz), 111.3 (tq, $J_{\text{CF}} = 255.2, 38.3$ Hz), 118.3 (qt, $J_{\text{CF}} = 284.8, 34.3$ Hz), 126.7, 128.5, 129.2, 140.9. IR (thin film): 3853, 3732, 3628, 3298, 2960, 2873, 1558, 1457, 1428, 1367, 1260, 1201, 1178, 1107, 1045, 1005, 970, 938, 839, 806, 774, 758, 699, 667, 604, 565 cm^{-1} . HRMS (ESI-TOF) m/z calculated for $\text{C}_{14}\text{H}_{17}\text{F}_5\text{NO}_3\text{S}$ [$\text{M}-\text{H}^+$]: 374.0849, found 374.0841.

2,2,3,3,3-pentafluoropropyl (4-methyl-1-phenylpentyl)sulfamate (5u). The general C–H amination procedure B was followed using 137 mg of 2,2,3,3,3-pentafluoropropyl sulfamate (**2u**) (0.60 mmol). The crude mixture was purified by silica gel flash chromatography eluting with 20% diethyl ether in hexanes to give the product as a colorless oil in 60% yield (118 mg), $R_f = 0.5$ (20% ether in hexanes). ^1H NMR (300 MHz, CDCl_3): δ 0.86 (d, $J = 6.6$ Hz, 6H), 1.00–1.34 (m, 2H), 1.55 (sept, $J = 6.8$ Hz, 1H), 1.72–1.99 (m, 2H), 4.08 (sex, $J = 12.8$ Hz, 2H), 4.39 (q, $J = 7.5$ Hz, 1H), 5.23 (s, 1H), 7.23–7.41 (m, 5H). ^{13}C NMR (125 MHz, CDCl_3): δ 22.5, 22.6, 27.9, 34.9, 35.2, 60.1, 64.0 (t, $J_{\text{CF}} = 28.0$ Hz), 111.3 (tq, $J_{\text{CF}} = 255.1, 38.1$ Hz), 118.3 (qt, $J_{\text{CF}} = 284.6, 34.3$ Hz), 126.7, 128.5, 129.2, 140.7. IR (neat): 3301, 2958, 2872, 1496, 1456, 1428, 1367, 1295, 1258, 1201, 1178, 1107, 1038, 1008, 956, 908, 809, 774, 736, 699, 669, 622, 566 cm^{-1} . HRMS (ESI-TOF) m/z calculated for $\text{C}_{15}\text{H}_{20}\text{F}_5\text{NO}_3\text{S}$ [$\text{M}+\text{Na}^+$]: 412.0982, found 412.0992.

2,2,3,3,3-pentafluoropropyl((1*R*,4*aS*,10*aR*)-1-((3,7-dimethyloctanamido)met

hyl)-7-isopropyl-1,4a-dimethyl-1,2,3,4,4a,9,10,10a-octahydrophenanthren-9-yl)sulfamate (6u). The general procedure B was followed using 104 mg 2,2,3,3,3-pentafluoropropyl sulfamate (0.45 mmol, 1.2 equiv) and 165 mg of substrate (0.38 mmol, 1.0 equiv). Purification by chromatography on silica gel eluting with 20% EtOAc in hexanes afforded the desired product as a colorless oil in 55% yield (139 mg, inseparable 1:1 diastereomeric mixture), $R_f = 0.35$ (20% EtOAc in hexanes); ^1H NMR (400 MHz, CDCl_3) δ 0.76–0.84 (m, 18H), 0.93 (s, 6H), 1.10–1.14 (m, 4H), 1.15 (s, 6H), 1.22 (d, $J = 6.8$ Hz, 12H), 1.25–1.47 (m, 8H), 1.68–1.78 (m, 4H), 1.82–1.98 (m, 4H), 2.09–2.19 (m, 4H), 2.24–2.31 (m, 4H), 2.51–2.59 (m, 2H), 2.86 (sept, $J = 6.8$ Hz, 2H), 3.61–3.69 (m, 2H), 4.52–4.62 (m, 2H), 4.72–4.75 (m, 2H), 4.82–4.92 (m, 2H), 5.77 (t, $J = 6.0$ Hz, 2H), 6.74 (d, $J = 7.2$ Hz, 1H), 6.78 (d, $J = 7.2$ Hz, 1H), 7.09 (d, $J = 8.4$ Hz, 2H), 7.15 (d, $J = 8.4$ Hz, 2H), 7.34 (s, 1H), 7.35 (s, 1H). ^{13}C NMR (100 MHz, CDCl_3) δ 18.4, 19.5, 19.6, 19.7, 19.8, 22.5, 22.6, 22.7, 23.8, 24.0, 24.5, 24.7, 25.0, 25.1, 26.5, 26.6, 27.8, 27.9, 30.7, 30.8, 33.5, 33.6, 35.4, 36.8, 36.9, 37.3, 37.4, 37.8, 37.9, 38.4, 38.9, 39.0, 39.1, 44.7, 44.8, 48.9, 52.4, 52.5, 63.6, 63.9, 64.2, 123.6, 126.3, 126.4, 126.7, 128.4, 128.5, 133.0, 133.1, 146.7, 146.8, 147.1, 147.2, 174.2. ^{19}F NMR (376 MHz, decoupled, CDCl_3) δ –83.9, –123.8. IR (thin film): 3403, 3306, 2958, 2929, 2870, 1646, 1535, 1498, 1460, 1366, 1205, 1183, 1046, 1004, 801 cm^{-1} . HRMS (ESI-TOF) m/z calculated for $\text{C}_{33}\text{H}_{52}\text{F}_5\text{N}_2\text{O}_4\text{S}$ $[\text{M}+\text{H}]^+$: 667.3568, found 667.3562.

GC-MS Traces

All crude Rh-catalyzed C–H amination reactions were analyzed by GC to determine benzylic-to-tertiary ratios. Each product mixture was then analyzed by GC-

MS to confirm the identity of the benzylic and tertiary product peaks by analyzing their corresponding fragmentation patterns. As a representative example, GC-MS traces of the proposed fragmentation of the benzylic and tertiary isoamylbenzene amination products, resulting from the Rh-catalyzed amination reaction, are shown in Figure 3.14.

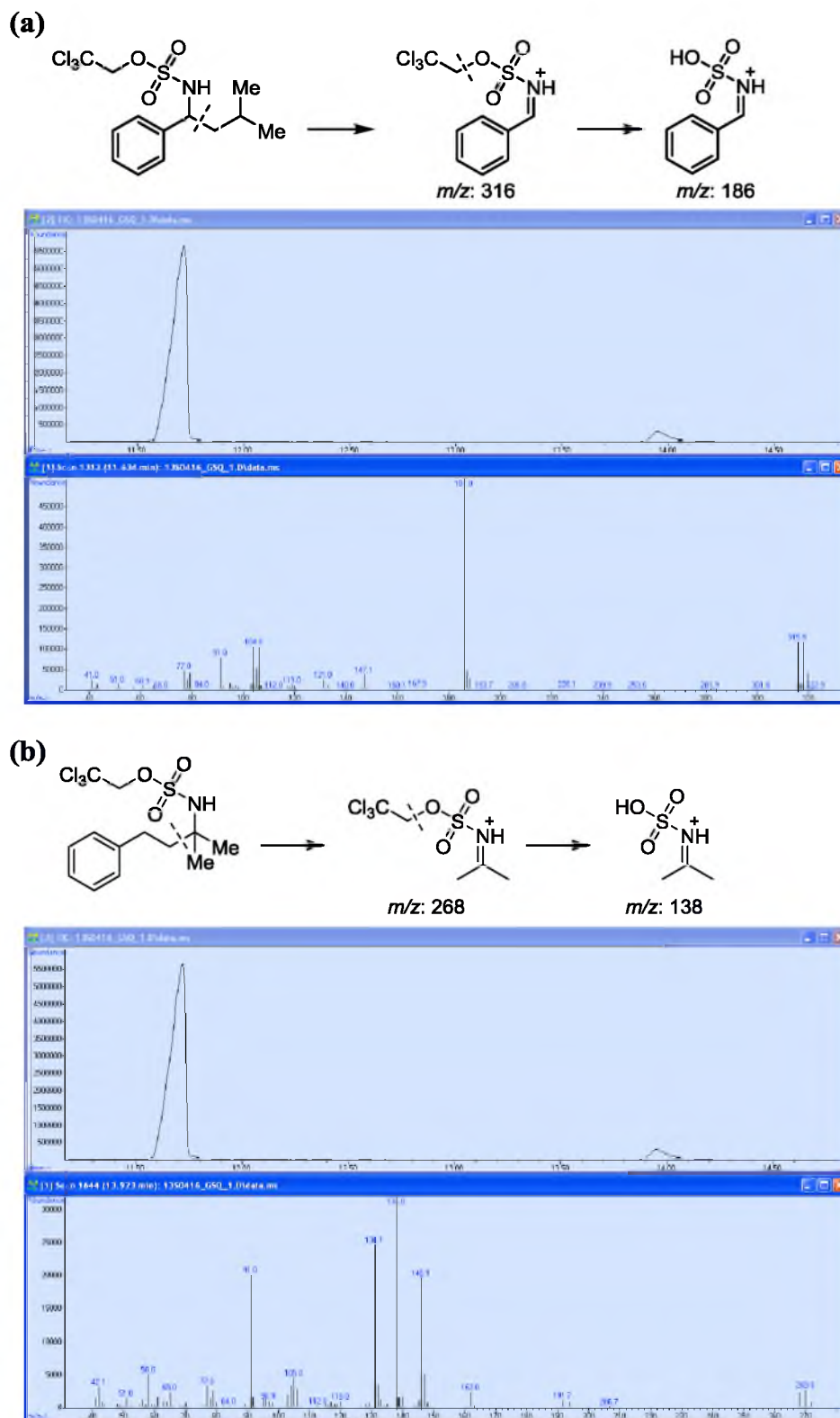


Figure 3.14. Representative proposed fragmentation of amination products with corresponding GC-MS traces. **(a)** Benzylic product. **(b)** Tertiary product.

References

1. Carlson, R. *Design and Optimization in Organic Synthesis*. Elsevier: Amsterdam, 1992; Vol. 8.
2. Deming, S. N.; Morgan, S. L. *Experimental Design: A Chemometric Approach*. Elsevier: Amsterdam, 1993; Vol. 11.
3. Gutekunst, W. R.; Baran, P. S. C-H Functionalization Logic in Total Synthesis. *Chem. Soc. Rev.* **2011**, *40*, 1976–1991.
4. Roizen, J. L.; Harvey, M. E.; Du Bois, J. Metal-Catalyzed Nitrogen-Atom Transfer Methods for the Oxidation of Aliphatic C–H Bonds. *Acc. Chem. Res.* **2012**, *45*, 911–922.
5. Roizen, J. L.; Zalatan, D. N.; Du Bois, J. Selective Intermolecular Amination of C–H Bonds at Tertiary Carbon Centers. *Angew. Chem. Int. Ed.* **2013**, *52*, 11343–11346.
6. Wells, P. R. Linear Free Energy Relationships. *Chem. Rev.* **1963**, *63*, 171–219.
7. Hansch, C.; Leo, A.; Taft, R. W. A Survey of Hammett Substituent Constants and Resonance and Field Parameters. *Chem. Rev.* **1991**, *91*, 165–195.
8. Hammett, L. P. Some Relations between Reaction Rates and Equilibrium Constants. *Chem. Rev.* **1935**, *17*, 125–136.
9. Hammett, L. P. The Effect of Structure upon the Reactions of Organic Compounds. Benzene Derivatives. *J. Am. Chem. Soc.* **1937**, *59*, 96–103.
10. Taft, R. W. Polar and Steric Substituent Constants for Aliphatic and o-Benzoate Groups from Rates of Esterification and Hydrolysis of Esters. *J. Am. Chem. Soc.* **1952**, *74*, 3120–3128.
11. Taft, R. W. Linear Steric Energy Relationships. *J. Am. Chem. Soc.* **1953**, *75*, 4538–4539.
12. Charton, M. Steric Effects. I. Esterification and Acid-Catalyzed Hydrolysis of Esters. *J. Am. Chem. Soc.* **1975**, *97*, 1552–1556.
13. Bess, E. N.; Sigman, M. S. Linear Free Energy Relationships (LFERs) in Asymmetric Catalysis. In *Asymmetric Synthesis II: More Methods and Applications*, Christmann, M.; Bräse, S., Eds. Wiley-VCH Verlag GmbH & Co. KGaA: Weinheim, 2012.
14. Harper, K. C.; Sigman, M. S. Using Physical Organic Parameters To Correlate Asymmetric Catalyst Performance. *J. Org. Chem.* **2013**, *78*, 2813–2818.

15. Harper, K. C.; Sigman, M. S. Three-Dimensional Correlation of Steric and Electronic Free Energy Relationships Guides Asymmetric Propargylation. *Science* **2011**, *333*, 1875–1878.
16. Harper, K. C.; Sigman, M. S. Predicting and Optimizing Asymmetric Catalyst Performance Using the Principles of Experimental Design and Steric Parameters. *Proc. Natl. Acad. Sci. U.S.A.* **2011**, *108*, 2179–2183.
17. Jensen, K. H.; Sigman, M. S. Systematically Probing the Effect of Catalyst Acidity in a Hydrogen-Bond-Catalyzed Enantioselective Reaction. *Angew. Chem. Int. Ed.* **2007**, *46*, 4748–4750.
18. Johnson, C. D. Linear Free Energy Relations and the Reactivity-Selectivity Principle. *Chem. Rev.* **1975**, *75*, 755–765.
19. Shorter, J. The Separation of Polar, Steric, and Resonance Effects in Organic Reactions by the Use of Linear Free Energy Relationships. *Chem. Soc. Rev.* **1970**, *24*, 433–453.
20. Gustafson, J. L.; Sigman, M. S.; Miller, S. J. Linear Free-Energy Relationship Analysis of a Catalytic Desymmetrization Reaction of a Diarylmethane-bis(phenol). *Org. Lett.* **2010**, *12*, 2794–2797.
21. Harper, K. C.; Bess, E. N.; Sigman, M. S. Multidimensional Steric Parameters in the Analysis of Asymmetric Catalytic Reactions. *Nat. Chem.* **2012**, *4*, 366–374.
22. Milo, A.; Bess, E. N.; Sigman, M. S. Interrogating Selectivity in Catalysis Using Molecular Vibrations. *Nature* **2014**, *507*, 210–214.
23. Denmark, S. E.; Gould, N. D.; Wolf, L. M. A Systematic Investigation of Quaternary Ammonium Ions as Asymmetric Phase-Transfer Catalysts. Application of Quantitative Structure Activity/Selectivity Relationships. *J. Org. Chem.* **2011**, *76*, 4337–4357.
24. Gormisky, P. E.; White, M. C. Catalyst-Controlled Aliphatic C–H Oxidations with a Predictive Model for Site-Selectivity. *J. Am. Chem. Soc.* **2013**, *135*, 14052–14055.
25. Harper, K. C.; Vilardi, S. C.; Sigman, M. S. Prediction of Catalyst and Substrate Performance in the Enantioselective Propargylation of Aliphatic Ketones by a Multidimensional Model of Steric Effects. *J. Am. Chem. Soc.* **2013**, *135*, 2482–2485.
26. Winstein, S.; Holness, N. J. Neighboring Carbon and Hydrogen. XIX. *t*-Butylcyclohexyl Derivatives. Quantitative Conformational Analysis. *J. Am. Chem. Soc.* **1955**, *77*, 5562–5578.
27. Curtin, D. Y. Stereochemical Control of Organic Reactions Differences in

- Behaviour of Diastereoisomers. *Rec. Chem. Prog.* **1954**, *15*, 110–128.
28. Verloop, A.; Hoogenstraaten, W.; Tipker, J. Development and Application of New Steric Substituent Parameters in Drug Design. In *Drug Design*, Ariens, E. J., Ed. Academic Press: New York, 1976; Vol. VII, pp 165–207.
 29. Verloop, A.; Tipker, J. A Comparative Study of New Steric Parameters in Drug Design. *Pharmacochem. Libr.* **1977**, *2*, 63–81.
 30. Verloop, A.; Tipker, J. Physical Basis of STERIMOL and Related Steric Constants. *Pharmacochem. Libr.* **1987**, *10*, 97–102.
 31. Hansch, C.; Leo, A.; Hoekman, D. *Exploring QSAR: Volume 2: Hydrophobic, Electronic, and Steric Constants*. American Chemical Society: Washington, D.C., 1995.
 32. Lewis, E. S. Rate-Equilibrium LFER Characterization of Transition States: The Interpretation of α . *J. Phys. Org. Chem.* **1990**, *3*, 1–8.
 33. Frisch, M. J.; Trucks, G. W.; Schlegel, H. B.; Scuseria, G. E.; Robb, M. A.; Cheeseman, J. R.; Scalmani, G.; Barone, V.; Mennucci, B.; Petersson, G. A., et al. *Gaussian 09, Revision C.01*, Gaussian, Inc.: Wallingford, CT, 2009.
 34. Zhao, Y.; Truhlar, D. G. The M06 Suite of Density Functionals for Main Group Thermochemistry, Thermochemical Kinetics, Noncovalent Interactions, Excited States, and Transition Elements: Two New Functionals and Systematic Testing of Four M06-Class Functionals and 12 Other Functionals. *Theor. Chem. Acc.* **2007**, *120*, 215–241.
 35. Valero, R.; Gomes, J. R. B.; Truhlar, D. G.; Illas, F. Good Performance of the M06 Family of Hybrid Meta Generalized Gradient Approximation Density Functionals on a Difficult Case: CO Adsorption on MgO(001). *J. Chem. Phys.* **2008**, *129*, 124710.
 36. Schäfer, A.; Horn, H.; Ahlrichs, R. Fully Optimized Contracted Gaussian Basis Sets for Atoms Li to Kr. *J. Chem. Phys.* **1992**, *97*, 2571.
 37. Schäfer, A.; Huber, C.; Ahlrichs, R. Fully Optimized Contracted Gaussian Basis Sets of Triple Zeta Valence Quality for Atoms Li to Kr. *J. Chem. Phys.* **1994**, *100*, 5829.
 38. Brown, H. C.; Okamoto, Y. Electrophilic Substituent Constants. *J. Am. Chem. Soc.* **1958**, *80*, 4979–4987.
 39. Fiori, K. W.; Du Bois, J. Catalytic Intermolecular Amination of C–H Bonds: Method Development and Mechanistic Insights. *J. Am. Chem. Soc.* **2007**, *129*, 562–568.

40. Fiori, K. W.; Espino, C. G.; Brodsky, B. H.; Du Bois, J. A Mechanistic Analysis of the Rh-Catalyzed Intramolecular C–H Amination Reaction. *Tetrahedron* **2009**, *65*, 3042–3051.
41. MATLAB. *version 8.1.0.604 (R2013a)*. The MathWorks, Inc.: Natick, MA, 2013.
42. Arlot, S.; Celisse, A. A Survey of Cross-Validation Procedures for Model Selection. *Statist. Surv.* **2010**, *4*, 40–79.
43. Coates, J. Interpretation of Infrared Spectra, A Practical Approach. In *Encyclopedia of Analytical Chemistry*, Meyers, R. A., Ed. John Wiley & Sons Ltd: Chichester, 2000; pp 10815–10837.
44. Tanaka, J.; Nojima, M.; Kusabayashi, S.; Nagase, S. Protonation and Alkylation of 1-Arylpropenyl-Lithium. *J. Chem. Soc., Perkin Trans. 2* **1987**, 673–678.
45. Kündig, E. P.; Cunningham Jr, A. F. 1,3-Benzodithiole Tetraoxide as a CH₂²-Synthon. *Tetrahedron* **1988**, *44*, 6855–6860.
46. Imai, T.; Nishida, S.; Tsuji, T. Ring Opening Alkylation of Cyclic Ethers with [α]-Halogenoalkyllithiums in the Presence of Boron Trifluoride-Diethyl Ether. *J. Chem. Soc., Chem. Commun.* **1994**, 2353–2354.
47. Yamamoto, H.; Ho, E.; Sasaki, I.; Mitsutake, M.; Takagi, Y.; Imagawa, H.; Nishizawa, M. Intermolecular Amination of Allyl Alcohols with Sulfamates: Effective Utilization of Mercuric Catalyst. *Eur. J. Org. Chem.* **2011**, *2011*, 2417–2420.
48. Winum, J.-Y.; Vullo, D.; Casini, A.; Montero, J.-L.; Scozzafava, A.; Supuran, C. T. Carbonic Anhydrase Inhibitors: Inhibition of Transmembrane, Tumor-Associated Isozyme IX, and Cytosolic Isozymes I and II with Aliphatic Sulfamates. *J. Med. Chem.* **2003**, *46*, 5471–5477.

CHAPTER 4

A DESIGNER SUBSTRATE SCOPE LIBRARY AMENABLE TO QUANTITATIVE DESCRIPTION AND PREDICTIVE MODELLING OF REACTION PERFORMANCE*

Introduction

Assessment of reaction substrate scope is often a qualitative endeavor that provides general indications of substrate sensitivity to a measured reaction outcome. Unfortunately, this field standard typically falls short of enabling the quantitative prediction of reaction outcomes for substrates not evaluated in the scope library. The disconnection between a reaction's development and the quantitative prediction of new substrates' behavior limits the applicative usefulness of many methodologies.

Founded on the work presented in Chapters 2 and 3, we considered that the approach developed for mathematically exploring reaction mechanism and optimizing reaction outcomes, when applied to reaction scope, would advantageously impact the quality of data gathered from this key aspect of reaction development. This concept was evaluated in the context of rhodium-catalyzed asymmetric transfer hydrogenation. This chapter will explore the process of devising a Design of Experiments (DoE) founded

* This chapter is based on the author's reported work that is herein reproduced with permission from Bess, E. N.; Bischoff, A. J.; Sigman, M. S. Designer Substrate Library for Quantitative, Predictive Modeling of Reaction Performance. *Proc. Natl. Acad. Sci. U.S.A* **2014**, *111*, 14698–14703.

substrate scope library, developing models to quantify the molecular features that influence enantioselection, and, in so doing, lend mechanistic insight to the modes of asymmetric induction.

Product distributions of chemical reactions are dictated by a myriad of interactions between molecular species. Identifying which of these features impacts reaction selectivity is a key facet for mechanistically understanding a transformation. Such insight often facilitates optimization, as well as indicates which types of substrates (substrate scope) are well-suited to the method. Unfortunately, the assessment of impactful features is frequently a qualitative endeavor that would significantly benefit from quantitation. Founded upon the modelling concepts investigated in Chapters 2 and 3 and expanding the previously established applications of DoE, a robust method is demonstrated for developing a varied substrate scope library of ketones, identifying quantitative descriptors of mechanistic significance, and applying these descriptors to mathematically elucidate trends in enantioselective reaction outcomes of rhodium-catalyzed asymmetric transfer hydrogenation. The developed mathematical relationships are used to predict future outcomes of new ketone substrates.

Human brains are highly experienced at recognizing patterns in observed data. Organizing information and drawing connections between data enables general conclusions to be made: fast or slow; good or bad; high or low. While these qualitative assessments are routinely crafted, they are subject to biases, causing evaluations to differ from one individual to another.¹ The examination of a reaction's substrate scope often takes on a similarly qualitative air.²⁻⁵ A substrate scope for a developed synthetic method typically provides an indication of functional group tolerance and general trends in

reaction outcomes for sterically and/or electronically varied substrates. This qualitative approach, which lacks quantitation of how substrate features will influence a reaction's outcome, particularly product selectivity, often limits a reaction's application to contexts with high degrees of similarity to the initial scope library. Additionally, it can be difficult to predict, beyond generalities such as poorly versus well behaved, how a new substrate will perform under the reaction conditions. Addressing this limitation through quantitative prediction of reaction outcomes would significantly affect how one both develops and applies a new synthetic method while simultaneously imparting fundamental mechanistic insight.⁶

To accomplish this goal, an entirely new approach to examining a reaction's substrate scope is required. As the ultimate goal is to mathematically predict a broad range of reaction outcomes, an initial library of substrates would need to be carefully designed to represent many of the impactful features influencing the reaction, as was successfully demonstrated with the sulfamate ester library for rhodium-catalyzed C–H amination (Chapter 3). Specifically, one would need to include systematic variation of steric and electronic features of a given substrate class while also limiting the initial size of the substrate library to make this a practical venture. With this in mind, exploiting the tenets of Design of Experiments (DoE) and regression modeling is required, where broadly descriptive models are built from data that systematically samples the experimental space to be described.^{7,8} Following the pattern prescribed in the previous chapters, the results of this sampling are then correlated to chemical descriptors—which are predicted to define relevant interactions between a substrate and catalyst—using linear regression algorithms for the prediction of reaction outcomes.⁹⁻¹⁷

In the context of enantio- or site-selective reactions, it is anticipated that this type of strategy would have two far-reaching effects: 1) provide mechanistic information about the properties of a substrate that are essential for differentially engaging a catalyst, where one product is favored over others and 2) enable quantified predictions of how future substrates will behave under the reaction conditions, prior to performing the experiment. Numerical depiction of patterns in reaction outcomes expands the applicability of developed reaction methods, adding a quantitatively accurate and precise dimension to qualitative expectations of chemical behavior.¹⁸ Herein is described an approach for constructing a substrate library of ketones that is sterically and electronically varied according to DoE principles and, thus, is amenable to descriptive, predictive quantitative modelling, wherein mechanistic patterns in reaction outcomes are robustly delineated. Particularly, the objective is to develop a ketone library that is defined by molecular descriptors that broadly represent properties that are influential in a variety of mechanistically distinct reactions.

The following sections describe a four-step process to designing a substrate scope library, which is suited to eventual quantitative modelling of reaction outcomes (Figure 4.1). These steps are 1) identify parameters to describe reaction sensitivities and define the virtual experimental space; 2) organize ketones that systematically sample the experimental space and evaluate these ketones' performance in enantioselective reactions; 3) connect molecular descriptors of ketones to reaction outcomes via linear regression modelling; and 4) apply models to quantitatively predict the performance of new ketones.

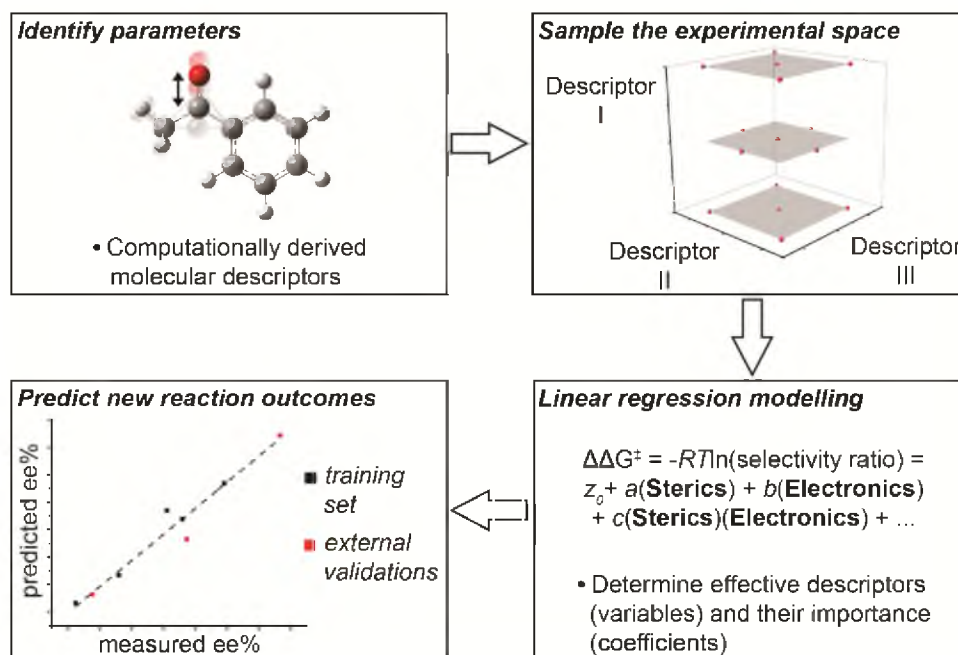


Figure 4.1. Approach to developing a sterically and electronically modulated substrate library amenable to quantitative modelling of reaction outcomes. First, parameters are selected based on hypotheses of their mechanistic relevance to define the experimental substrate scope space. Second, the experimental space is systematically sampled in a reaction of interest. Third, linear regression modelling is used to identify quantitative relationships between reaction outcomes and molecular descriptors. Finally, the developed model is used to predict the reaction outcomes of new substrates, prior to experimental assessment.

Identify Substrate Parameters and Define the Ketone Experimental Space

Quantitative modelling initiates with consideration of the experimental ketone space to be described. What substrate changes impact reaction outcomes and why? Hypothesizing a reaction's sensitivity to substrate modifications and identifying a system by which these changes are numerically depicted sets the stage for a systematic substrate analysis focused on facets of mechanistic relevance. This process was recently demonstrated in our analysis of Nozaki-Hiyama-Kishi (NHK) propargylation of alkyl ketones.¹¹ Measuring dimensional information according to Sterimol parameters, a library of sterically varied methyl ketones and ligands was prepared, according to DoE principles (Figures 4.2a–c).¹⁹⁻²¹ Subjected to NHK propargylation reaction conditions, enantiomeric ratios resulting from each ligand/ketone combination in this library were measured. Linear regression modelling was used to develop a mathematical relationship that related steric features of the substrates (Sterimol B₁, minimum substituent radius; Sterimol B₅, maximum substituent radius) and ligands (B₁) to $\Delta\Delta G^\ddagger$ ($\Delta\Delta G^\ddagger = -RT \cdot \ln(\text{enantioselectivity})$, Figure 4.2d). This model enabled the robust prediction of enantioselectivity afforded for new methyl ketones, ligands, and combinations thereof. Additionally, this model quantifies specific aspects of steric differentiation that are key features of ketone facial discrimination.

A constraint of this study was its inability to predictively describe electronically perturbed and more complex ketone substrates, as the training set (data points used for model development) was limited to alkyl methyl ketones. Thus, we aimed to build an expanded, DoE-founded library of ketones, bearing steric and electronic variation at both ketone substituent sites, which adds significant complexity to the experimental design.

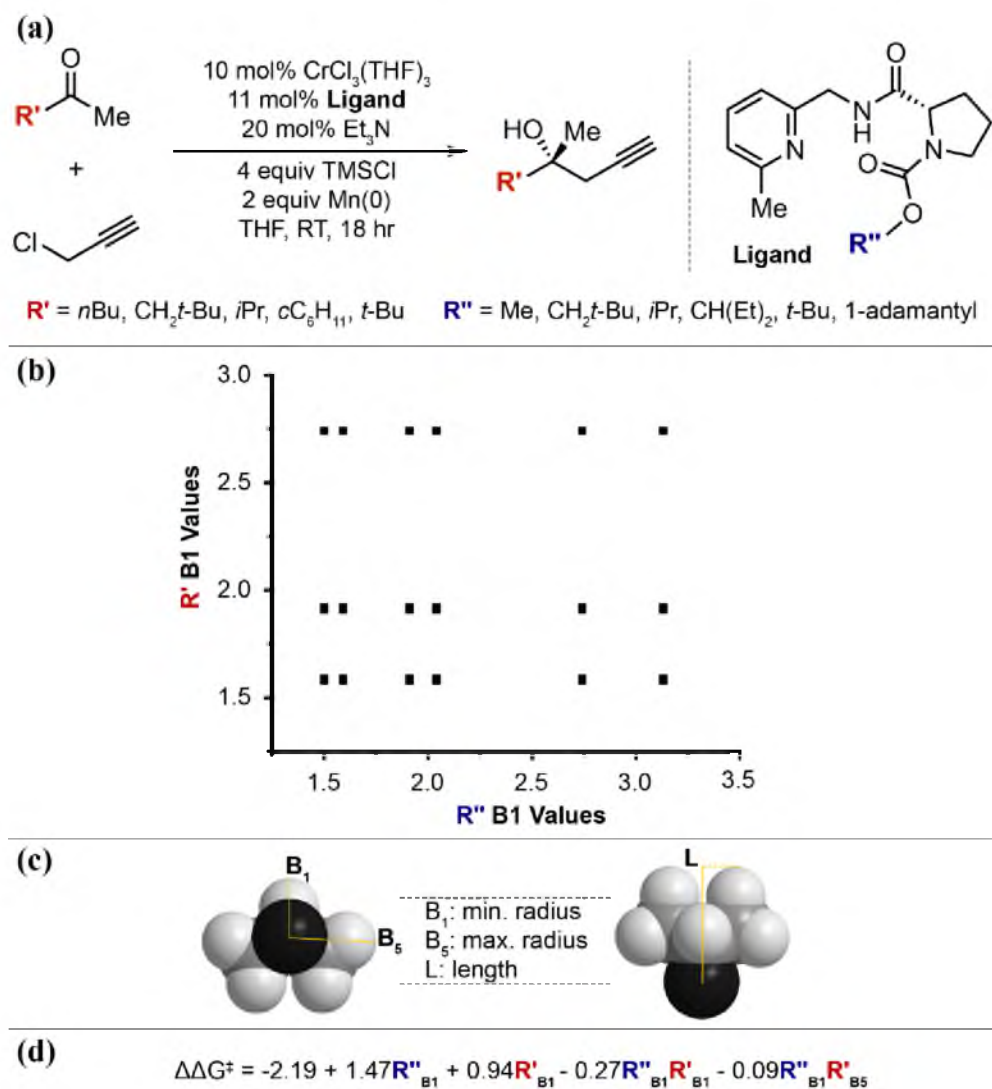


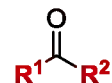
Figure 4.2. Using design of experiments to evaluate steric effects. (a) NHK propargylation of alkyl ketones, with steric effects varied at the substrate R' and ligand R'' positions. (b) Design of Experiments (DoE) approach to substrate and ligand variation. The plot demonstrates the relatively even distribution of substituent changes, as measured by Sterimol B_1 values. (c) Depiction of an isopropyl substituent's Sterimol measurements. (d) Mathematical model of NHK propargylation.

Two salient molecular features of ketones that we hypothesized to be important considerations for describing them are differential steric size between a ketone's two substituents, which can enable discrimination between ketone faces, and carbonyl electrophilicity, which likely modulates the early or late nature of the corresponding transition states involved in determining selectivity.²² Due to the demonstrated effective use of Sterimol parameters for describing the relative size of methyl ketones (*vide supra*), this multidimensional steric measure—particularly B_1 and B_5 , which measure the minimum and maximum size near the reactive carbonyl—seemed an appropriate choice for describing differential steric bulk between R^1 and R^2 (Figure 4.3).

An interest in describing ketone variation at both R-group sites, for alkyl and aryl substituents, limits the range of parameters that could be effective electronic descriptors. For instance, the commonly employed Hammett σ value (the acidity of benzoic acid derivatives) could not be used to parameterize this library, as σ values are limited to describing electronic changes on phenyl rings at *meta* and *para* positions, also precluding description of heteroaromatic arenes and alkyl chains.²³ While σ values are too limited a descriptor for this library, these values are well-correlated to carbonyl infrared (IR) stretching frequencies.^{24,25} IR vibrational frequencies originate from differential charges and masses across a bond and, therefore, inherently describe, without limitation, carbonyl electronics and the groups bonded to the carbonyl carbon.^{9,18,26} The demonstrated success of IR vibrational data effectively describing reaction outcomes (Chapters 2 and 3) prompted the use of this powerful descriptor for quantitating ketone features.

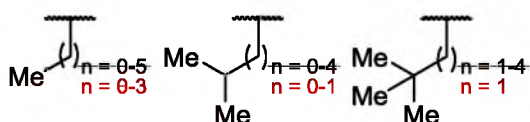
Using Sterimol parameters and carbonyl IR stretching frequencies as general descriptors of the anticipated reaction of ketones, it was next necessary to assess the

Objective: Develop library of ketones that displays broad steric and electronic variation at R^1 and R^2 .

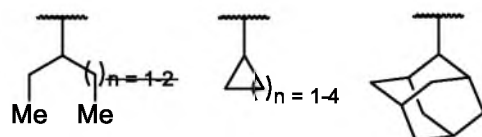
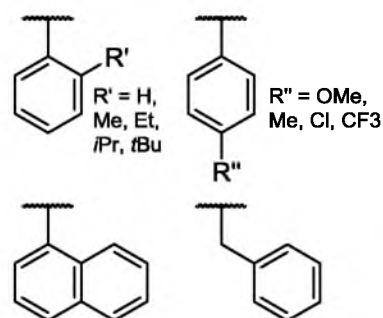


(a)

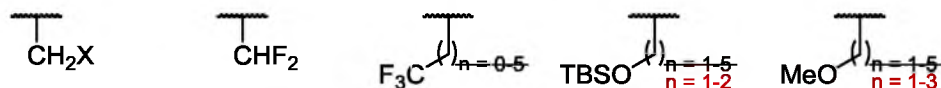
Aliphatic R Groups



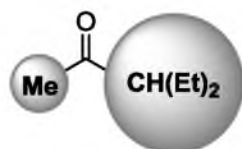
Aromatic R Groups



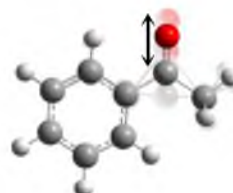
Halogenated/Oxygenated Aliphatic R Groups



(b)



• Differential steric bulk (Sterimol values)



• Carbonyl electrophilicity ($\nu_{C=O}$)

Figure 4.3. Building the experimental space. (a) A 52-membered set of methyl ketones that sample the steric and electronic ketone space was constructed. Redundancy within the library was reduced by assessing each ketone according to (b) putative mechanistically relevant descriptors (Sterimol values and carbonyl IR stretching frequency, $\nu_{C=O}$). This reduction resulted in the 32-membered library depicted in (a).

sensitivity limits of these parameters. This determination was undertaken by first virtually populating three categories of ketone substituents: aliphatic, halogenated/oxygenated aliphatic, and arene (Figure 4.3a). The resulting 52 defined groups were each included as a substituent on a methyl ketone. Energy minimization and frequency calculations (M06-2X/TZVP) were carried out for this diverse set in order to evaluate each ketone's carbonyl IR stretching frequency and Sterimol values (Figure 4.3b).²⁷⁻³¹

From structurally related ketone subsets, carbonyl IR stretches' sensitivity to R-group variation was determined. Performing this sensitivity analysis was designed to alleviate redundancy in the ketone library so as not to oversample any region of the experimental space. This analysis was performed by analyzing graphed comparisons of ketone carbonyl IR stretching frequency, representative examples of which are given in Figure 4.4. Considering the analysis of the *i*Pr-derived subset as a template for all such analyses, comparison of *i*Pr, CH(Et)₂ and CH(Pr)₂ demonstrate little change in carbonyl IR stretching frequency for the latter two methyl ketones. Thus, of this trio, only the *i*Pr group was determined to be within the descriptive range of the carbonyl IR stretch parameter. For the CF₃-derived substituents, the electron-withdrawing effect of trifluoromethyl does not impact the carbonyl IR stretching frequency when the group is more than one methylene unit removed from the carbonyl, so only the CH₂CF₃ group was maintained from this series. The results of similar analyses for other R-group subsets are presented in Figure 4.3a. Once complete, this sensitivity analysis reduced the initial 52-membered ketone set to 32 methyl ketones, each hypothesized to be distinct according to the Sterimol and carbonyl stretching parameters.

The next stage was to consider how the experimental space for multisite,

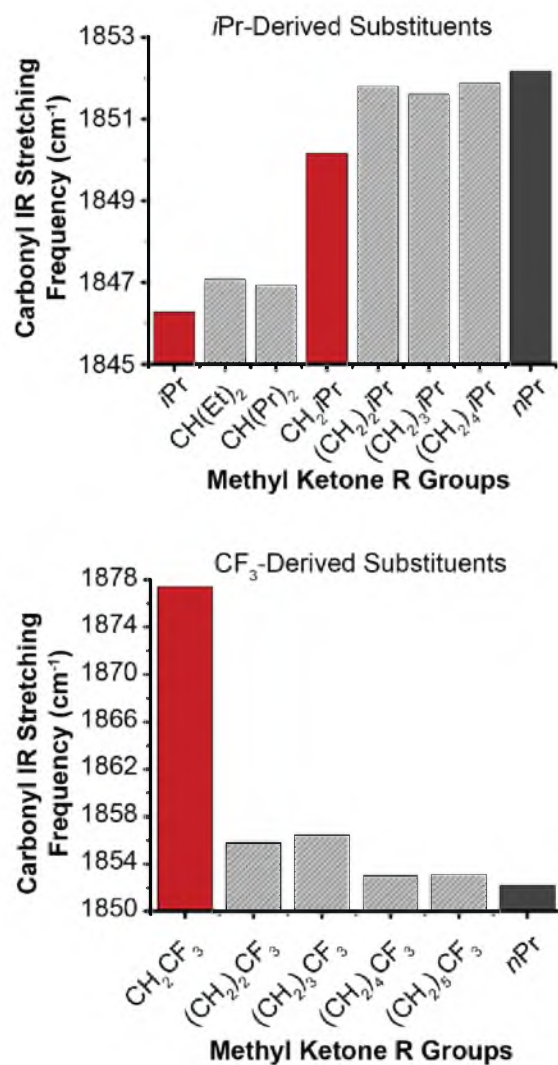


Figure 4.4. Representative sensitivity analyses given for *i*Pr- and CF₃-derived substituents.

multieffect ketone variation could be identified. To accomplish this, eight methyl ketone R groups were selected in DoE fashion (Figure 4.5) to representatively sample the methyl ketone library. All unique combinations of these eight groups at R¹ and R² yielded 28 ketones for which differential Sterimol values (Sterimol values_{R1} – Sterimol values_{R2}) and carbonyl IR stretch frequency were measured from energy minimized structures. The identified ketone experimental space is given in Figure 4.6.

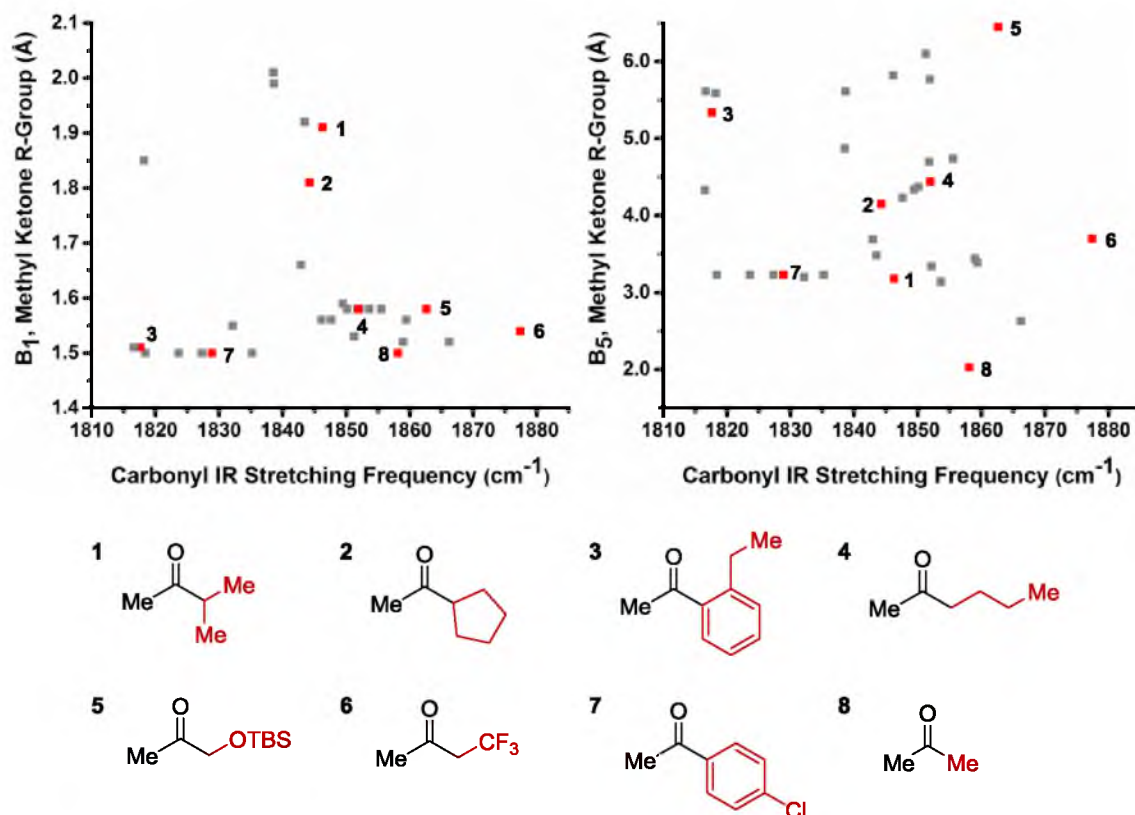


Figure 4.5. Plots of Sterimol B₁ and Sterimol B₅ versus carbonyl IR stretching frequencies of the 32-membered set of methyl ketones that was identified via sensitivity analyses. The red data points represent a reasonably even, DoE-type sampling of these sterically and electronically described spaces.

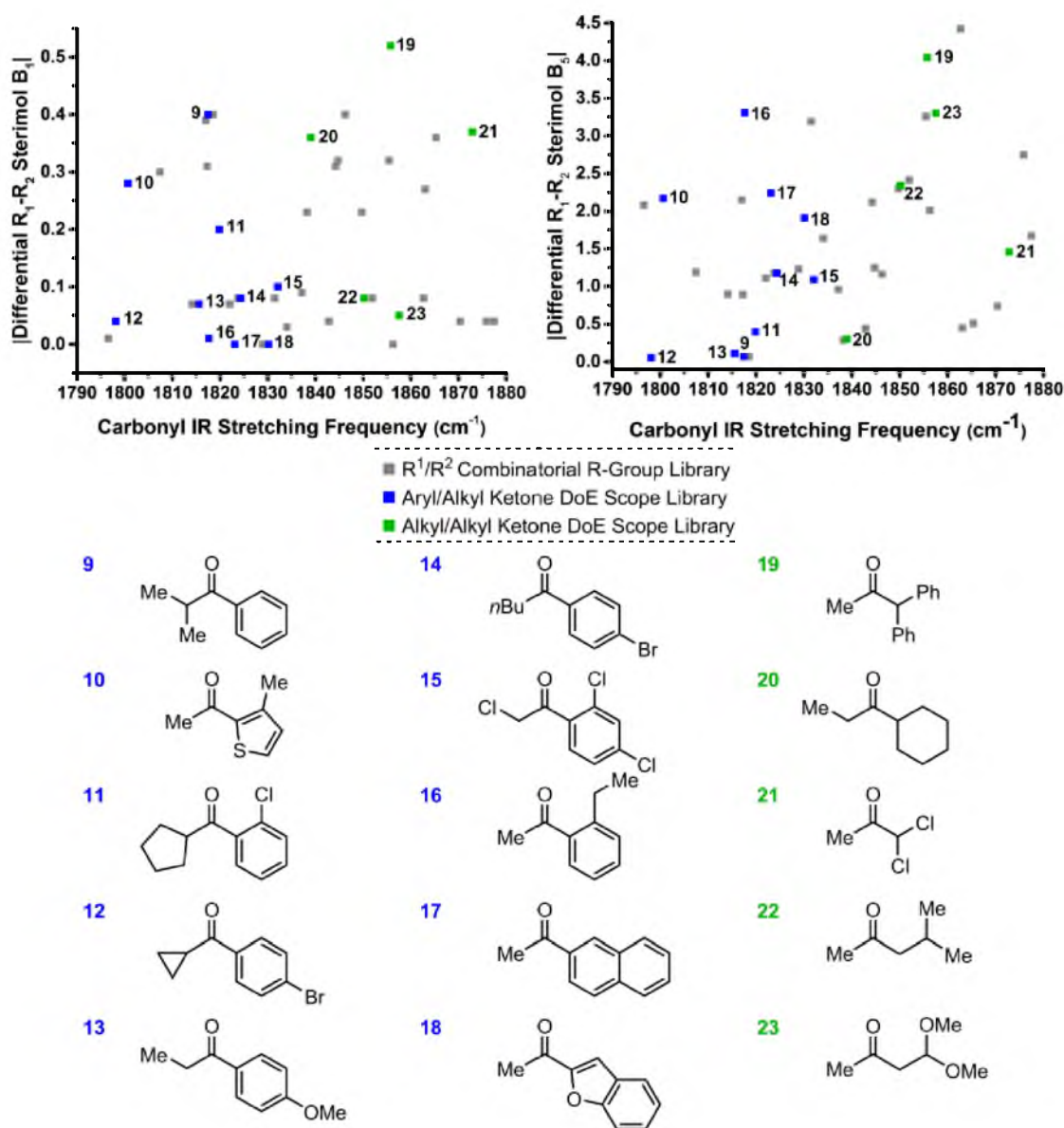


Figure 4.6. Identify ketones that systematically sample the experimental ketone scope space. (a) Plot of the R¹/R² combinations of the eight R groups represented in Figure 4.5 (■). Presumably, this space, defined by differential Sterimol B₁ and B₅ values and carbonyl IR stretching frequencies, defines a relevant ketone scope. This space was evenly sampled, ■ and ■, according to DoE principles. Substrates that systematically populate the ketone scope, as delineated by the electronic and steric descriptors applied, are depicted.

Organize and Evaluate Ketones that Systematically Sample the Experimental Space

After the substrate scope space was defined, this bounded region was populated with ketones that broadly span its dimensions (Figure 4.6). All but one of these ketones, **16**, are commercially available, enabling ready evaluation of this designer library (hereafter termed the DoE library). The conceptual framework upon which the DoE library was built is best evaluated by subjecting the ketones to a chemical transformation and measuring reaction outcomes. Then, linear regression models can be developed to describe the observed outcomes as related to ketone changes. Finally, the model's validity is determined by assessing how well the model predicts the reaction outcomes of new ketones.

To limit factors that would confound assessment of the described approach's effectiveness for DoE library development, it was desirable to subject the library to reaction conditions where measured reaction outcomes 1) are highly reproducible, 2) are sensitive to structural changes to ketones, and 3) have been rationalized according to previous mechanistic work. These requirements allow the method of DoE library development to be assessed in a manner that is not contingent upon the reaction itself. Additionally, corroborating the developed model with prior mechanistic work adds credence to the use of future DoE-founded modelling approaches for lending mechanistic insight in the absence of computational transition state models.

Rhodium-catalyzed asymmetric transfer hydrogenation (ATH) is a reaction that satisfies the requirements for DoE library assessment.³²⁻³⁴ Of particular note, computational models of the ruthenium ATH variant's selectivity determining transition state have been investigated.³⁵ These models suggest that the favored diastereomeric

transition state benefits from a key stabilizing C–H/ π interaction between a C–H bond of the pentamethylcyclopentadienyl (Cp*) ligand’s methyl group and the pi cloud of a ketone substrate’s arene (Figure 4.7). This proposed transition state model suggests that aryl/alkyl ketones, which can engage with the catalyst through a C–H/ π interaction, and alkyl/alkyl ketones, which cannot participate in this intermolecular interaction, may behave as two distinct substrate classes in the ATH reaction.³⁶

Supposing that these two types of ketones rely on different modes of asymmetric induction, we determined that each ketone class should be independently modelled. This two-pronged approach allows for an optimal description of the unique features relevant to each ketone class’s selectivity-determining interactions. Interestingly, assessment of the DoE library’s graphical depiction according to carbonyl IR stretching frequencies and Sterimol values demonstrates a natural divide between the two ketone classes (Figure 4.6).

Quantitatively Connect Reaction Outcomes and Molecular Descriptors of Ketones

The aryl/alkyl and alkyl/alkyl ketone DoE libraries were each subjected to ATH conditions, and the resulting enantiomeric ratios, in the form of $\Delta\Delta G^\ddagger$ ($\Delta\Delta G^\ddagger = -RT^* \ln([S]/[R])$), were tabulated (see “Methods”).^{10,37} To quantitate and interpret the key selectivity determinants in each ketone class’s library, a set of ketone parameters that is capable of detailing the selective process was required. Measured from computationally energy-minimized ketone structures, parameters were included in this set based on hypotheses of their mechanistic significance. In the initial stages of model development, we often include only the parameters we propose to be most impactful and add

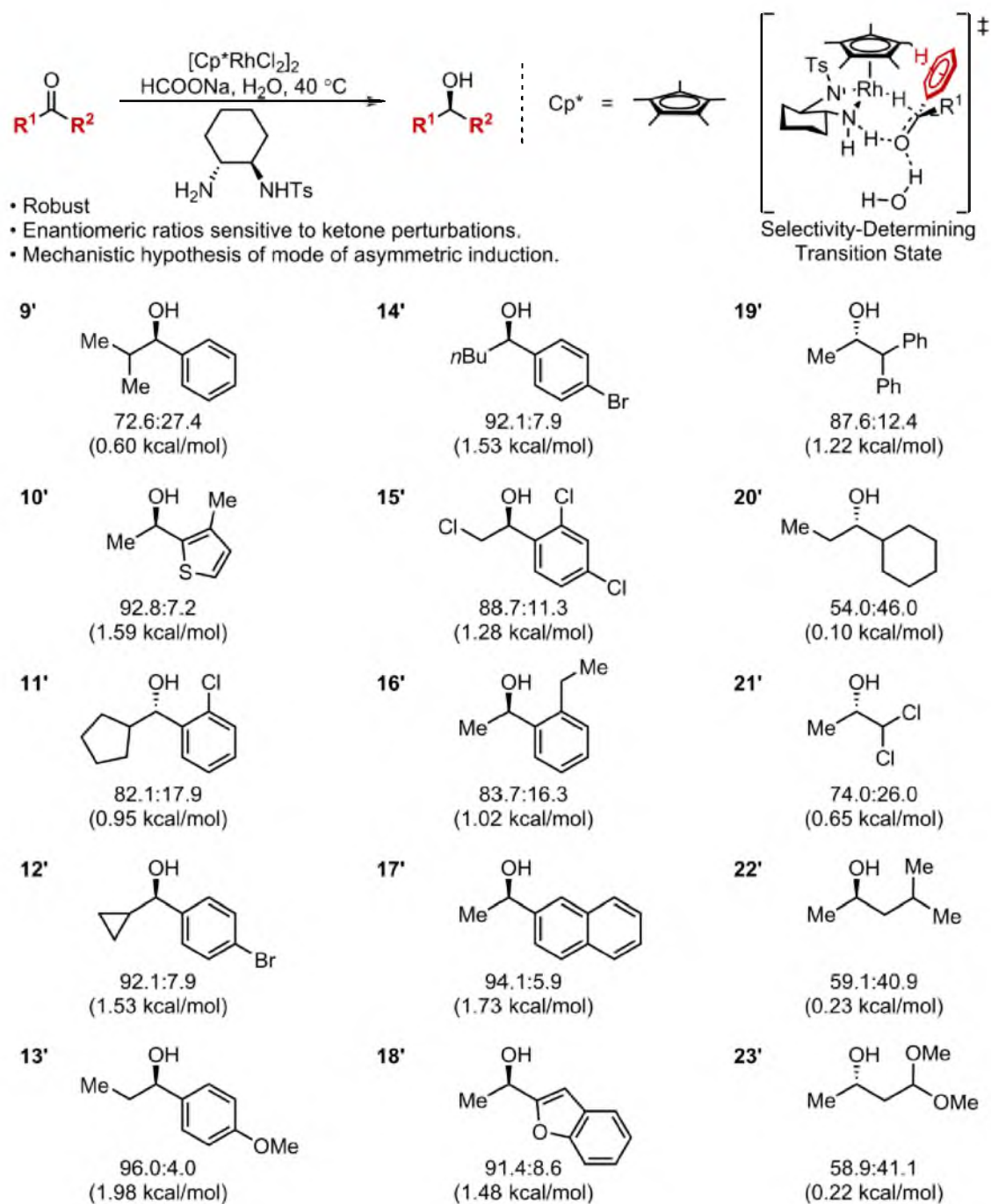


Figure 4.7. Rhodium-catalyzed asymmetric transfer hydrogenation (ATH) reaction, to which conditions the DoE library was subjected to assess the robustness of the library for developing broadly descriptive, accurate, and precise mathematic models. The transformations' proposed selectivity-determining transition state is presented. The training set of reduced ketone products and their corresponding enantiomeric ratios are presented, with $\Delta\Delta G^\ddagger$ values given in parentheses.

parameters to improve the models, as needed. The mechanistic hypotheses are continually informed and refined in a dynamic, iterative process according to the failures and successes of the explanatory parameters that are evaluated via regression. For instance, and as described in greater detail below, previously established steric parameters were ineffective descriptors of the enantioselective role of differential steric effects in the ATH system. This deficiency fueled development of a new steric measure more well-suited to the demands of the ATH system (and potentially other systems) and provided insight into the steric dimensions of mechanistic relevance. While there are many other unique parameter combinations with potential descriptive relevance, below is described the logic employed to arrive at the parameter set that was used for regression modelling.

To begin constructing the parameter set, the relevant electronic details of ketones were proposed to be described by three descriptors (Figure 4.8). First, the vibrational frequency of the carbonyl IR stretch ($\nu_{C=O}$) used to define the library was included. The intensity of this stretch ($I_{C=O}$) was also considered for its representation of electronic variation. An alternative measure of electronic nature was incorporated through point charges at the four atoms that are conserved throughout the ketone library (C–C(O)–C).

Turning to structural features of the library, it is plausible that the degree of asymmetric induction for aryl/alkyl ketone substrates is influenced by the degree of torsion (*Tor*) between the carbonyl and the arene (Figure 4.8). This parameter may describe the energy expenditure/stabilization balance between various torting of aryl/alkyl ketones from their energetic minima to conformations where transition state-stabilizing C–H/ π interactions can occur. Indeed, in the absence of this term, robust

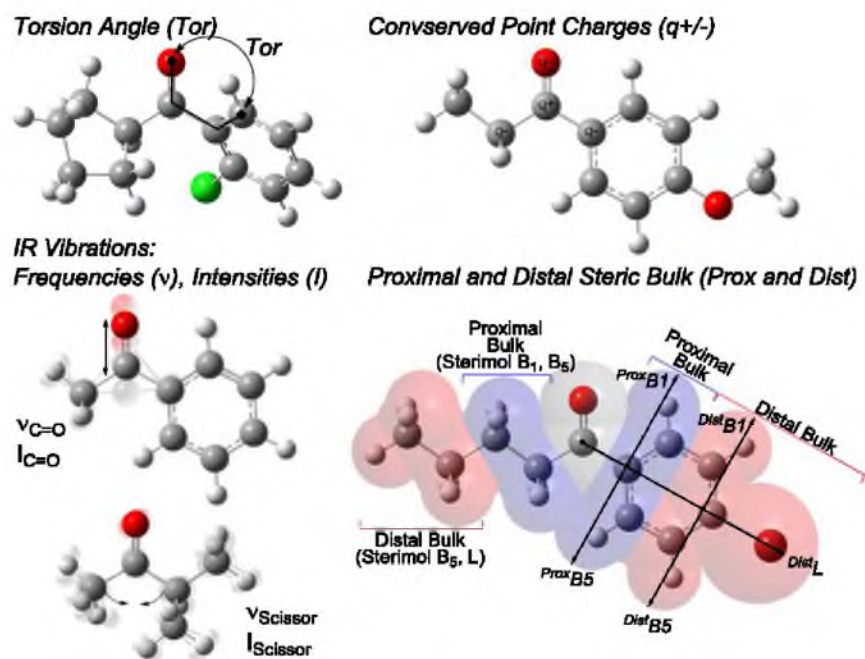


Figure 4.8. Numeric molecular descriptors hypothesized to be relevant predictors of ATH enantioselectivity.

models were not developed (*vide infra*).

While this torsion angle cannot be used to describe alkyl/alkyl ketones, where facial discrimination cannot arise from C–H/ π stabilizing interactions, a surrogate was envisioned in a scissoring IR vibrational mode. Termed ν_{scissor} and I_{scissor} , the frequency and intensity of this vibration, which induces a compression of the two carbons alpha to the carbonyl (Figure 4.8), were added to the alkyl/alkyl ketone descriptor set. Although several other vibrations, and combinations thereof, might describe similar molecular dynamics, this scissoring term was selected due to the confidence with which it could be consistently identified in all computed alkyl/alkyl ketones.

Finally, the initial DoE library descriptors of sterics, Sterimol B_1 and B_5 values, were revisited for inclusion in the parameter set. Sterimol values provided an ineffective representation of ATH enantioselection, which precluded identification of robust models and, consequently, instigated a reanalysis of how to treat steric effects. As size proximal to the reactive carbonyl moiety is likely to play a different role in enantioselection than distal steric effects, we assessed means of partitioning steric measures into these distinct units. Sterimol measurements of ethyl and *n*butyl substituents highlight the necessity of this distinction (Figure 4.9). While the B_1 measures of ethyl and *n*butyl are nearly identical, the B_5 measures differ substantially. Ethyl's B_5 measurement is 3.15 Å, while for *n*butyl this parameter measures 4.45 Å, the width to the distal end of the aliphatic chain. Practically, each substituent's steric dimensions that are proximal to the carbonyl are more similar to one another than these measurements indicate.

The discrepancy between the Sterimol measure of size and practically relevant proximal sterics was addressed by slicing R groups into two portions. For aliphatic

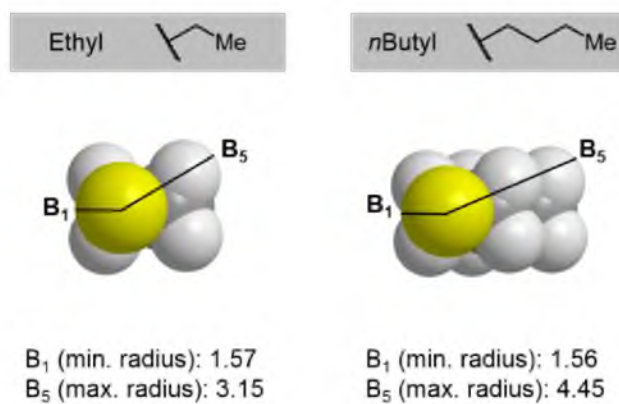


Figure 4.9. Comparison of Sterimol measurements for ethyl and *n*butyl substituents, highlighting Sterimol values' deficiency for distinguishing between proximal and distal bulk.

groups, the proximal effect is defined as the first two carbons and its associated hydrogens; any atoms beyond the proximal segment comprise the distal fragment (Figure 4.8). B_1 and B_5 were measured for the proximal unit. B_5 and L were measured for the distal unit.

Arenes were segmented in a similar fashion. Proximal sterics is defined as positions spatially equivalent to the *ortho* position on a phenyl ring, beyond which is distal sterics. For each steric fragment, two measurements of arene width were obtained, as depicted in Figure 4.8. The Sterimol length parameter, L , was measured for the distal steric slice.

From this set of ketone parameters, the combinations thereof that describe the observed trends in the DoE library's enantioselectivity were identified through an iterative process of constructing and assessing various combinations of parameters via MATLAB stepwise regression algorithms (see Methods and SI: Model Development for details).³⁸ This automated mathematical process involves evaluating p -value statistical measures for each parameter to determine whether the term is an appropriate descriptor of the system. From starting models of both no parameters and all parameters of the descriptor set, terms are added to (p -value < 0.05) or removed from (p -value > 0.1) the models based on p -value thresholds (see Methods and SI: Model Development for details). Through this process, a model for each ketone class was developed. The majority of terms in the model that describes the aryl/alkyl ketones were anticipated to be effective descriptors, as the carbonyl IR stretching frequency ($\nu_{C=O}$) and differential steric bulk were two design parameters (Figure 4.10). Yet, with the developed mathematical model, these terms' mechanistic significance on the reaction's enantioselectivity can now be

$$\Delta\Delta G^\ddagger = -RT\ln([S]/[R]) = -0.10 - 0.38(\nu_{C=O}) - 0.80(\text{ProxB1}_{\text{Alkyl}}) + 0.29(\text{ProxB1}_{\text{Aryl}}) - 0.52(\text{Tor}) - 1.46(\nu_{C=O})(\text{ProxB1}_{\text{Alkyl}})$$

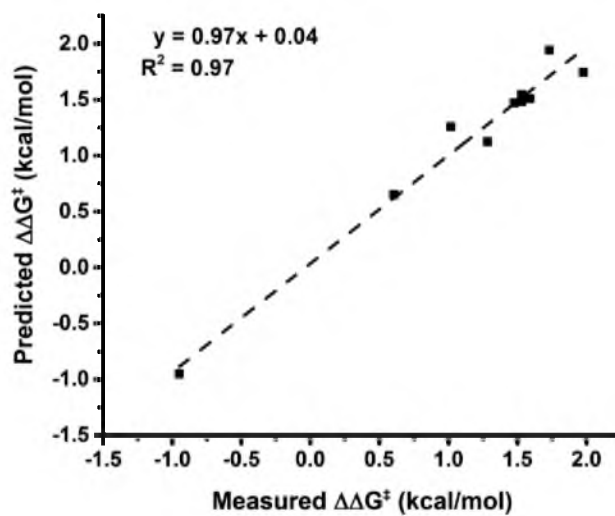


Figure 4.10. Quantitative description of ATH reaction enantioselectivities for the aryl/alkyl ketone library, with a graphical demonstration of the high degree of correlation between predicted and measured $\Delta\Delta G^\ddagger$ values.

more precisely, quantitatively understood.

The carbonyl/aryl torsion angle (*Tor*) was hypothesized to be relevant due to the proposed C–H/ π interaction.³⁵ The normalized regression model (Figure 4.11) conveys the relative importance of the torsion term via the magnitude of its coefficient. Bearing the third largest coefficient, the torsion term plays a significant role in the prediction of $\Delta\Delta G^\ddagger$. In the raw regression model (see “Experimental Information”), *Tor* bears a negative coefficient, indicating that increases in torsion angle erode enantioselectivity. The correlation is graphically represented in Figure 4.11, where deviation from this pattern is described by the model’s other parameters. The relationship between torsion and enantioselectivity does directly support that a C–H/ π interaction is operative in face selection, which is consistent with the computational structural models.³⁵ *Tor*’s relevance in the mathematical model emphasizes the capability of this linear regression approach for delineating distinct mechanistic features amongst a multitude of potential effects.

Description of the various steric and electronic effects playing a role in enantioselection for the alkyl/alkyl library was afforded with $\nu_{C=O}$ and steric measures (Figure 4.12; for a detailed description of model development, see “Experimental Information”). However, the greatest predictor of enantioselectivity is the crossterm (largest parameter coefficient) describing the synergistic influence of the scissoring vibrational frequency and intensity. While these parameters are difficult to mechanistically deconvolute, the origin of vibrational frequency and intensity in differential mass and charge across a bond indicate the appropriateness of such a parameter.

Robustness of the models for describing the steric and electronic variation in the

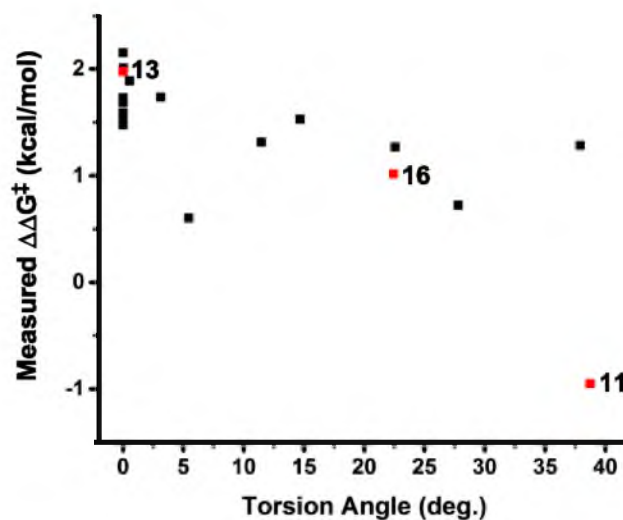


Figure 4.11. Demonstrated correlation between measured enantioselectivities and torsion angle for aryl/alkyl ketone library.

$$\Delta\Delta G^\ddagger = -RT\ln([S]/[R]) = -0.52 - 0.33(v_{C=O}) - 0.73(\text{ProxB1}_{\text{Alkyl, Small}})(v_{\text{Scissor}}) - 1.75(v_{\text{Scissor}})(f_{\text{Scissor}})$$

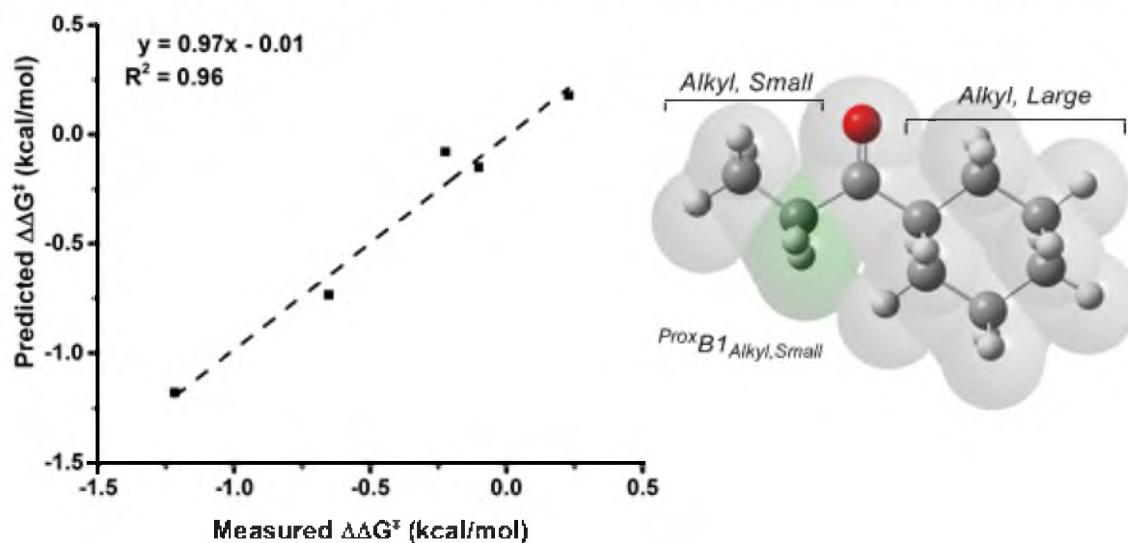


Figure 4.12. Normalized mathematical model describing how attributes of alkyl/alkyl ketones modulate enantioselective ATH reaction outcomes. Graphical depiction of model accuracy is given in the form of a predicted versus measured enantioselectivity plot. Representation of the model-relevant steric effect is presented.

DoE libraries is determined by correlating experimentally measured enantioselectivity to the enantioselective reaction outcomes predicted by the developed models. Plotting these comparisons, shown in Figures 4.9 and 4.11, demonstrates that both models exhibit an ability to accurately (R^2 value near one) and precisely (slope near one and y-intercept near zero) predict enantioselection for the ketones used in model development.

Predict the Performance of New Ketone Substrates

An important application of the developed models lies with their potential to predict the enantioselective outcomes of new ketone substrates. Demonstrating the models' predictive power provides a validation of model robustness and a measure of the models' broad applicability. That is, optimal models represent generalized patterns in reaction outcomes. The reliability of the models was evaluated through external validation experiments (Figures 4.12a and 4.12b). Nine aryl/alkyl ketones (**24–32**) and three alkyl/alkyl ketones (**33–35**) were subjected to ATH conditions, and enantiomeric ratios were subsequently determined. Using the developed models for each ketone class, predictions of enantioselectivity were made. Figure 4.13a demonstrates the excellent agreement between predicted and measured enantioselectivities.

Conclusions

In the absence of quantitative models, expected levels of asymmetric induction, i.e., the mechanistic influences of multieffect substrate variation, are difficult to forecast beyond the generalities of good, average, or poor. Certainly, qualitatively predicting reversal of face selection, such as observed for the enantiomeric products **36** and **37**

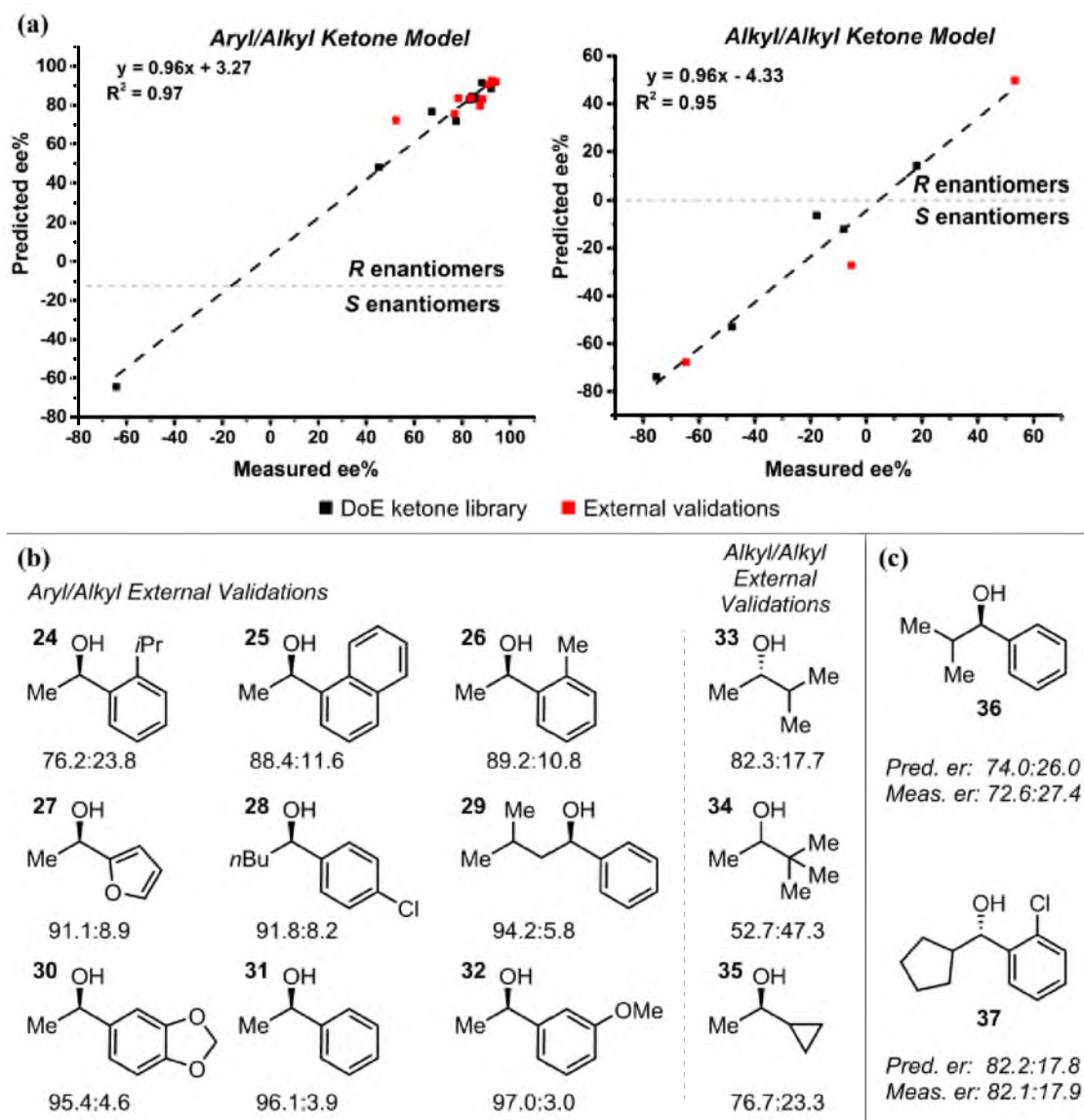


Figure 4.13. Predicting the enantioselective performance of new ketones. (a) Plots depicting robust external validation of the aryl/alkyl and alkyl/alkyl ketone models, respectively. (b) Products of aryl/alkyl and alkyl/alkyl external validation, with associated enantiomeric ratios. (c) Predicted and measured enantiomeric ratios (er) for two substrates, where the aryl/alkyl model predicted the observed, yet unexpected, reversal of enantioselection

(Figure 4.13c), is even more challenging. Asymmetric catalysis, as a field, has numerous demonstrated apparent outliers, similar to the one described above, that may be predicted more accurately by utilizing the techniques described herein. It is also noteworthy to consider the advancements of the presented approach for comprehensively modelling electronically and structurally diverse substrates. Classic electronic (Hammett) and steric (Charton) linear free-energy relationship analyses are unable to describe the developed multivariate ketone scope libraries, as the substrates boast significant variability of ketone steric and electronic effects.^{23,39} From *ortho*-substituted phenyl rings to heteroaromatics to electronically perturbed alkyl substituents, each of these R groups represents a limitation of Hammett and Charton descriptors. An ability to design this broadly diverse ketone library that is also amenable to quantitative modelling demonstrates a new, information-rich approach to reaction scope assessment. Presenting a reaction's substrate scope with a robust quantitative model renders the substrate assessment greater than the sum of its experimentally analyzed constituents. Robust quantitative models enable recognition of patterns by which the reaction outcomes of novel substrates can be predicted, effectively expanding a substrate scope.

While a significant amount of both intellectual and applied effort was required to develop the approach by which an appropriate DoE-founded library is constructed, following the outlined process will enable libraries of new substrate classes to be readily developed. We have demonstrated that with model training sets of only five to 10 substrates, on par with or even less than scope breadths of modern synthetic reports, robust models were developed. Additionally, it is often simple and rapid to perform ground state computations (completed in a matter of hours) in order to tabulate data for

substrate-specific parameters. Thus, applying the developed methodology requires only a modest effort beyond the standard timeline for reaction method development. Each unique investigation is enabled by the ability to develop parameter sets that are tailored to the features of hypothesized mechanistic importance in order to afford information-rich quantitative models. Simply through thoughtful designs of requisite substrate scope interrogations, the extent of meaningful data obtained from this necessary aspect of reaction development can be significantly enhanced.

Methods

All parameters used for linear regression modelling were measured from energy-minimized structures (M06-2X/TZVP) using Gaussian09.²⁷ Torsion, IR, and natural bond orbital (NBO) point charge parameters were measured using GaussView 5.0.⁴⁰ Sterimol-derived measurements were made using Mol2Mol.⁴¹ Invoking these parameters for descriptive model development is an iterative process of identifying mechanistically relevant parameter combinations. The explanatory aptness of the selected parameters was investigated by subjecting the aryl/alkyl DoE ketone library's enantioselective outcomes and descriptor set (Figure 4.5a: torsion angle, carbonyl IR stretching frequency and intensity, point charges, and Sterimol values for distal and proximal units) to an initial round of stepwise linear regression modelling using MATLAB algorithms (see SI: Model Development for further details). From this analysis, it was found that $^{Prox}BI_{Alkyl}$, Tor , $^{Prox}B5_{Alkyl}$, and $^{Dist}L_{Alkyl}$, ordered according to predictive significance, provide a reasonable representation of the DoE library's ATH enantioselective outcomes. External validation data were used to further distinguish this initial model as one bearing terms appropriately

descriptive of ketones that were not used for model identification.

This analysis enabled refinement of the descriptor set; point charges, not part of this initial model, were precluded from further modelling attempts, while *Tor* was maintained. Given the initial design hypothesis that carbonyl IR vibrational frequency is an effective descriptor of ketone reaction behavior, the carbonyl IR frequency was retained. Descriptors of proximal steric bulk, some of which proved effective in the first modelling attempt, were incorporated in the second stage of model development due to their hypothesized relevance.

Through hypothesis-driven model development, this honed collection of parameters, and cross-terms thereof, was iteratively reduced until the precise, accurate model given in Figure 4.5b was identified. While this quantitative relationship demonstrates predictive robustness, it represents one of many potential models. This can be understood by considering the interrelatedness of many of the parameters employed in model development. For instance, steric bulk can impact torsion angles, which alters carbonyl/arene conjugation and, thus, the carbonyl IR stretching frequency. Although various combinations of these interdependent molecular descriptors may reveal other unique models of similar robustness, this does not diminish the information-rich nature of the externally validated model.

A similar process was undertaken for the alkyl/alkyl DoE ketone library, where enantioselective outcomes and the library's descriptor set (Figure 4.5a: carbonyl and scissoring IR vibrational frequencies and intensities, NBO point charges, and Sterimol values for distal and proximal units) were subjected to stepwise linear regression MATLAB algorithms. Initial modelling attempts overwhelmingly suggested that the

point charges on the carbonyl oxygen and carbon atoms were relevant descriptors of the observed enantioselection trends (see SI: Model Development). However, through external validation this model was refuted. As point charges were not necessary for describing the aryl/alkyl ketone library, it was hypothesized that this measure could be excluded from the second stage of modelling.

With this simplified descriptor set (IR vibrational frequencies and intensities of carbonyl stretching and alkyl/alkyl scissoring; proximal and distal steric bulk measurements) modelling attempts were still ineffective. It was presumed that this limitation was associated with the broad steric and electronic variation represented in the relatively small ketone library. Thus, three additional ketones (**33–35**) were included in the library to facilitate the elucidation of a relevant descriptive subset of terms. Using standard MATLAB stepwise linear regression algorithms, followed by removal of redundant terms, a model with the terms $^{Dist}L_{Alkyl, Large}$, $v_{Scissor}$, $I_{Scissor}$, and $(v_{Scissor})(I_{Scissor})$ was afforded. Next, the five-membered DoE library of enantioselectivities was fitted to these terms, and the resultant model was subsequently evaluated for its robustness through external validation (using **33–35**). While this model was not able to predict the enantioselectivities of these new ketones, this result yielded confidence that this process could still yield models where external validation remained an appropriate measure of robustness.

To initiate the third stage of model development, it was proposed that proximal steric effects would be more likely to influence asymmetric induction than distal steric bulk. Thus, $^{Dist}L_{Alkyl, Large}$ was eliminated from the descriptor set, and stepwise linear regression proceeded from the remaining terms— $v_{Scissor}$, $I_{Scissor}$, $(v_{Scissor})(I_{Scissor})$ —and

$v_{C=O}$. The resultant model, afforded after removing superfluous terms, bore four parameters: $v_{C=O}$, $^{Prox}B1_{Alkyl,Small}$, $v_{Scissor}$, and $(v_{Scissor})(I_{Scissor})$. Wary of overfitting the data set, parameter reduction was successfully approached via combining $^{Prox}B1_{Alkyl,Small}$ and $v_{Scissor}$ into a single cross-term. Again, the five-membered alkyl/alkyl library was used to determine the coefficients (weighting) of each term (details provided in SI: Model Development). The model was determined to be robustly descriptive of a variety of alkyl/alkyl ketones via external validation, where the previous model had failed at the external validation stage.

Experimental Information

General Information

Tetrahydrofuran (THF) and dichloromethane (DCM) were prepared by passing through an activated alumina column, under a nitrogen atmosphere, prior to use. Triethylamine was used after distillation from CaH_2 . Dimethylsulfoxide (DMSO) was dried with 3 Å molecular sieves prior to use. Unless otherwise noted, all other reagents were used as received from commercial sources.

Thin-layer chromatography was performed using silica gel 60 F₂₅₄ and the eluents specified, then visualized via a 254 nm UV lamp and/or stained with phosphomolybdic acid, potassium permanganate, 2,4-dinitrophenylhydrazine, or vanillin stains. SiliaFlash[®] F60 40–63 µm silica gel was used for flash column chromatography, as designated. ¹H and ¹³C NMR spectra were acquired on a Varian Unity spectrometer at the MHz specified. Spectral referencing was performed relative to the $CHCl_3$ 7.26 ppm singlet (¹H NMR) and the center peak of the $CHCl_3$ 77.16 ppm triplet (¹³C NMR). All multiplicities

reported are apparent. Abbreviations s, d, t, q, p, sex, sep, dd, ddd, td, bs, and m represent the resonance multiplicities singlet, doublet, triplet, quartet, pentet, sextet, septet, doublet of doublets, doublet of doublets of doublets, triplet of doublets, broad singlet, and multiplet, respectively. IR spectroscopy data were obtained using a Nicolet 380 FT-IR instrument. High-resolution mass spectrometry (HRMS) data were obtained using an Agilent LCTOF. Melting points were measured using a Thomas Hoover Unimelt capillary melting point apparatus. All melting points are uncorrected. Super critical fluid chromatography (SFC) analysis was performed using a Thar instrument under the conditions indicated. Gas chromatography analysis was performed using a Hewlett Packard HP6890 instrument under the conditions indicated. Specific rotations were determined using a PerkinElmer 343 Polarimeter, the 589 nm wavelength (sodium D line), and a 1 dm cell path length, with concentrations given in units of g/100 mL.

Synthetic Procedures

Method A: Asymmetric transfer hydrogenation. This method (Figure 4.14) was used to afford enantioenriched alcohols. To a 20 mL test tube, equipped with a stirbar, was added 1.5 mg of $[\text{Cp}^*\text{RhCl}_2]_2$ (0.0025 mmol, 0.005 equiv), 1.6 mg of N-((1R,2R)-2-aminocyclohexyl)-4-methylbenzenesulfonamide, and 1 mL of deionized water. The resulting suspension was stirred in a 40 °C oil bath for 1 hour before adding 0.1700 g of HCOONa (2.5 mmol, 5.0 equiv) and the respective ketone (0.5 mmol, 1.0 equiv). The reaction mixture was stirred for 2 hours before cooling to room temperature, extracting with diethyl ether, and drying with Na_2SO_4 . The resulting organic solution was passed through a silica plug prior to analytical separation of enantiomers via GC or SFC,

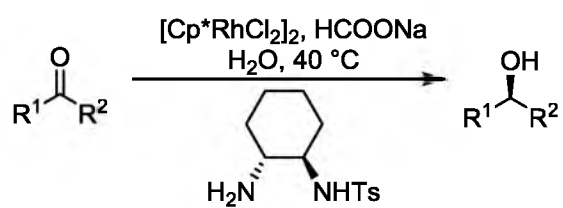


Figure 4.14. Rhodium-catalyzed asymmetric transfer hydrogenation.

as noted.

Method B: Racemic ketone reduction. This racemic reduction method (Figure 4.15) was used to prepare racemic alcohols by dissolving the corresponding ketone (1 equiv) in THF (5 mL/mmol). The reaction mixture was cooled to 0 °C, NaBH₄ (2 equiv) was added, and then the suspension was stirred under a nitrogen atmosphere until formation of product was observed, often requiring heating to reflux. The reaction was quenched with saturated NH₄Cl_(aq) and extracted three times with ethyl acetate. The resulting organic solution was washed with brine and then dried with Na₂SO₄.

(R)-2-methyl-1-phenylpropan-1-ol. This alcohol, for which literature characterization data are available,⁴² was synthesized according to Method A to afford enantiomeric ratios of 71.9:28.1 and 73.2:26.8 for two experimental runs. Experimental specific rotation: $[\alpha]_D^{20} = +22.5$ (*c* 0.16, CHCl₃, 71.9:28.1 er (*R*)). Literature specific rotation:⁴³⁻⁴⁵ $[\alpha]_D^{23} = +12.3$ (*c* 1.2, CHCl₃, 69.2:30.9 er (*R*)). SFC Enantiomeric Separation Conditions: Chiralpak[®] AD-H column (4.6 mm x 250 mm, 5 μm particle size), 3% isopropanol, 3 mL min⁻¹, 40 °C, 160 bar. R_T = 4.62, 5.02 min.

(R)-1-(3-methylthiophen-2-yl)ethanol. This alcohol, for which literature characterization data are available,⁴⁶ was synthesized according to Method A to afford enantiomeric ratios of 92.9:7.1 and 92.7:7.3 for two experimental runs. Experimental specific rotation: $[\alpha]_D^{20} = +46.2$ (*c* 0.84, CHCl₃, 92.9:7.1 er (*R*)). Literature specific rotation:⁴⁷ $[\alpha]_D^{25} = +13.0$ (*c* 3.4, CHCl₃, 80.5:19.5 er (*R*)). SFC Enantiomeric Separation Conditions: Chiralpak[®] AD-H column (4.6 mm x 250 mm, 5 μm particle size), 1% isopropanol, 4 mL min⁻¹, 40 °C, 160 bar. R_T = 5.03, 5.57 min.

(S)-(2-chlorophenyl)(cyclopentyl)methanol. This alcohol, for which literature

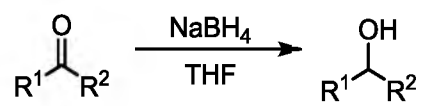


Figure 4.15. Racemic ketone reduction.

characterization data are available,⁴⁸ was synthesized according to Method A to afford enantiomeric ratios of 81.8:18.2 and 82.5:17.5 for two experimental runs. Experimental specific rotation: $[\alpha]_D^{20} = -30.0$ (c 0.26, CHCl_3 , 81.8:18.2 er (*S*)). Literature specific rotation:⁴⁸ $[\alpha]_D^{20} = -12.2$ (c 0.42, CHCl_3 , 81:19 er (*S*)). SFC Enantiomeric Separation Conditions: Chiralpak[®] AY-H column (4.6 mm x 250 mm, 5 μm particle size), 4% isopropanol, 1 mL min⁻¹, 28 °C, 160 bar. $R_T = 14.32, 15.26$ min.

(*R*)-(4-bromophenyl)(cyclopropyl)methanol. This alcohol was synthesized according to Method A to afford enantiomeric ratios of 91.7:8.3 and 92.5:7.5 for two experimental runs. Method B was used to synthesize the racemic sample by dissolving 1.576 g of (4-bromophenyl)(cyclopropyl)methanone (7.0 mmol, 1 equiv) in THF (35mL). The reaction mixture was cooled to 0 °C, 0.530 g NaBH₄ (14.0 mmol, 2 equiv) was added, and then the suspension was stirred under a nitrogen atmosphere for 3 hours, gradually warming to room temperature, followed by heating to reflux for 40 hours. The reaction was quenched with saturated NH₄Cl_(aq) and extracted three times with ethyl acetate. The resulting organic solution was washed with brine and then dried with Na₂SO₄, affording a clear, pale yellow oil, which was purified via flash silica-gel column chromatography (20% ethyl acetate in hexanes) and was afforded in 85% yield (5.971 mmol, 1.356 g). TLC (30% ethyl acetate in hexanes) $R_f = 0.61$. ¹H NMR (500 MHz, CDCl₃) δ : 0.34–0.40 (m, 1H), 0.43–0.49 (m, 1H), 0.53–0.60 (m, 1H), 0.60–0.67 (m, 1H), 1.12–1.21 (m, 1H), 1.93–2.06 (m, 1H), 3.97 (dd, $J = 8.31$ Hz, 3.42 Hz, 1H), 7.28–7.32 (m, 2H), 7.45–7.49 (m, 2H). ¹³C NMR (126 MHz, CDCl₃) δ : 3.1 (s), 3.7 (s), 19.4 (s), 78.0 (s), 121.4 (s), 127.9 (s), 131.6 (s), 142.9 (s). IR (thin film): 3339, 3080, 3004, 2872, 2360, 1903, 1591, 1484, 1399, 1290, 1191, 1136, 1101, 1069, 1028, 1008, 947, 918, 866, 813,

763, 712, 629, 545 cm^{-1} . HRMS $\text{C}_{10}\text{H}_{11}\text{OBrNa}$ $[\text{M}+\text{Na}]^+$ calculated 248.9891, observed 248.9894. Experimental specific rotation: $[\alpha]_D^{20} = -19.1$ (c 2.02, CHCl_3 , 92.5:7.5 er (R)). Literature specific rotation for analogous cyclopropyl(phenyl)methanol:³² $[\alpha]_D^{27} = -28.3$ (c 1.01, CHCl_3 , 97.8:2.2 er (R)). SFC Enantiomeric Separation Conditions: Chiralpak[®] AD-H column (4.6 mm x 250 mm, 5 μm particle size), 5-50% isopropanol, 2 mL min^{-1} , 25 $^\circ\text{C}$, 160 bar. $R_T = 5.54, 5.85$ min.

(R)-1-(4-methoxyphenyl)propan-1-ol. This alcohol, for which literature characterization data are available,⁴⁹ was synthesized according to Method A to afford enantiomeric ratios of 96.0:4.0 and 96.0:4.0 for two experimental runs. Experimental specific rotation: $[\alpha]_D^{20} = +36.4$ (c 2.84, CHCl_3 , 96.0:4.0 er (R)). Literature specific rotation:⁵⁰ $[\alpha]_D^{24} = -23.4$ (c 0.30, CHCl_3 , 82.6:17.4 er (S)). SFC Separation Conditions: Chiralpak[®] AS-H (4.6 mm x 250 mm, 5 μm particle size), 2% isopropanol, 3 mL min^{-1} , 26 $^\circ\text{C}$, 160 bar. $R_T = 5.54, 6.36$ min.

(R)-1-(4-bromophenyl)pentan-1-ol. This alcohol, for which literature characterization data are available,⁵¹ was synthesized according to Method A to afford enantiomeric ratios of 92.3:7.7 and 91.9:8.1 for two experimental runs. Experimental specific rotation: $[\alpha]_D^{20} = +22.0$ (c 3.22, CHCl_3 , 92.3:7.7 er (R)). Literature specific rotation:^{43,51} $[\alpha]_D^{20} = -25.8$ (c 1.0, CHCl_3 , 97:3 er (S)). SFC Enantiomeric Separation Conditions: Chiralpak[®] AD-H column (4.6 mm x 250 mm, 5 μm particle size), 3% isopropanol, 5 mL min^{-1} , 29 $^\circ\text{C}$, 160 bar. $R_T = 8.11, 9.19$ min.

(S)-2-chloro-1-(2,4-dichlorophenyl)ethanol. This alcohol, for which literature characterization data are available,⁵² was synthesized according to Method A to afford enantiomeric ratios of 88.7:11.3 and 88.7:11.3 for two experimental runs. Experimental

specific rotation: $[\alpha]_D^{20} = +29.8$ (c 3.9, CHCl_3 , 88.7:11.3 er (*S*)). Literature specific rotation:⁵² $[\alpha]_D^{20} = -57$ (c 1.0, CHCl_3 , >99.5:0.5 er (*R*)). SFC Enantiomeric Separation Conditions: Chiralpak[®] AD-H column (4.6 mm x 250 mm, 5 μm particle size), 5% isopropanol, 2 mL min^{-1} , 40 $^\circ\text{C}$, 160 bar. $R_T = 14.40, 16.22$ min.

(*R*)-1-(2-ethylphenyl)ethanol. This alcohol was synthesized according to Method A to afford enantiomeric ratios of 83.7:16.3 and 83.6:16.4 for two experimental runs. The racemic sample was synthesized through the following procedure. Magnesium turnings (470 mg, 19.3 mmol, 1.4 equiv), ground with a mortar and pestle, were added to an oven-dried round bottom flask equipped with a magnetic stir bar. Next, the flask was brought under a nitrogen atmosphere, 3 mL of THF were added, and the suspension was stirred for 5 minutes before adding 2 drops of 1,2-dibromoethane (passed through a plug of activated basic alumina prior to use). After stirring until the solution phase became grey in color, approximately 10 minutes, 1-bromo-2-ethylbenzene (2.4 mL, 17.3 mmol, 1.25 equiv) in 3 mL of THF was added all at once. Following stirring for an additional 10 minutes, 10.5 mL of THF were added. The reaction mixture was stirred at room temperature for 0.5 hours, followed by refluxing for 2 hours. Upon cooling to room temperature, acetaldehyde (0.78 mL, 0.608g, 13.8 mmol, 1 equiv) in 12.5 mL of THF was added. After the reaction mixture was stirred for 4 hours, H_2O was added to quench the reaction, followed by addition of saturated aqueous NH_4Cl . The organic phase was extracted and washed with NH_4Cl and subsequently brine. The resulting organic phase was dried with Na_2SO_4 , concentrated, and purified via flash silica-gel column chromatography (50% diethyl ether in pentane) to afford a clear, colorless oil in 31% yield (4.2 mmol, 0.635 g). TLC (10% ethyl acetate in hexanes) $R_f = 0.22$. ^1H NMR (400

MHz, CDCl₃) δ : 1.25 (t, $J = 7.57$ Hz, 3H), 1.50 (d, $J = 6.35$ Hz, 3H), 1.75 (bs, 1H), 2.70 (qd, $J = 7.49$ Hz, 3.42, 2H), 5.19 (q, $J = 6.35$ Hz, 1H), 7.15–7.27 (m, 3H), 7.54 (dd, $J = 7.3, 2.0$, 1H). ¹³C NMR (126 MHz, CDCl₃) δ : 15.9 (s), 24.9 (s), 25.3 (s), 66.3 (s), 125.0 (s), 126.5 (s), 127.6 (s), 128.8 (s), 140.6 (s), 143.4 (s). IR (thin film): 3335, 2967, 2930, 2874, 1604, 1487, 1449, 1370, 1276, 1209, 1180, 1127, 1080, 1003, 945, 894, 798, 754, 613, 551 cm⁻¹. HRMS C₁₀H₁₄OAg [M+Ag]⁺ calculated 257.0096, observed 257.0100. Experimental specific rotation: $[\alpha]_D^{20} = +36.7$ (c 1.38, CHCl₃, 83.6:16.4 er (*R*)). Literature specific rotation:⁵³ $[\alpha]_D^{20} = +68.5$ (c 0.54, CHCl₃, 91.5:8.5 er (*R*)). GC Enantiomeric Separation Conditions: Supelco Beta DEX 120 (30 m x 0.25 mm x 0.25 μ m); 50 °C for 2 min., then ramp 3.5 °C/min to 160 °C and hold for 5 min.; 13.5 psi, 6.8 mL min⁻¹, 25.0:1 split ratio, H₂ carrier gas. R_T = 28.4, 29.6 min.

1-(2-ethylphenyl)ethanone. This ketone, which was ultimately subjected to ATH conditions, was synthesized from 1-(2-ethylphenyl)ethanol according to a previously published oxidation procedure, and characterization data have been previously reported.^{54,55}

(*R*)-1-(naphthalen-2-yl)ethanol. This alcohol, for which literature characterization data are available,⁵⁶ was synthesized according to Method A from 1-(naphthalen-2-yl)ethan-1-one, which was recrystallized from EtOH/H₂O prior to use, to afford enantiomeric ratios of 93.2:6.8 and 95.0:5.0 for two experimental runs. Experimental specific rotation: $[\alpha]_D^{20} = +38.3$ (c 2.6, CHCl₃, 95.0:5.0 er (*R*)). Literature specific rotation:⁵⁷ $[\alpha]_D^{28} = -39$ (c 1.0, CHCl₃, 91.5:8.5 er (*S*)). SFC Enantiomeric Separation Conditions: Chiralcel[®] OJ-H column (4.6 mm x 250 mm), 10% isopropanol, 2 mL min⁻¹, 40 °C, 160 bar. R_T = 11.36, 14.44 min.

(R)-1-(benzofuran-2-yl)ethanol. This alcohol, for which literature characterization data are available,⁵⁸ was synthesized according to Method A to afford enantiomeric ratios of 90.8:9.2 and 92.1:7.9 for two experimental runs. Experimental specific rotation: $[\alpha]_D^{20} = +14.6$ (*c* 3.24, CHCl₃, 92.1:7.9 er (*R*)). Literature specific rotation:⁵⁹ $[\alpha]_D = +16.83$ (*c* 0.53, CHCl₃, 92:8 er (*R*)). SFC Separation Conditions: Chiralcel[®] OZ-H column (4.6 mm x 250 mm, 5 μm particle size), 5–50% isopropanol (4.5% cosolvent increase per minute), 3 mL min⁻¹, 26 °C, 160 bar. R_T = 3.77, 4.14 min.

(S)-1,1-diphenylpropan-2-ol. This alcohol, for which literature characterization data are available,⁶⁰ was synthesized according to Method A from 1,1-diphenylpropan-2-one, which was recrystallized from EtOH/H₂O prior to use, to afford enantiomeric ratios of 86.8:13.2 and 88.4:11.6 for two experimental runs. Experimental specific rotation: $[\alpha]_D^{20} = -4.6$ (*c* 0.96, 88.4:11.6 er (*S*)). Literature specific rotation:^{61,62} $[\alpha]_D^{20} = -5.92$ (*c* 2.5, CHCl₃, 98.3:1.7 er (*S*)). SFC Enantiomeric Separation Conditions: Chiralpak[®] AY-H column (4.6 mm x 250 mm, 5 μm particle size), 2% methanol, 2 mL min⁻¹, 40 °C, 160 bar. R_T = 9.92, 10.87 min.

(S)-1-cyclohexylpropan-1-ol. This alcohol, for which literature characterization data are available,⁶³ was synthesized according to Method A to afford enantiomeric ratios of 53.6:46.4 and 54.5:45.5 for two experimental runs. The alcohol was benzoyl-protected, according to a previously reported procedure⁶⁴, for enantiomeric separation. Experimental specific rotation: $[\alpha]_D^{20} = -1.9$ (*c* 1.55, CDCl₃, 53.6: 46.4 er (*S*)). Literature specific rotation:^{65,66} $[\alpha]_D^{28} = +4.5$ (*c* 1.00, CHCl₃, 97:3 er (*R*)). SFC Enantiomeric Separation Conditions: Chiralpak[®] AD-H column (4.6 mm x 250 mm, 5 μm particle size), 1–5% isopropanol, 2 mL min⁻¹, 40 °C, 160 bar. R_T = 4.62, 5.02 min.

(S)-1,1-dichloropropan-2-ol. This alcohol, for which literature characterization data are available,⁶⁷ was synthesized according to Method A to afford enantiomeric ratios of 73.9:26.1 and 74.2:25.8 for two experimental runs. The alcohol was benzoyl-protected, according to a previously reported procedure,⁶⁴ for enantiomeric separation. Experimental specific rotation: $[\alpha]_D^{20} = -0.9$ (*c* 0.55, CDCl₃, 74.2:25.8 er (*S*)). Literature specific rotation:⁶⁷ $[\alpha]_D^{21} = -2.92$ (*c* 3.2, CHCl₃, 81:19 er (*S*)). SFC Enantiomeric Separation Conditions: Chiralpak[®] AY-H column (4.6 mm x 250 mm, 5 μm particle size), 1–5% isopropanol, 2 mL min⁻¹, 40 °C, 160 bar. R_T = 1.86, 2.24 min.

(R)-4-methylpentan-2-ol. This alcohol, for which literature characterization data are available,⁶⁸ was synthesized according to Method A to afford enantiomeric ratios of 59.1:40.9 and 59.1:40.9 for two experimental runs. Experimental specific rotation: $[\alpha]_D^{20} = -2.5$ (*c* 0.41, CDCl₃, 59.1:40.9 er (*R*)). Literature specific rotation:^{69,70} $[\alpha]_D^{25} = +19.5$ (*c* not reported, CHCl₃, 85.5:14.5 er (*S*)). GC Enantiomeric Separation Conditions: Supelco Beta DEX 120 (30 m x 0.25 mm x 0.25 μm), 40 °C, 13.5 psi, 7.2 mL min⁻¹, 25:1 split ratio, H₂ carrier gas. R_T = 17.4, 18.6 min.

(S)-4,4-dimethoxybutan-2-ol. This alcohol, for which literature characterization data are available⁷¹, was synthesized according to Method A to afford enantiomeric ratios of 59.8:40.2 and 58.0:42.0 for two experimental runs. Experimental specific rotation: $[\alpha]_D^{20} = -2.2$ (*c* 1.65, CDCl₃, 59.8:40.2 er (*S*)). Literature specific rotation:⁷² $[\alpha]_D^{20} = +12.0$ (*c* 1.00, CHCl₃, >99.95:0.05 er (*R*)). GC Enantiomeric Separation Conditions: Supelco Beta DEX 120 (30 m x 0.25 mm x 0.25 μm), 60 °C, 15.8 psi, 3 mL min⁻¹, 25:1 split ratio, H₂ carrier gas. R_T = 37.3, 38.2 min.

(R)-1-(2-isopropylphenyl)ethanol. This alcohol was synthesized according to

Method A to afford enantiomeric ratios of 75.5:24.5 (stirring reaction for 5 hours once ketone was added) and 76.9:23.1 (standard ketone reaction time of 2 hours) for 2 experimental runs. The racemic sample was synthesized through the following procedure. Magnesium turnings (38.72 mmol, 1.4 equiv), ground with a mortar and pestle, were added to an oven-dried round bottom flask equipped with a magnetic stir bar. Next, the flask was brought under a nitrogen atmosphere, 6 mL of THF were added, and the suspension was stirred for 5 minutes before adding 2 drops of 1,2-dibromoethane (passed through an activated basic alumina plug prior to use). After stirring until the solution phase became grey, approximately 10 minutes, the corresponding bromide (35.2 mmol, 1.25 equiv) in 6 mL of THF was added all at once. After stirring for an additional 10 minutes, 21 mL of THF were added. The reaction mixture was stirred at room temperature for 1 hour, followed by refluxing for 20 hours. Upon cooling to room temperature, the corresponding aldehyde (28.16 mmol, 1 equiv) in 28 mL of THF was added. After the reaction mixture was stirred for 6 hours, H₂O was added to quench the reaction, followed by addition of saturated aqueous NH₄Cl. The organic phase was extracted and washed with NH₄Cl and subsequently brine. The resulting organic phase was dried with Na₂SO₄, concentrated, and purified via flash silica-gel column chromatography (15% ethyl acetate in hexanes) to afford isolated product, a clear, yellow oil, in 22% yield (6.08 mmol, 0.999 g). TLC (15% ethyl acetate in hexanes) R_f = 0.20. ¹H NMR (500 MHz, CDCl₃) δ: 1.23–1.28 (m, 6H), 1.50 (d, *J* = 6.35 Hz, 3H), 1.65 (bs, 1H), 3.26 (sep, *J* = 6.84 Hz, 1H), 5.28 (q, *J* = 6.35 Hz, 1H), 7.20–7.30 (m, 3H), 7.53 (dd, *J* = 7.33 Hz, 1.47 Hz, 1H). ¹³C NMR (126 MHz, CDCl₃) δ: 24.1 (s), 24.5 (s), 25.2 (s), 28.2 (s), 66.3 (s), 124.9 (s), 125.5 (s), 126.3 (s), 127.7 (s), 142.5 (s), 145.4 (s). IR (thin film):

3329, 3061, 3029, 2964, 2927, 2869, 2362, 1603, 1488, 1447, 1384, 1367, 1268, 1219, 1183, 1110, 1068, 1035, 1003, 947, 897, 755, 614, cm^{-1} . HRMS $\text{C}_{11}\text{H}_{16}\text{ONa}$ $[\text{M}+\text{Na}]^+$ calculated 187.1099, observed 187.1092. Experimental specific rotation: $[\alpha]_D^{20} = +23.9$ (c 0.28, CHCl_3 , 76.9:23.1 er (*R*)). Literature specific rotation for analogous 1-(2-ethylphenyl)ethanol⁵³: $[\alpha]_D^{20} = +68.5$ (c 0.54, CHCl_3 , 91.5:8.5 er (*R*)). SFC Separation Conditions: : Chiralpak[®] AS-H (4.6 mm x 250 mm, 5 μm particle size), 2% isopropanol, 3 mL min^{-1} , 26 $^\circ\text{C}$, 160 bar. $R_T = 5.54, 6.36$ min.

1-(2-isopropylphenyl)ethan-1-one. This ketone was synthesized from 1-(2-isopropylphenyl)ethanol according to a previously published Swern oxidation procedure^{54,55} and purified via flash silica-gel column chromatography (10% ethyl acetate in hexanes) to afford isolated product, a clear, colorless oil, in 52% yield (3.08 mmol, 0.499 g). TLC (10% ethyl acetate in hexanes) $R_f = 0.36$. ^1H NMR (500 MHz, CDCl_3) δ : 1.24 (d, $J = 6.84$ Hz, 6H), 2.57 (s, 3H), 3.46 (sep, $J = 6.84$ Hz, 1H), 7.20–7.26 (m, 1H), 7.41–7.43 (m, 2H), 7.46–7.49 (m, 1H). ^{13}C NMR (126 MHz, CDCl_3) δ : 24.3 (s), 29.4 (s), 30.8 (s), 125.5 (s), 126.6 (s), 127.7 (s), 131.2 (s), 139.0 (s), 147.8 (s), 203.9 (s). IR (thin film): 3064, 2964, 2869, 2361, 1685, 1599, 1572, 1485, 1463, 1444, 1383, 1356, 1279, 1243, 1204, 1166, 1100, 1059, 1032, 1012, 956, 757, 602, 570, 542 cm^{-1} . HRMS $\text{C}_{11}\text{H}_{14}\text{ONa}$ $[\text{M}+\text{Na}]^+$ calculated 185.0942, observed 185.0945.

(*R*)-1-(naphthalen-1-yl)ethanol. This alcohol, for which literature characterization data are available,⁶³ was synthesized according to Method A to afford enantiomeric ratios of 88.3:11.7 and 88.5:11.4 for two experimental runs. Experimental specific rotation: $[\alpha]_D^{20} = +42.1$ (c 1.43, CHCl_3 , 88.3:11.7 er (*R*)). Literature specific rotation:⁷³ $[\alpha]_D^{20} = -57.4$ (c 0.86, CHCl_3 , 95.5:1.5 er (*S*)). SFC Enantiomeric Separation

Conditions: Chiralcel[®] OD column (4.6 mm x 250 mm), 15% isopropanol, 4 mL min⁻¹, 40 °C, 160 bar. R_T = 3.21, 4.10 min.

(R)-1-(o-tolyl)ethanol. This alcohol, for which literature characterization data are available,⁵³ was synthesized according to Method A to afford enantiomeric ratios of 88.7:11.3 and 89.7:10.3 for two experimental runs. Experimental specific rotation: $[\alpha]_D^{20} = +57.1$ (*c* 3.75, 89.7:10.3 er (*R*)). Literature specific rotation:⁵³ $[\alpha]_D^{20} = +68.5$ (*c* 0.54, CHCl₃, 91.5:8.5 er (*R*)). GC Enantiomeric Separation Conditions: Supelco Beta DEX 120 (30 m x 0.25 mm x 0.25 μm); 50 °C for 2 min., then ramp 2 °C/min to 150 °C; 13.5 psi, 6.8 mL min⁻¹, 0.1:1 split ratio, H₂ carrier gas. R_T = 38.5, 40.6 min.

(R)-1-(furan-2-yl)ethan-1-ol. This alcohol, for which literature characterization data are available,⁷⁴ was synthesized according to Method A to afford enantiomeric ratios of 93.9:6.1 and 93.6:6.4 for two experimental runs. Experimental specific rotation: $[\alpha]_D^{20} = +17.3$ (*c* 1.54, 93.6:6.4 er (*R*)). Literature specific rotation:⁷⁵ $[\alpha]_D^{25} = +20.8$ (*c* 1.27, CHCl₃, >97.5:2.5 er (*R*)). GC Enantiomeric Separation Conditions: Supelco Beta DEX 120 (30 m x 0.25 mm x 0.25 μm); 55 °C, 13.5 psi, 6.8 mL min⁻¹, 25.0:1 split ratio, H₂ carrier gas. R_T = 39.8, 44.2 min.

(R)-1-(4-chlorophenyl)pentan-1-ol. This alcohol was synthesized according to Method A to afford enantiomeric ratios of 91.7:8.3 and 91.9:8.1 for two experimental runs. The racemic sample was synthesized through the following procedure. Magnesium turnings (41.3 mmol, 1.4 equiv), ground with a mortar and pestle, were added to an oven-dried round bottom flask equipped with a magnetic stir bar. Next, the flask was brought under a nitrogen atmosphere, 6 mL of THF were added, and the suspension was stirred for approximately 5 minutes before adding 2 drops of 1,2-dibromoethane (passed through

a plug of activated basic alumina prior to use). After stirring until the solution phase became grey in color, approximately 10 minutes, 6 mL of THF was added followed by 1-bromobutane (37.5 mmol, 1.25 equiv), which was passed through activated basic alumina prior to use. After stirring for an additional 10 minutes, 21 mL of THF were added. The reaction mixture was stirred at room temperature for 50 minutes, followed by refluxing for 3 hours. Upon cooling to room temperature, 30 mL of THF and 4-chlorobenzaldehyde (30.0 mmol, 1 equiv) were added. After the reaction mixture was stirred for 4 hours, H₂O was added to quench the reaction, followed by addition of saturated aqueous NH₄Cl. The organic phase was extracted and washed with saturated NH₄Cl_(aq) and, subsequently, brine. The resulting organic phase was dried with Na₂SO₄, concentrated, and purified via flash silica-gel column chromatography (30% ethyl acetate in hexanes) to afford a clear, pale yellow oil in 45% yield (13.391 mmol, 2.661 g). TLC (20% ethyl acetate in hexanes) R_f = 0.37. ¹H NMR (500 MHz, CDCl₃) δ: 0.88 (t, *J* = 7.33 Hz, 3H), 1.20–1.28 (m, 1H), 1.29–1.42 (m, 3H), 1.63–1.71 (m, 1H), 1.73–1.80 (m, 1H), 1.82 (s, 1H), 4.62–4.67 (m, 1H), 7.26–7.29 (m, 2H), 7.30–7.33 (m, 2H). ¹³C NMR (126 MHz, CDCl₃) δ: 14.1 (s), 22.7 (s), 28.0 (s), 39.0 (s), 74.1 (s), 127.4 (s), 128.7 (s), 133.2 (s), 143.5 (s). IR (thin film): 3344, 2956, 2931, 2860, 2361, 2339, 1597, 1578, 1491, 1466, 1409, 1379, 1342, 1198, 1090, 1041, 1013, 972, 941, 897, 831, 773, 731, 668, 550 cm⁻¹. HRMS C₁₁H₁₄ClO [M-H]⁻ calculated 197.0733, observed 197.0744. Experimental specific rotation: [α]_D²⁰ = +24.0 (*c* 4.33, CHCl₃, 91.9:8.1er (*R*)). Literature specific rotation for analogous 1-(4-bromophenyl)pentan-1-ol:^{43,51} [α]_D²⁰ = -25.8 (*c* 1.0, CHCl₃, 97:3 er (*S*)). SFC Enantiomeric Separation Conditions: Chiralpak[®] AD-H column (4.6 mm x 250 mm, 5 μm particle size), 4% isopropanol, 5 mL min⁻¹, 30 °C, 160 bar. R_T = 4.88, 5.37 min.

1-(4-chlorophenyl)pentan-1-one. This ketone was synthesized from 1-(4-chlorophenyl)pentan-1-ol (5.03 mmol, 1.0 equiv.) according to a previously published Swern oxidation procedure⁵⁴ and purified via flash silica-gel column chromatography (10% ethyl acetate in hexanes) to afford a white solid in 68% yield (3.43 mmol, 0.674 g). TLC (10% ethyl acetate in hexanes) $R_f = 0.41$. M.P.: 30–31 °C. ¹H NMR (500 MHz, CDCl₃) δ : 0.95 (t, $J = 7.33$ Hz, 3H), 1.36–1.45 (m, 2H), 1.67–1.75 (m, 2H), 2.93 (t, $J = 7.33$ Hz, 2H), 7.41–7.45 (m, 2H), 7.87–7.92 (m, 2H). ¹³C NMR (126 MHz, CDCl₃) δ : 14.1 (s), 22.6 (s), 26.5 (s), 38.5 (s), 129.0 (s), 129.6 (s), 135.5 (s), 139.4 (s), 199.4 (s). IR (thin film): 3093, 2966, 2955, 2929, 2873, 2362, 2340, 1676, 1592, 1572, 1488, 1466, 1455, 1406, 1376, 1342, 1270, 1207, 1177, 1095, 1013, 980, 839, 794, 733, 668, 567 cm⁻¹. HRMS C₁₁H₁₄ClO [M+H]⁺ calculated 197.0733, observed 197.0733.

(R)-3-methyl-1-phenylbutan-1-ol. This alcohol, for which literature characterization data are available,⁷⁶ was synthesized according to Method A from 3-methyl-1-phenylbutan-1-one, which was passed through activated basic alumina prior to use, to afford enantiomeric ratios of 94.4:5.6 and 94.0:6.0 for two experimental runs. Experimental specific rotation: $[\alpha]_D^{20} = +35.6$ (c 2.9, CHCl₃, 94.0:6.0 er (*R*)). Literature specific rotation:⁷⁷ $[\alpha]_D = +23$ (c 1.2, CHCl₃, 87:13 er (*R*)). SFC Enantiomeric Separation Conditions: Chiralcel[®] OZ-H column (4.6 mm x 250 mm, 5 μ m particle size), 1% isopropanol, 2 mL min⁻¹, 40 °C, 160 bar. $R_T = 12.57, 13.69$ min.

(R)-1-(benzo[d][1,3]dioxol-5-yl)ethanol. This alcohol, for which literature characterization data are available,⁷⁸ was synthesized according to Method A to afford enantiomeric ratios of 95.0:5.0 and 95.8:4.2 for two experimental runs. Experimental specific rotation: $[\alpha]_D^{20} = +30.0$ (c 0.34, CHCl₃, 95.0:5.0 er (*R*)). Literature specific

rotation:⁷⁹ $[\alpha]_D^{23} = +46.5$ (*c* 1.01, CHCl₃, 98.5:1.5 er (*R*)). SFC Enantiomeric Separation Conditions: Chiralcel[®] OJ-H column (4.6 mm x 250 mm), 1–3% methanol (0.17% cosolvent increase per minute), 1 mL min⁻¹, 25 °C, 160 bar. R_T = 10.71, 11.52 min.

(*R*)-1-phenylethanol. This alcohol, for which literature characterization data are available,⁵⁶ was synthesized according to Method A from acetophenone, which was passed through activated basic alumina prior to use, to afford enantiomeric ratios of 96.7:3.3 and 95.6:4.4 for two experimental runs. Experimental specific rotation: $[\alpha]_D^{20} = +47.4$ (*c* 3.0, CHCl₃, 96.7:3.3 er (*R*)). Literature specific rotation:⁵⁶ $[\alpha]_D^{25} = -39.6$ (*c* 2.46, CHCl₃, 91:9 er (*S*)). Enantiomeric Separation Conditions: Chiralcel[®] OD column (4.6 mm x 250 mm), 3% methanol, 5 mL min⁻¹, 33 °C, 160 bar. R_T = 2.32, 2.83 min.

(*R*)-1-(3-methoxyphenyl)ethanol. This alcohol, for which literature characterization data are available,⁵⁸ was synthesized according to Method A to afford enantiomeric ratios of 97.1:2.9 and 96.8:3.2 for two experimental runs. Experimental specific rotation: $[\alpha]_D^{20} = +35.9$ (*c* 2.49, CHCl₃, 97.1:2.9 er (*R*)). Literature specific rotation:⁵⁸ $[\alpha]_D^{20} = -38.9$ (*c* 1.27, CHCl₃, 95.5:4.5 er (*S*)). SFC Separation Conditions: Chiralcel[®] OJ-H column (4.6 mm x 250 mm), 1–5% methanol (0.27% cosolvent increase per minute), 3 mL min⁻¹, 40 °C, 160 bar. R_T = 6.32, 7.16 min.

(*S*)-3-methylbutan-2-ol. This alcohol, for which literature characterization data are available,⁸⁰ was synthesized according to Method A to afford enantiomeric ratios of 82.1:17.9 and 82.6:17.4 for two experimental runs. Experimental specific rotation: $[\alpha]_D^{20} = +1.6$ (*c* 0.67, CDCl₃, 82.1:17.9 er (*S*)). Literature specific rotation:⁸⁰⁻⁸² $[\alpha]_D^{24} = +7.91$ (*c* 1.0, CH₂Cl₂, 87:13 er (*S*)). GC Enantiomeric Separation Conditions: Supelco Beta DEX 120 (30 m x 0.25 mm x 0.25 μm), 32 °C, 15.9 psi, 3.5 mL min⁻¹, 100:1 split

ratio, H₂ carrier gas. R_T = 17.6, 18.4 min.

3,3-dimethylbutan-2-ol. This alcohol, for which literature characterization data are available,⁸³ was synthesized according to Method A to afford enantiomeric ratios of 52.7:47.3 and 52.6:47.4 for two experimental runs. GC Enantiomeric Separation Conditions: Supelco Beta DEX 120 (30 m x 0.25 mm x 0.25 μm), 50 °C, 13.5 psi, 6.8 mL min⁻¹, 25:1 split ratio, H₂ carrier gas. R_T = 9.36, 9.96 min.

(R)-1-cyclopropylethanol. This alcohol, for which literature characterization data are available,⁸⁴ was synthesized according to Method A to afford enantiomeric ratios of 77.0:23.0 and 76.3:23.7 for two experimental runs. Experimental specific rotation: $[\alpha]_D^{20} = -4.4$ (*c* 1.14, 76.3:23.7 er (*R*)). Literature specific rotation:⁸⁴ $[\alpha]_D^{25} = -10.5$ (*c* 8.5, CHCl₃, 92.5:7.5 er (*R*)). GC Enantiomeric Separation Conditions: Supelco Beta DEX 120 (30 m x 0.25 mm x 0.25 μm), 40 °C, 13.5 psi, 7.2 mL min⁻¹, 25:1 split ratio, H₂ carrier gas. R_T = 11.7, 12.3 min.

Tabulated Enantioselectivities and Molecular Descriptors

All parameters used for linear regression modelling were measured from energy-minimized structures (M06-2X/TZVP) using Gaussian09.²⁷ Torsion, IR, and NBO point charge parameters were measured using GaussView 5.0.⁴⁰ Sterimol-derived measurements were made using Mol2Mol.⁴¹ Occasionally, Mol2Mol software gave anomalous Sterimol values for substituents that are structurally identical. Thus, Sterimol-derived measurements have been standardized. For example, all phenyl rings that are structurally identical at the *ortho* or *meta* positions are tabulated such that their identical features are numerically represented in an appropriate manner.

Model Development

Stepwise linear regression algorithms from MATLAB's Statistics Toolbox were used for model development. This process and the MATLAB commands employed are outlined below. All data are normalized prior to performing linear regression. All R^2 values represent adjusted R^2 .

Modelling Aryl/Alkyl Ketones

The four commands described below were used for initial assessment of the full library set (descriptors x1-x16, as presented in Table 4.1). X is the descriptor matrix. Y is the matrix of $\Delta\Delta G^\ddagger$ values. Each stepwise algorithm adds or removes terms according to p -value tolerance levels. For terms with p -values <0.05 , the term is added to the model. Terms are removed for p -values >0.10 . For each line of command, the initial terms in the model varies. "FitForward" begins with no terms in the model. "FitBackL" begins with all linear terms in the model. "FitBackI" begins with all interaction/cross-terms in the model. "FitQuad" begins with quadratic terms in the model.

The command "FitForward = LinearModel.stepwise(X, Y)" resulted in Eq. 4.1, which has an R^2 value of 0.974. The command "FitBackL = LinearModel.stepwise(X, Y, 'linear')" resulted in Eq. 4.2, which has an R^2 value of 1.00.

$$y = -0.13 - 0.67x3 + 0.48x4 - 0.32x6 - 0.63x12 \quad \text{Eq. 4.1}$$

$$y = -0.45 + 1.09x9 - 0.55x10 + 0.32x11 - 0.49x12 - 0.17x13 - 0.78x14 - 1.17x15 - 0.09x16 \quad \text{Eq. 4.2}$$

Table 4.1. Aryl/alkyl ketone DoE library and external validations.

	<i>Y</i>	<i>x1</i>	<i>x2</i>	<i>x3</i>	<i>x4</i>	<i>x5</i>	<i>x6</i>		
R1	R2	Avg $\Delta\Delta G^\ddagger$	$\nu_{C=O}$ (cm^{-1})	$I_{C=O}$ (a.u.)	ProxB1_{Alkyl}	ProxB5_{Alkyl}	DistB5_{Alkyl}	DistL_{Alkyl}	
DoE Library									
1	<i>i</i> Pr	Ph	0.60	1817.47	178.7993	1.90	3.19	0.00	0.00
2	CyPent	2-Cl Ph	-0.95	1819.87	186.7459	1.86	3.19	3.82	5.54
3	CH ₂ Cl	2,4-diCl Ph	1.28	1832.09	219.7283	1.51	3.46	0.00	0.00
4	CyPr	4-Br Ph	1.53	1798.11	163.0239	1.54	3.21	0.00	0.00
5	<i>n</i> Bu	4- Br Ph	1.53	1824.33	186.668	1.56	3.13	4.45	6.72
6	Me	3-Me-2-thiophenyl	1.59	1800.69	223.8738	1.51	2.03	0.00	0.00
7	Me	2-benzofuran	1.48	1830.13	264.0216	1.51	2.03	0.00	0.00
8	Me	2-naphthyl	1.73	1823.1	279.6375	1.51	2.03	0.00	0.00
9	Me	2-Et Ph	1.02	1817.65	217.7746	1.5	2.03	0.00	0.00
10	Et	4-OMe Ph	1.98	1815.56	196.9634	1.57	3.15	0.00	0.00
External Validations									
11	Me	2-furyl	1.69	1825.25	244.8105	1.51	2.03	0.00	0.00
12	Me	3-OMe Ph	2.15	1824.58	202.8848	1.51	2.03	0.00	0.00
13	<i>n</i> Bu	4-Cl Ph	1.50	1823.82	183.8004	1.56	3.13	4.45	6.72
14	Me	Ph	2.01	1827.3	216.1813	1.51	2.03	0.00	0.00
15	Me	2-Me Ph	1.31	1816.53	217.7209	1.51	2.03	0.00	0.00
16	Me	1-(benzo[d][1,3]dioxol-5-yl)	1.89	1820.24	235.6685	1.51	2.03	0.00	0.00
17	Me	1-naphthyl	1.27	1816.64	192.4465	1.50	2.03	0.00	0.00
18	CH ₂ <i>i</i> Pr	Ph	1.74	1819.86	174.7183	1.57	3.13	4.36	5.55
19	Me	2- <i>i</i> Pr Ph	0.72	1818.22	213.1045	1.50	2.03	0.00	0.00

Table 4.1. Continued.

	<i>x7</i>	<i>x8</i>	<i>x9</i>	<i>x10</i>	<i>x11</i>	<i>x12</i>	<i>x13</i>	<i>x14</i>	<i>X15</i>	<i>x16</i>
	ProxB1 _{Aryl}	ProxB5 _{Aryl}	DistB1 _{Aryl}	DistB5 _{Aryl}	DistL _{Aryl}	Tor (deg)	Charge R1 Carbon ^a	Charge R2 Carbon ^a	NBO Charge Carbonyl Carbon ^a	NBO Charge Carbonyl Oxygen ^a
DoE Library										
1	3.14	3.14	3.14	3.14	6.77	5.45	-0.315	-0.167	0.573	-0.532
2	3.14	4.55	3.14	3.14	6.77	38.74	-0.340	-0.174	0.589	-0.521
3	3.14	4.54	3.14	3.14	8.2	37.92	-0.467	-0.187	0.548	-0.488
4	3.14	3.14	3.14	3.14	8.51	14.66	-0.353	-0.154	0.558	-0.552
5	3.14	3.14	3.14	3.14	8.51	0.00	-0.501	-0.166	0.567	-0.525
6	3.18	4.20	2.60	2.60	6.20	0.00	-0.708	-0.336	0.534	-0.532
7	2.56	3.07	2.99	3.52	8.43	0.00	-0.702	0.161	0.517	-0.508
8	3.14	3.14	3.14	4.34	8.92	0.00	-0.709	-0.162	0.555	-0.521
9	3.14	5.34	3.14	3.14	6.77	22.43	-0.709	-0.168	0.562	-0.533
10	3.14	3.14	3.14	3.14	8.8	0.00	-0.503	-0.201	0.564	-0.539
External Validation Set										
11	2.55	3.07	2.52	2.78	6.02	0.00	-0.701	0.13	0.517	-0.515
12	3.14	3.14	3.14	5.36	6.77	0.00	-0.709	-0.143	0.558	-0.526
13	3.14	3.14	3.14	3.14	8.2	0.00	-0.501	-0.168	0.568	-0.526
14	3.14	3.14	3.14	3.14	6.77	0.03	-0.710	-0.168	0.557	-0.522
15	3.14	4.33	3.14	3.14	6.77	11.44	-0.708	-0.169	0.556	-0.529
16	3.14	3.14	3.14	3.62	7.81	0.52	-0.708	-0.169	0.556	-0.528
17	3.14	5.61	3.14	5.61	6.96	22.57	-0.708	-0.132	0.559	-0.529
18	3.14	3.14	3.14	3.14	6.77	3.13	-0.503	-0.165	0.572	-0.537
19	3.14	5.59	3.14	3.14	6.76	27.80	-0.709	-0.165	0.564	-0.532

^aNatural bond orbital (NBO) point charges.

The command “FitBackI = LinearModel.stepwise(X, Y, 'interactions')” resulted in Eq. 4.3, which has an R^2 value of 0.982.

$$y = -2.03 + 1.01x_5 - 1.82x_{13} - 3.75x_{14} + 1.44x_{15} + 0.95x_{16} - 1.99x_{13}:x_{16} - 3.79x_{15}:x_{16} \quad \text{Eq. 4.3}$$

The command “FitQuad = LinearModel.stepwise(X, Y, 'purequadratic')” resulted in Eq. 4.4, which has an R^2 value of 0.999.

$$y = 1 + 0.94x_{13} - 0.34x_{14} - 2.54x_{15} + 0.37x_{16} + 2.03x_{14}:x_{16} - 0.52(x_{13})^2 - 1.68(x_{14})^2 - 0.20(x_{16})^2 \quad \text{Eq. 4.4}$$

It is often the case that models with fewer terms provide more general descriptions of a system and, thus, are more robust. As the model with the fewest terms (Eq. 4.1) was afforded via the FitForward algorithm, its validity was assessed via external validation (Figure 4.16), which indicated that the model provides a reasonable description of ATH asymmetric induction.

At this stage, the descriptor library was refined, eliminating the NBO point charges and measures of distal steric bulk. Invoking the initial hypothesis that carbonyl IR stretching frequency and differential steric bulk are effective descriptors of enantioselective outcomes, MATLAB stepwise linear regression was performed using the single-term descriptor set x_1 , x_3 , x_4 , x_7 , x_8 , x_{12} and began from the defined model initiation point of descriptors x_1 , x_3 , x_7 , and x_{12} . The command “UserDefinedStep =

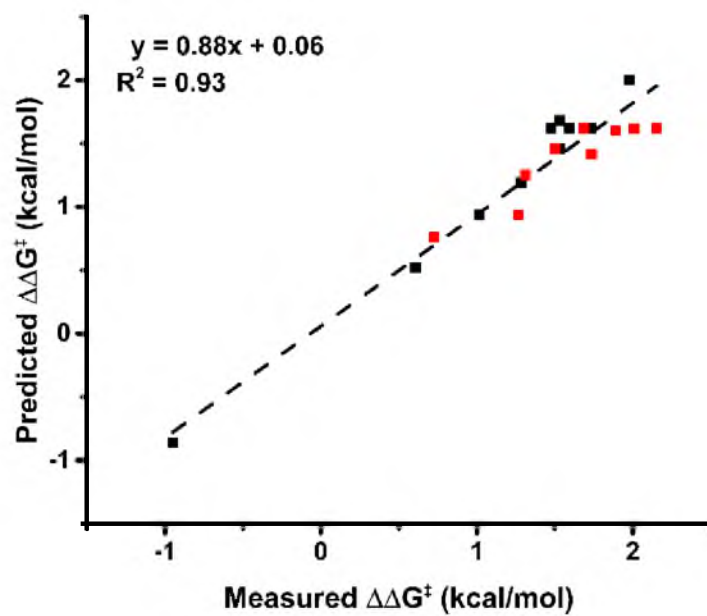


Figure 4.16. Predicted versus measured aryl/alkyl library $\Delta\Delta G^\ddagger$ values depicting the model in Eq. 4.1. ■ represents the aryl/alkyl DoE library, and ■ represents external validation data.

LinearModel.stepwise($X, Y, 'y \sim 1 + \mathbf{x1} + \mathbf{x3} + \mathbf{x7} + \mathbf{x12}'$)” resulted in Eq. 4.5, which has an R^2 value of 0.931, and is the final descriptive model for the aryl/alkyl ketone library.

$$y = -0.10 - 0.38\mathbf{x1} - 0.80\mathbf{x3} + 0.29\mathbf{x7} - 0.52\mathbf{x12} - 1.46\mathbf{x1}:\mathbf{x3} \quad \text{Eq. 4.5}$$

The robustness of this model, as described above, is graphically represented in Figure 4.16. Further information regarding the descriptive capabilities of this model is gathered by assessing the regression model that is fit using raw (not normalized) data. Raw data models provide insight into whether a parameter augments or diminishes enantioselectivity. The aryl/alkyl raw linear regression model is given in Eq. 4.6.

$$\begin{aligned} \Delta\Delta G^\ddagger = -RT\ln([S]/[R]) = & -2884 + 1.59(\mathbf{v}_{\text{C=O}}) + 1883(\text{Prox}\mathbf{B1}_{\text{Alkyl}}) \quad \text{Eq. 4.6} \\ & + 1.07(\text{Prox}\mathbf{B1}_{\text{Aryl}}) - 0.03(\mathbf{Tor}) - 1.04(\mathbf{v}_{\text{C=O}})(\text{Prox}\mathbf{B1}_{\text{Alkyl}}) \end{aligned}$$

Modelling Alkyl/Alkyl Ketones

The enantioselectivity data (Y) and descriptor set (X) represented in Table 4.2 were used for linear regression modelling. The MATLAB command “FitForward = LinearModel.stepwise(X, Y)” afforded no model. “FitBackL = LinearModel.stepwise($X, Y, 'linear'$),” “FitBackI = LinearModel.stepwise($X, Y, 'interactions'$),” and “FitQuad = LinearModel.stepwise($X, Y, 'purequadratic'$)” afforded identical models, represented in Eq. 4.7, with R^2 values of 0.94.

$$y = -10.54 - 1.27\mathbf{x13} - 30.02\mathbf{x14} \quad \text{Eq. 4.7}$$

Table 4.2. Alkyl/alkyl ketone DoE library and external validations.

			<i>Y</i>	<i>x1</i>	<i>x2</i>	<i>x3</i>	<i>x4</i>	<i>x5</i>
R1^a	R2^b	Avg $\Delta\Delta G_{\ddagger}^{\ddagger}$	$\nu_{C=O}$ (cm⁻¹)	I_{C=O} (a.u.)	ProxB1_{Alkyl.Small}	ProxB5_{Alkyl.Small}	ProxB1_{Alkyl.Large}	
DoE Library								
1	Me	CH(Ph) ₂	-1.22	1855.72	144.3298	1.50	2.03	1.80
2	Me	CH ₂ <i>i</i> Pr	0.23	1850.16	164.7989	1.50	2.03	1.58
3	Et	CyHexyl	-0.10	1839.02	156.1775	1.57	3.14	1.91
4	Me	CHCl ₂	-0.65	1872.86	191.5912	1.50	2.04	1.87
5	Me	CH ₂ CH(OMe) ₂	-0.22	1857.52	178.1931	1.50	2.04	1.55
6	Me	<i>t</i> Bu	-0.07	1840.16	186.3692	1.50	2.03	2.74
7	Me	CyPr	0.74	1832.14	165.9745	1.50	2.03	1.55
8	Me	<i>i</i> Pr	-0.96	1846.28	184.1163	1.50	2.03	1.91

^aSmaller of the two alkyl groups. ^bLarger of the two alkyl groups.

Table 4.2. Continued.

	<i>x6</i>	<i>x7</i>	<i>x8</i>	<i>x9</i>	<i>x10</i>	<i>x11</i>	<i>x12</i>	<i>x13</i>	<i>x14</i>
						Charge	Charge	Charge	Charge
				ν_{scissor}	I_{scissor}	R1	R2	Carbonyl	Carbonyl
	<i>Prox</i> B5 _{Alkyl, Large}	<i>Dist</i> B5 _{Alkyl, Large}	<i>Dist</i> L _{Alkyl, Large}	(cm^{-1})	(a.u.)	Carbon ^c	Carbon ^c	Carbon ^c	Oxygen ^c
DoE Library									
1	2.94	6.07	5.96	337.67	2.0924	-0.714	-0.363	0.612	-0.526
2	3.12	4.37	5.55	438.08	0.8314	-0.710	-0.505	0.586	-0.535
3	3.17	3.45	6.66	454.11	0.6835	-0.509	-0.320	0.602	-0.537
4	3.49	0.00	0.00	432.94	1.7475	-0.726	-0.302	0.545	-0.483
5	3.15	5.33	6.72	351.95	2.9498	-0.709	-0.551	0.594	-0.528
External Validation Set									
6	3.19	0.00	0.00	464.57	2.2826	-0.719	-0.158	0.599	-0.533
7	3.20	0.00	0.00	380.6	3.9854	-0.703	-0.360	0.574	0.552
8	3.18	0.00	0.00	439.36	3.2453	-0.717	-0.321	0.588	-0.530

^c Natural bond orbital (NBO) point charges.

Although three of four stepwise regression commands applied to the alkyl/alkyl library of data yield the model given in Eq. 4.7, graphical representation of the model's external validation statistics (Figure 4.17) indicates that this model lacks broad descriptive abilities.

To identify a mathematical equation with more robust predictive capabilities, the relevance of point charge parameters was assessed by excluding them from the descriptor set. From the remaining terms ($x1-x10$), additional rounds of linear regression modelling were pursued.

The commands “FitForward = LinearModel.stepwise(X , Y),” “FitBackI = LinearModel.stepwise(X , Y , 'interactions')” and “FitQuad = LinearModel.stepwise(X , Y , 'purequadratic')” resulted in no models, while “FitBackL = LinearModel.stepwise(X , Y , 'linear')” yielded Eq. 4.8, which has an R^2 value of 0.993.

$$y = -2.75 + 2.43x1 + 3.27x8 + 1.78x9 \quad \text{Eq. 4.8}$$

Although “FitBackL” afforded a model, this model did not perform well when assessed for external validation robustness (Figure 4.18).

To facilitate elucidation of the relevant combination of descriptors that robustly describes the observed enantioselectivity trends, data for three ketones (Table 4.2, entries 6–8) were added to the matrix, and the same four-membered series of exploratory algorithms was executed. X_{all} and Y_{all} represent the expanded library of eight ketones. Performing the MATLAB commands “FitForward = LinearModel.stepwise(X_{all} , Y_{all})” and “FitBackL = LinearModel.stepwise(X_{all} , Y_{all} , 'linear')” afforded no models.

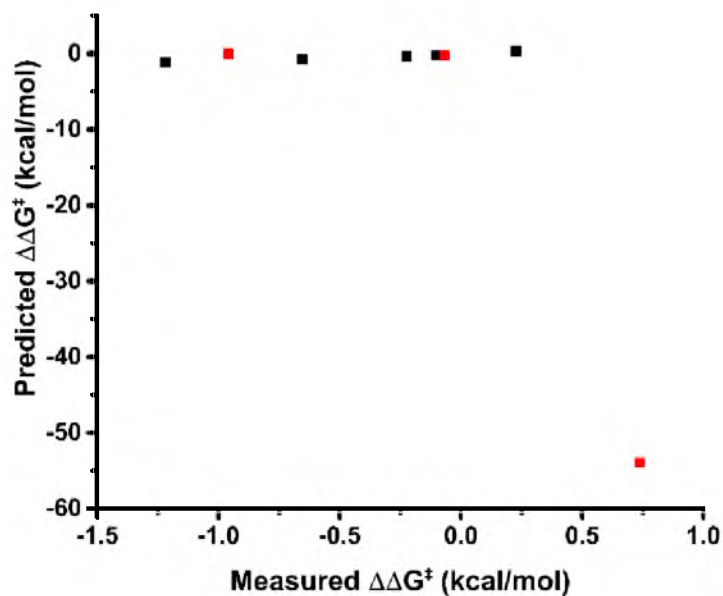


Figure 4.17. Predicted versus measured alky/alkyl library $\Delta\Delta G^\ddagger$ values depicting the model in Eq. 4.7. ■ represents the alky/alkyl DoE library, and ■ represents external validation data.

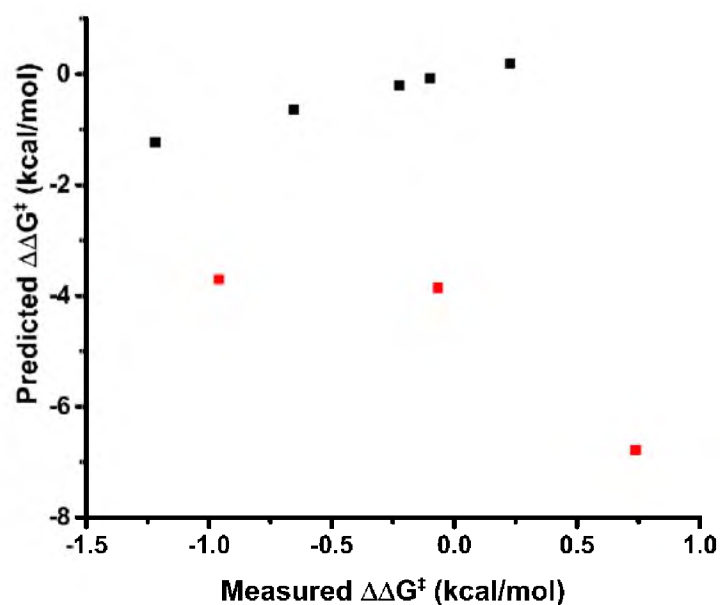


Figure 4.18. Predicted versus measured alky/alkyl library $\Delta\Delta G^\ddagger$ values depicting the model in Eq. 4.8. ■ represents the alky/alkyl DoE library, and ■ represents external validation data.

However, “FitBackI = LinearModel.stepwise(*Xall*, *Yall*, 'interactions')” yielded the relationship in Eq. 4.9, which has an R^2 value of 0.977.

$$y = -0.98 + 3.69x_7 + -3.28x_8 + 1.49x_9 + 0.77x_{10} - 2.59x_9:x_{10} \quad \text{Eq. 4.9}$$

“FitQuad = LinearModel.stepwise(*Xall*, *Yall*, 'purequadratic')” produced the model in Eq. 4.10, which has an R^2 value of 0.332.

$$y = -0.70 + 0.07x_{10} + 0.80x_{10}^2 \quad \text{Eq. 4.10}$$

From the model presented in Eq. 4.9, the proposed combination of terms yielded by “FitBackI” (x_7 , x_8 , x_9 , x_{10} , $x_9:x_{10}$) was further investigated for its robustness. To fit the five-membered alkyl/alkyl DoE library set (Table 4.2, entries 1–5) to this five-term model, the relationship was first simplified by removing the term with the largest p -value and smallest coefficient, x_{10} , affording the necessary scenario of more data points than descriptors. Next, the five-membered DoE library was fit to the resulting model template (Eq. 4.11).

$$y \sim 1 + x_7 + x_8 + x_9 + x_9:x_{10} \quad \text{Eq. 4.11}$$

External validation was then performed using the three ketones presented in Table 4.2, entries 6–8 (Figure 4.19). Importantly, while the relationship described in Eq. 4.11 poorly predicted the results of ketone external validations, this negative result provided a

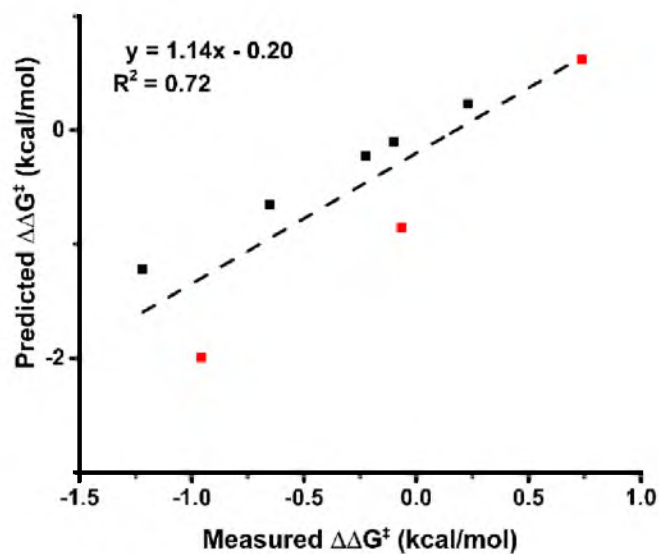


Figure 4.19. Predicted versus measured alkyl/alkyl library $\Delta\Delta G^\ddagger$ values depicting the model in Eq. 4.11. ■ represents the alkyl/alkyl DoE library, and ■ represents external validation data.

test of the described approach, i.e., expanding the library to enable the elucidation of relevant descriptor combinations, then reverting the library to its original DoE members for determining coefficient weights. This negative result yielded confidence that this process could still yield models where external validation remained an appropriate measure of robustness. Steps employing this method for arriving at the final alkyl/alkyl model are presented below. Although the model from the “FitBackI” algorithm was not robust, it suggested an interesting descriptor, $x_9 * x_{10}$, i.e., $v_{Scissor} + I_{Scissor} + (v_{Scissor})(I_{Scissor})$. Evaluating this term in combination with the presumably appropriate descriptor, x_1 ($v_{C=O}$), as the starting point for stepwise regression (“TailoredStep = LinearModel.stepwise(*Xall*, *Yall*, 'y ~ 1 + x1 + x9*x10'”, where *Xall* and *Yall* represent the expanded library of eight ketones) yielded Eq. 4.12, which has an R^2 value of 0.973.

$$y = -0.64 - 0.40x_1 - 0.69x_3 + 0.40x_9 - 0.02x_{10} - 1.69x_{19}:x_{10} \quad \text{Eq. 4.12}$$

Removing the term with largest p -value and smallest coefficient, x_{10} , and fitting the data to the remaining terms produced Eq. 4.13, which has an R^2 value of 0.982.

$$y = -0.64 - 0.39x_1 - 0.68x_3 + 0.41x_9 - 1.69x_9:x_{10} \quad \text{Eq. 4.13}$$

The model was further simplified by combining x_3 and x_9 into a cross-term ($x_3:x_9$) and fitting the data to the resulting template (“ManualFit = LinearModel.fit(*Xall*, *Yall*, 'y ~ 1 + x1 + x3:x9 + x9:x10'”), yielding the favorable model presented in Eq. 4.14, which has an R^2 value of 0.961.

$$y = -0.39 - 0.42x_1 - 0.81x_3 \cdot x_9 - 1.67x_9 \cdot x_{10} \quad \text{Eq. 4.14}$$

$$y = -0.52 - 0.33x_1 - 0.73x_3 \cdot x_9 - 1.75x_9 \cdot x_{10} \quad \text{Eq. 4.15}$$

Next, this identified parameter combination served as a template model to which the original, five-membered ketone library data (Table 4.2, entries 1–5) was fit. Eq. 4.15 (R^2 is 0.89) was the ultimate result of this iterative linear regression analysis, providing a robust description of the alkyl/alkyl ketones evaluated, as demonstrated in Figure 4.5c and 4.6c.

References

1. Linhares, A.; Chada, D. M. What is the Nature of the Mind's Pattern-Recognition Process? *New Ideas Psychol.* **2013**, *31*, 108–121.
2. Collins, K. D.; Glorius, F. A Robustness Screen for the Rapid Assessment of Chemical Reactions. *Nat. Chem.* **2013**, *5*, 597–601.
3. Collins, K. D.; Rühling, A.; Glorius, F. Application of a Robustness Screen for the Evaluation of Synthetic Organic Methodology. *Nat. Protocols* **2014**, *9*, 1348–1353.
4. Collins, K. D.; Rühling, A.; Lied, F.; Glorius, F. Rapid Assessment of Protecting-Group Stability by Using a Robustness Screen. *Chem. Eur. J.* **2014**, *20*, 3800–3805.
5. Malik, H. A.; Taylor, B. L. H.; Kerrigan, J. R.; Grob, J. E.; Houk, K. N.; Du Bois, J.; Hamann, L. G.; Patterson, A. W. Non-Directed Allylic C-H Acetoxylation in the Presence of Lewis Basic Heterocycles. *Chem. Sci.* **2014**, *5*, 2352–2361.
6. Trost, B. M. Selectivity: A Key to Synthetic Efficiency. *Science* **1983**, *219*, 245–250.
7. Carlson, R. *Design and Optimization in Organic Synthesis*. Elsevier: Amsterdam, 1992; Vol. 8.
8. Deming, S. N.; Morgan, S. L. *Experimental Design: A Chemometric Approach*. Elsevier: Amsterdam, 1993; Vol. 11.
9. Milo, A.; Bess, E. N.; Sigman, M. S. Interrogating Selectivity in Catalysis Using Molecular Vibrations. *Nature* **2014**, *507*, 210–214.
10. Harper, K. C.; Sigman, M. S. Using Physical Organic Parameters To Correlate Asymmetric Catalyst Performance. *J. Org. Chem.* **2013**, *78*, 2813–2818.
11. Harper, K. C.; Vilardi, S. C.; Sigman, M. S. Prediction of Catalyst and Substrate Performance in the Enantioselective Propargylation of Aliphatic Ketones by a Multidimensional Model of Steric Effects. *J. Am. Chem. Soc.* **2013**, *135*, 2482–2485.
12. Harper, K. C.; Bess, E. N.; Sigman, M. S. Multidimensional Steric Parameters in the Analysis of Asymmetric Catalytic Reactions. *Nat. Chem.* **2012**, *4*, 366–374.
13. Harper, K. C.; Sigman, M. S. Predicting and Optimizing Asymmetric Catalyst Performance Using the Principles of Experimental Design and Steric Parameters. *Proc. Natl. Acad. Sci. U.S.A.* **2011**, *108*, 2179–2183.
14. Harper, K. C.; Sigman, M. S. Three-Dimensional Correlation of Steric and

- Electronic Free Energy Relationships Guides Asymmetric Propargylation. *Science* **2011**, *333*, 1875–1878.
15. Donoghue, P. J.; Helquist, P.; Norrby, P.-O.; Wiest, O. Prediction of Enantioselectivity in Rhodium Catalyzed Hydrogenations. *J. Am. Chem. Soc.* **2009**, *131*, 410–411.
 16. Kozłowski, M. C.; Ianni, J. C. Quantum Molecular Interaction Field Models of Substrate Enantioselection in Asymmetric Processes. *J. Mol. Catal. A: Chem.* **2010**, *324*, 141–145.
 17. Ianni, J. C.; Annamalai, V.; Phuan, P.-W.; Panda, M.; Kozłowski, M. C. A Priori Theoretical Prediction of Selectivity in Asymmetric Catalysis: Design of Chiral Catalysts by Using Quantum Molecular Interaction Fields. *Angew. Chem. Int. Ed.* **2006**, *45*, 5502–5505.
 18. Bess, E. N.; DeLuca, R. J.; Tindall, D. J.; Oderinde, M. S.; Roizen, J. L.; Du Bois, J.; Sigman, M. S. Analyzing Site Selectivity in Rh₂(esp)₂-Catalyzed Intermolecular C–H Amination Reactions. *J. Am. Chem. Soc.* **2014**, *136*, 5783–5789.
 19. Verloop, A.; Hoogenstraaten, W.; Tipker, J. Development and Application of New Steric Substituent Parameters in Drug Design. In *Drug Design*, Ariens, E. J., Ed. Academic Press: New York, 1976; Vol. VII, pp 165–207.
 20. Verloop, A.; Tipker, J. A Comparative Study of New Steric Parameters in Drug Design. *Pharmacochem. Libr.* **1977**, *2*, 63–81.
 21. Verloop, A.; Tipker, J. Physical Basis of STERIMOL and Related Steric Constants. *Pharmacochem. Libr.* **1987**, *10*, 97–102.
 22. Jacobsen, E. N.; Zhang, W.; Guler, M. L. Electronic Tuning of Asymmetric Catalysts. *J. Am. Chem. Soc.* **1991**, *113*, 6703–6704.
 23. Hammett, L. P. Some Relations between Reaction Rates and Equilibrium Constants. *Chem. Rev.* **1935**, *17*, 125–136.
 24. Jones, R. N.; Forbes, W. F.; Mueller, W. A. The Infrared Carbonyl Stretching Bands of Ring Substituted Acetophenones. *Can. J. Chem.* **1957**, *35*, 504–514.
 25. Brown, H. C.; Okamoto, Y. Electrophilic Substituent Constants. *J. Am. Chem. Soc.* **1958**, *80*, 4979–4987.
 26. Coates, J. Interpretation of Infrared Spectra, A Practical Approach. In *Encyclopedia of Analytical Chemistry*, Meyers, R. A., Ed. John Wiley & Sons Ltd: Chichester, 2000; pp 10815–10837.
 27. Frisch, M. J.; Trucks, G. W.; Schlegel, H. B.; Scuseria, G. E.; Robb, M. A.;

- Cheeseman, J. R.; Scalmani, G.; Barone, V.; Mennucci, B.; Petersson, G. A., et al. *Gaussian 09, Revision C.01*, Gaussian, Inc.: Wallingford, CT, 2009.
28. Zhao, Y.; Truhlar, D. G. The M06 Suite of Density Functionals for Main Group Thermochemistry, Thermochemical Kinetics, Noncovalent Interactions, Excited States, and Transition Elements: Two New Functionals and Systematic Testing of Four M06-Class Functionals and 12 Other Functionals. *Theor. Chem. Acc.* **2007**, *120*, 215–241.
 29. Valero, R.; Gomes, J. R. B.; Truhlar, D. G.; Illas, F. Good Performance of the M06 Family of Hybrid Meta Generalized Gradient Approximation Density Functionals on a Difficult Case: CO Adsorption on MgO(001). *J. Chem. Phys.* **2008**, *129*, 124710.
 30. Schäfer, A.; Horn, H.; Ahlrichs, R. Fully Optimized Contracted Gaussian Basis Sets for Atoms Li to Kr. *J. Chem. Phys.* **1992**, *97*, 2571.
 31. Schäfer, A.; Huber, C.; Ahlrichs, R. Fully Optimized Contracted Gaussian Basis Sets of Triple Zeta Valence Quality for Atoms Li to Kr. *J. Chem. Phys.* **1994**, *100*, 5829.
 32. Ohkuma, T.; Koizumi, M.; Doucet, H.; Pham, T.; Kozawa, M.; Murata, K.; Katayama, E.; Yokozawa, T.; Ikariya, T.; Noyori, R. Asymmetric Hydrogenation of Alkenyl, Cyclopropyl, and Aryl Ketones. RuCl₂(xylbinap)(1,2-diamine) as a Precatalyst Exhibiting a Wide Scope. *J. Am. Chem. Soc.* **1998**, *120*, 13529–13530.
 33. Murata, K.; Ikariya, T.; Noyori, R. New Chiral Rhodium and Iridium Complexes with Chiral Diamine Ligands for Asymmetric Transfer Hydrogenation of Aromatic Ketones. *J. Org. Chem.* **1999**, *64*, 2186–2187.
 34. Wu, X.; Xiao, J. Aqueous-Phase Asymmetric Transfer Hydrogenation of Ketones—A Greener Approach to Chiral Alcohols. *Chem. Commun.* **2007**, 2449–2466.
 35. Yamakawa, M.; Yamada, I.; Noyori, R. CH/π Attraction: The Origin of Enantioselectivity in Transfer Hydrogenation of Aromatic Carbonyl Compounds Catalyzed by Chiral η⁶-Arene-Ruthenium(II) Complexes. *Angew. Chem. Int. Ed.* **2001**, *40*, 2818–2821.
 36. Ahlford, K.; Lind, J.; Maler, L.; Adolfsson, H. Rhodium-Catalyzed Asymmetric Transfer Hydrogenation of Alkyl and Aryl Ketones in Aqueous Media. *Green Chem.* **2008**, *10*, 832–835.
 37. Bess, E. N.; Sigman, M. S. Linear Free Energy Relationships (LFERs) in Asymmetric Catalysis. In *Asymmetric Synthesis II: More Methods and Applications*, Christmann, M.; Bräse, S., Eds. Wiley-VCH Verlag GmbH & Co. KGaA: Weinheim, 2012.

38. MATLAB. *version 8.1.0.604 (R2013a)*. The MathWorks, Inc.: Natick, MA, 2013.
39. Charton, M. Steric Effects. I. Esterification and Acid-Catalyzed Hydrolysis of Esters. *J. Am. Chem. Soc.* **1975**, *97*, 1552–1556.
40. Dennington, R. D., II; Keith, T. A.; Millam, J. M. *GaussView 5.0.8*, Shawnee Mission KS, 2009.
41. Gunda, T. E. *Mol2Mol*, 5.6.3; University of Debrecen: Debrecen, Hungary, 2011.
42. Sheppard, C. I.; Taylor, J. L.; Wiskur, S. L. Silylation-Based Kinetic Resolution of Monofunctional Secondary Alcohols. *Org. Lett.* **2011**, *13*, 3794–3797.
43. MacLeod, R.; Welch, F. J.; Mosher, H. S. Asymmetric Reductions. VII. The Action of the Grignard Reagent from (+)-1-Chloro-2-methylbutane on a Series of Alkyl Phenyl Ketones 1-3. *J. Am. Chem. Soc.* **1960**, *82*, 876–880.
44. Brown, H. C.; Jadhav, P. K.; Mandal, A. K. Hydroboration. 62. Monoisopinocampheylborane; An Excellent Chiral Hydroborating Agent for Trans-Disubstituted and Trisubstituted Alkenes. Evidence for a Strong Steric Dependence in such Asymmetric Hydroborations. *J. Org. Chem.* **1982**, *47*, 5074–5083.
45. Wang, F.; Liu, H.; Cun, L.; Zhu, J.; Deng, J.; Jiang, Y. Asymmetric Transfer Hydrogenation of Ketones Catalyzed by Hydrophobic Metal–Amido Complexes in Aqueous Micelles and Vesicles. *J. Org. Chem.* **2005**, *70*, 9424–9429.
46. Ganter, C.; Brassat, L.; Ganter, B. Diastereoselective Synthesis of Tricarbonyl(thiophene)chromium Complexes. *Chem. Ber.* **1997**, *130*, 659–662.
47. Cherng, Y.-J.; Fang, J.-M.; Lu, T.-J. Pinane-Type Tridentate Reagents for Enantioselective Reactions: Reduction of Ketones and Addition of Diethylzinc to Aldehydes. *J. Org. Chem.* **1999**, *64*, 3207–3212.
48. Qi, S.-B.; Li, M.; Li, S.; Zhou, J.-N.; Wu, J.-W.; Yu, F.; Zhang, X.-C.; Chan, A. S. C.; Wu, J. Copper-dipyridylphosphine-Catalyzed Hydrosilylation: Enantioselective Synthesis of Aryl- and Heteroaryl Cycloalkyl Alcohols. *Org. Biomol. Chem.* **2013**, *11*, 929–937.
49. Cheng, Y.-N.; Wu, H.-L.; Wu, P.-Y.; Shen, Y.-Y.; Uang, B.-J. Enantioselective Addition of Dialkylzincs to Aldehydes Catalyzed by (–)-MITH. *Chem. Asian. J.* **2012**, *7*, 2921–2924.
50. Dean, M. A.; Hitchcock, S. R. Divergent Enantioselective Pathways in the Catalytic Asymmetric Addition of Diethylzinc to Aldehydes in the Presence and Absence of Titanium Tetraisopropoxide. *Tetrahedron: Asymmetry* **2008**, *19*, 2563–2567.

51. Fernández-Mateos, E.; Maciá, B.; Yus, M. Catalytic Asymmetric Addition of Alkylolithium Reagents to Aromatic Aldehydes. *Eur. J. Org. Chem.* **2012**, *2012*, 3732–3736.
52. Mangas-Sánchez, J.; Busto, E.; Gotor-Fernández, V.; Malpartida, F.; Gotor, V. Asymmetric Chemoenzymatic Synthesis of Miconazole and Econazole Enantiomers. The Importance of Chirality in Their Biological Evaluation. *J. Org. Chem.* **2011**, *76*, 2115–2122.
53. Martins, J. E. D.; Wills, M. Ir(III) Complexes of Diamine Ligands for Asymmetric Ketone Hydrogenation. *Tetrahedron* **2009**, *65*, 5782–5786.
54. Reetz, M. T.; Drewes, M. W.; Schwickardi, R. Preparation of Enantiomerically Pure α -N,N-Dibenzylaminoaldehydes: S-2-(n,n-Dibenzylamino)-3-Phenylpropanal. *Org. Synth.* **1999**, *76*, 110.
55. Cahiez, G.; Luart, D.; Lecomte, F. Unexpected Cross-Coupling Reaction between *o*-Chloroaryl Ketones and Organomanganese Reagents. *Org. Lett.* **2004**, *6*, 4395–4398.
56. Kantam, M. L.; Laha, S.; Yadav, J.; Likhar, P. R.; Sreedhar, B.; Jha, S.; Bhargava, S.; Udayakiran, M.; Jagadeesh, B. An Efficient Copper–Aluminum Hydrotalcite Catalyst for Asymmetric Hydrosilylation of Ketones at Room Temperature. *Org. Lett.* **2008**, *10*, 2979–2982.
57. Langlotz, B. K.; Wadepohl, H.; Gade, L. H. Chiral Bis(pyridylimino)isoindoles: A Highly Modular Class of Pincer Ligands for Enantioselective Catalysis. *Angew. Chem. Int. Ed.* **2008**, *47*, 4670–4674.
58. Li, Y.; Yu, S.; Wu, X.; Xiao, J.; Shen, W.; Dong, Z.; Gao, J. Iron Catalyzed Asymmetric Hydrogenation of Ketones. *J. Am. Chem. Soc.* **2014**, *136*, 4031–4039.
59. Sokeirik, Y. S.; Mori, H.; Omote, M.; Sato, K.; Tarui, A.; Kumadaki, I.; Ando, A. Synthesis of a Fluorous Ligand and Its Application for Asymmetric Addition of Dimethylzinc to Aldehydes. *Org. Lett.* **2007**, *9*, 1927–1929.
60. Xu, D.; Wang, S.; Shen, Z.; Xia, C.; Sun, W. Enantioselective Oxidation of Racemic Secondary Alcohols Catalyzed by Chiral Mn(III)-Salen Complexes with *N*-Bromosuccinimide as a Powerful Oxidant. *Org. Biomol. Chem.* **2012**, *10*, 2730–2732.
61. Cram, D. J.; Elhafez, F. A. A. Studies in Stereochemistry. XXII. Rearrangement of the 1,1-Diphenyl-2-propyl into the 1,2-Diphenyl-1-propyl System¹. *J. Am. Chem. Soc.* **1954**, *76*, 28–33.
62. Mandal, S. K.; Jensen, D. R.; Pugsley, J. S.; Sigman, M. S. Scope of Enantioselective Palladium(II)-Catalyzed Aerobic Alcohol Oxidations with (–)-

- Sparteine. *J. Org. Chem.* **2003**, *68*, 4600–4603.
63. Liu, S.; Wolf, C. Chiral Amplification Based on Enantioselective Dual-Phase Distribution of a Scalemic Bisoxazolidine Catalyst. *Org. Lett.* **2007**, *9*, 2965–2968.
64. DeLuca, R. J.; Sigman, M. S. The Palladium-Catalyzed Anti-Markovnikov Hydroalkylation of Allylic Alcohol Derivatives. *Org. Lett.* **2012**, *15*, 92–95.
65. Tanaka, T.; Yasuda, Y.; Hayashi, M. New Chiral Schiff Base as a Tridentate Ligand for Catalytic Enantioselective Addition of Diethylzinc to Aldehydes. *J. Org. Chem.* **2006**, *71*, 7091–7093.
66. Burrows, E. P.; Welch, F. J.; Mosher, H. S. Asymmetric Reductions. VIII. the Action of the Grignard Reagent from (+)-1-Chloro-2-methylbutane on Cyclohexyl Alkyl Ketones. *J. Am. Chem. Soc.* **1960**, *82*, 880–885.
67. Ramachandran, P. V.; Gong, B.; Teodorović, A. V. The Influence of Fluorine on the Asymmetric Reduction of Fluoromethyl Ketones. *J. Fluorine Chem.* **2007**, *128*, 844–850.
68. Blake, A. J.; Cunningham, A.; Ford, A.; Teat, S. J.; Woodward, S. Enantioselective Reduction of Prochiral Ketones by Catecholborane Catalysed by Chiral Group 13 Complexes. *Chem. Eur. J.* **2000**, *6*, 3586–3594.
69. Brown, H. C.; Ayyangar, N. R.; Zweifel, G. Hydroboration. XVIII. The Reaction of Diisopinocampheylborane with Representative cis-Acyclic, Cyclic, and Bicyclic Olefins. A Convenient Synthesis of Optically Active Alcohols and Olefins of High Optical Purity and Established Configuration. *J. Am. Chem. Soc.* **1964**, *86*, 397–403.
70. Yadav, J. S.; Nanda, S.; Reddy, P. T.; Rao, A. B. Efficient Enantioselective Reduction of Ketones with *Daucus carota* Root. *J. Org. Chem.* **2002**, *67*, 3900–3903.
71. Durrwachter, J. R.; Wong, C. H. Fructose 1,6-Diphosphate Aldolase-Catalyzed Stereoselective Synthesis of C-Alkyl and N-Containing Sugars: Thermodynamically Controlled C-C Bond Formations. *J. Org. Chem.* **1988**, *53*, 4175–4181.
72. Matsuda, M.; Yamazaki, T.; Fuhshuku, K.-i.; Sugai, T. First Total Synthesis of Modiolide A, Based on the Whole-Cell Yeast-Catalyzed Asymmetric Reduction of a Propargyl Ketone. *Tetrahedron* **2007**, *63*, 8752–8760.
73. Jing, Q.; Sandoval, C. A.; Wang, Z.; Ding, K. Complete Chiral Induction from Enantiopure 1,2-Diamines to Benzophenone-Based Achiral Bisphosphane Ligands in Noyori-Type RuII Catalysts. *Eur. J. Org. Chem.* **2006**, *2006*, 3606–3616.

74. Yu, X.; O'Doherty, G. A. De Novo Asymmetric Synthesis and Biological Evaluation of the Trisaccharide Portion of PI-080 and Vineomycin B2. *Org. Lett.* **2008**, *10*, 4529–4532.
75. Kusakabe, M.; Kitano, Y.; Kobayashi, Y.; Sato, F. Preparation of Optically Active 2-Furylcarbinols by Kinetic Resolution Using the Sharpless Reagent and Their Application in Organic Synthesis. *J. Org. Chem.* **1989**, *54*, 2085–2091.
76. Carter, M. B.; Schiott, B.; Gutierrez, A.; Buchwald, S. L. Enantioselective Hydrosilylation of Ketones with a Chiral Titanocene Catalyst. *J. Am. Chem. Soc.* **1994**, *116*, 11667–11670.
77. Bandini, M.; Bottoni, A.; Cozzi, P. G.; Miscione, G. P.; Monari, M.; Pierciaccante, R.; Umani-Ronchi, A. Chiral C2-Boron-Bis(oxazolines) in Asymmetric Catalysis – A Theoretical Study of the Catalyzed Enantioselective Reduction of Ketones Promoted by Catecholborane. *Eur. J. Org. Chem.* **2006**, *2006*, 4596–4608.
78. Wettergren, J.; Bøgevig, A.; Portier, M.; Adolfsson, H. Ruthenium-Catalyzed Enantioselective Reduction of Electron-Rich Aryl Alkyl Ketones. *Adv. Synth. Catal.* **2006**, *348*, 1277–1282.
79. Hashiguchi, S.; Fujii, A.; Haack, K.-J.; Matsumura, K.; Ikariya, T.; Noyori, R. Kinetic Resolution of Racemic Secondary Alcohols by RuII-Catalyzed Hydrogen Transfer. *Angew. Chem. Int. Ed.* **1997**, *36*, 288–290.
80. Gonzalez, A. Z.; Román, J. G.; Gonzalez, E.; Martinez, J.; Medina, J. R.; Matos, K.; Soderquist, J. A. 9-Borabicyclo[3.3.2]decenes and the Asymmetric Hydroboration of 1,1-Disubstituted Alkenes. *J. Am. Chem. Soc.* **2008**, *130*, 9218–9219.
81. Pickard, R. H.; Kenyon, J. Investigations on the Dependence of Rotatory Power on Chemical Constitution. Part IV. The Rotations of the Normal Secondary Alcohols of the Formula $C_2H_5CH(OH)R$. *J. Chem. Soc.* **1913**, 1923–1959.
82. Brown, H. C.; Chandrasekharan, J.; Ramachandran, P. V. Chiral Synthesis via Organoboranes. 14. Selective Reductions. 41. Diisopinocampheylchloroborane, An Exceptionally Efficient Chiral Reducing Agent. *J. Am. Chem. Soc.* **1988**, *110*, 1539–1546.
83. Soni, R.; Collinson, J.-M.; Clarkson, G. C.; Wills, M. An Unexpected Directing Effect in the Asymmetric Transfer Hydrogenation of α,α -Disubstituted Ketones. *Org. Lett.* **2011**, *13*, 4304–4307.
84. Eagon, S.; Kim, J.; Yan, K.; Haddenham, D.; Singaram, B. Asymmetric Reductions Using the Chiral Boronic Ester TarB–H: A Practical and Inexpensive Procedure for Synthesizing Chiral Alcohols. *Tetrahedron Lett.* **2007**, *48*, 9025–9029.

CHAPTER 5

ONGOING AND PROPOSED APPLICATIONS OF MODEL DEVELOPMENT

Introduction

In the last 5 years, the Sigman group has made significant advances in the mathematical description of site- and enantioselective reactions. From one-dimensional linear free-energy relationships to multidimensional mathematical models, the types of reactions to which quantitative modelling can be applied has been substantially expanded. Reactions are no longer limited to description with only classical, relative rate-derived parameters. Instead, a myriad of potential molecular descriptors—computationally derived and, thus, tailored to the specific species under evaluation—are used to numerically identify relationships between chemical structure and $\Delta\Delta G^\ddagger$. The applicative usefulness of these models has been demonstrated through their support of mechanistic hypotheses and their facilitation of reagent optimization. While prediction of optimized reaction species from numerical trends is fairly facile, work continues on identifying effective methods for interpreting the mechanistic implications of multiparameter models.

The work presented in Chapter 4—the mathematical description of a rigorously designed ketone scope library—is a culmination of the Design of Experiments (DoE) and modelling techniques examined and refined in the preceding two chapters. Thus, the

ongoing goals of this program, representing an extension of this work, are now focused on applying the developed ketone library, and libraries to be constructed for other substrate classes, to several mechanistically diverse reactions. Identifying and comparing appropriate predictive models for a variety of reactions of ketones is expected to ultimately reveal the interactions between substrates and catalysts that are conserved throughout each application and those that are uniquely important, broadly impacting mechanistic analyses on a substrate class-wide scale.

Extending Free-Energy Relationships to Enzyme Engineering

The ability to accurately predict the enantioselective outcomes of unique sterically and electronically perturbed ketone substrates demonstrates the effectiveness of the DoE approach for constructing a training set from which a broadly descriptive mathematical model can be developed. Considering the demonstrated value of abiding by DoE precepts, we hypothesized that these principles could be analogously applied to the systematic investigation of enzyme-catalyzed transformations to afford models of the form in Eq. 5.1. In collaboration with Professor Vlada Urlacher of the University of Düsseldorf and Dr. Stephan Lütz of the Novartis-Basel Bioreactions group, we have begun to extend this methodology to enzyme engineering using the P450 BM-3 enzyme from *Bacillus megaterium*.

$$\Delta\Delta G^\ddagger = z_0 + a(\text{Steric Bulk}) + b(\text{Hydrophobicity}) + c(\text{Steric Bulk})(\text{Hydrophobicity}) + \quad \text{Eq. 5.1}$$

Natively, P450 BM-3 uses an iron(IV)-oxo species, embedded in a porphyrin, to selectively oxidize hydrocarbon bonds of medium chain length fatty acids. Directed evolution and site-directed mutagenesis have been extensively employed to this enzyme's oxidizing active site, with the objective of empirically gaining qualitative insight into the enzyme's structural features required for selective substrate oxidation.¹ Even with the information that these approaches afford, the absence of quantifiable evidence about the origin of selectivity makes it difficult, at best, to mutate active sites in order to achieve predictable and desired oxidation selectivities for non-wild-type substrates. A deeper, quantitative understanding of enzymes' impeccable selectivity may be afforded by using statistical methods expounded upon in previous chapters—Principal Component Analysis (PCA), Design of Experiments (DoE), and linear regression modeling—to interrogate the active site.²⁻⁴

From review of the P450 BM-3 engineering literature, it can be inferred that substrate binding pockets with restricted volume, and thus substrates with limited degrees of freedom, facilitate the proper orienting of substrates relative to the enzyme's iron(IV)-oxo oxidant, thereby enabling oxidation.^{1,5-7} We identified three hydrophobic active site residues that are hypothesized to provide key, synergistic modulation of the enzyme's capacity for selective oxidation: Phe87, Ala264, and Ala328 (Figure 5.1).¹ To delineate and optimize each of these residues' contributions to selectivity, these positions must be systematically mutated. Probing the relationship between these three residues is enabled through their simultaneous mutation (via DoE), parameterizing the mutant enzymes via molecular descriptors that quantify residue steric bulk and hydrophobicity (PCA).

The five natural amino acids with the most hydrophobic side chains (Ala, Val, Ile,

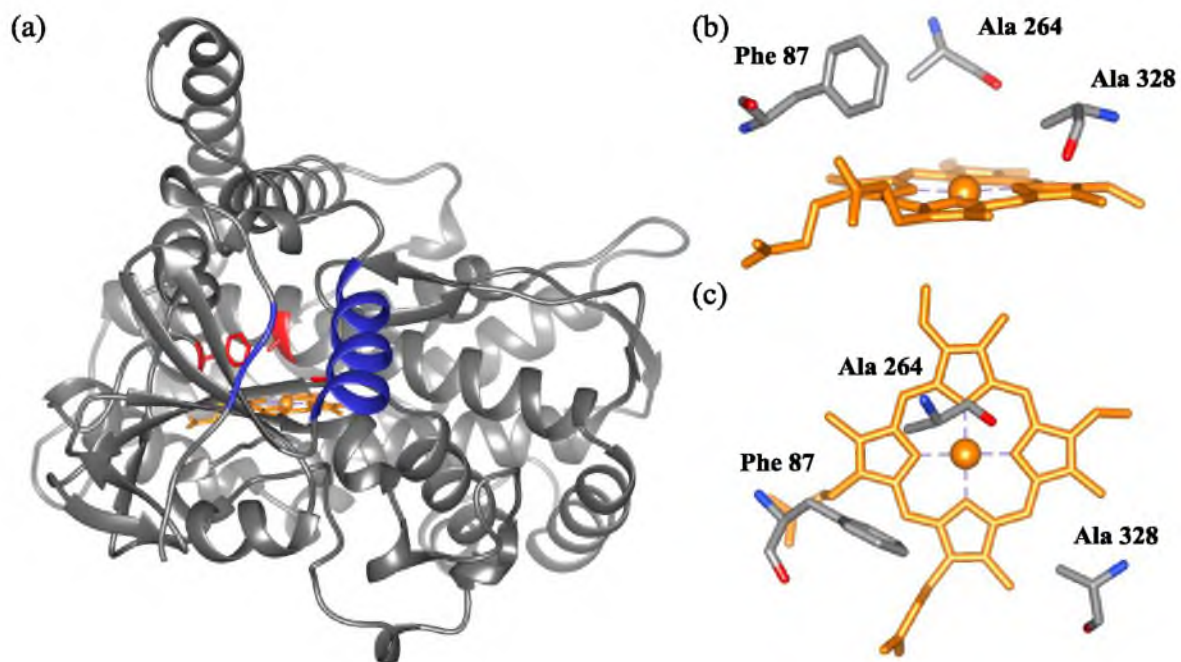


Figure 5.1. P450 BM-3 oxidizing enzyme. (a) Enzyme's iron-porphyrin active site, with the residues lining the substrate access channel highlighted in blue. Residues colored red are the three active site positions undergoing systematic mutation: Phe 87, Ala 264, Ala 328. (b) Side and (c) top views of the porphyrin and the residues to be mutated.

Leu, Phe) were considered for their ability to systematically perturb the relevant molecular features of the three active site residues under evaluation. However, as assessment of each of these combinations would require 5^3 (125) mutants, means of minimizing the size of this mutant library were considered in the context of DoE principles. Library reduction was accomplished by first hypothesizing relevant molecular descriptors of hydrocarbon bond oxidation selectivity. With the presumption that active site hydrophobicity and volume modulate selectivity profiles (*vide supra*), Sterimol (B_1 , B_5 , L), $\log P$ (hydrophobicity partition coefficient), and substituent volume (vol) were measured for Ala, Val, Ile, Leu, and Phe (Table 5.1).

The resulting data matrix of residue descriptors was subjected to PCA. Application of PCA allows identification of a subset of the five hydrophobic amino acids that represents the greatest systematic variation across the multi-descriptor-defined space. PCA enables this by identifying the orthogonal directions of greatest variation within a data set and defining each as a linear combination of the original variables.³ As applied to the data set of the five amino acids and their respective Sterimol, $\log P$, and volume descriptors, this resulted in five new principal components (PCs), the first two of which—PC₁ (Eq. 5.2) and PC₂ (Eq. 5.3)—represent 97% of the variation within the dataset (Figure 5.2a). Thus, by plotting the five hydrophobic amino acids according to these vectors, it is visually simple to select the amino acids that evenly and broadly span this experimental space as Ala, Ile, and Phe (Figure 5.2b).

$$PC_1 = 0.00B_1 + 0.47B_5 + 0.49L + 0.52 \log P + 0.52 vol \quad \text{Eq. 5.2}$$

$$PC_2 = -0.91B_1 + 0.33B_5 - 0.25L - 0.02 \log P - 0.03 vol \quad \text{Eq. 5.3}$$

Table 5.1. Parameter measurements on which Principal Component Analysis (PCA) was performed.

	B₁	B₅	L	logP	vol
Ala	1.52	2.04	2.87	-2.96	25.9
Val	1.90	3.17	4.11	-2.26	59.8
Ile	1.90	3.49	4.92	-1.72	76.8
Leu	1.52	4.45	4.92	-1.52	76.9
Phe	1.52	6.04	4.62	-1.52	93.6

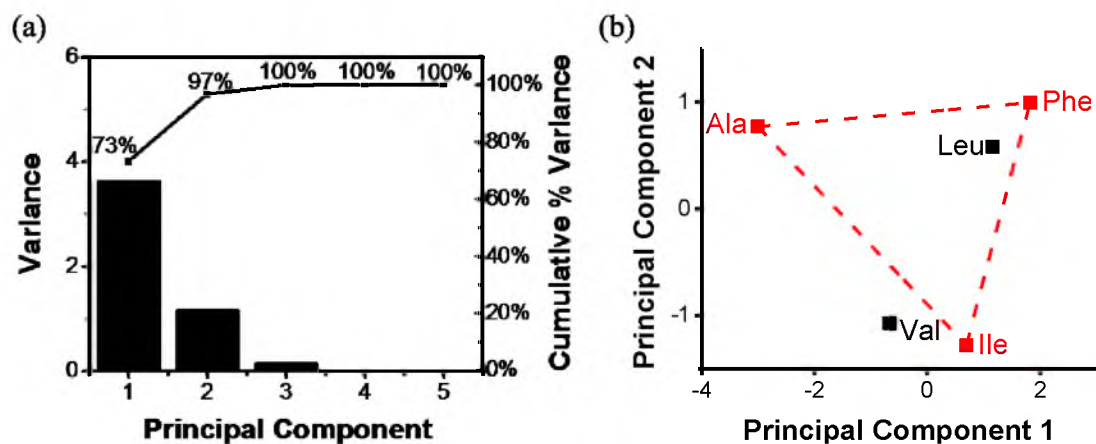


Figure 5.2. Results of Principal Component Analysis, which was performed on the data in Table 5.1. (a) Plot of variance in each Principal Component. (b) Graphical representation of hydrophobic amino acids, which are plotted according to Principal Components 1 and 2. Red data points, connected with a triangle, represent the DoE-based sampling of the Principal Component-described space.

In other words, according to DoE principles, evaluating all combinations of Ala, Ile, and Phe in residue positions 87, 264, and 328 is hypothesized to afford the same breadth and depth of information as testing all five of the amino acids would afford. This reduction from five to three amino acids is significant. Rather than synthesizing 5^3 (125) mutants to test every possible mutant combination, the reduction to three amino acids requires that only 3^3 (27) mutants be synthesized and evaluated—a 78% reduction in the number of required experiments.

It is proposed that through the simultaneous mutation and mechanistically relevant parameterization of mutated residues, a linear regression-derived mathematical model can be generated to quantitatively relate active site properties to selectivity in the enzyme-mediated oxidation (Eq. 5.1). By simultaneously mutating the designated active site residues, it is hypothesized that synergistic interactions amongst residues will be elucidated, yielding novel insight into the active site requirements for hydrocarbon oxidation. Synthesis of the enzyme library has begun and will be continued by the Urlacher lab. Following the synthesis and expression of all 27 mutated plasmids, the library will be applied to the oxidation of several substrates, ranging from the simple hydrocarbon, octane, to indole-derived substrates, each of which will be mathematically modelled to determine the substrates' mechanistic origins of selectivity.⁸ Additionally, correlating changes in substrate to changes in the active site features that dictate site selectivity may inform enzyme tailoring in order accommodate previously incompatible substrate types.

Conclusions

The foundations for mathematical modelling developed in this work, particularly the applications for DoE concepts, demonstrate the flexibility of these quantitative methods for describing a variety of mechanistically distinct scenarios. Great potential exists for advancing means of mechanistically interpreting these models. Efforts in the Sigman group are focused on this objective, and standardized parameter sets for distinct molecule classes are being developed. Through multiple applications of such standardized sets, trends in the broad mechanistic implications of these parameters may be identified. This information would allow newly developed parameters to be used and interpreted in a manner analogous to the venerable, information-rich Hammett parameter. With continued development and refinement of these parameters and modelling techniques, the trend towards increased sophistication and precision of identifying and describing subtlety in molecular interactions will continue to expand mathematical models' usefulness for understanding the underlying order of chemistry.

References

1. Whitehouse, C. J. C.; Bell, S. G.; Wong, L.-L. P450BM3 (CYP102A1): Connecting the Dots. *Chem. Soc. Rev.* **2012**, *41*, 1218–1260.
2. Barton, R. R. *Graphical Methods for the Design of Experiments*. Springer-Verlag: New York, 1999; Vol. 143.
3. Carlson, R. *Design and Optimization in Organic Synthesis*. Elsevier: Amsterdam, 1992; Vol. 8.
4. Deming, S. N.; Morgan, S. L. *Experimental Design: A Chemometric Approach*. Elsevier: Amsterdam, 1993; Vol. 11.
5. Peters, M. W.; Meinhold, P.; Glieder, A.; Arnold, F. H. Regio- and Enantioselective Alkane Hydroxylation with Engineered Cytochromes P450 BM-3. *J. Am. Chem. Soc.* **2003**, *125*, 13442–13450.
6. Zilly, F. E.; Acevedo, J. P.; Augustyniak, W.; Deege, A.; Häusig, U. W.; Reetz, M. T. Tuning a P450 Enzyme for Methane Oxidation. *Angew. Chem. Int. Ed.* **2011**, *50*, 2720–2724.
7. Weber, E.; Seifert, A.; Antonovici, M.; Geinitz, C.; Pleiss, J.; Urlacher, V. B. Screening of a Minimal Enriched P450 BM3 Mutant Library for Hydroxylation of Cyclic and Acyclic Alkanes. *Chem. Commun.* **2011**, *47*, 944–946.
8. Urlacher, V. B.; Girhard, M. Cytochrome P450 Monooxygenases: An Update on Perspectives for Synthetic Application. *Trends Biotechnol.* **2012**, *30*, 26–36.